Titre: Title:	Improving Performance Characteristics of Poly (Lactic Acid) (PLA) Through Blending With Poly (Butylene Adipate-Co-Terephthalate) (PBAT) And Incorporation of Cellulose Nanocrystals (CNCs)
Auteur: Author:	Mojtaba Mohammadi
Date:	2021
Type:	Mémoire ou thèse / Dissertation or Thesis
Référence: Citation:	Mohammadi, M. (2021). Improving Performance Characteristics of Poly (Lactic Acid) (PLA) Through Blending With Poly (Butylene Adipate-Co-Terephthalate) (PBAT) And Incorporation of Cellulose Nanocrystals (CNCs) [Ph.D. thesis, Polytechnique Montréal]. PolyPublie. https://publications.polymtl.ca/9137/

POLYTECHNIQUE MONTRÉAL

affiliée à l'Université de Montréal

Improving Performance Characteristics Of Poly (lactic acid) (PLA) Through Blending With Poly (butylene adipate-co-terephthalate) (PBAT) And Incorporation Of Cellulose Nanocrystals (CNCs)

MOJTABA MOHAMMADI

Département de génie chimique

Thèse présentée en vue de l'obtention du diplôme de *Philosophiæ Doctor*

Génie chimique

Août 2021

POLYTECHNIQUE MONTRÉAL

affiliée à l'Université de Montréal

Cette thèse intitulée :

Improving Performance Characteristics Of Poly (lactic acid) (PLA) Through Blending With Poly (butylene adipate-co-terephthalate) (PBAT) And Incorporation Of Cellulose Nanocrystals (CNCs)

présentée par **Mojtaba MOHAMMADI**

en vue de l'obtention du diplôme de *Philosophiæ Doctor*

a été dûment acceptée par le jury d'examen constitué de :

Jason Robert TAVARES, président

Pierre CARREAU, membre et directeur de recherche

Marie-Claude HEUZEY, membre et codirectrice de recherche

Abdellah AJJI, membre

Alain DUFRESNE, membre externe

DEDICATION

To my family and my beloved spouse, Rezvan.

ACKNOWLEDGEMENTS

First and foremost, I am extremely grateful to my supervisor, Professor Pierre Carreau, and my co-supervisors, Professor Marie-Claude Heuzey for their support, patience, immense knowledge and for providing me with a friendly and comfortable atmosphere for doing research.

Thanks to Professor Jason-Robert Tavares, Professor Abdellah Ajji, and Professor Alain Dufresne for taking part in my thesis committee.

I would like to extend my sincere thanks to Professor Aurélie Taguet and Dr. Charles Bruel for their insightful comments and suggestions and for their contribution to the papers.

I would like to thank all the student members of the Rheology Group who have generously shared their knowledge and experiences with me during the productive discussions.

I also would like to thank the technical and administrative staff of the Chemical Engineering Department of École Polytechnique de Montréal, especially Matthieu Gauthier.

I would like to convey my heartfelt thanks to all my friends and colleagues who have supported and helped me during my PhD studies and my life in Montréal.

Last but not least, I would like to thank my parents and brother, who have always supported me throughout my life. A special thanks to my wife, Rezvan, who has always stood by me and supported me through the good times and bad.

RÉSUMÉ

Dans cette recherche, notre objectif était de développer des nanocomposites poly (acide lactique) (PLA) et poly (butylène adipate-co-téréphtalate) (PBAT)/ cellulose nanocristaux (CNC) et des mélanges PLA/PBAT (75% wt/25% wt) contenant 1 wt % CNC aux propriétés très améliorées par rapport à celles des PLA de base (semi-cristallins (sc) et amorphes (a)) et des PBAT. Du PBAT d'origine pétrolière, mais biodégradable, a été mélangé avec du PLA et des nanocristaux de cellulose biosourcée (CNC) comme charge pour produire un mélange hybride biodégradable de nanocomposites. Les CNC ont des propriétés intrinsèquement hydrophiles qui limitent leur utilisation à quelques polymères hydrosolubles ou à base de latex. En tant qu'agent de renforcement dans les polymères hydrophobes ou les mélanges de polymères, la modification de surface ou la compatibilité est nécessaire pour obtenir une bonne dispersion et distribution, qui à leur tour entraînent une amélioration des propriétés des polymères ou des mélanges de polymères. Cependant, dans cette thèse, nous avons utilisé des CNC vierges qui ont été dispersées dans des PLA et des PBAT grâce à une nouvelle méthode basée sur la sélection thermodynamique des solvants pour la dispersion et la distribution des CNC et la dissolution des polymères, respectivement.

Dans la phase initiale, les nanocomposites PLA/CNC et PBAT/CNC ont été étudiés en utilisant une technique de coulée par solvant de nanocomposites renforcés par CNC de PLA et de PBAT afin de produire des matériaux entièrement biodégradables. L'analyse thermodynamique reposant sur la théorie des paramètres de solubilité de Hansen (HSP) a identifié le diméthylsulfoxyde/tétrahydrofurane (DMSO/THF) comme un système de solvants optimal pour incorporer les CNC dans les PLA et les PBAT. Les CNC et les polymères ont été dispersés et dissous dans du DMSO et du THF, respectivement. Cela nous a conduit à proposer une méthodologie qui s'appuie sur deux solvants : l'un pour disperser les CNC, et l'autre pour dissoudre les polymères. Les teneurs en CNC dans les PLA et les PBAT étaient de 1, 2 et 3 % en poids. Ensuite, l'effet des CNC sur les propriétés des PLA et du PBAT pour les états fondus et solides a été étudié. La présence d'une structure des CNC bien dispersée dans les matrices PLA et PBAT a été observée en utilisant la microscopie électronique à balayage (MEB) et la microscopie à force atomique (AFM). En incorporant des CNC à 1 % en poids et des teneurs plus élevées, la viscosité complexe et les modiles de stockage et de perte ont été considérablement améliorés, en particulier aux basses fréquences. La création d'un réseau interconnecté de CNC au sein des matrices PLA et

PBAT est à l'origine de ces améliorations. En outre, la présence d'un réseau 3D a été mise en évidence par la détermination d'un seuil de contrainte apparente en ajustant le modèle Herschel-Bulkely modifié aux données de cisaillement oscillatoire de faible amplitude de déformation (SAOS). La concentration seuil de percolation, calculée à l'aide d'un modèle empirique en loi de puissance ajusté aux données rhéologiques du module de stockage en fonction de la concentration en CNC, était aussi faible que 1 % en poids pour aPLA et 0.3 % en poids pour scPLA et PBAT. L'effet des traces de solvant sur les propriétés rhéologiques et morphologiques de l'aPLA, du scPLA et du PBAT a été étudié et tandis que les PLA conservaient des traces de solvant, entraînant un effet plastifiant significatif, l'élimination du solvant a été complète dans le PBAT.

Dans la deuxième phase, les propriétés morphologiques et rhéologiques des PLA, PBAT, et de leurs mélanges (75/25% en poids ; PLA/PBAT) ont été étudiées en présence de cellulose nanocristaux (CNC) préparés à partir d'une technique de coulée à l'aide d'un seul solvant, le N,N-diméthylformamide (DMF)., suivi d'un mélange à l'état fondu. La localisation de l'équilibre thermodynamique des particules de CNC devrait être dans la phase PBAT. En outre, la tension interfaciale entre le PLA et le PBAT a été obtenue à partir des meilleurs ajustements des données viscoélastiques linéaires en utilisant le modèle de Palierne pour des mélanges purs préparés à partir de granulés et de coulée en solution suivie d'un mélange à l'état fondu. Les valeurs calculées étaient assez différentes de celles obtenues à partir de l'équation de la moyenne harmonique. La viscosité complexe et le module de stockage des nanocomposites polymères purs préparés à partir de la coulée en solution ont augmenté considérablement avec la teneur en CNC, en particulier aux basses fréquences. De plus, des dépassements prononcés ont été observés dans la croissance des contraintes dans des essais de démarrage. Les CNC hautement dispersés dans les nanocomposites coulés en solution ont été agglomérés après mélange à l'état fondu. Lors du mélange à l'état fondu, la viscosité complexe et le module de stockage des nanocomposites purs coulés en solution ont nettement diminué en raison de la ré-agglomération des CNC dispersées, peut-être en raison d'une mauvaise affinité des CNC avec les polymères et de la désulfatation des CNC à des températures plus élevées. Pour préparer les nanocomposites des mélanges, les CNC ont été initialement localisées dans la matrice, dispersées ou les deux phases lors de l'étape de coulée en solution, et la localisation finale des CNC a été étudiée après le mélange à l'état fondu. Les micrographies SEM de mélanges purs cryo-fracturés PLA (scPLA ou aPLA)/PBAT ont montré que le mélange à l'état fondu a un effet substantiel sur la morphologie des mélanges purs, et les échantillons sont plus

homogènes avec des morphologies plus fines par rapport aux mélanges purs préparés à partir de la coulée en solution . L'ajout de CNC au mélange aPLA/PBAT a entraîné une diminution du rayon moyen en volume de la phase dispersée, peu importe si les CNC étaient initialement localisées dans la matrice, dispersées ou les deux phases. Dans le cas du scPLA/PBAT, lorsque les CNC ont été initialement localisées dans PBAT, le rayon moyen en volume des gouttelettes était presque le même que pour le mélange pur scPLA/PBAT. Dans les autres cas, lorsque les CNC étaient initialement localisées dans la matrice ou dans les deux phases, des gouttelettes de PBAT allongées ont été observées avec une tendance à convertir la morphologie matrice-gouttelette en une morphologie co-continue. De plus, différentes localisations des CNC ont été caractérisées à l'aide de SEM et d'AFM. Des essais de SAOS et de croissance de contrainte en démarrage ont également été menés pour étudier le rôle des CNC et leur localisation sur les propriétés des mélanges nanocomposites et leur stabilité morphologique sous cisaillement. Lorsque les CNC étaient initialement dispersées dans le PLA ou les deux phases, ils avaient tendance à être localisées à l'interface des phases PLA et PBAT, ce qui était favorable pour stabiliser la morphologie du mélange sous cisaillement. Lorsque les CNC ont été introduites dans les mélanges via la phase PBAT, une morphologie matrice-gouttelette a été obtenue. Lorsque les CNC localisées à l'interface, des augmentations significatives et légères des courbes de viscosité complexe des nanocomposites de mélange scPLA/PBAT et aPLA/PBAT, respectivement, ainsi qu'un plateau dans le module de stockage des nanocomposites de mélange scPLA/PBAT, indicateur de la transformation de comportement liquide à solide. L'épaulement dans le module de stockage (plus évident pour scPLA/PBAT/CNC) et l'arc de relaxation des gouttelettes dans les courbes Cole-Cole disparaissent suite à la localisation interfaciale de CNC à 1 % en poids. Dans les mélanges nanocomposites aPLA/PBAT/CNC, cette localisation interfaciale n'a pas modifié les morphologies matrice-gouttelettes d'où la disparition du deuxième arc des courbes Cole-Cole et de l'épaulement du module de stockage du aPLA/PBAT/CNC était une indication que la relaxation de la phase PBAT est fortement réduite. D'autre part, pour les mélanges nanocomposites scPLA/PBAT/CNC, la morphologie est passée d'une matrice-gouttelettes à une structure continue et l'épaulement du module de stockage et l'arc de relaxation dans les courbes Cole-Cole ont disparu. L'application d'un taux de cisaillement de 0.1 s^{-1} a induit une coalescence de gouttelettes prononcée dans les mélanges PLA/PBAT purs, tandis que l'ajout de CNC à 1 % en poids a significativement empêché la coalescence de gouttelettes de PBAT.

Dans la troisième phase, pour mieux comprendre l'efficacité de la méthode à deux solvants, les propriétés thermiques et mécaniques des échantillons préparés par une méthode à un seul solvant (DMF) ont été comparées à ceux de la méthode des deux solvants (DMSO/THF). En outre, les propriétés morphologiques et rhéologiques des nanocomposites purs préparés par une méthode de solvant ont été étudiées dans la deuxième phase avant de préparer le mélange de nanocomposites. Dans les deux méthodes, la calorimétrie différentielle à balayage (DSC) a montré que le contenu cristallin total des nanocomposites scPLA/CNC augmentait (effet dû à un agent de nucléation), alors qu'il diminuait dans les systèmes PBAT/CNC (effet de restriction de la mobilité de la chaîne polymère). Dans les deux cas, la température de cristallisation a été augmentée avec la teneur en CNC. Tous les nanocomposites préparés par la méthode des deux solvants ont présenté un comportement cassant. Au contraire, pour la méthode à un solvant, l'allongement à la rupture a augmenté de 28 et 95 % dans le scPLA et l'aPLA, respectivement, mais a diminué de 80 % dans le PBAT par incorporation de 3 % en poids de CNC. De plus, pour la méthode à un solvant, l'incorporation de 3 % en poids de CNC a amélioré les propriétés d'impact de 32 et 9 % dans scPLA et aPLA, respectivement, mais les propriétés d'impact des nanocomposites PBAT ont été diminuées de 4 %. Dans l'analyse thermique mécanique dynamique (DMTA), le module de stockage des systèmes scPLA/CNC et PBAT/CNC a augmenté de manière significative, en particulier dans la région caoutchouteuse avec des augmentations correspondantes de 5 à 85 MPa et 105 à 155 MPa, respectivement. À l'aide d'un modèle de percolation, la force du réseau de percolation du CNC a pu être déterminée. Elle s'est avérée dépendante de la température et affectée par des traces de solvant principalement dans les nanocomposites scPLA. Ces résultats ont confirmé que les deux méthodes de coulée en solution conduisaient à une bonne dispersion des CNC hydrophobes dans les matrices PLA et PBAT, mais que le solvant restant avait des effets négatifs sur les propriétés mécaniques et thermiques, en particulier lorsque la méthode à deux solvants était utilisée.

Enfin, dans la quatrième phase, l'effet des localisations interfaciales des CNC après mélange à l'état fondu a été étudié sur les propriétés morphologiques, rhéologiques, thermiques et mécaniques de mélanges de PLA/PBAT contenant 1 % en poids de CNC. Il a été montré dans la deuxième phase que la localisation initiale de 1 % en poids de CNC dans la matrice (PLA) ou dans les deux phases entraînait une localisation interfaciale des CNC dans les nanocomposites du mélange PLAs/PBAT. Peu importe la localisation initiale, alors que la localisation interfaciale dans aPLA/PBAT/CNC a conduit à des morphologies matrice-gouttelettes plus fines, dans scPLA/PBAT/CNC la

morphologie matrice-gouttelettes a été converties en une morphologie co-continue. De plus, ces observations ont été confirmées par une analyse rhéologique. De plus, les propriétés thermiques (d'après l'analyse DSC) ont confirmé l'effet de nucléation des CNC dans les mélanges PLAs/PBAT et amélioré la cristallisation de scPLA et PBAT dans les mélanges de scPLA/PBAT et aPLA/PBAT, respectivement, avec des augmentations de la température de cristallisation et le degré de cristallinité. La localisation interfaciale des CNC a amélioré l'allongement à la rupture et la résistance aux chocs de 52 à 171 % et de 57 à 140 %, respectivement, dans les mélanges nanocomposites scPLA/PBAT par rapport aux PLA purs. Cette amélioration était moindre dans les mélanges nanocomposites aPLA/PBAT en raison d'une moindre efficacité de la localisation des CNC à l'interface en raison de plus de traces de solvant dans aPLA/PBAT/CNC et d'une meilleure affinité des CNC avec le solvant par rapport aux polymères, d'où une adhérence interfaciale plus faible entre les phases aPLA et PBAT. En raison de cet effet, bien que la perte dans le module de stockage du système aPLA/PBAT n'ait pas été compensée par l'ajout de CNC, les CNC dans le scPLA/PBAT ont pu créer une meilleure adhérence entre les phases et améliorer le module de stockage jusqu'à la valeur de scPLA pur.

ABSTRACT

In this research, our objective was to develop poly (lactic acid) (PLA) and poly (butylene adipate-co-terephthalate) (PBAT)/ cellulose nanocrystal (CNC) nanocomposites and PLA/PBAT (75 wt%/25 wt%) blends containing 1 wt% cellulose nanocrystals (CNCs) with highly improved properties in comparison to those of neat PLAs (semicrystalline (sc) and amorphous (a)) and PBAT. Petroleum-sourced, but biodegradable PBAT was blended with PLA and bio-based CNCs as a filler to produce biodegradable hybrid blend nanocomposites. The CNCs are intrinsically hydrophilic properties that limit their usage to a few water-soluble or latex-based polymers. As a reinforcing agent in hydrophobic polymers or polymer blends, Surface modification or compatibilization is necessary to achieve a good dispersion and distribution, which in turn result in improvement in polymers or polymer blend properties. However, in this thesis, we used pristine CNCs that were dispersed in PLAs and PBAT through a novel method based on the thermodynamic selection of solvents for dispersion and distribution of CNCs and dissolution of polymers, respectively.

In the initial phase, PLA/CNC and PBAT/CNC nanocomposites were investigated using solvent casting of pristine CNCs reinforced nanocomposites of PLAs and PBAT in order to produce fully biodegradable materials. Thermodynamic analysis relying on the Hansen solubility parameter (HSP) theory identified dimethyl sulfoxide/tetrahydrofuran (DMSO/THF) as an optimal solvent system to incorporate CNCs into PLAs and PBAT. The CNCs and the polymers were dispersed and dissolved in DMSO and THF, respectively. It led us to propose a methodology that relies on two solvents: one to disperse the CNCs, and the other to dissolve the polymers. The CNC contents in both PLAs and PBAT were 1, 2, and 3 wt%. Then, the effect of the CNCs was investigated on the properties of the PLAs and PBAT for both molten and solid states. The presence of a well-dispersed CNC structure within the PLAs and PBAT matrices was observed using scanning electron microscopy (SEM) and atomic force microscopy (AFM). By incorporating 1 wt% CNCs and greater contents, the complex viscosity, storage, and loss moduli were considerably enhanced, especially at low frequencies. The creation of an interconnected network of CNCs within the PLAs and PBAT matrices was credited with these improvements. Also, the presence of a 3D network was evidenced by the determination of apparent yield stress by fitting a modified Herschel-Bulkely model to the strain amplitude oscillatory shear (SAOS) data. The percolation threshold concentration, calculated using an empirical power-law model fitted to the rheological data of the

storage modulus as a function of CNC concentration, was as low as 1 wt% for aPLA and 0.3 wt% for both scPLA and PBAT. The effect of solvent traces on the rheological and morphological properties of aPLA, scPLA, and PBAT was investigated and while PLAs retained solvent traces, leading to a significant plasticizing effect, solvent removal was complete in PBAT.

In the second phase, the morphological and rheological properties of PLAs, PBAT, and their blends (75/25 wt%; PLA/PBAT) were investigated in the presence of CNCs prepared from solution casting using a single solvent, N, N-dimethylformamide (DMF), followed by melt mixing. The thermodynamic equilibrium localization of CNCs particles should be in the PBAT phase. Also, the interfacial tension between both PLA and PBAT was obtained from the best fits of the linear viscoelastic data using the Palierne model of the neat blends prepared both from granules and from solution casting followed by melt mixing. The calculated values were quite different than those obtained from the harmonic-mean equation. The complex viscosity and storage modulus of the neat polymer nanocomposites prepared from solution casting increased markedly with CNC content, particularly at low frequencies. Also, pronounced overshoots were observed in the stress growth coefficient. The highly dispersed CNCs in the solution cast nanocomposites were agglomerated after melt mixing. Upon melt mixing the complex viscosity and storage modulus of the solution cast neat nanocomposites decreased markedly due to re-agglomeration of the dispersed CNCs, possibly due to poor affinity of CNCs with the polymers and desulfation of CNCs at higher temperatures. For preparing the blend nanocomposites, the CNCs were initially localized in the matrix, dispersed, or both phases during the solution casting step, and the final localization of CNCs were studied after melt mixing. SEM micrographs of cryo-fractured neat blends PLA (scPLA or aPLA)/PBAT showed that melt mixing has a substantial effect on the morphology of the neat blends, and the samples are more homogenous with finer morphologies compared to the prepared neat blends from solution casting. Adding CNCs to the aPLA/PBAT blend were resulted in a decrease of the volume average radius of the dispersed phase no matter if the CNCs were initially localized in the matrix, dispersed, or both phases. In the case of scPLA/PBAT, when the CNCs were initially localized in PBAT the volume average radius of droplets was almost the same as for the neat scPLA/PBAT blend. In the other cases, when CNCs were initially localized in the matrix or both phases, elongated PBAT droplets were observed with a tendency of converting the matrix-droplet morphology to a co-continuous one. Also, different localization of CNCs were characterized using SEM and AFM. SAOS and stress growth tests were also conducted to

investigate the role of the CNCs and their localization on the blend nanocomposite properties and their morphological stability under shear flow. When CNCs were initially dispersed in PLA or both phases, they tended to be localized at the interface of the PLAs and PBAT phases, which was favorable to stabilize the blend morphology under shear flow. When CNCs were introduced to the blend nanocomposites through the PBAT phase, a matrix-droplet morphology was obtained. When CNCs localized at the interface, significant and slight increases in the complex viscosity plots of scPLA/PBAT and aPLA/PBAT blend nanocomposites and also a plateau in the storage modulus of scPLA/PBAT blend nanocomposites were an indication of the transform from liquid to solid-like behavior. Both the shoulder in complex modulus (more obvious for scPLA/PBAT/CNC) and the droplet relaxation arc in the Cole-Cole plots disappear following the interfacial localization of 1 wt% CNCs. In the aPLA/PBAT/CNC blend nanocomposites, this interfacial localization did not change the matrix-droplet morphologies, hence the disappearance of the second arc of Cole-Cole plots and shoulder in complex modulus of aPLA/PBAT/CNC was an indication that the relaxation of the PBAT dispersion phase is greatly reduced. On the other hand, for the scPLA/PBAT/CNC blend nanocomposites, the morphology changed from matrix-droplet to a continuous structure, and both the shoulder in complex modulus and relaxation arc in Cole-Cole plot of scPLA/PBAT/CNC disappear. Applying a shear rate of 0.1 s^{-1} induced a pronounced droplet coalescence in the neat PLA/PBAT blends, whereas adding 1 wt % CNCs significantly prevented PBAT droplet coalescence.

In the third phase, to have a better understanding of the effectiveness of the two solvents method, the thermal and mechanical properties of the samples prepared by one solvent method (DMF) were compared to those of the two solvents (DMSO/THF) method. Also, the morphological and rheological properties of neat nanocomposites prepared by one solvent method were investigated in the second phase before preparing the blend nanocomposites. In both methods, differential scanning calorimetry (DSC) showed that the total crystalline content of the scPLA/CNC nanocomposites increased (nucleating agent effect), whereas it decreased in the PBAT/CNC systems (polymer chain mobility restriction effect). In both cases, the crystallization temperature was increased with CNC content. All the nanocomposites prepared via the two solvents method exhibited a brittle behavior. On the contrary, for the one solvent method, the elongation at break increased by 28 and 95 % in the scPLA and aPLA, respectively, but decreased by 80 % in PBAT by incorporation of 3 wt% CNCs. Also, for the one solvent method, incorporating 3 wt% CNCs

were improved the impact properties by 32 and 9 % in scPLA and aPLA, respectively, but the impact properties of PBAT nanocomposites were decreased by 4%. In dynamic mechanical thermal analysis (DMTA) the storage modulus of scPLA/CNC and PBAT/CNC systems increased significantly, especially in the rubbery region with corresponding increases from 5 to 85 MPa and 105 to 155 MPa, respectively. Using a percolation model, the strength of the percolating CNC network could be determined and was found to be dependent on temperature and affected by traces of solvent mostly in the scPLA nanocomposites. These results confirmed that both solution cast methods led to a good dispersion of hydrophobic CNCs within PLA and PBAT matrices, but remaining solvent had some negative effects on the mechanical and thermal properties, especially when the two solvents method was used.

Finally, in the fourth phase, the effect of interfacial localizations of CNCs after melt mixing was investigated on morphological, rheological, thermal, and mechanical properties of blends of PLAs/PBAT containing 1 wt% CNCs. It was shown in the second phase that initial localization of 1 wt% CNCs in the matrix (PLAs) or both phases resulted in interfacial localization of CNCs in the PLAs/PBAT blend nanocomposites. No matter of initial localization, while interfacial localization in aPLA/PBAT/CNC led to finer matrix-droplet morphologies, in scPLA/PBAT/CNC the matrix-droplet morphologies were converted to a co-continuous one. Also, these, observation was confirmed by rheological analysis. Also, thermal properties (from DSC analysis) confirmed the nucleation effect of CNCs in PLAs/PBAT blends and improved the crystallization of scPLA and PBAT in the blends of scPLA/PBAT and aPLA/PBAT, respectively, with increases in the crystallization temperature and the degree of crystallinity. Interfacial localization of CNCs improved elongation at break and impact strength by 52 - 171 % and 57 -140 %, respectively, in scPLA/PBAT blend nanocomposites compared to the neat PLAs. This improvement was less in aPLA/PBAT blend nanocomposites due to less effectiveness of CNC localization at the interface because of more trace of solvent in aPLA/PBAT/CNC and better affinity of CNCs with solvent compared to polymers, hence resulted in lower interfacial adhesion between aPLA and PBAT phases. Due to this effect, although the loss in the storage modulus of aPLA/PBAT was not compensated by the addition of CNCs, the CNCs could create in scPLA/PBAT better adhesion between phases and improved the storage modulus up to the value of neat scPLA.

TABLE OF CONTENTS

LIST OF TABLES

LIST OF FIGURES

CHAPTER 1 INTRODUCTION

Today, we need a wide range of polymeric materials with their applications in different areas such as aerospace, aeronautical, automotive, medical, sensors, agriculture, etc. [1]. This is mainly because polymeric materials are light and have many advantages such as low cost, durability, water resistance, etc. in comparison to their metal counterparts. Most of the plastics that are in the environment are polyethylene (PE), polypropylene (PP), Polyethylene terephthalate (PET), polystyrene (PS), and polyvinyl chloride (PVC) which are non-biodegradable or fossil-based [2]. The fossil-based polymers produce a large quantity of waste in the environment. One way to resolve these problems in the environment is to substitute fossil-based polymers with bio-based polymers. Both bio and fossil-based polymers can be biodegradable or not [3]. Also, it is worth mentioning that biodegradability could not be the ultimate solution in replacing fossil-based polymers with bio-based one. For example, when the impacts of carbon sequestration in a landfill are taken into account, Poly (lactic acid) (PLA) and PP greenhouse gas emissions are equal [2]. PLA and Poly (butylene adipate-co-terephthalate) (PBAT) received remarkable attention from industrial and academic points of view. PLA is bio-based, biodegradable, biocompatible, and non-toxic [4]. PLA belongs to a family of aliphatic thermoplastic polyester, which has attractive mechanical and physical properties such as high modulus, high strength, and good clarity. So, it is a good candidate to replace petroleum-based polymers such as PS, PET, and PP [5]. It has a wide range of applications such as construction and automobile product, textile and fibers, films and packaging, and biomedical (drug delivery, blood vessels, tissue engineering, and scaffolding) [6]. However, it suffers from serious drawbacks such as low melt strength, low crystallization rate, poor processability, slow crystallization rate, low toughness, low service temperature, and high brittleness [5]. Also, PBAT has been identified as a promising biodegradable plastic candidate for packaging applications due to its high degree of flexibility, toughness, and ductility, as well as acceptable mechanical strength and good processability [7], [8]. In this context, PBAT has been proposed as a viable alternative to the commonly used PE-based films in flexible packaging [9], [10]. However, improvements in PBAT's viscoelastic and barrier properties, as well as mechanical strength and stiffness, may expand its applications in packaging and other areas. These disadvantages of PLA and PBAT can be improved through the development of PLA or PBAT-

based nanocomposites [11], [12]. Cellulose nanocrystals are rod-like nanoparticles made by acid hydrolysis of cellulose from the cell walls of various plants, sea creatures, and bacteria. Low density, renewability, biodegradability, high reactivity, big surface area per unit weight, and high strength and modulus are just a few of the benefits of CNC [13]. Recently, there has been a surge in interest in incorporating CNCs into PLA and PBAT in order to broaden their uses by improving mechanical and thermal properties over a wide temperature range[13]–[16]. CNC can help PLA and PBAT retain their unique qualities including biocompatibility, biodegradability, and transparency while improving their mechanical and thermal properties. This would result in completely biobased, biocompatible, and biodegradable composite materials that might be used to replace petroleum-based polymeric products in the packaging and automobile industries. When CNC particles are exposed to non-water-soluble polymers, strong hydrogen bonds between them result in the creation of large agglomerates. As a result, the application of CNC to improve the properties of polymers has increased, but it is still confined to a few water-soluble polymers and a few other materials. As a result, in most situations, surface modification or compatibilization are required to produce a high dispersion of CNCs, as well as a minimum requirement to significantly improve polymer characteristics [17]. Due to the plasticization effect of the modifiers or compatibilizers, improvements in mechanical properties have not always been observed despite adequate dispersion. What is more, pristine CNC has been used in solution casting, but as far as we know, no previous research has investigated how to select the best solvent for dispersing CNCs or dissolution of polymers. Both the melt and solid characteristics of nanocomposites are influenced by the creation of an interconnected network of particles. As a result, in this study, at first, we attempted to find an effective preparation process (selecting best solvent based on thermodynamic point of view) to incorporate CNCs in PLA and PBAT, and second, we compared the effectiveness of this method with the regular preparation solution casting using dimethylformamide (DMF) on the mechanical and thermal properties of PLA and PBAT/CNC nanocomposites. In addition to neat PLA and PBAT/CNC nanocomposites in this thesis, we developed biopolymer blend nanocomposites based on polylactide (PLA) with highly improved morphological and rheological, thermal, and mechanical properties in comparison to those of neat PLAs. PLA blending will open a new horizon for new or extended PLA applications [5]. The final properties of the blend depend on the inherent properties of components in the blend and blend morphology [5]. So, the properties can be improved by controlling the PLA ratio in the second

phase, use of another polymer as the third component (ternary blend systems), and developing hybrid systems through introducing nanoparticles, which can be localized in the matrix, in droplets, or at the interface [5]. One of the promising second components to blend with PLA is PBAT, which is a biodegradable synthetic fossil-based polymer. The final performance of polymer blends can be increased by introducing nanoparticles as reinforcements and can be considered hybrid materials. One of the promising nanoparticles is cellulose nanocrystals [18]. Although there is a wide range of investigations on the properties of polymer blends and nanocomposites, very few pay attention to the control and stabilization of the morphology of polymer blends using nanoparticles [19]. Also, CNCs localization could have a significant effect on rheological, thermal, and mechanical properties that should be addressed properly. So, in this work, we improved the morphological, rheological, thermal, and mechanical properties of PLA/PBAT blend nanocomposites by the addition of cellulose nanoparticles. The whole system as a hybrid system can be considered a green nanocomposite or bio-nanocomposite since PLA and CNC are bio-based and biodegradable and PBAT is biodegradable.

The main contributions of this research are found in four scientific articles; the first and second have been published in the journals of Cellulose and Nanomaterials, respectively, the third and fourth have been accepted with a revision in the journals of Polymer Composites, and Polymer, respectively.

This thesis consists of the following chapters:

- Chapter 1: Introduction
- Chapter 2: Literature review
- Chapter 3: Objectives
- Chapter 4: Organization of the articles
- Chapters 5 - 8: The four articles reporting the main results of this project.
- Chapter 9: General discussion
- Chapter 10: Conclusions and recommendations

CHAPTER 2 LITERATURE REVIEW

2.1 Biodegradable Polymers

Biodegradable polymers are polymers that undergo the mineralization process through chain scission by microbes present in the environment, which needs specific pH, humidity, oxygen level, and metals in order to become completely degradable in the environment [20]. It is important to state that bio-based plastics and biodegradable plastics are completely different from each other. A bio-based plastic can be biodegradable or not and if plastic is biodegradable, it does not mean that it is bio-based [3]. So, plastics from biomass feedstock materials that are bio-based can be biodegradable or not. Biodegradable plastics can be from renewable resources such as poly (lactic acid) (PLA) and polyhydroxyalkanoate (PHA) or can be from fossil resources such as polycaprolactone (PCL), polybutylene succinate (PBS), and poly (butylene adipate-co-terephthalate) (PBAT) (Figure 2.1) [3]. Despite their enormous potential, biodegradable (bio or fossil-based) plastics have yet to gain widespread adaptation in the plastic industry, owing to their higher costs and poor mechanical properties. Global bioplastics production capacities are expected to rise from around 2.11 million tons in 2020 to around 2.87 million tons in 2025, according to the latest industry data collected by European Bioplastics in collaboration with the Nova-Institute [21]. Biobased PLA and biodegradable PBAT global production capacity were around 294×10^3 and 280×10^3 tonnes in 2020 and the production of biodegradable plastics is expected to increase to 1.8 million tonnes in 2025 [21]. Bioplastic final cost is likely to be reduced as processing technologies and capability improve; however, the weak mechanical properties will continue to be a limiting factor. Biopolymers have a number of flaws, including brittleness, poor barrier properties, low thermal stability, thermal degradability, and processing window sensitivity [22].

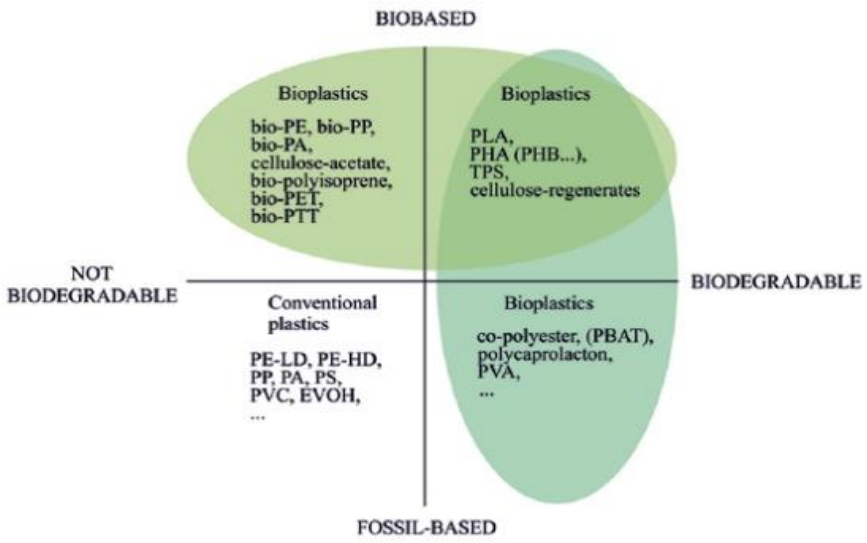

Figure 2.1 Biodegradability characteristic of conventional and bio-polymers [3]

2.1.1 Polylactide (PLA)

Poly (lactic acid) or polylactide (PLA) is a bio-based and biodegradable polymer produced from biomasses or resources such as cornstarch and sugarcane that belongs to the aliphatic thermoplastic polyester group and is produced industrially. PLA has one of the highest commercial potentials among biodegradable polyesters due to its widespread availability, mechanical properties, and low cost [23], [24]. Direct condensation and ring-opening polymerization of lactic acid monomer and cyclic lactic dimer, respectively, can be used to synthesize PLA (Figure 2.2) [5].

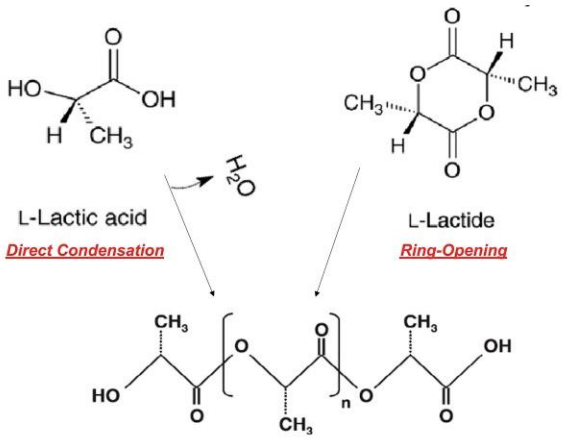

Figure 2.2 Different methods of PLA synthesis [6][5].

PLA is one of the few bioplastics that can match the mechanical strength of commodity polymers including polystyrene (PS) and polyethylene terephthalate (PET). PLA has a number of advantages, including high modulus (2-16 GPa), high strength (around 14-117 MPa), and transparency, but it also has a number of drawbacks that must be resolved in order for it to be used in broader applications. The brittleness, low barrier properties, and slow crystallization rate of PLA are its key drawbacks [5]. Different techniques for improving PLA toughness were discussed by Anderson et al. [25] and Rasal et al. [26], including changing the ratio of D and L mesoforms (ratio of D:L and native properties depend on the synthesis route taken; Chemically synthesized lactic acid gives the racemic mixture (50% D and 50% L), while fermentation-derived lactic acid typically consists of 99.5% of the L-isomer and 0.5% of the D-isomer), plasticization, copolymerization with other polyesters, and blending with other bioplastics. PLA resins containing more than 93 % of L-lactic acid are semi-crystalline. However, PLA with 50–93 % L-lactic acid is completely amorphous. Blending PLA with other bioplastics has gotten a lot of attention because it's cost-effective and improves not only the brittleness of PLA but also its other properties [5], [25].

2.1.2 Poly (butylene adipate-co-terephthalate) (PBAT)

PBAT is a synthetic polymer derived from fully biodegradable fossil resources, has a high elongation at break (up to 700%) [27]. Figure 2.3 shows the molecular structure of PBAT, which is made up of butylene terephthalate (BT) and butylene adipate (BA) parts. It is used in a variety of applications, including packaging, biomedical, and hygiene devices, among others [7].

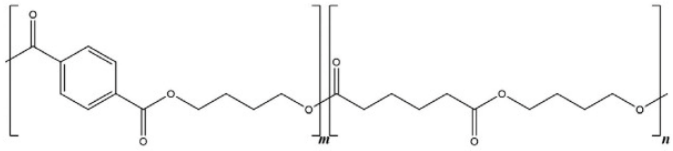

Figure 2.3 Chemical structure of PBAT [27].

The use of this biodegradable material is hampered by its high prices and poor thermo-physical and mechanical resistance as compared to non-biodegradable polymers [28]. As a result, the growth of a PBAT market will be possible only if production costs are reduced and their properties are enhanced [29]. PBAT has been identified as a promising biodegradable plastic candidate for packaging applications due to its high degree of flexibility, toughness, and ductility, as well as

good processability [30]. In this context, PBAT has been proposed as a viable alternative to the commonly used polyethylene (PE)-based films in flexible packaging [9], [10]. However, improvements in PBAT's viscoelastic and barrier properties, as well as mechanical strength and stiffness, may expand its applications in packaging and other areas.

2.2 Nanocellulose

Nanotechnology is defined as the study and control of materials with at least one dimension in the range of 100 nanometers. Nano dimensional materials with unique properties can lead to new advanced material applications. Nanomaterials derived from renewable resources, such as cellulosic and lignocellulosic biomass, have the potential to play a significant role in nanotechnology research. A suitable method or a combination of methods may be used to extract nanocellulose from lignocellulosic biomass. Extracted nanocellulose is a readily available and reusable biomaterial resource with unique properties for advanced materials applications. Nanocellulose's shape, scale, surface morphology, yield, and properties are all affected by the lignocellulosic biomass source, pretreatment, and preparation processes [31], [32]. Cellulosic nanomaterials such as bacterial nanocellulose (BNC) which is formed by certain strains of bacteria, cellulose nanofibers (CNF), and cellulose nanocrystals (CNC) which are isolated from lignocellulosic biomasses are all referred to as nanocellulose (Figure 2.4). The majority of cellulose nanocrystals (CNC) are rod-like nanoparticles with diameters of 10–20 nm and lengths of several hundred nanometers. Strong acid hydrolysis is used to make them from a variety of materials, including wood pulp, cotton, manila, tunicin, and bacteria. The nanocellulose and main amorphous components are eliminated during the acid hydrolysis process, leaving CNC particles with high crystallinity and a half ester sulfate group (OSO_3^-) on their surface. Cellulose nanofibrils (CNF) are flexible fibers with a diameter similar to or greater than CNC and a length of several μm [33]–[35]. Tempo-mediated oxidation (2,2,6,6,-tetramethylpipelidine-1-xoyl radical) is a typical manufacturing process [36], [37]. The resulting CNF has both amorphous and crystalline portions, giving it a lower crystallinity than CNC, and carboxylate groups are added during the TEMPO oxidation process. Due to the almost excellent crystalline structure of CNC or crystalline sections of CNF, together with intra- and inter-chain hydrogen bond networks, both CNC and CNF are nanomaterials with exceptional mechanical properties. Cellulose nanocrystals as a reinforcing phase have gotten a lot of interest because of their low cost, biodegradability, ease of availability,

high strength, renewability, and other excellent properties [38]. CNCs also could disperse more effectively than CNF in the matrix of polymers. Nanocelluloses have the ability to reinforce various polymer matrices with very low filler loadings to achieve targeted properties, with Young's modulus in the range of 100–130 GPa and a high specific surface area of several hundred m^2 g^{-1} [31].

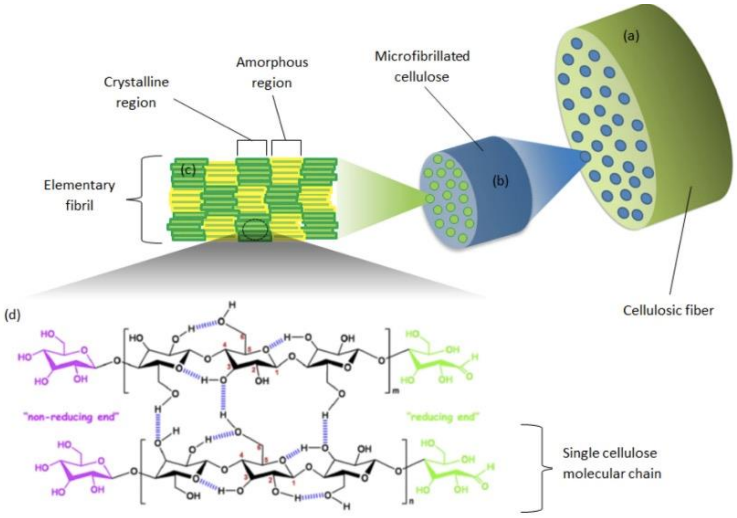

Figure 2.4 (a) Cellulosic fiber, (b) micro-fibrillated cellulose, (c) elementary fibril and (d) basic cellulose chemical structure [39].

Cellulose nanocrystals have some excellent characteristics that make them suitable for reinforcing phases in polymer matrices, including the following [31]:

1) High aspect ratio (length/width ratio) compared to micro cellulosic materials, allowing for good stress transfer between fillers and polymer matrix during loading.
2) Because of the nanosized dimensions, there is a large specific contact surface area, which means that a low concentration is required to disperse and distribute across the matrix and achieve the desired properties.
3) The large hydroxyl groups on the surface of the cellulosic nanofiller may form hydrogen bonds/participate in chemical reactions with the matrix, resulting in better matrix reinforcement.
4) Furthermore, the abundance of hydroxyl groups in nanocellulose allows for the functionalization of nanocellulose with suitable molecules for efficient nanocellulose reinforcement in polar and nonpolar matrix polymers.

5) Cellulose nanofillers are a form of nanofiller that is both environmentally friendly and renewable.

2.2.1 CNC Treatments

Apart from their intriguing features, CNCs, use in polymer nanocomposites is confined to a few hydrophilic polymers like polyvinyl alcohol (PVOH) [40]–[42] and polyethylene oxide (PEO) [43], and hydrophobic polymers in latex form [44]. This is owing to CNC's high hydrophilicity, which means they do not disperse well with more intriguing polymers like hydrophobic polyolefins, PLA, and other hydrophobic polymers. To achieve improved mechanical characteristics and excellent dispersion of CNCs into polymer matrices, compatibilization is required [45]. CNC treatments to make it more hydrophobic, polymer matrix functionalization to make it more hydrophilic or the use of compatibilizers should all be considered in this regard. CNC surface treatments include acetylation or esterification [46], tempo-mediated oxidation [36], [37], grafting [47]–[50], and cationization [51], as well as plasma [52] and corona [53] treatments and chemical alterations. For CNCs, these procedures must be followed by a post-treatment reaction such as grafting a long hydrophobic chain (surfactant) as a grafting agent to the carboxylate or carboxylic groups due to a lack of significant physical or chemical interactions with polymer matrices. This can make the entire treatment procedure costly, time-consuming, and difficult to manage. Also, to improve the compatibility of CNCs and polymer matrices, coupling agents and compatibilizers have been utilized [54], [55]. The plasticization effect of short chains grafted on the surface of CNCs, on the other hand, impairs the CNCs' reinforcing action.

2.3 Polymer Nanocomposites

Polymer nanocomposites have stimulated the interest of scientists and industry in recent years due to their ability to achieve substantial improvements in mechanical, thermal, thermomechanical, and solvent or gas barrier properties with respect to the polymer matrix at very low filler concentrations as compared to continuous phase materials [56]. Three major factors influence the properties of nanocomposites: polymer matrix and nano reinforcing phase properties, as well as the interfacial interaction between the filler surface and the polymer matrix. Moreover, the properties of polymeric nanocomposites are highly dependent on the dispersion and distribution of nanomaterials in the continuous matrix phase for a particular nano reinforcement and matrix of the

polymer [38]. As well distributed in polymers, cellulose nanocrystal (CNC) has the potential to generate new products due to its superior mechanical properties, low density, biodegradability, renewability, and low cost [17], [57]–[59]. While modified CNCs have been successfully applied to a variety of polymers in recent years, the use of unmodified CNCs in polymer matrices is still a question that needs to be answered. Furthermore, the incorporation of CNCs into polymer blends has received little attention and will be discussed in the section on polymer blends.

2.3.1 PLA/CNC and PBAT/CNC Nanocomposites

Since CNCs are bio-based, biodegradable, biocompatible, non-toxic, and derived from abundant resources on Earth, these materials that are entirely bio-based and biodegradable are becoming increasingly popular [60], [61]. Their growth is due to the ability to create polymer nanocomposites with improved properties while preserving the matrix's biodegradability. CNC's biggest drawback is that they are difficult to disperse in hydrophobic media such as PLA and PBAT since they are predominantly hydrophilic [62]. In order to create CNC-based nanocomposites, various methods such as solvent casting, melt mixing, and in situ polymerization have been used. [63]. Several recent advances in the production of these nanocomposites are detailed in several review articles [64]–[67]. Table 1 summarized the advantages and disadvantages of different methods in preparing CNC-based nanocomposites.

Table 2.1 Advantages and disadvantages of different methods in preparing CNC-based nanocomposites [63]

Methods	Advantages	Disadvantages
Solvent casting	The production process is easy, 3-dimensional CNC network	Solvent utilization and some solvents are toxic, not good for large scale production
Melt mixing	Large scale production, no solvent	CNC degradation, destruction of a 3-dimensional network through high shear rate, very bad dispersion in hydrophobic matrices
In situ polymerization	CNC network formation, making covalent bonding between polymer and CNCs, the possibility of large-scale production	CNC degradation during polymerization, dispersion of CNCs in monomer phase does not allow to go for a high degree of polymerization

The use of direct melt mixing to achieve well-dispersed CNCs in PLA and PBAT has not been extensively established. This is primarily due to the presence of interacting hydroxyl groups on the

CNC surface, which makes dispersion within PLA and PBAT difficult. The irreversible agglomeration of CNCs in the PLA/CNC and PBAT/CNC nanocomposites during melt mixing are caused by strong interactions among CNC particles, as well as their large surface area and high surface energy [68], [69]. Besides that, high processing temperatures combined with applied shear forces can cause further thermal degradation of CNCs that accelerate beyond 200 °C [68], [69]. The developed CNC agglomerates in the matrix could also serve as stress concentration sites, reducing the mechanical properties of nanocomposites dramatically. Many attempts have been made to boost the CNC dispersion in PLA and less in PBAT and, as a result, the final properties of their nanocomposites. CNC surface functionalization, the incorporation of surfactants/compatibilizers, and the use of hybrid processing methods are examples of these efforts [13]. Table 2 summarizes the research on CNC melt mixing in PLA, including the method of modifications, CNC content, percolation threshold concentration, and analysis. Among these studies, Kamal et al. [70] were able to melt mix spray-freeze-dried CNCs into a PLA matrix without modifying the CNCs or using additives. They obtained a percolation threshold of 3 wt% CNCs. Only a few studies have been published on melt mixing as a method of preparing PBAT/CNC nanocomposites. Using an internal melt mixer, Zhan et al. [71] integrated both unmodified and modified CNCs into PBAT. Morelli et al. [72] reported a slight increase in thermal stability and mechanical properties of PBAT reinforced by phenyl butyl isocyanate-modified CNCs, even by 10 wt% CNCs, prepared through melt-processed using a twin-screw extruder (TSE). A slight improvement in mechanical properties was reported by Pinherio et al. [16], where they prepared PBAT/octadecyl isocyanate-modified CNCs in an internal melt mixer.

Table 2.2 Melt mixing of PLA/CNCs [13]

Melt process	CNC content and modification	Results
Twin-Screw Extruder[73]	Using Beycostat A B09 as a surfactant (5 wt%)	CNC dispersion increased, but PLA degraded at 20 wt%
Twin-Screw Extruder[74]	CNC-grafted PLA (2, 4, and 8 wt%)	--
Twin-Screw Extruder[75]	Silanation (3 wt%)	Still the presence of agglomerates
Twin-Screw Extruder[76]	Esterification (0.5, 1, and 2 wt%)	Increase in interfacial interaction without any effect on the crystallization
Twin-Screw Extruder[77]	CNC-HCL, CNC-AA, and CNC-LA (5 wt%)	PLA had better interaction with LA in comparison to the AA and HCL

Twin-Screw Extruder[78]	CNC hydrolysis with H_2SO_4, HCL, H_3PO_4, HNO_3	CNC hydrolysis with H_3PO_4 resulted in good dispersion
Twin-Screw Extruder [47]	CNC grafted PLLA (1, 2, 3 wt%)	Agglomeration increased with CNC content
Twin-Screw Extruder [79]	CNC grafted PMMA (5 wt%)	Good dispersion of CNCs
Twin-Screw Extruder [80]	--- (4 wt%)	Up to 10 μm CNC agglomerates
Internal Mixer [81]	CNC-ASA (5 wt%)	Better dispersion in comparison to unmodified CNCs
Internal Mixer [82]	--- (3 and 6 wt%)	10 μm agglomerates of CNCs at CNC content of 3 wt%
Internal Mixer [82]	CNC-grafted PLA (3 and 6 wt%)	Good dispersion of CNCs
Internal Mixer [83]	Freeze dry and spray dry CNC (0.5, 1, 1.5, 3, 5, 7 wt%)	Had a good dispersion even at 7 wt%
Internal Mixer [84]	CNC-grafted PLLA (1,2,3 wt%)	Good dispersion of CNC
Internal Mixer [85]	Lignin coated CNCs	Up to 30 μm agglomerates of CNCs
CNC-ASA=CNCs modified with alkenyl succinic anhydride, CNC-LA=lactic acid modified CNCs, CNC-AA=acetate modified CNCs, CNC-HCl =Hydro chloric acid modified CNCs, CNC-H_2SO_4 = CNCs hydrolyzed through H_2SO_4, CNC-H_3PO_4 = CNCs hydrolyzed through H_3PO_4, CNC-HNO_3 = CNCs hydrolyzed through HNO_3, CNC-g-PMMA= CNCs grafted with poly(methyl methacrylate)		

Since it's difficult to get a good CNC dispersion in PLA and PBAT using melt mixing, several studies have looked at how to boost it using solvent casting. Solution casting implies dissolving PLA and PBAT chains in a polar solvent such as N, N-dimethylformamide (DMF) [86], dimethyl sulfoxide (DMSO), formic acid, dimethylacetamide (DMAc), pyridine, chloroform [87]–[89], dichloromethane [90], and a few more solvents [62] in order to disperse CNC inside the PLA and PBAT chains. After the solvent has evaporated, a strong CNC solid percolation network can form. As solution casting is used, thermal degradation of PLA and CNC can be avoided. Also, the combination of wet (solution casting) and dry (melt mixing) methods can be an effective method in the preparation of PLA/CNC and PBAT/CNC nanocomposites. Few researchers obtained interesting results without modification of CNCs and studies conducted on modified CNCs can be found in a recent review paper conducted by Vatansever et al. [13]. Among different studies conducted on unmodified PLA/CNC nanocomposites [13], [87], [91]–[94], Bagheriasl et al. [80], [95] demonstrated that using DMF as the solvent, well-dispersed CNC particles could be obtained in PLA. They compared their findings to samples prepared using a melt mixing (TSE) directly.

When comparing melt mixing (Figure 2.5, first row) and solution casting (Figure 2.5, second row) in PLA nanocomposite with 4 wt% of CNCs, the scanning electron microscopy (SEM) and transmission electron microscopy (TEM) images in Figure 2.5 shows that when using solution casting in PLA nanocomposite well distributed CNCs were obtained.

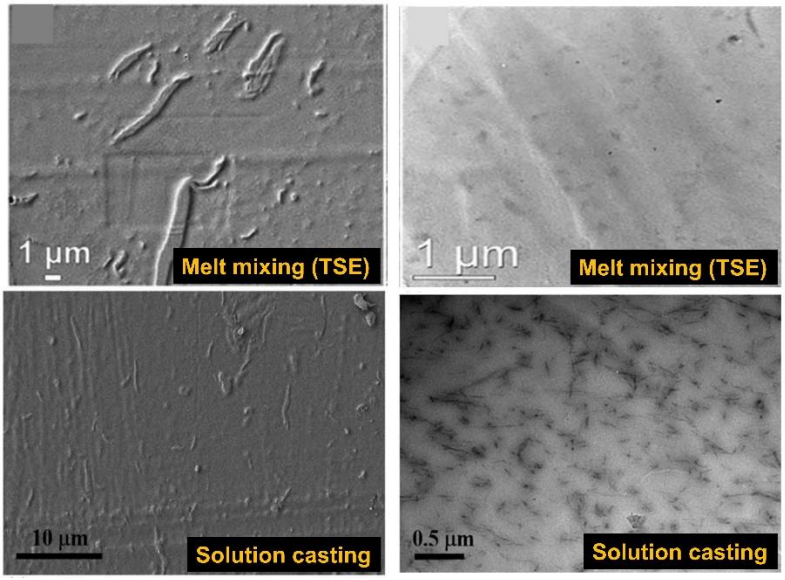

Figure 2.5 Images of PLA/CNC nanocomposite (containing 4 wt% CNCs) prepared by solution casting and melt mixing; SEM (left) and TEM (right) [80], [95].

The importance of PLA molecular weight and crystallizability on CNC dispersion efficiency was reported by Vatanserver et al. [96]. Due to a better interpenetration of PLA molecules and CNC nanoparticles within each other during the solution preparation process, it was shown that the CNCs could be better distributed in a lower molecular weight PLA. They also showed that the high crystallizability of PLA could improve the CNC dispersion quality by preventing agglomeration during the solvent evaporation step. Figure 2.6 displays TEM images of PLA/CNC nanocomposites with a CNC content of 5 wt%. The existence of CNC agglomerates in high molecular weight PLAs could be seen (Figure 2.6, first column). In low molecular weight PLA, however, the CNC dispersion appears to be better (Figure 2.6, second column). Comparing Figures 2.5 and 2.6 show, although Vatanserver et al. [96], used the same methods for the preparation of lower molecular weight PLA/CNC nanocomposites, they achieved a lower dispersion of CNCs in low molecular weight PLA. Morelli et al. [97], using solution casting, obtained 120 % and 40 % improvement in tensile modulus and strength when incorporated 10 wt% aromatic isocyanate-grafted CNCs in

PBAT matrix. Also, Ferreira et al. [98] could achieve an improvement in storage modulus for PBAT/3 wt% unmodified and adipic acid-modified CNCs prepared from solution casting. Despite the fact that solution casting has been performed in several studies to prepare polymer-CNC nanocomposite, none of them consider how to select a solvent for CNC dispersion and polymer dissolution. Furthermore, the impact of residual solvent on rheological, mechanical, and morphological properties is still a challenging topic that needs to be addressed properly.

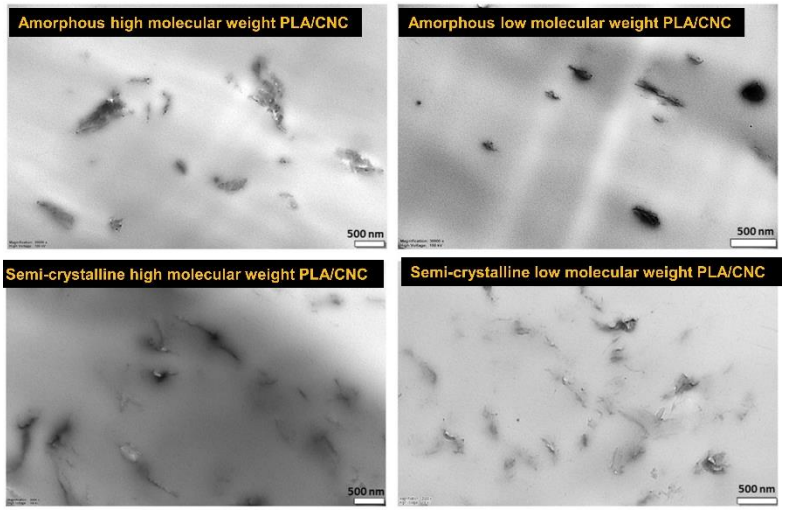

Figure 2.6 TEM images of PLA/CNC nanocomposites (amorphous and semicrystalline with different molecular weights) with 5 wt% CNCs prepared by solution casting [96].

Researchers recently merged the two methods to prepare a better dispersion of CNCs not only from solvent casting but also from both solvent casting and melt mixing, in order to make it industrially acceptable. Most of them used solution casting to create a masterbatch, which is then diluted in the melt mixing process. To stop CNC agglomeration inside PLA, Oksman et al. [99] investigated a liquid-assisted nanocellulose feeding into the extruder. Their goal was to remove the need for CNC drying before processing, which could cause irreversible aggregation due to strong hydrogen bonding. During the process, they also used (polylactide-graft-maleic anhydride) PLA-g-MA and poly (ethylene glycol) (PEG) as a compatibilizer in the system. Other researchers used the same liquid-assisted feeding process but were unable to achieve a high degree of CNC dispersion in the PLA matrix [99]–[103]. More researchers have recently concentrated on the masterbatch method, which uses a polymer as the CNC carrier. Solution casting [104]–[106], spin coating [107], and in-situ polymerization [14], [108] are popular methods for creating masterbatches. Bitinis et al. [109] used solution casting to prepare PLA masterbatches with pristine CNCs, PLA-grafted-CNC, and

alkyl-grafted-CNC (C18-g-CNC). They discovered that using C18-g-CNC resulted in a more uniform CNC dispersion in PLA. Similarly, Heshmati et al. [110] used a solvent casting process and DMF as the solvent to prepare a masterbatch of PLA/CNC and PLA/PEO-CNC by high-pressure homogenization and freeze-drying. The masterbatch was then diluted with the aid of an internal mixer. Atomic force microscopy (AFM) images show an acceptable dispersion of 2 wt% of CNCs (with or without PEO) in the PLA (Figure 2.7). The dispersion of CNCs was better when the CNCs were functionalized with PEO, as seen in the images; a percolation threshold of 1.5 wt% was reached.

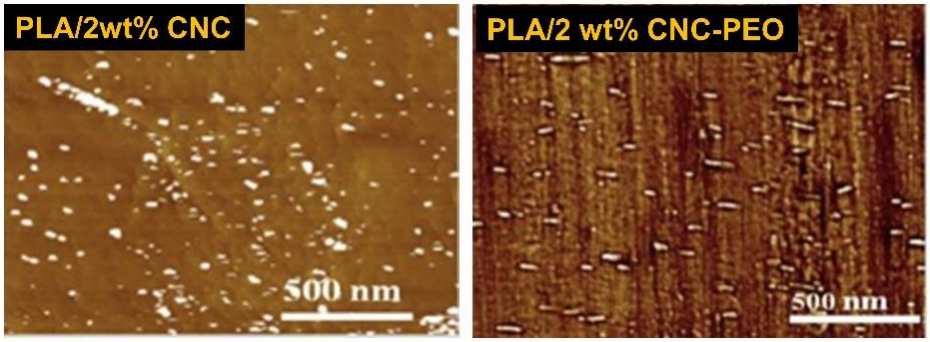

Figure 2.7 AFM images of PLA/2 wt% CNC and PLA/2 wt% CNC-PEO nanocomposites prepared by dilution of masterbatch in an internal mixer [110], [111].

In a recent study, Bagheriasl et al. [80] prepared PLA/4 wt% CNC through TSE subsequent to dilution of a masterbatch (prepared via solution casting). Although the TEM images of samples prepared by solution casting and melt mixing (Figure 2.8) are close to those obtained by solution casting alone (Figure 2.5), the rheological properties of samples prepared by solution casting are significantly improved. However, they discovered that the tensile strength remained nearly constant while the modulus increased only slightly. This may be due to the difference in surface energies between PLA and CNC particles, which results in poor interfacial strength.

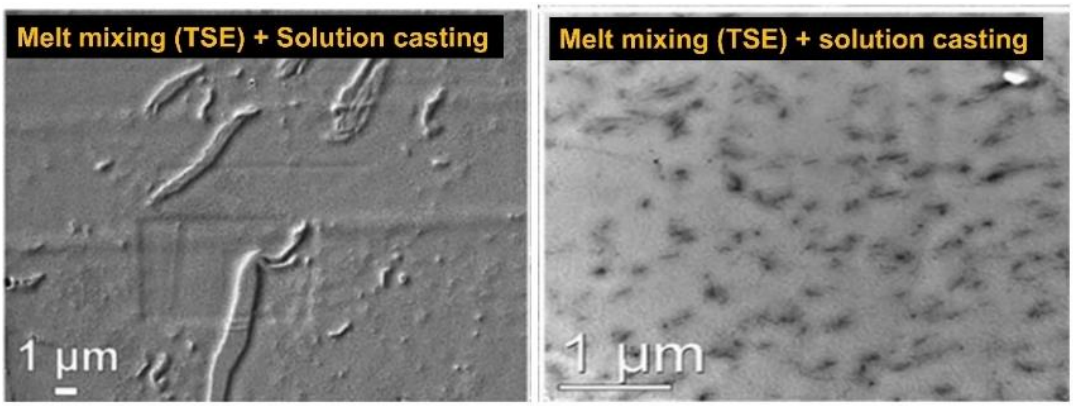

Figure 2.8 Images PLA/CNC nanocomposite (containing 4 wt% CNCs) prepared by dilution of masterbatch in the TSE; SEM (left) and TEM (right) [80].

Shojaeiarani et al. [107] compared two masterbatches of PLA/CNC-PEO made by spin-coating and solvent casting and then diluted with a twin-screw extruder. The dispersion of CNC was better from the spin-coating method at low CNC contents up to 3 wt%, but as the CNC content increased to 5 wt%, the dispersion from solvent casting was better than spin-coating. The existence of a significant amount of residual solvent associated with a large volume of spin-coated masterbatches at 5 wt% CNCs hampered the CNC dispersion within PLA, according to the authors. They also suggested that the CNC agglomeration could be caused by insufficient shear or a shorter residence time. They didn't display TEM or AFM images of the dispersed CNCs to see whether they could get a better dispersion of CNCs in the PLA. Water-soluble polymers including polyvinyl alcohol (PVOH), polyethylene oxide (PEO), and polyvinyl(acetate) (PVAc) have also been used as carrier polymers to make masterbatches and then PLA/CNC nanocomposites [82], [112]–[114]. Arias et al. [82] successfully dispersed CNCs at a nano-level scale through a novel two-step process. First, they encapsulated CNCs with polyethylene oxide (PEO) using a solution mixing method followed by freeze-drying. Second, they prepared PLA/PEO-CNC in the molten state. They used a high and low molecular weight of PEO and showed that using low molecular weight resulted in a finer dispersion of CNCs. Also, they compared their result with direct mixing of CNCs and PLA and the result showed 10 µm agglomerates of CNCs at CNC content of 3 wt%. Moreover, they showed that the brittle behavior PLA transferred to the ductile behavior by increasing the amount of low molecular PEO. Regarding PBAT/CNC nanocomposites, in a study conducted by Vatansever et al. [105], CNC reinforced PBAT nanocomposites with CNC contents of 1, 3, and 5% were made by solution casting or melt mixing of a PBAT/CNC masterbatch. They discovered that solution-cast

nanocomposites had a much finer CNC dispersion, while melt mixing resulted in CNC agglomerates (Figure 2.9). They did not observe any significant differences in thermal degradation, and mechanical properties of PBAT/CNC prepared from solution casting or dilution of masterbatch through melt mixing.

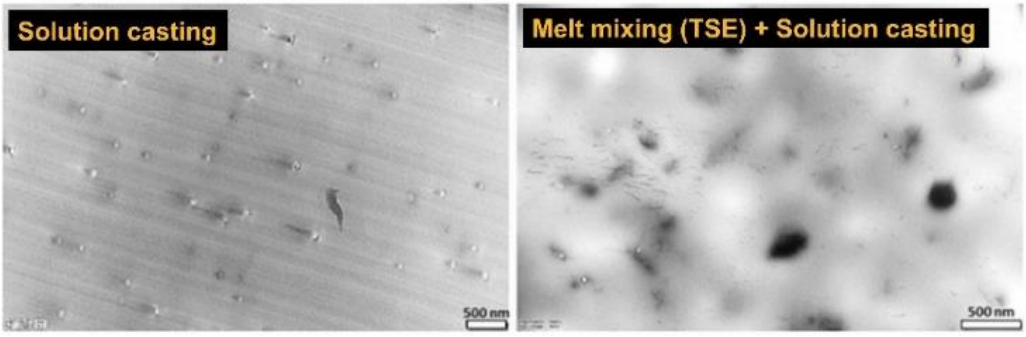

Figure 2.9 TEM images of PBAT/5 wt% CNC nanocomposites prepared by solution casting or dilution of master batch prepared by solution casting in a TSE [105].

2.3.2 Rheological Properties of PLA/CNC and PBAT/CNC Nanocomposites

From rheological analysis, it is possible to predict or estimate the properties of polymers containing CNCs. Variations in complex viscosity and storage modulus as a function of frequency are widely used to describe the morphology (e.g., CNC dispersion) of CNC-based nanocomposites [115]. Using the information from the storage and loss modulus (G' and G'', respectively) and the complex viscosity (η^*) as a function of frequency, the rheological behavior of the polymer can be described. Kamal's group [116] identified the following rheological characteristics as indicators of solid-network formation initiation: (a) a sudden shortening of the linear viscoelastic region, (b) a higher G' (than G'') at low frequencies, (c) an upturn in complex viscosity at low frequencies. When the CNC distribution and dispersion are homogenous throughout the polymer, G' and G'' increase with the filler content, and the increases are more important at low frequencies [115]. On the other hand, there is a wide range of investigations that showed that adding a filler (nano) to the polymers will result in increases or decreases in the complex viscosity. The decrease in complex viscosity can be due to the degradation of the polymer matrix in the presence of a filler. Mariano et al. [115] prepared PLA/CNC nanocomposites through melt mixing where the CNCs were modified by two PLLA-based surfactants (imidazole group (Im-PLLA) and polyethylene glycol (PEG) block (PEG-b-PLLA)). They showed that adding a large amount of CNCs increased the complex viscosity of

the system. Zhang et al. [117] showed that the addition of 3 wt.% CNC to the polymer nanocomposite of PBAT/CNC resulted in an increase in the complex viscosity. On the other hand, Pinherio et al. [118] showed that modified CNCs with octadecyl isocyanate in PBAT/CNC nanocomposites had a reverse effect on the complex viscosity. In another study, Ben Azouz et al. [119] investigated the effect of CNCs on polyoxyethylene (PEO)/CNC nanocomposite. They showed that the viscosity decreased with increasing CNC content up to 6 wt.%, probably this is due to interactions between the oxygen groups of PEO and the hydroxyl groups of cellulose, which result in a strong affinity between PEO chains and the cellulosic surface.; beyond that concentration, the viscosity started to increase. Because most of the polymers are hydrophobic and the CNCs are hydrophilic, there is not a good interfacial interaction between CNCs and polymers, which results in agglomeration or poor dispersion of CNCs in the polymer matrix [120], [121]. In addition to the effects of CNCs on the storage modulus, loss modulus, and complex viscosity, it can produce another effect by providing a three-dimensional network, which connects through the polymer. This three-dimensional network is considered above a percolation threshold at which the rheological properties of polymer composites increase exponentially and the systems exhibit an apparent yield stress [122]. Bagheriasl et al. [122] investigated the shear rheology of PLA/CNC nanocomposite which is produced through solvent casting and they showed that the system reached a percolation threshold at the CNCs wt% of 0.66 for PLA/CNC nanocomposites. In another study conducted by Arslan et al. [106], the rheological properties of the PLA/CNC nanocomposites confirmed the CNC dispersion variation in the samples prepared through solution casting and dilution of a master batch in a twin-screw extruder (TSE). The CNC percolation network in nanocomposites prepared by solution casting was found to be between 1 and 3 wt% CNC, while the solid network formation concentration in nanocomposites prepared by TSE was calculated to be greater than 5 wt% CNC. Vatanserver et al. [105] confirmed the dispersion and distribution of CNC in PBAT through the rheological experiments. The CNC percolation network concentration in nanocomposites prepared by solution casting was calculated to be around 2.18 wt% CNCs, while the solid network formation concentration in nanocomposites prepared by TSE was calculated to be around 3.15 wt% CNCs.

A very good comparison in the review of Vatansever et al. [13] focuses on the rheological behavior of PLA/CNC nanocomposites at a frequency of 0.1 rad/s from different reports (Figure 2.10). According to Figure 2.10, it is obvious that Bagheriasl et al. [123] and Gupta et al. [124] reached

a very high value in the complex viscosity and storage modulus, which is an indication of a CNC network formation at a very low amount of CNCs (around 0.6 wt%). The decrease in the complex viscosity from the work of Bagheriasl et al. [123] at a CNC content of 7 wt% is an indication of CNC agglomeration in the PLA matrix (Figure 2.10).

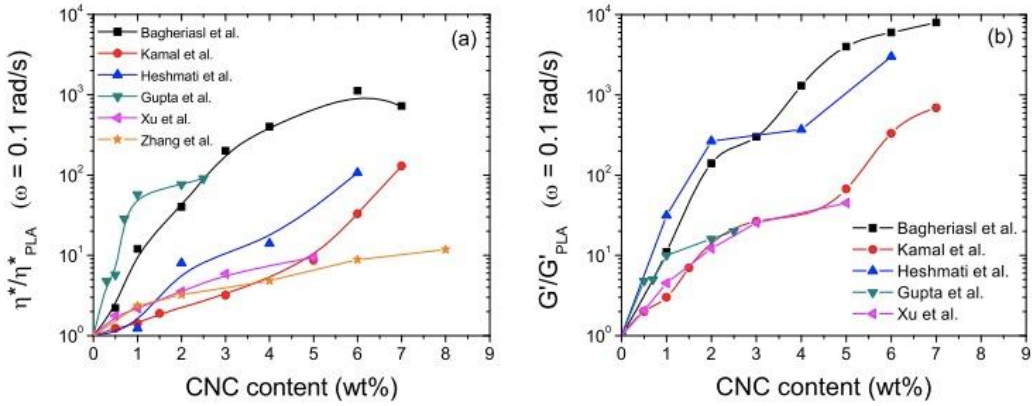

Figure 2.10 Relative (a) complex viscosity and (b) storage modulus of PLA/CNC nanocomposites from different reports as a function of CNC content [13], [83], [111], [123]–[126].

By applying the empirical power-law equation (Equation 2.1) to the experimental data of storage modulus versus CNC material, the percolation threshold in polymer nanocomposites could be determined.

$$G' = \beta_c G \left(\frac{m - m_c G}{m_c G} \right)^{n_2} \qquad \text{for } m > m_c G \qquad \text{(Equation 2.1)}$$

In this equation $\beta_c G$ and n_2 are power-law constants, m is the CNC concentration (wt%) and $m_c G$ is the rheological percolation threshold (wt%) [96], [123], [127]–[130]. By fitting this empirical model to the rheological data, percolation thresholds could be calculated for CNC nanocomposites. The onset of CNC percolation threshold concentrations were identified by Bagherasli et al. [123] and Gupta et al. [85] as 0.66 and 0.68 wt%, respectively, which is consistent with their experimental results. Vatanserver et al. [96] used this approach to determine the CNC rheological percolation threshold for PLA/CNC nanocomposites, which was 7.8 and 4.8 wt% for high and low molecular weight (MW) PLA with amorphous content, and 6.6 and 2.8 wt% for high and low MW PLA with semicrystalline content, respectively.

2.3.3 Thermal and Crystalline Properties PLA/CNC and PBAT/CNC Nanocomposites

Differential scanning calorimetry was used to investigate the effect of CNCs on the crystallization and spherulite growth of biodegradable polymers from the melt. CNCs act as nucleating agents, increasing the melting temperature (T_m), crystallization temperature (T_c), and degree of crystallinity (X_c) of the polymer, according to several authors [63]. The presence of thicker polymer crystalline lamellae can lead to a rise in melting temperature [97], whereas the crystallization of slightly less-perfect polymer crystals can lead to a decrease in melting temperature [72]. When a nanofiller serves as a nucleating agent, the nanocomposite's crystallization temperature is typically raised slightly above that of the neat polymer, which is directly linked to an increased number of heterogeneous nuclei for crystallization. When CNCs act as an anti-nucleating agent, however, T_c decreases, which may be due to polymer chain restriction, which impedes crystalline growth [131], [132]. Chen et al. [133] investigated the effect of modified and unmodified CNCs on the poly(β-hydroxybutyrate) composites. They showed that unmodified CNCs increased the crystallization temperature due to the nucleating effects on CNCs, but modified polylactide-grafted CNCs showed a lower crystallization temperature in comparison to the unmodified CNCs and the neat polymer. The degree of nucleation dispersion, nanocomposite processing method, polymer chemical structure, filler structure, and other factors all influence the crystallization process of polymeric nanocomposites. Various observations were reported in the literature on the impact of CNC on polymer crystallinity. CNCs have an effect on the crystallinity of polymers and this is related not only to the role of CNCs as nucleating agents but also through increasing the interfacial interaction between filler-matrix [72], [134], [135]. This effect was shown by Pei et al. [136]. They investigated the effects of CNCs and silylated CNCs on the crystallinity of PLLA-based nanocomposite. They showed that unmodified CNCs did not have any effect on the crystallinity of PLLA, but the modified CNCs increased the degree of crystallinity of PLLA from 14.3 to 30.4 %. These findings show that the increase in crystallinity of PLLA resulted from a better interfacial interaction between silylated CNCs and PLLA and also from a better dispersion throughout the PLLA matrix. Despite the rise in T_c as the amount of CNC increased, the crystallinity of PBAT did not change significantly, according to Morelli et al. [97]. Hameed et al. [137] found a similar behavior while working with PHBV. Morelli et al. [14] observed that after adding modified CNCs with a low molecular weight poly (butylene glutarate), T_c of PBAT increased while X_c decreased.

Several other investigations on PLA/CNC nanocomposites reported both increase [116], [136]–[142] and decrease [140], [142]–[145] in crystallization rate and crystallinity of PLA. As a result of these contradictory findings, cellulose nanocrystals (especially modified CNCs) can function as nucleating agents, affecting the interfacial interaction between the filler-matrix, T_c, and X_c of the polymer. As a result, it's a good idea to look into the nucleation effect of CNCs for each system, as it can change and alter the final material properties.

2.3.4 Mechanical Properties PLA/CNC and PBAT/CNC Nanocomposites

The enhancement of the host matrix mechanical properties appears normal, given cellulose's inherent mechanical role in nature. The use of CNCs in various polymer matrices to produce nanocomposites with adequate mechanical properties is critical for the better utilization of these materials in various fields. When these materials are used as packaging, for example, they must have a high elongation at break and a high tear resistance [146]. In biomedical applications, the material should be flexible with high elongation at break, whereas high stiffness and strength are needed in automotive applications [147], [148]. The inclusion of a hard phase (CNCs) in the comparatively softer polymer matrix can be linked to an increase in the mechanical properties of the nanocomposites, which absorb part of the external stress due to their high Young's modulus and also dissipate this external stress through particle-particle and particle-polymer friction, as previously described [149]. Other possibilities in improving the mechanical properties can be related to polymer crystallinity. As explained in the previous section, the crystallinity of CNC-based nanocomposites increased by adding CNCs to the matrix [136]. In addition to many efforts for studying the effect of CNCs on mechanical properties of polymer nanocomposites [150]–[153], other authors have shown experimentally that adding CNCs as reinforcement improves the mechanical properties of various polymer matrices. In thermoplastic nanocomposites such as PLA-CNC or PBAT/CNC, decreases in the elongational at break are reported in different publications and this is mainly related to intrinsic properties of thermoplastic nanocomposites, which are common in all of them. Fortunati et al. [154] investigated the PLA/modified CNC nanocomposites and showed despite the increase of 83 % in Young modulus, the elongational at break decrease by adding 5 wt% modified CNCs. On the other hand, Pinherio et al. [118] investigated mechanical properties of PBAT/CNC nanocomposites, for which the CNCs were modified with octadecyl isocyanate. They showed that elongation at break of PBAT increased with increasing the CNCs

content up to the theoretical percolation threshold (CNC content of 3 wt%). They explained that a homogenous dispersion of CNCs was achieved up to the theoretical percolation threshold and this resulted in better dissipation of external stresses. Above the theoretical percolation threshold, the CNC agglomeration takes place and produces stress concentration spots in the matrix. Many other investigations on mechanical properties of PLA/CNC and PBAT/CNC were extensively reviewed by Vatnatserver et al. [13] and Ferreira et al. [63].

2.4 Polymer Blends

From a thermodynamic standpoint, the Gibbs free energy will explain the mixing structure of two polymers. The Gibbs free energy of mixing is shown in Equation 2.2 [155]:

$$\Delta G_m = RTX_{AB}\varphi_A\varphi_B + RT\left[\frac{\rho_A\varphi_A ln\varphi_A}{Mw_A} + \frac{\rho_B\varphi_B ln\varphi_B}{Mw_B}\right] \quad \text{Equation 2.2}$$

where ΔG_m, φ_i, X_{AB}, Mw_i, ρ_i, R, and T are Gibbs free energy of mixing, volume fraction of component *i*, Flory-Huggins interaction parameters, molecular weight of polymers, density of polymers, gas constant, and absolute temperature, respectively. In the Gibbs free energy description, $\Delta G = \Delta H + RT\Delta S$, the first term is the enthalpy of mixing, and the second term is the contribution of the entropy of mixing. Binary polymer blends are divided into three categories based on Gibbs free energy of mixing [155]:

1) Completely miscible ($\Delta G < 0$, $\frac{\partial^2 \Delta G}{\partial^2 \phi} > 0$ (in all compositions))
2) Partially miscible ($\Delta G < 0$ (in all compositions), $\frac{\partial^2 \Delta G}{\partial^2 \phi} > 0$ (parts of composition))
3) Immiscible ($\Delta G > 0$(in all composition range))

Both components of miscible polymer blends are miscible down to the molecular scale, whereas immiscible polymer blends form two distinct phases of the polymers. Again, two phases form in partially miscible systems, but each phase is a miscible mixture of both polymer components. Because of the positive enthalpy of mixing and negligible entropy of mixing caused by high molecular weights and a low degree of freedom of polymers, the majority of polymer mixtures are immiscible. As a result, most polymer mixtures have a positive Gibbs free energy of mixing, resulting in immiscibility. The morphology of immiscible polymer blends has a significant impact on final blend efficiency and must be managed to achieve the desired properties [5]. Figure 2.11

depicts various possible morphologies in binary polymer systems as well as their potential properties [156].

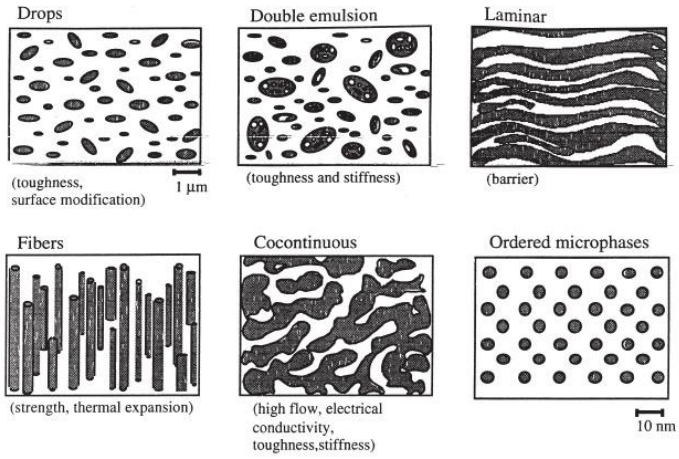

Figure 2.11 Immiscible polymer blends in various morphologies and their possible properties [156].

Controlling the polymer blend ratio, viscoelastic properties of the materials, and processing methods and conditions will result in the morphologies shown in Figure 2.11 [157], [158]. Also, the interfacial tension between the phases has a significant impact on the morphology of immiscible polymer blends [159]. Conversely, the interfacial tension between two polymers is proportional to their surface tension (energy). The work needed to increase the surface area of a solid or a liquid by one unit of area is known as surface tension [160]. The surface tension is measured in J/m^2 or N/m. The contact angle method [161], [162] is the most popular method for measuring the surface tension of polymers in the solid-state among various techniques. There are unavoidable errors in contact angle measurements, such as the roughness of the solid polymer surface, the purity of the liquid probes, and the droplet image resolution. The pendant drop method [163], [164], on the other hand, has been commonly used to determine the surface tension of polymer melts. This approach is accurate and has a limited range of error, and it can be used with both Newtonian and viscoelastic fluids [165]. Interfacial tension is a reversible work that is needed to minimize an interfacial area by the unit area [160]. The interfacial tension arises from the unbalanced forces at the interface and has the same units as the surface tension (J/m^2 or N/m). The interfacial tension in a binary blend can be calculated through the geometric mean equation (Equation 2.3) [160]. The surface tension of the components can be used to calculate the interfacial tension between two polymers, or a

polymer melt and a solid. To estimate interfacial tension, Good and Girifalco [166] used the work of adhesion concept:

$$\gamma_{12} = \gamma_1 + \gamma_2 - W_a \quad \text{Equation 2.3}$$

where γ_{12} represents the interfacial tension between the two components, γ_1 and γ_2 represent the surface tensions of components 1 and 2, respectively, and W_a represents the work of adhesion between the two components. Wu [167] proposed the harmonic mean approach (Equation 2.4) for systems with low surface tensions based on the principle of energy additivity and the contribution of polar and dispersive components in adhesion work:

$$\gamma_{ij} = \gamma_i + \gamma_j - 4\left(\frac{\gamma_i^d \gamma_j^d}{\gamma_i^d + \gamma_j^d} + \frac{\gamma_i^p \gamma_j^p}{\gamma_i^p + \gamma_j^p}\right) \quad \text{Equation 2.4}$$

where γ_i^d and γ_i^p are the surface tension's dispersive and polar elements, respectively. Wu [167] also discovered that using the geometric mean equation (Equation 2.5) to estimate the interfacial tension between two materials with highly different polarities is inaccurate. In these systems, he calculated the adhesion work using the geometric mean method.

$$\gamma_{ij} = \gamma_i + \gamma_j - 2\left[\sqrt{\gamma_i^d \gamma_j^d} + \sqrt{\gamma_i^p \gamma_j^p}\right] \quad \text{Equation 2.5}$$

From a rheological analysis, in the small-amplitude oscillation shear (SAOS), Palierne [168] proposed a model for predicting the rheological properties of viscoelastic emulsions with a narrow droplet size distribution ($R_v/R_n \leq 2$, where R_v and R_n is the volume and number-average diameter, respectively). The storage modulus of a polymer blend, according to his model, is written as (Equations 2.6 and 2.7): [169]:

$$G_b^*(\omega) = G_m^*(\omega)\frac{1+3\phi H^*(\omega)}{1-2\phi H^*(\omega)} \quad \text{Equation 2.6}$$

and

$$H^*(\omega) = \frac{4\left(\frac{\gamma_{12}}{R_v}\right)\left[2G_m^*(\omega)+5G_d^*(\omega)\right]+\left[G_d^*(\omega)-G_m^*(\omega)\right]\left[16G_m^*(\omega)+19G_d^*(\omega)\right]}{40\left(\frac{\gamma_{12}}{R_v}\right)\left[G_m^*(\omega)+G_d^*(\omega)\right]+\left[2G_d^*(\omega)+3G_m^*(\omega)\right]\left[16G_m^*(\omega)+19G_d^*(\omega)\right]} \quad \text{Equation 2.7}$$

where ϕ, ω, and γ_{12} are the volume fraction of droplets of volume average radius, R_v, the angular frequency, and the interfacial tension, respectively. $G_b^*(\omega)$, $G_m^*(\omega)$, and $G_d^*(\omega)$ are the storage modulus of the blend, matrix, and dispersed phase, respectively. The interfacial tension is

calculated using this method by fitting the Palierne model to the rheological details. The rheological approach can only estimate interfacial tension in systems where the second plateau in the storage modulus is experimentally available.

2.4.1 Morphology Development in Immiscible Polymer Blends

Most polymers are immiscible due to their high molecular weight, which results in a small entropy gain when mixed [170]. Nonetheless, there is a small number of miscible polymer pairs, and a few of them have commercial applications [170]. The degree of molecular mixing in such systems is sufficient to produce macroscopic properties consistent with a single-phase material [170]. When immiscible polymers are mixed, they form multi-phasic materials with a specified phase morphology. While blending two polymers is the most popular method, ternary blends have also attracted a lot of attention. Shokoohi and Arefazar [171] recently analyzed the various morphologies that occur in ternary blends. It is well understood that the properties of immiscible blends are influenced not only by the blend component characteristics and concentrations but also by the phase morphology. Thus, tailoring the blend morphology allows for the optimization of product properties [172]. Only binary immiscible polymer blends will be included in this thesis. Such structures are made up of two co-continuous phases or dispersed domains in a continuous phase. The change of the droplet-like morphology to a continuous morphology occurs when the minor phase concentration is increased. In the dispersion step, this process occurs by droplet break-up and coalescence and crossing the percolation threshold. Finally, co-continuous morphology is obtained when both phases are 100 % continuous. Many studies have been conducted on the effects of various parameters on the morphological development of polymer blends, including rheological characteristics (viscosity and elasticity ratios), interfacial tension, compatibilizer, the presence of a third component (polymer or filler), processing method, and conditions (shear rate, time, and temperature) [159], [173]–[175]. Deformation, retraction, breakup, and coalescence of droplets cause morphology growth in a droplet-like morphology (Figure 2.12). As a consequence, the binary polymer blend droplet morphology is the result of a competition between droplet coalescence and breakup. The system free energy can be reduced by increasing the size of the minor phase or matrix structure, which can be achieved by a quiescent process.

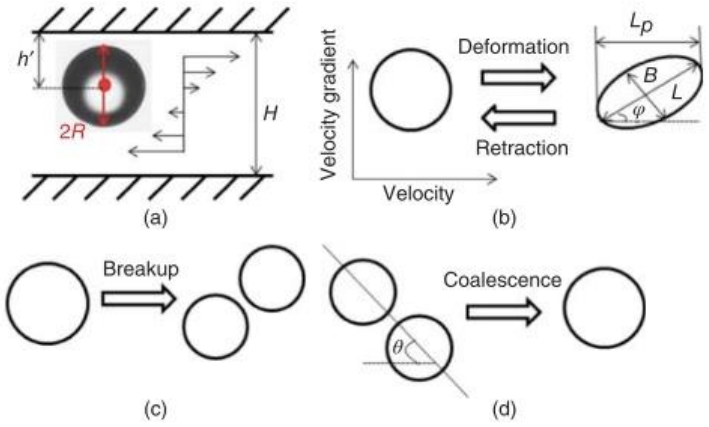

Figure 2.12 Morphology growth in a droplet-like morphology (a) droplet in shear flow, (b) droplet deformation and retraction, (c) droplet breakup, and (d) droplet coalescence [172].

2.5 PLA/PBAT Blends

As previously mentioned, mixing PLA with other bioplastics has been proposed as a viable method for PLA toughness [5]. PLA/PBAT blends [19], [176], [185]–[191], [177]–[184] have gotten a lot of attention because of PBAT's high impact strength and elongation at break. Furthermore, the PBAT polyester design makes it compatible with PLA. Using a TSE, Jiang et al. [192] produced immiscible PLA/PBAT blends. They discovered that PBAT improved blend toughness and elongation at break while lowering tensile strength and modulus. PLA crystallization was also accelerated by PBAT. Nofar et al. [193] recently demonstrated that by incorporating 25% PBAT in a high molecular weight amorphous PLA without the use of a compatibilizer and using a TSE, PBAT droplet sizes below 1 μm within the PLA matrix could be achieved, increasing the blend ductility to about 265 percent with respect to PLA. Deng et al. [194] also found that raising the PBAT content from 10 wt% to around 20 wt% improved the ductility of the PLA/PBAT blend system from around 10% to around 300%. Lee et al. [195] demonstrated that ultrasound sonication significantly improved the interfacial adhesion between PLA and PBAT. Previous research on the mechanical properties of PLA/PBAT has found that adding PBAT lowers tensile strength and modulus while increasing elongation at break as compared to the neat PLA. Several studies have looked into the impact of different additives as plasticizers or compatibilizers on the properties of PLA/PBAT. Coltelli et al. [196] demonstrated that adding acetyl tributyl citrate (ATBC) as a plasticizer (up to 30 wt%) could increase the strain at break of a PLA/PBAT blend by 300%

compared to the neat PLA. Al-Itry et al. [197]–[199] demonstrated that the epoxy-based Joncryl chain-extender (CE) could improve the PLA/PBAT blend modulus, strain at break (up to 135%), and melt strength. Two CEs (Joncryl and 1,6- hexanediol diglycidyl ether) were studied by Dong et al. [200]. By combining multiple CEs, the compatibility of PLA and PBAT was significantly improved, and the strain at break was increased by up to 500% without losing too much strength. Dong et al. [201] looked at the effect of compatibilizers including phthalic anhydride (PA) and bioxazoline (BOZ) on the mechanical and morphological properties of PLA/PBAT blends. Due to reduced domain sizes, small amounts of anhydride (PA) or bioxazoline (BOZ) increased elongation at break by up to 515 % without affecting the tensile strength. Zhang et al. [202] found that using glycidyl methacrylate (GMA) improved the surface adhesion between the PLA and PBAT phases, as well as the phases compatibility and, as a result, the rheological properties. The strain at break was also raised by 180% while the tensile strength remained unchanged. They also showed a three-fold increase in impact strength. The effect of mixing ratio and 2,5-dimethyl 2,5-di (tert butylperoxy) hexane as a reactive compatibilizer investigated by Nishida et al. [203]. When the mixing ratios were 50/50 and 30/70 (wt%/wt%), the inclusion of the crosslinking agent considerably boosted elongation at break. The findings were compared to those of Izod impact tests, which quantify material fracture toughness. Coltelli et al. [204] used the same compatibilizer and found that the blend viscosity increased with a better phase surface adhesion and the elongation at break increased by up to 60%. According to Zhang et al. [205], adding epoxy-functional styrene acrylic as a reactive compatibilizer increased the impact toughness of the blends by three times and increased the elongation at breakup by 150%. The use of poly-(dichloro)-phosphazene (DCP) as a reactive compatibilizer reduced the size of PBAT domains, improved interfacial adhesion with PLA, and increased melt strength and elongation at break by 300 percent, while tensile strength remained unchanged [206], [207]. Gu et al. [177] investigated the melt rheological properties of PLA/PBAT blends. Due to the PLA/PBAT interface contribution, the storage modulus of the blend increased with PBAT material at lower frequencies. Nofar et al. [19] investigated the rheological and interfacial properties of PLA/PBAT blends with a fixed weight ratio of 75/25 wt%, as well as various processing techniques and two different molecular weight PLAs. They measured the interfacial tension between PLA and PBAT to be 1.2 mN/m using the Palierne model [168]. They also confirmed that PBAT droplet coalescence can occur in shear flow and can be controlled using rheometry, and that the effect of coalescence can be predicted using the Palierne model. Using the

Palierne model, Jalali Dil et al. [191] discovered that when a low molecular weight PBAT was distributed in a PLA, the interfacial tension between the PLA and PBAT could be as low as 0.6 mN/m.

2.6 PLA/PBAT Blend Nanocomposites

While adding PBAT to PLA can boost some properties, it can also reduce the strength and modulus of the blends. The incorporation of nanoparticles into immiscible polymer blends has been studied over the past decade in order to enhance their overall physical properties. A reduction in the size of the dispersed phase, as well as a reduction in interfacial tension and an improvement in interfacial adhesion between the two polymeric phases, are indicative of the nanofiller compatibilizing effect. The effectiveness of a nanofiller as a compatibilizer is determined by its shape, specific surface area, surface chemistry, and localization in the blend. Furthermore, it is important to remember that localization is influenced not only by the shape, aspect ratio, and surface chemistry of the nanoparticles (NPs) but also by the processing parameters. It has also been stated that by selectively localizing nanoparticles within the blend structure, various morphologies with desired properties can be obtained [208]. We will discuss this topic in more detail in the next section. The nanoparticle localization in blends affects dramatically their rheological behavior [209]. The state of dispersion and localization of the nanofillers can be determined using viscoelastic properties in the molten state. They will also give you an idea of how efficient the processing characteristics are on the dispersion and finally on the final properties. Several studies have looked into the properties of PLA/PBAT blends with nanoparticles like nanoclay [187], [210]–[213], graphene [213], [214], carbon nanotubes [190], [215], [216], and nanosilica [188], [189]. To the best of our knowledge, Ma et al. [217] and Sarul et al. [218] were the only authors to analyze the properties of PLA/PBAT/CNC blend nanocomposites. Ma et al. [217] only focused on the antimicrobial properties and Sarul et al. [218] investigated the preparation of PLA/PBAT/CNC blend nanocomposites through solution casting followed by melt mixing via a twin-screw extruder.

2.6.1 Morphology Development Based on Nanoparticle Localization in the Polymer Blend

The final morphology of blend nanocomposites is generally highly dependent on the final localization of the nanoparticles in the blend [208], [219]. Understanding the processes involved

in the localization of solid particles in polymer blends is therefore critical for achieving the desired properties in the final blend. It is important to briefly discuss the implications of the most critical thermodynamic and kinetic parameters on the localization of solid particles in polymer blends and the impact of different nanoparticle localization on the morphology of binary polymer blends will be discussed in the following section.

The localization of the nano-inclusion can be qualitatively measured from a thermodynamics standpoint by comparing the surface tensions of the three components. The location of the nano-inclusion after mixing is determined by the differences in surface tensions. The Young equation (Equation 2.8) [220] can be used to calculate the distribution coefficient ω_a:

$$\omega_a = \frac{\gamma_{1s} - \gamma_{2s}}{\gamma_{12}} \qquad \text{Equation 2.8}$$

where γ_{1s}, γ_{2s}, and γ_{12} are the interfacial tensions between polymer 1 and solid particles, polymer 2 and solid particles, and polymers 1 and 2, respectively. The interfacial tensions between solid particles and polymers, as seen in Young's model, play key roles in the particle final thermodynamics localization. Thermodynamically, the particles would be localized in phase 2 when $\omega_a > 1$, while phase 1 is the preferred location of the solid particles when $\omega_a < -1$. The solid particles will be thermodynamically localized at the interface when $-1 \leq \omega_a \leq 1$. As is discussed in the previous sections, The two key methods for calculating the interfacial tension are the harmonic-mean (Equation 2.4) and geometry-mean (Equation 2.5) approach. However, since only the thermodynamics equilibrium state of the materials is taken into account in the calculations, this simple method of estimating the localization can not always be accurate. Elias et al. [221] demonstrated that in polypropylene/polystyrene, PP/PS (70/30 wt%) blend, hydrophobic and hydrophilic silica particles were found in the PP phase or at the interface, and in the PS phase, respectively, after components were mixed at the same time using a twin-screw mini-extruder. The results showed an agreement between the thermodynamics predictions and the final localization of silica particles after mixing. In another recent study conducted by Jalali Dil et al. [222] two mixing strategies were adopted to localize copper nanowires (CuNWs) in a high interfacial tension PLA/LDPE (70/30 wt%) (PLA/CnNWs masterbatch blended with LDPE (Pr1), LDPE/CuNWs masterbatch blended with PLA (Pr2)). They reported in both strategies, by providing sufficient shear rate and mixing time, the polar CuNWs localized in a more polar phase (PLA in PLA/LDPE blend) (Figure 2.13).

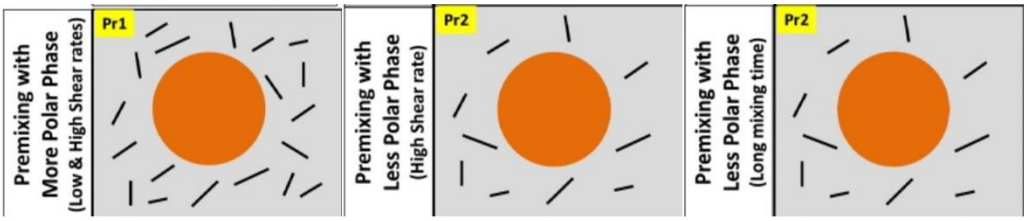

Figure 2.13 Different localizations of CuNWs in PLA/LDPE (70/30 wt%). (Pr1) PLA/CnNWs masterbatch blended with LDPE and (Pr2) LDPE/CuNWs masterbatch blended with PLA [222].

On the other hand, there are many reports that show contradictions between predictions of nanoparticle localization using thermodynamics point of view and final localization after processing [208], [220], [223]–[225]. Therefore, other parameters, such as kinetics mechanisms including mixing strategies, viscosity ratio, and mixing time to name a few as well as size/shape of the nanoinclusions play an important role in the selective localization of nanoparticles [208]. It is worth mentioning that the differences in the melting temperatures of the polymeric phases, as well as the variability in the surface energy data of the materials, have been reported as another reason why the localization predicted by Young's model did not match with their observation [208]. What is more, the surface energy of solid particles can be measured using a variety of techniques, which can result in a variety of surface energy data. Furthermore, the surface energy of polymers at room temperature was taken from the literature of most previous studies and then extrapolated to higher temperatures.

2.6.2 Localization of Nanoparticle Affected by Kinetics Parameters

As it is mentioned in the previous section the kinetics parameters could have a substantial effect on the migration of nano-inclusion to their favorable phases predicted by Young's equation (Equation 2.8). Particle migration is thermodynamically advantageous since it lowers the system's free energy. As long as surface energy effects are dominant, all of the theoretical predictions are usually right. Therefore, in this section, the effect of kinetics parameters including mixing strategies, viscosity, the effect of aspect ratio of particles, and nano-inclusion dispersion will be reviewed.

2.6.2.1 **Mixing Strategy Effect**

The effect of the sequence in which components are added to polymer blends is the most studied kinetics parameter in the literature. The majority of previous studies find that adding all of the

components to the mixing chamber or adding solid particles to a polymer melt results in particle localization in their thermodynamics equilibrium localization [221], [223], [234]–[242], [226]–[233]. Nanoparticles may be premixed with a thermodynamically incompatible phase to trigger migration of the nanoparticles to a more thermodynamically compatible phase during melt processing [111], [188], [190], [221], [233], [243]. As a result, nanoparticle interfacial entrapment with optimized properties could be achieved [187], [190], [222]. For example, Jalali Dil et al. [189] investigated the localization of micro and nano silica in the bend of PLA/PBAT (70/30 wt%). They showed that nano silica particles were found to be localized at the interface when mixed with low or high viscosity PLA phases. When micro-silica particles were premixed with the high viscosity PLA, on the other hand, they were trapped in the high viscosity PLA. In the literature, viscosity is the most frequently reported kinetics barrier for solid particle migration. In the following section, the impact of this parameter will be discussed. In another study conducted by Jalali Dil et al. [190] three mixing procedures were used to investigate the effect of the mixing sequence on the localization of multiwall carbon nanotubes (MWCNTs) (MWCNTs added to the PLA/PBAT melt (Pr1), MWCNTs initially dispersed in the PLA phase and then mixed with PBAT (Pr2), and MWCNTs initially dispersed in the PBAT and then mixed with PLA (Pr3)) in PLA/PBAT blends (80/20 wt% and 50/50 wt%). While the MWCNTs localized in the PBAT phase through Pr1 and Pr3 (in accordance with thermodynamics analysis), they localized in both PLA and PBAT phases and at the interface through Pr2 (Figure 2.14). Nofar et al. [187] also investigated the effect of mixing protocol on localization of nanoclay in the blend of PLA/PBAT (75/25 wt%) and observed different localization based on thermodynamics and kinetics effects.

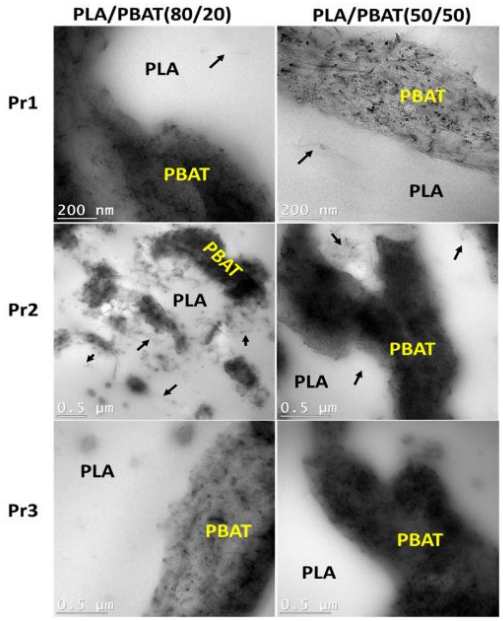

Figure 2.14 Schematic of possible localization of MWCNTs in the blends of PLA/PBAT (80/20 and 50/50 wt%). MWCNTs added to the PLA/PBAT melt (Pr1), MWCNTs initially dispersed in the PLA phase and then mixed with PBAT (Pr2), and MWCNTs initially dispersed in the PBAT and then mixed with PLA (Pr3) [190].

2.6.2.2 **Viscosity Effect**

Nanoparticle migration toward stable localization is known to be hampered by viscosity, which acts as a powerful kinetics barrier. Elias et al. [223] investigated the localization of fumed silica in PP/ethylene-co-vinyl acetate (EVA) blend, which melt mixed in a twin-screw mini extruder. They reported that using low viscosity EVA resulted in localization of fumed silica at the interface and the PP phase, but high viscosity EVA caused this localization to be in the EVA and at the interface. Also, Jalali Dil et al. [189], [244] investigated the effect of viscosity on the localization of nano and micro silica particles in a PLA/PBAT blend (low interfacial tension) and a PLA/LDPE blend (high interfacial tension) in two separate studies. Using high viscosity LDPE as an initial phase for dispersing the micro-silica, microparticles could not migrate to the PLA or at the interface. However, low viscosity LDPE facilitated this migration to the PLA phase. On the other hand, nano-silica migrated to the PLA phase and at the interface no matter the high or low viscosity LDPE. In the other study that they used PBAT instead of LDPE, they used both high and low viscosity PLAs to see the effect of the viscosity on the localization of micro and nano-silica in the PLA/PBAT

blend [189]. When micro and nanosilica were added to the melt of PLA/PBAT (one-step process), it resulted in localization of both micro and nanosilica in the PBAT phase (the favorable phase from a thermodynamics point of view) (Figure 2.15).

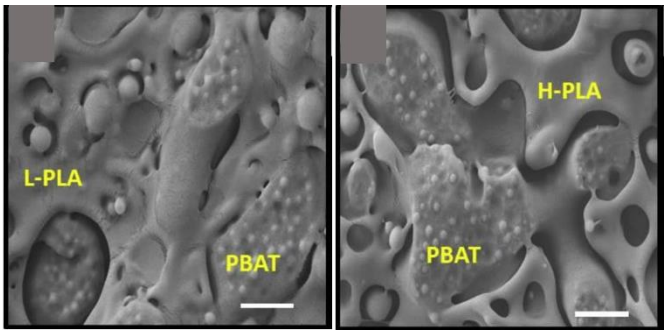

Figure 2.15 SEM images of the 3 wt% micro-silica localized in PLA/PBAT blends using a one-step process. The scale bar is 2 μm [189].

On the other hand, for premixing of silica particles with the PLA phase followed by mixing with PBAT (two-step process), micro-silica migrated to the interface in the case of low viscosity PLA but stay in PLA phase for high viscosity PLA (Figure 2,16). In this process, nano-silica migrated to the interface for both low and high viscosity PLAs.

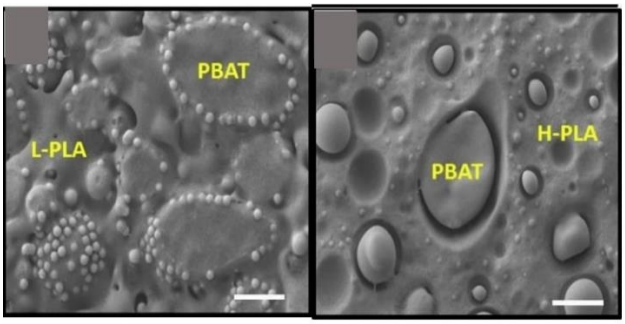

Figure 2.16 SEM images of the 3 wt% micro-silica localized in PLA/PBAT blends using two-step process. The scale bar is 2 μm [189].

2.6.2.3 **Effect of Size, Shape, and Quality of the Dispersion of Nanoparticles**

Since the agglomerate strength of nanoparticles increases as particle size decreases, achieving a high degree of nanoscale dispersion of nanoparticles is difficult [81]. Nanoparticle agglomeration influences not only the reinforcement efficacy of nanoparticles but also their migration and localization in binary polymer blends due to poor dispersion [245], [246]. Jalali Dil et al. [244] investigated the localization of nano-silica in PLA/LDPE (80/20 wt%) blend. They prepared the

blend nanocomposites by premixing nano-silica with HDPE and observed while dispersed nanosilica migrate to the PLA phase, the aggregates of nano-silica remained in the LDPE phase (Figure 2.17)

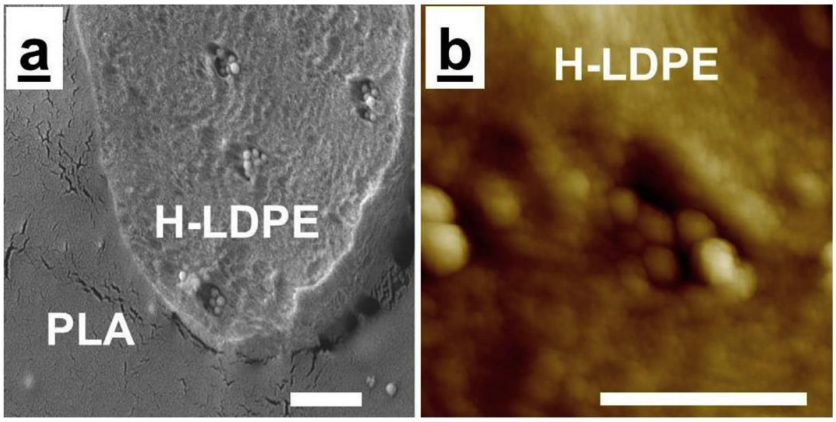

Figure 2.17 The localization of nano-silica particles in PLA/H-LDPE (80/20 wt%) blend, (a) SEM image of nano-silica aggregates in H-LDPE, (b) AFM image of nano-silica aggregates in the H-LDPE phase. All the white scale bars show 1 µm.

Goldel et al. [247], compared the migration of carbon nanotube (CNT) and carbon black (CB) particles from Styrene-acrylonitrile (SAN) to polycarbonate (PC) in a PC/SAN blend to see how the aspect ratio of solid particles affected migration. They discovered that CB particles migrate at the interface considerably slower than CNT particles. They hypothesized a method known as the "slim-fast-mechanism," or SFM, in which the migration is driven solely by the interface curvature. They stated that when a low aspect ratio particle migrates through an interface, the interface curvature, and thermodynamic driving force decrease, which can lead to particle trapping at the interface (Figure 2.18). The interface, on the other hand, cannot relax until the particle has completely passed through the interface during the migration of a high aspect ratio particle (Figure 2.19).

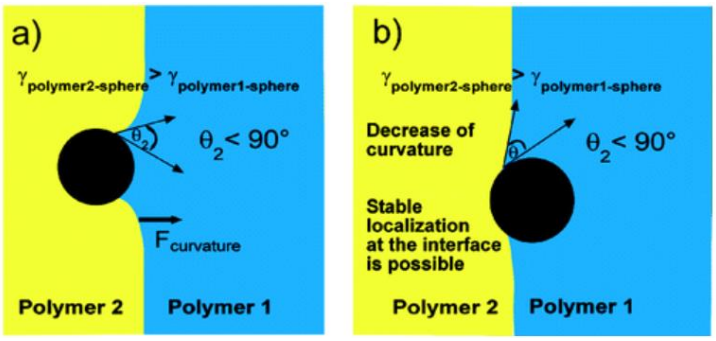

Figure 2.18 Ideal low aspect ratio filler (not slim) at the blend interface during melt mixing. The interfacial curvature can relax while θ_2 is constant, and thus the driving force $F_{curvature}$ is decreasing during the transfer [247].

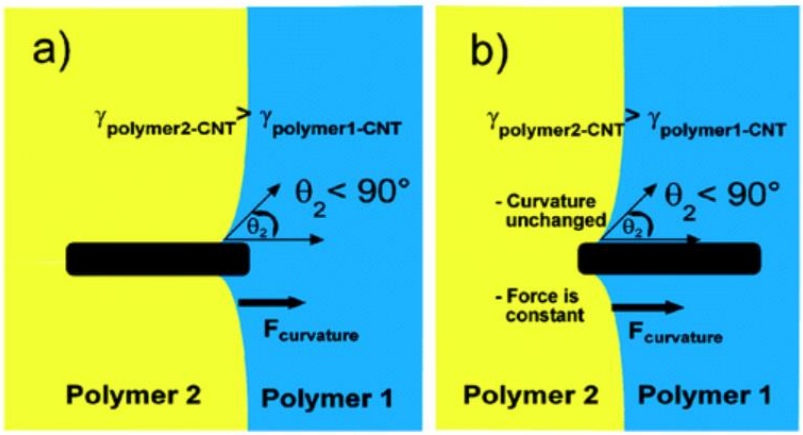

Figure 2.19 High aspect ratio filler (slim) at the blend interface. The interfacial curvature is not able to relax when θ_2 remains constant. Thus, the driving force is not decreasing during the transfer [247].

Using the SLM mechanism, Salehyian et al. [248] investigated the effect of the aspect ratio of CNT on CNT migration and consequently viscoelastic properties of PLA/polyvinylidene fluoride (PVDF) blend (70/30 wt%). They showed that, while higher-aspect-ratio CNTs (L-CNTs) were found at the interface and within the PLA matrix, the low-aspect-ratio CNTs (S-CNTs) were localized in the PLA phase. Also, regarding the size of nanoparticles Jalali Dil et al. [244] investigated the localization of micro and nano-silica in the blend of PLA/PBAT (70/30 wt%). They demonstrated that in samples prepared by localizing micro or nano-silica in a less thermodynamically stable phase (PLA), micro-silica particles were still visible in the PLA matrix since nanosilica particles fully migrated to the interface and stabilized there. This discovery implies

that larger particles need more energy to move. This should not be confused with the "slim-fast mechanism," which is concerned with the penetration rate. Because of the maximum instabilities at the interface, it is hypothesized that removing larger particles needs less energy.

2.7 Nanoparticle Localization: Morphological Stabilization and Rheological Responses

Apart from their reinforcing capacity, nanoparticles have been shown to play a role in tailoring the morphology of immiscible blends in a large number of studies over the last decade [208], [220]. Nanoparticles have been added to immiscible blends to help achieve some uniformity, based on their concentrations and localization. It should be noted that when using traditional compatibilizers (co-polymers or reactive compatibilizers), the morphologies cannot be as fine as when using nanoparticles. A reduction in the size of the dispersed phase, as well as a reduction in interfacial tension and an increase in the interfacial adhesion between the two polymeric phases, characterizes the compatibilization effect of nanofillers. In different systems, it is reported that different localization (in the dispersed phase, at the interface, and in the matrix phase) can have a compatibilization effect. Rheological experiments on filled blends can be used to quantify their performance as compatibilizers. There are numerous articles or book chapters on the rheological behavior of nanoparticle-filled polymers, particularly general reviews [249]–[252]. The structure of nanocomposite materials, especially the combination of the mesoscopic structure and the strength of the interaction between the polymer and the NPs, is known to have a significant impact on viscoelastic properties in the molten state [253]. The most unique rheological behavior of polymer blend nanocomposites can be categorized as follow:

1) The shifting relaxation spectra are obtained from the loss and elastic modulus because when nanofillers are added to polymeric chains, their mobility is limited.
2) The change of nonlinear domain to lower strains with the increase of nanofillers [249]
3) The dramatic increase of the complex viscosity at low frequency (nonterminal zone of relaxation) is due to the formation of the network as a result of highly dispersed nanoparticles.

In the following, the most highlighted researches are presented, which were done on morphological stabilization and rheological responses due to the addition of nanoparticles and different

localizations. Also, other investigations in this area can be found in different books, book chapters, and review papers [208], [209], [219], [254]–[256].

In a recent study, Jalali Dil et al. [190] investigated in depth the effects of MWCNT localization in PLA/PBAT blends (80/20 wt% and 50/50 wt%) on the morphology, and rheological properties. Based on the mixing protocol the MWCNTs were located either in PBAT (mixing all three components (Pr1) or premixing MECNTs with PBAT and then mixing with PLA (Pr3)) or PLA, PBAT, and at the interface (premixing MWCNTs with PLA and then mix with PBAT (Pr2)) (Figure 2.20). The localization of MCNTs using Pr1 and Pr3 were in the PBAT phase and were in accordance with the thermodynamics predictions (Equation 2.8). They showed that adding 3wt% MWCNTs in the PLA/PBAT (80/20 wt%) blend using Pr2 converted the dispersed phase morphology to a continuous one (Figure 2.20 b & d) and in the Pr3, dangling of MWCNTs at the interface make a bridging effect between PLA and PBAT phases (Figure 2.20 c & e). On the other hand, in the co-continuous PLA/PBAT (50/50 wt%), the addition of 3wt% MWCTs induced a phase coarsening compared to the PLA/PBAT blend (Figure 2.20 g-i). In the rheological analysis (Figure 2.20 k & l), both blends (70/30 and 50/50 wt%) irrespective of the mixing sequence, at low frequencies, the addition of MWCNTs caused a viscosity upturn and a rise in storage modulus. While, in the matrix/dispersed morphology the obtained rheological results presented the existence of a 3D network of PBAT/MWCNTs in the bulk of these samples, indicating a change from viscoelastic liquid to viscoelastic solid behavior, in the co-continuous blend it is an indication of increased resistance to phase deformation when MWCNTs are added to the blend. Other investigations also show that the selective localization of solid particles in the dispersed phase could promote the formation of a continuous network [257]–[260]. Furthermore, the observed higher viscosity and storage modulus of the sample prepared by Pr2 can be due to the MWCNTs bridging effect in both blend nanocomposites (Figure 2.20 k & l).

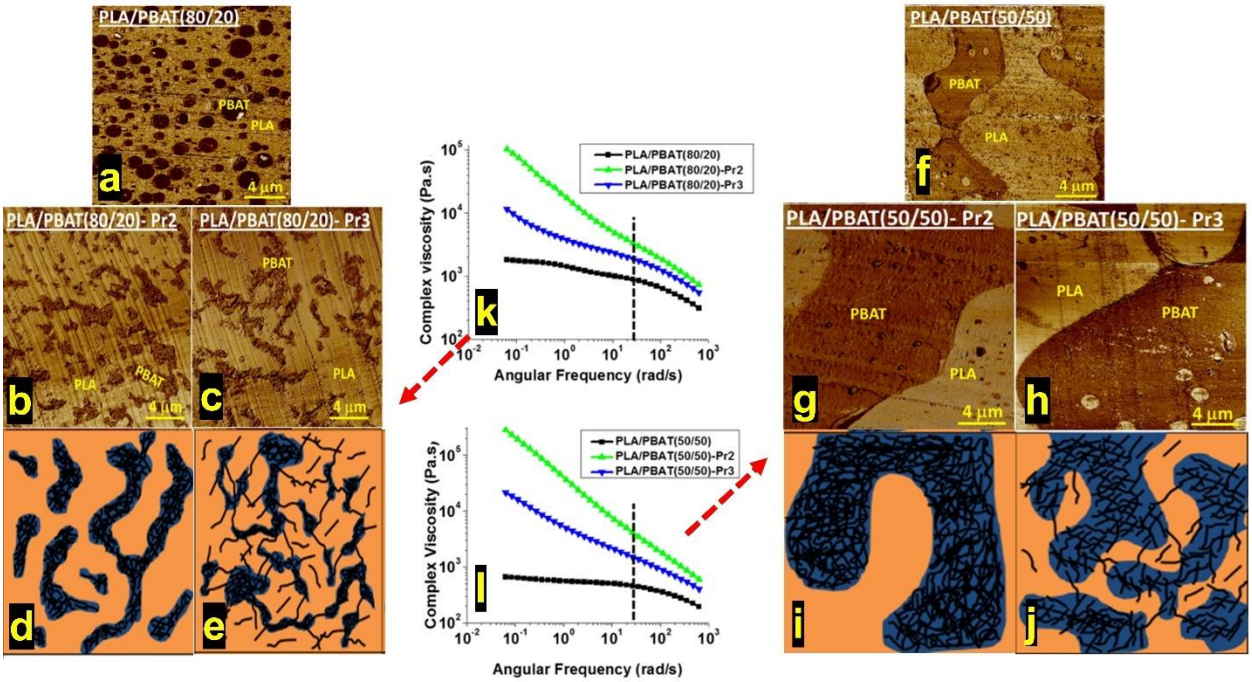

Figure 2.20 AFM images (a-c & f-g) showing the effects of the addition of 3 wt % MWCNTs using mixing sequences of Pr2 (premixing with PLA; b, g, d, and i) and Pr3 (premixing with PBAT; c, d, h, and j) on morphologies of PLA/PBAT (80/20) and PLA/PBAT (50/50). (a) & (f): show the morphology of the pure blend without MWCNTs. (k) and (l): effect of the addition of 3 wt % MWCNTs using different mixing strategies on complex viscosity of PLA/PBAT (80/20; k and 50/50; l) blends. The dashed lines in each plot show an estimated shear rate of 25 s^{-1} at the processing condition [190].

Filippone et al. [261] investigated the morphology evolution of a blend of polyethylene (PE)/ nylon 6 (PA6) (75/25 vol.% or 25/75 vol.%) in the presence of organoclay nanoparticles. Since the filler enriches the more hydrophilic polyamide phase (PA6) preferentially, different effects on the microstructure of the blends were observed depending on whether the host PA6 was the main or minor blend constituent. In the former case, even at low filler loadings, an unexpected decrease in the average size of the dispersed PE inclusions was observed. In fact, the organoclay plays the role of a physical barrier that prevents colliding droplets from merging during melt mixing. In the other case, the organoclay causes incremental refinement of the morphology, which remains globular at low filler contents; at filler loadings larger than a critical threshold, the filled polyamide assembles into a highly continuous structure finely interpenetrated with the major polyethylene phase (Figure 2.21).

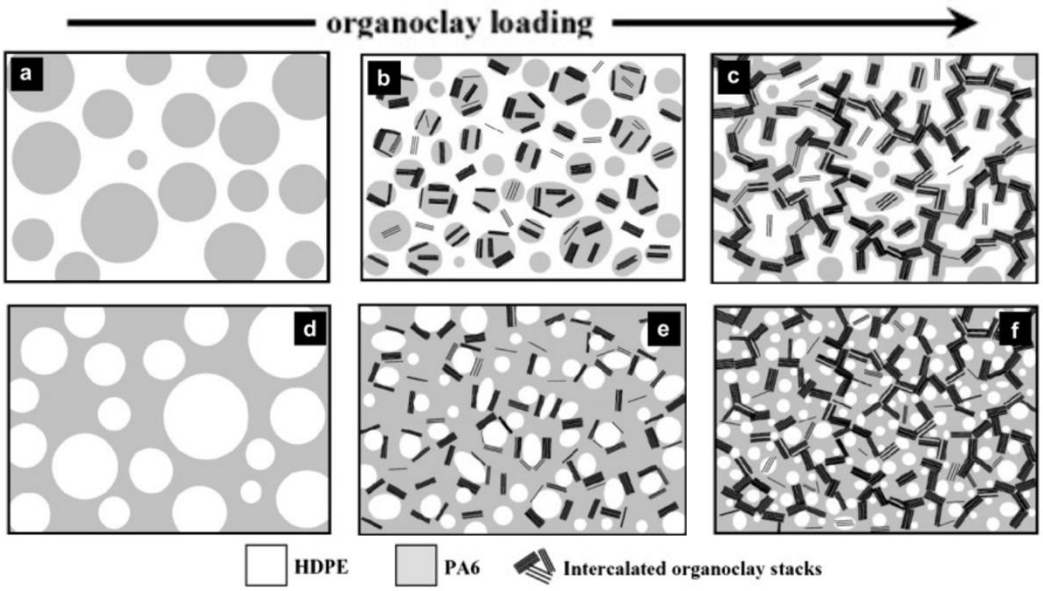

Figure 2.21 Schematic illustration of the evolutions of the microstructure in the blends with polyamide as the minor (a–c) or major (d–f) phase as a result of the addition of organoclay. The greyish color shows the PA6 as major or minor phases [261].

The effect of 1 and 5 wt% of Cloisite 30B (C30B) nanoclay and localization on the morphological and viscoelastic properties of PLA/PBAT/C30B blend nanocomposites studied by Nofar et al. [187]. Three separate mixing protocols were used to investigate the localization of C30B in the blends. S1) combining all three components at the same time, S2) premixing C30B with PLA and then blending with PBAT, and S3) premixing C30B with PBAT and then blending with PLA). They investigated the effect of shear rate (0.01 and 0.05 S^{-1}) on morphology stabilization of PLA/PBAT blend nanocomposites. The results showed that shear rates of 0.01 S^{-1} caused substantial droplet coalescence in the neat PLA-PBAT blend (Figure 2.22 a) while incorporating 1 and 5 wt% C30B at the PLA-PBAT interface (in accordance with thermodynamics predictions (Equation 2.8)) significantly suppressed PBAT droplet coalescence (Figure 2 22 b & c). The nanoclays were found in both the PLA matrix and at the interface at a higher C30B content of 5 wt%, depending on the mixing protocols. When the blend nanocomposites were blended simultaneously or when PLA and C30B were premixed before blending with PBAT, no coalescence occurred. Premixing PBAT with C30B before blending with PLA, on the other hand, resulted in the highly concentrated C30B at the interface moving towards the PLA matrix during shearing. The coalescence was even more visible at a higher shear rate of 0.05 S^{-1}. C30B was

mainly at the interface in the S3, and the viscoelastic responses were the highest of all the nanocomposites (Figure 2.22 d & e)

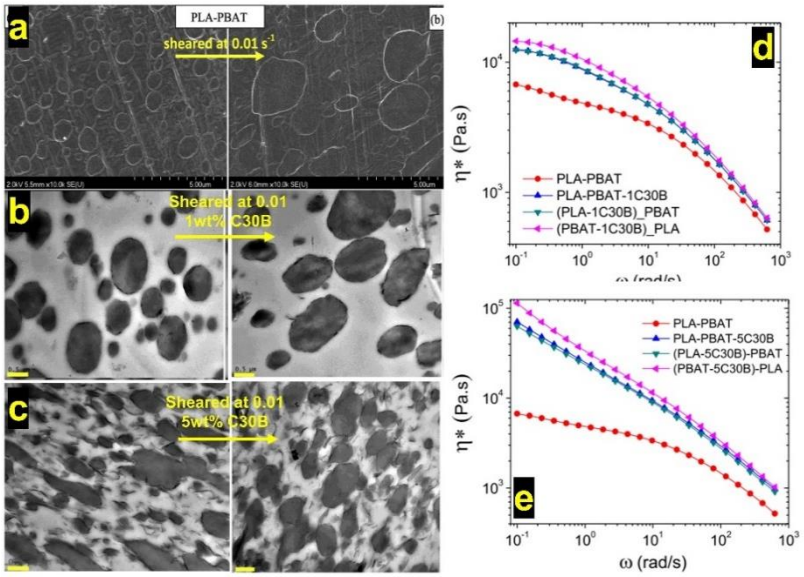

Figure 2.22 SEM images showing the dispersed PBAT phase in the PLA matrix after molding (i.e., non-sheared) (a) and sheared at a rate of 0.01 s^{-1} using 1 wt% C30B (b) and 5 wt% C30B (c). The scale bars in (a) are 5 µm and in (b) and (c) are 0.5 µm. (d) and (e): complex viscosity of PLA/PBAT blend nanocomposites containing 1 and 5 wt% C30B [187].

On a similar blend (PLA/PBAT (70/30 wt%)) Jalali Dil et al. [188] observed similar morphological and rheological transitions for silica nanoparticles localized at the PLA/PBAT blend interface. When 1 wt% silica nanoparticles were localized at the interface, the PBAT droplet size decreased from approximately 1.7 (Figure 2.23 a) to 1.0 µm (Figure 2.23 b). When the concentration was increased to 3 wt%, the droplet-matrix morphology converted to a co-continuous one (Figure 2.23 c). Figure 2.23 d & e shows the corresponding rheological responses to interfacial localization of 1 (circles) and 3 wt % (upper triangles) silica nanoparticles. These figures show that increasing silica nanoparticles from 1 to 3 wt%, resulted in a sudden upturn in complex viscosity and a plateau in storage modulus at low frequencies which is an indication of the transition from liquid to solid-like behavior. Also, Figure 2.23 f shows that by adding 3 wt%, the second arc in the Cole-Cole plot which is related to the relaxation of PBAT droplet was disappeared and it is in accordance to Figure 2.23 c which shows conversion of matrix-droplet morphology to co-continuous one.

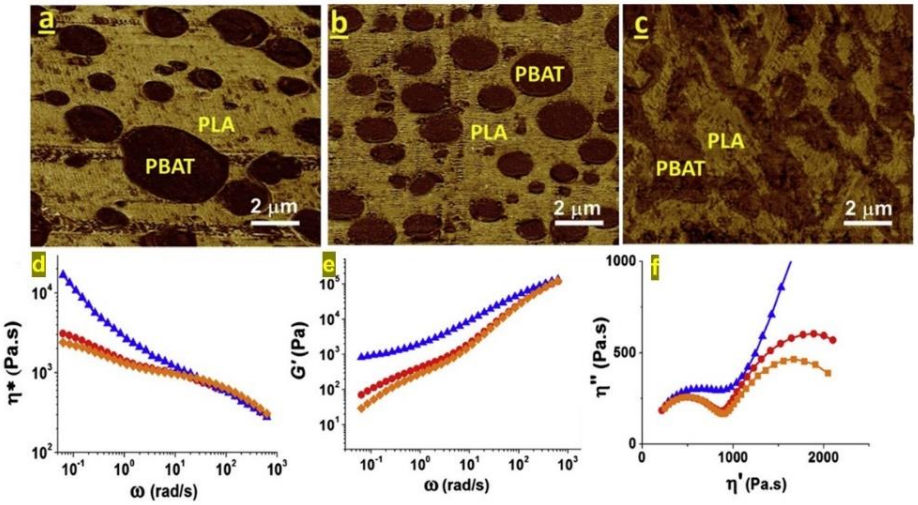

Figure 2.23 Effect of the interfacial localization of nanosilica in PLA/PBAT (70/30 wt%) blend nanocomposites; AFM images of a) neat blend, b) PLA/PBAT/1 wt% nanosilica, and c) PLA/PBAT/3 wt% nanosilica. (d) Complex viscosity and (e) storage modulus versus angular frequencies and (f) Cole–Cole (imaginary part of the viscosity (η'') vs. real part of the viscosity (η') plot. In the rheological data diamonds or squares are neat PLA/PBAT blend, circles are PLA/PBAT loaded with 1 wt% and upper triangles are PLA/PBAT loaded with 3 wt% [188].

Also, Nofar et al [210] investigated the localization of C30B in the blend of amorphous and semicrystalline PLA/PBAT (75/25 wt%). They prepared the blends using both TSE and an internal mixer. They found that when semicrystalline PLA was used the 1 wt% C30B had a tendency to be localized at the interface of PLA and PBAT and can migrate to the PLA phase in the presence of a larger amount of C30B (in accordance with thermodynamics predictions (Equation 2.8)). On the other hand, when they used an amorphous PLA, the clay was found throughout the blend structure. Also, they claimed during the internal mixer longer mixing time the nanoclays could migrate to the more thermodynamically favorable phase. Because of the longer exposure to shear conditions, the morphology could have stabilized even further. Also, Shahlari and Lee [262] observed C30B clays at the interface of PBAT/PLA (80/20) wt%) blends, resulted in slightly smaller PLA domain sizes. This was due to the clay physical barrier effect at the interface, which prevented coalescence. Wu et al. [240] looked at how clay and carbon nanotubes affected the morphology of PLA/PCL blends (70/30 wt%). Clays were seen at the interface region, which inhibited the coalescence of PCL droplets. CNTs, on the other hand, were mainly found within PCL domains and to a lesser degree

at the interface. Because of the lower viscosity ratios, the latter case strengthened the morphologies by preferring droplet breakup.

The use of compatibilizers for morphology stabilization could be eliminated if nanoparticles are localized at the interface. This interfacial localization of nanoparticles over compatibilizers could include their additional influence on improving the final thermomechanical and viscoelastic properties of the blends, in addition to their morphological stabilization. On the other hand, the use of a compatibilizer or surface modification of nanoparticles has also been attempted to thermodynamically control the localization of nanoparticles at the interface. Aghjeh et al. [263] investigated the localization of C30B (1, 3, and 5 wt%) in the blend of PLA/ethylene-vinyl acetate (EVA) (75/25 wt%) with/without using a compatibilizer (Elvaloy® PTW; terpolymer of ethylene, butyl acrylate (BA) and glycidyl methacrylate (GMA)). They demonstrated that the organoclay selectively localized in the PLA phase (Figure 2.24 a & b) and that the existence of a compatibilizer has a significant impact on the organoclay localization and led to the organoclay migration toward the interface (Figure 2.24 c & d). With this localization, the EVA droplet size decreased, and the rheological responses substantially improved, with a strong plateau modulus at low to medium frequencies (Figure 2.24 e & f). Figure 2.24e shows the storage modulus at higher frequencies, while Figure 2.24f shows the storage modulus at lower frequencies.

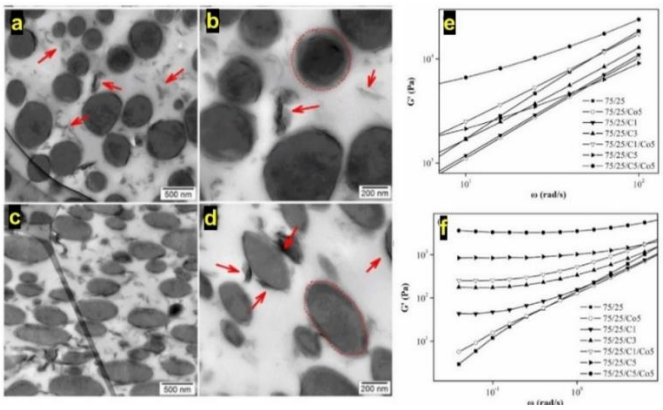

Figure 2.24 Morphology-rheology dependency in PLA/EVA blends on clay localization and on the addition of compatibilizer. (a) and (b) are the TEM micrographs of blend nanocomposites without compatibilizer and (c) and (d) are the TEM micrographs of blend nanocomposites with compatibilizer. (b) and (d) are higher magnification of (a) and (c). C and Co in the legends of storage modulus curves ((e) higher frequencies and (f) lower frequencies) represent the clay and compatibilizer respectively and their forthcoming numbers indicate their weight ratios [210].

In another study, Yousefzade et al. [263] tuned the localization of carbon nanotubes (CNTs) at the interface of poly(L-lactide) (PLLA) and a thermoplastic polyurethane (TPU) using commercial multifunctional styrene-acrylic oligomers (BASF, Joncryl®ADR-4368) as a reactive agent. When samples were prepared by non-reactive and reactive melt mixing, respectively, MWCNTs were mostly found in the TPU phase (Figure 25a) and at the interface (Figure 25b). Both storage and loss modulus increased significantly for samples prepared by reactive melt mixing, particularly in low-frequency regions, according to rheological data. As a thermodynamic compatibilizer for immiscible polyvinylidene fluoride/poly l-lactide (PVDF/PLLA; 50/50 wt%) blends, Zhao et al. [264] used CNTs with reactive epoxide groups and long poly(methyl methacrylate) (PMMA) tails. The CNTs localized at the interface with this functionalization and the storage modulus from the rheological analysis was remarkably enhanced with an evident solid-like behavior at low frequencies. Some investigations demonstrated different effects of compatibilizers based on their type as well as the type of nanoparticles [212], [265].

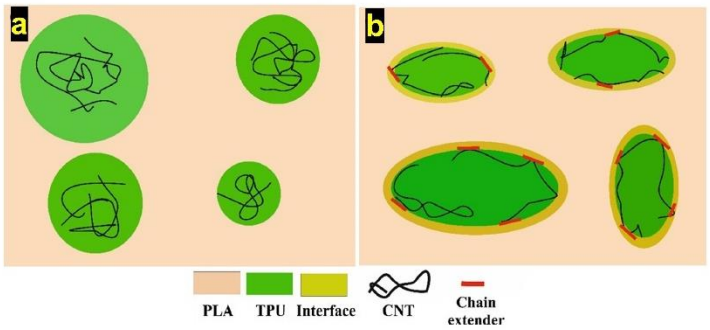

Figure 2.25 Schemes showing droplet morphology in blends of PLLA/TPU containing CNTs and prepared by non-reactive (a) and reactive (b) melt mixing [263].

2.7.1 PLA-Based Blends containing CNCs

There are few pieces of research on the PLA blends containing CNCs. It can be categorized as PLA/polyhydroxy butyrate (PHB)/freeze-dried-CNC [266]–[268], PLA/ polybutylene succinate (PBS)/CNC [269], [270], PLA/polyvinyl alcohol (PVAc)/CNC [114], and PLA/NR/CNC [271], [272]. However, none of them reports a very good dispersion of CNCs as shown by TEM or AFM images. On the other hand, Heshmati et al. [110] used a procedure based on a combination of solvent dissolution, casting (to prepare neat nanocomposites), and melt mixing processing (to prepare blend nanocomposites through dilution of a masterbatch of neat nanocomposites) to

localize CNC particles into an entirely bio-based PLA/PA11 blend (70/30, 30/70, and 50/50 wt%). They proved a high level of dispersion of CNC in the matrix of PLA and PA11 through microscopy and rheological analysis. They showed that irrespective of the preparing process (using PLA/CNC or PA11/CNC masterbatch) and the composition of blend, the spray-dried CNCs prefer to stay in the PA11 phase, which is the thermodynamically favorable phase for CNCs (Figure 2.26).

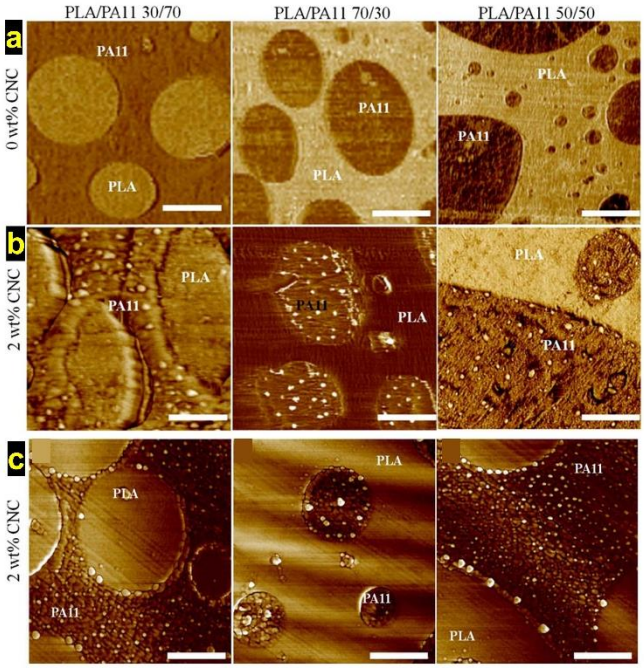

Figure 2.26 AFM phase micrographs of the PLA/PA11 blends without (a) and with (b & c; 2 wt%) CNC particles. CNC was fed into the blend through the PA11/CNC (b) and PLA/CNC (c) mixtures. The scale bar is 500 nm [110].

While the localized CNCs did not have any effect on the size of the dispersed phase even at 3 wt% (both 70/30 and 70/30 PLA/PA11), they showed with the incorporation of 1 wt% CNCs the co-continuous phase (PLA/PA11; 50/50 wt%) thickness drops from 13 to 3 µm, resulting in a dramatic coalescence suppression effect (Figure 2.27).

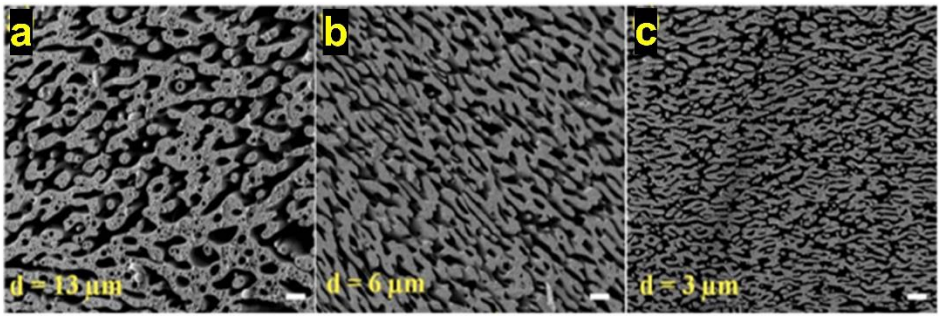

Figure 2.27 Morphology evolution of the PLA/PA11 (50/50 wt%) blend in the presence of CNC particles: (a) 0 wt% CNC, (b) 0.5 wt% CNCs, (c) 1 wt% CNCs. The scale bars are 10 µm and d is the pore diameter [110].

Also, Heshmati et al. [111] showed that modification of CNCs with PEO and preparing the same blend with the same procedure resulted in the localization of the CNCs in the PLA, which is opposite to the thermodynamically favorable phase for the CNCs. They incorporated the PEO/CNC in the blend of PLA/PA11 through premixing with PLA or PA11. Irrespective of the premixing procedure the CNC localized in the PLA phase. It is worth mentioning that they used 5 vol% of PEO, which was miscible with PLA and creating one phase. Similar to regular PLA/PA11/CNC, when the PLA-5PEO/PA11 blend was in a matrix/dispersed phase form, the localization of PEO-coated CNCs in the PLA phase does not affect the morphology of the blend. The presence of 2 wt% PEO-coated CNCs in the PLA phase of a co-continuous (PLA-5PEO)/PA11 blend reduced the pore size from 11 to 4 µm. In both investigations of Heshmati et al. [110], [111], although they presented the rheological properties of the neat nanocomposites that confirmed a good dispersion of CNCs in both phases (increases of the complex viscosity and plateau in storage modulus at low frequencies), they did not present any information about the rheological properties of PLA/PA11/CNC blend nanocomposites to confirm their observations from SEM or AFM. Also, they did not prove the morphological and rheological stabilization of the PLA/PA11 blends. Shakouri and Nazockdast [273], [274] used CNCs with various dimensions in a PLA/TPU blend (80/20 wt%) (Figure 2.28a), including spherical (Figure 2.28d), rod-like (Figure 2.28b), and cylindrical (Figure 2.28c) CNCs. They prepared the samples through the combination of solution casting and melt mixing of masterbatches of PLA/CNC. Spherical and cylindrical CNCs were found to be localized in the PLA matrix and/or interface (Figure 2. 28 c & d), while rod-like CNCs were found mostly in the TPU phase (Figure 2.28 b), which was in line with thermodynamic predictions. The addition of 3 wt% spherical and cylindrical CNCs to the blend has significantly

reduced the particle size of TPU (Figure 2.28 c & d). The rod-like CNCs, on the other hand, had no effect on the TPU size reduction (Figure 2.28 b). The presented rheological analysis confirms these localizations with an upturn in the complex viscosity and plateau in storage modulus for spherical and cylindrical CNCs (Figure 2.28 e). In their work the morphological and rheological stabilization of the blend nanocomposites were not investigated.

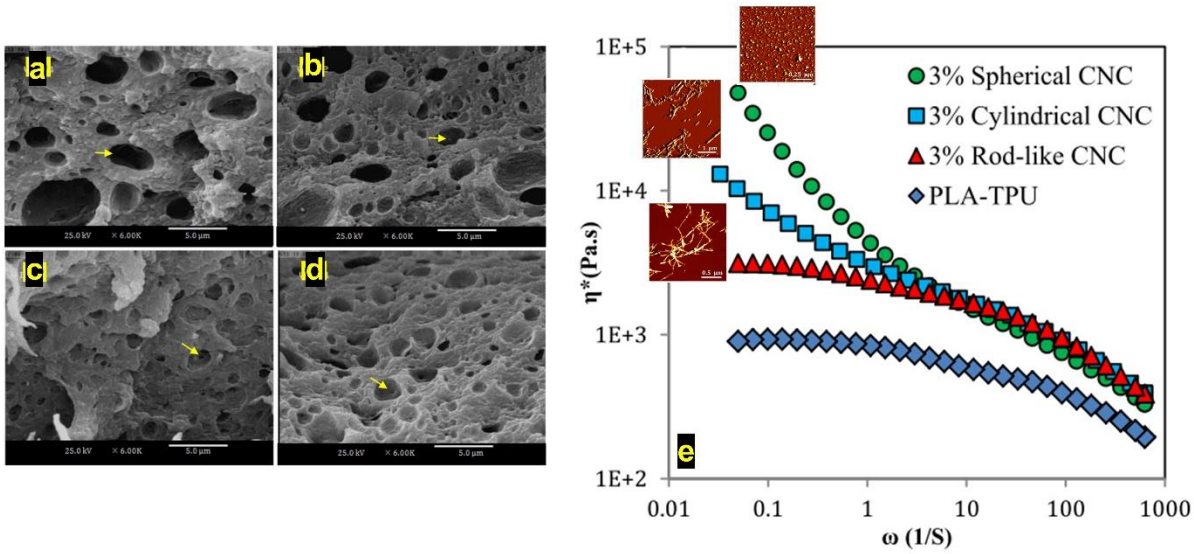

Figure 2.28 FE-SEM micrographs of PLA/TPU (80/20) blend (a), blend nanocomposites containing 3 wt% rod-like (148 ±19 μm) CNCs (b), cylindrical (204 ±26 μm) CNCs (c) and spherical (54 ±8 μm) CNCs (d). e: complex viscosity versus frequency for PLA/TPU (80/20 wt%) blend and blend nanocomposites containing 3 wt% of various CNCs [273].

The only work investigating the CNC incorporation in the blend of PLA and PBAT was that presented by Sarul et al. [218]. They investigated the preparation of PLA/PBAT/CNC blend nanocomposites through solution casting followed by melt mixing via a twin-screw extruder. However, the authors did not report on the CNC dispersion in the neat polymers. Their analysis of the effect of the localization of CNCs was based on expectations from thermodynamics considerations and they did not present a microscopic analysis to localize the CNCs and confirm their thermodynamics analysis. They did not present a strong explanation in the rheological analysis section (with no information about the rheological properties of the neat polymer matrices before and after melt mixing). According to their rheological analysis on blend nanocomposites, with the addition of 3 and 5 wt% CNCs, a large increase in the complex viscosity and storage modulus at low frequencies were observed in the samples prepared by solution casting (Figure

2.29). They claimed that it can be attributed to the formation of the CNC network in the PLA matrix. Also, they mentioned since re-agglomeration of CNCs will suppress the melt properties of nanocomposites (melt mixing; TSE), no significant improvement in rheological properties was observed (Figure 2.29).

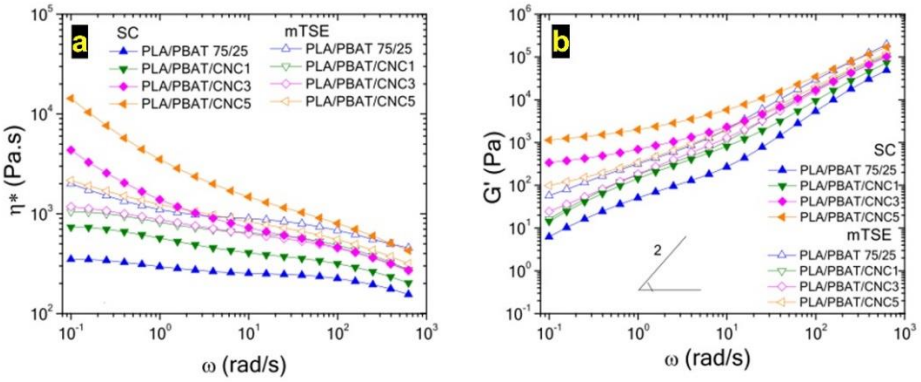

Figure 2.29 (a) Complex viscosity, η^*, and (b) storage modulus, G', of the blends and blend nanocomposites at 170 °C prepared with solution casting and melt mixing using TSE [218].

2.8 Summary

Although many efforts have been devoted to prepare neat nanocomposites from solution casting especially PLA/CNC nanocomposites, none of them presented how to select a solvent for the dispersion of CNCs and dissolution of PLA, and most of them were just based on experience or trial and error. Also, none of these investigations paid attention to the effect of solvent on the morphological, rheological, thermal, and mechanical properties. Therefore, this research is planned to fill this gap in the literature by using a thermodynamics analysis to select the best solvent for the dispersion and dissolution of CNCs and polymers, respectively, and to propose an efficient method of preparation that lead to the development of PLA/CNC or PBAT/CNC nanocomposites with a dispersed structure and enhanced properties. Also, a systematic investigation of the preparation method is needed to compare the morphological, rheological, and mechanical properties of prepared polymer nanocomposites. Despite the fact that PLA/PBAT/CNC blend nanocomposites can be considered as green blend nanocomposites (all the components are biodegradable), none of the previous investigations thoroughly analyzed their morphological, rheological, thermal, and mechanical properties. Also, in the investigated blend nanocomposites containing CNCs some of the investigators presented the rheological properties of the neat nanocomposites that confirmed a

good dispersion of CNCs in both phases. However, none of them presented complete analysis of the rheological properties of the blend nanocomposites to confirm their observations from microscopic analysis, and none of them paid attention to the morphological and rheological stabilization of the blends in the presence of CNCs. So, efforts have to be devoted to the preparation of blend nanocomposites of PLA/PBAT/CNC with enhanced properties. Morphological, rheological, mechanical, and thermal properties of neat and blended nanocomposites were investigated thoroughly, and the results have been published or submitted for publication to peer review journals.

CHAPTER 3 OBJECTIVES

3.1 Main Objective

The main objective of this Ph.D. research is to develop high performance poly (lactic acid) (PLA) system through blending with poly (butylene adipate terephthalate) PBAT and incorporation of CNCs. Petroleum-sourced but biodegradable (PBAT) blended with PLA and bio-based cellulose nanocrystals (CNCs) as filler to produce a biodegradable hybrid blend nanocomposite. We aim at obtaining properties comparable to commercial polyethylene terephthalate (PET) and polypropylene (PP). PET and PP have a modulus of elasticity of around 2800 and 1800 MPa, respectively, and elongation at break of around 200 and 580 %, respectively [275]. Upon blending with PBAT, the elongation at break of PLA will be improved due to high elongation at break of PBAT (around 800%), but its modulus of elasticity will be decreased which will be compensated by incorporation of CNCs and making a balance between stiffness and toughness in PLA and the results will be comparable with commodity polymers of PET and PP. The improvement in properties of this polymer blend nanocomposite will depend on the quality of CNC dispersion and interfacial tension between polymer components and CNCs. Moreover, the final properties of immiscible polymer blends could be altered as a result of droplet coalescence or breakup, and it is important to note that droplet coalescence should be averted or minimized. What is more, to the best of our knowledge there have been no attempts to investigate PLA/PBAT/CNC nanocomposites by combining solution and melt mixing methods. So, the main goal of this thesis is to achieve well dispersed and localized PLA/PBAT/CNC nanocomposites with a stable morphology by solution and melt mixing.

3.2 Specific objectives

Combination of solvent casting and melt mixing methods used to well-disperse CNCs in the neat PLA, neat PBAT, and PLA/PBAT polymer blends. The solvents selected based on thermodynamic analysis and the most used solvent in the previous studies. Based on thermodynamic analysis the best solvent for dispersing and dissolution of CNCs and PLA or PBAT were DMSO and THF, respectively. Also, DMF used as the most used solvent based on published articles for dispersing

and dissolution of both CNCs and polymers, respectively. So, in order to meet the main objective, the following specific objectives need to be considered:

1. Prepare well dispersed unmodified CNCs in the neat PLA (semi-crystalline and amorphous) and PBAT using a solvent casting method through two or one solvents, to investigate the effect of dispersed structure on the melt rheological, morphological, and mechanical properties as well as the effectiveness of using two or one solvents.
2. Prepare well dispersed unmodified CNCs in the biodegradable PLA/PBAT blends using a solution method (one solvent method) followed by a melt mixing method (internal mixing)
3. Control the localization of finely dispersed CNC in order to minimize the coalescence during processing as well as stabilize the morphology of PLA/PBAT blends.
4. Control the localization of finely dispersed CNC at the interface to achieve desirable morphological, rheological, thermal, and mechanical properties in the blends of PLA/PBAT.

CHAPTER 4 ORGANIZATION OF THE ARTICLES

The primary findings of this study are reported in three publications, which are discussed in Chapters 5, 6, 7, and 8.

In chapter 5 a novel method based on a thermodynamic approach was adopted to select the best solvents for dispersion and dissolution of CNCs and PLA (semicrystalline and amorphous) or PBAT, respectively. Morphological and rheological data presented the effectiveness of this method to achieve highly disperse and distributive CNCs in the matrix of PLA and PBAT. Also, the effect of remaining solvents in the polymers was investigated thoroughly. The chapter was published as a scientific article in Cellulose (impact factor: 5.271)

Chapter 6 deals with the preparation of blend nanocomposite of PLA/PBAT (75/25 wt%) containing cellulose nanocrystals. The blend nanocomposites including both semicrystalline and amorphous PLA were prepared through a combination of solvent casting (one solvent, DMF, for dispersion and dissolution of CNCs and PLA or PBAT, respectively) followed by melt mixing in an internal mixer. CNCs dispersion and distribution in the neat nanocomposites were investigated using microscopic and rheological analysis for both samples from solution casting and the ones followed by melt mixing. What is more, morphological properties of PLA/PBAT blend nanocomposites were investigated with/without CNCs, and the effect of CNCs and their localization (from thermodynamic and processing points of view) after melt mixing were analyzed thoroughly. All the morphological observation was confirmed by rheological analysis. Finally, morphological stabilization in the presence of CNCs was investigated under shear flow and the results compared with the neat blends of PLA/PBAT. The chapter was published as a scientific article in Nanomaterials (impact factor: 5.346).

Chapter 7 is dedicated to a comparison of the mechanical and thermal properties of neat nanocomposites of PLA (amorphous and semicrystalline)/CNC and PBAT/CNC prepared from two solvents (prepared samples in chapter 5) and one solvent (prepared samples in chapter 6) methods. Through microscopic analysis, CNCs dispersion was investigated for both methods. Differential scanning calorimetry (DSC) was used to investigate the thermal properties of neat nanocomposites. For the mechanical analysis both tensile and impact properties are reported in

chapter 7 and also thermomechanical analysis was done using dynamic mechanical thermal analysis (DMTA). Finally, a percolation model (modified Takayanagi model), the strength of the percolating CNC network was determined and was found to be dependent on temperature and affected by traces of solvent The chapter was accepted with a revision as a scientific article to Polymer Composites (impact factor: 3.171).

In Chapter 8, the effect of interfacial localization of CNCs in the blends of PLA (semicrystalline and amorphous)/PBAT prepared through solution casting followed by melt mixing (the method is described in chapter 6) are shown on the morphological, rheological, thermal, and mechanical properties. The chapter was accepted with a revision scientific article to Polymer (impact factor: 4.430)

CHAPTER 5 ARTICLE 1: CNC DISPERSION IN PLA AND PBAT USING TWO SOLVENTS: MORPHOLOGICAL AND RHEOLOGICAL PROPERTIES[1]

Mojtaba Mohammadi, Charles Bruel, Marie-Claude Heuzey, Pierre J. Carreau*

Center for High Performance Polymer and Composite systems (CREPEC), Department of Chemical Engineering, École Polytechnique de Montréal, Montreal, Québec, H3T 1J4, Canada

5.1 Abstract

Cellulose nanocrystals (CNCs) were dispersed via solution casting in amorphous (A) and semi-crystalline (SC) poly (lactic acid) (PLA) and poly (butylene adipate-co-terephthalate) (PBAT). The protocol, optimized following the Hansen solubility parameter theory, relies on binary mixtures of tetrahydrofuran and dimethyl sulfoxide for the polymers and CNCs, respectively. First highlighted through atomic force microscopy, good filler dispersion and distribution were confirmed by a decrease of the linear viscoelastic region and significant increases of the complex viscosity, storage modulus, and apparent yield stress of the nanocomposites with CNC content, specifically at low frequencies. CNC percolation thresholds of 1, 0.3, and 0.3 wt% were determined in A-PLA, SC-PLA, and PBAT, respectively. These are the lowest to be reported in the literature until now. While PLA retained solvent traces, leading to a significant plasticizing effect, solvent removal was complete in PBAT. It was attributed to the crystallization of PBAT at the drying temperature (70°C).

Keywords: Nanocomposites; Cellulose nanocrystals (CNCs); PLA; PBAT; Solvent selection; HSP theory

---

[1] Published in Cellulose 27, 9877–9892 (2020)

5.2 Introduction

Polymeric materials have advantageously replaced their metallic counterparts in industries as diverse as aerospace, aeronautics, automotive, medical, sensors, or agriculture [1]. This is notably due to their lightness, low cost, durability, and water resistance [1]. Non-biodegradable fossil-based polymers, such as polyethylene, polypropylene, polystyrene, and poly (vinyl chloride), are the most employed and contribute disproportionally to the wastes released to the environment [2]. This issue could, in part, be addressed by using biodegradable plastics produced from bio/fossil-based resources [3]. Poly (lactic acid) (PLA) and poly (butylene adipate-co- terephthalate) (PBAT) have recently received significant attention. Their properties such as biodegradability and biocompatibility make them suitable for automobile products, textiles and fibers, films and packaging, and biomedical applications (drug delivery, blood vessels, tissue engineering, and scaffolding) [4], [5].

In addition to its eco-friendly advantages [6], PLA has interesting mechanical and physical properties, among which high modulus (2-16 GPa), high tensile strength (14-117 MPa), good clarity, and barrier properties. However, it suffers from serious drawbacks such as low melt strength, toughness, and service temperature; slow crystallization rate, poor processability, and high brittleness. By comparison, PBAT is more flexible with a Young modulus of 20-35 MPa, a tensile strength of 32-36 MPa, and an elongation at break that reaches up to 700% [5], [7]. However, it has high production costs and low thermophysical and mechanical resistances [4], [5]. While developing copolymers, blends, or composites, are all promising ways to address these drawbacks [4], [8], using nanofillers as reinforcing agents has proved to be one of the most effective methods to remediate the shortcomings of both PLA and PBAT [7], [9]. Natural fibers and cellulose derivatives, being low-cost, biodegradable, and biocompatible, are promising materials to produce green composites. Among them, cellulose nanocrystals (CNCs), have gained considerable attention during the last decade [10]–[12]. Even though CNCs can be well dispersed in hydrophilic polymers such as polyethylene oxide (PEO) [13], their dispersion in hydrophobic polymers remains difficult. It is due to the strong interparticle interactions caused by the hydrogen bonds they may form at their surface [11], [12]. Compatibilizers and surface modification are efficient at improving CNC dispersion in hydrophobic polymer matrices [14]–[17]. However, the dispersion of pristine CNCs, without modification or compatibilizers, remains challenging in polymer nanocomposites.

Rheological measurements are efficient at assessing its quality: upon good nanoparticle dispersion, the linear viscoelastic (LVE) region in terms of strain amplitude will decrease while the complex viscosity, storage modulus, and loss modulus, will increase at low frequencies [18]. It is worth pointing out that increases in viscosity upon CNC addition and dispersion has not been unanimously observed in the literature [9]. Ferreira et al. [19] further reviewed the rheological behaviors of CNC-based nanocomposite as a function of CNC size, filler/matrix interactions, and preparation method.

Different processing methods such as melt mixing using an internal mixer or a twin-screw extruder, solvent casting, or combination of these methods have been used to disperse CNCs in PLA and PBAT [16], [20]–[22]. A good dispersion of CNCs in hydrophobic PLA and PBAT can improve considerably the properties of these materials. Da Silva Gois et al. [23] investigated the PLA biodegradability in the presence of cellulose nanowhiskers (CNW) and surfactant modified CNW. The results showed better biodegradation of PLA matrix. In another study, Mathew et al. [24] showed that PLA biodegradability has been improved in the presence of microcrystalline cellulose. In the case of PBAT, unmodified nanofillers such as pristine CNCs [25] and nanoclays [26] have even been reported to improve the biodegradability of the matrix. The melt mixing of pristine CNCs is rather unsuccessful, as the shear forces applied in the melt cannot overcome the strong hydroxyl-hydroxyl H-bonds between CNC particles, while working at high temperatures may also degrade the cellulose nanocrystals. Therefore, melt mixing usually requires surface functionalization, or the use of surfactants or compatibilizers to reach a good CNC dispersion [16], [20]. Kamal et al. [22] could, however, disperse pristine spray-freeze-dried CNCs in a PLA matrix through melt mixing and obtained a rheological percolation threshold at a concentration of 3wt%. They reported that the spray-freeze-dried CNCs resulted in porous agglomerated structures that facilitate the infiltration of the polymer melt into these structures [27]. Solvent casting yields a better outcome [21], [28], [29]. Polymers are dissolved and CNCs dispersed in solvents such as dimethylformamide (DMF) [21], [30], chloroform [31], [32], or dichloromethane [33]. Bagheriasl et al. [21], [34], [35] used DMF to prepare CNC suspensions in PLA solutions. They obtained a high degree of dispersion of pristine CNCs in hydrophobic PLA for the first time and reached a rheological percolation threshold of 0.66 wt%. Therefore, and while solvent casting is unattractive from an industrial point of view, it remains the most effective method to achieve a good CNC dispersion in PLA or PBAT [36]. Combining solvent casting with melt mixing was hence suggested as a compromise towards

a more industrially acceptable solution. This is usually done by preparing a masterbatch through solvent casting [32], [37], or by *in-situ* polymerization [16], [38], which is then diluted through melt-mixing. This strategy was successfully applied in PLA and PEO [13], [39]–[41]. However, and to the best of our knowledge, there is no published investigation on the dispersion of pristine CNCs in PBAT through any solvent-based method.

In this work, we investigated the solvent casting of pristine CNC reinforced nanocomposites of PLA (2 different grades) and PBAT in order to produce fully biodegradable materials. A specific effort was made to select the best solvents for dispersing CNCs and dissolving the polymers based on the Hansen solubility parameter, HSP, theory. It led us to propose a methodology that relies on two solvents: one to disperse the CNCs, and the other to dissolve the polymers. The media were then mixed and casted. The nanocomposites are investigated with a focus on the morphological and rheological properties. While a good CNC dispersion was achieved in both PLA and PBAT, the PLA (especially the amorphous one) retained solvent traces that provided a plasticizing effect. The PBAT however did not, which is relevant for the objective of producing biodegradable materials.

5.3 Experimental

5.3.1 Materials

Two commercial PLAs were obtained from NatureWorks LLC (Minnetonka, MN, USA). These are Ingeo 4060D (amorphous, A-PLA) with a weight average molecular weight of 190 kg/mol and a D-lactide content of 12 mol% and Ingeo 3251D (semi-crystalline, SC-PLA) with a weight average molecular weight of 55 kg/mol and a D-lactide content of 1.4 mol%. The other polymer was PBAT (Ecoflex® FBX 7011) purchased from BASF, with a density of 1.23 g/cm^3, melt flow index (MFI) of 2 g/10 min, and a weight average molecular weight of 24.4 kg/mol. Freeze-dried CNCs were kindly provided by FPInnovations (Pointe-Claire, QC, Canada) and the information on CNC preparation can be found elsewhere [42]. Dimethyl sulfoxide (DMSO) and tetrahydrofuran (THF), anhydrous 99.8 %, were purchased from Fisher Scientific Canada Co.

5.3.2 Thermodynamics of solvent selection

Investigating solvent dispersibility of CNCs, our research group found the Hansen solubility parameter (HSP) theory [43] appropriate to map the chemical affinity of CNCs [44], [45] and to predict both their level of colloidal stability and their behavior upon solvent casting [46], [47]. The HSP theory indeed quantifies a chemical potential for interactions through a solubility (or cohesion) parameter, δ_T. Expressed in $MPa^{1/2}$, δ_T is the square-root of an energy density. It is split into three components, δ_D, δ_P, and δ_H (Equation.5.1), which respectively account for the dispersive, dipole-dipole, and hydrogen-bonding (and other Lewis acid/base) interactions. Each chemical has his own set of parameters $\{\delta_D; \delta_P; \delta_H\}$ that may directly be plotted in a 3D graph [48]. The main affinity of CNCs was characterized as having a HSP set of $\{\delta_{D,CNC}; \delta_{P,CNC}; \delta_{H,CNC}\}$ = {18.1; 20.4; 15.3} ± {0.5; 0.5; 0.4} $MPa^{1/2}$ [45].

$$\delta_T^2 = \delta_D^2 + \delta_P^2 + \delta_H^2 \qquad \text{Equation 5.1}$$

The chemical distance between two substrates A $\{\delta_{D,A}; \delta_{P,A}; \delta_{H,A}\}$ and B $\{\delta_{D,B}; \delta_{P,B}; \delta_{H,B}\}$, $R_{a,A\text{-}B}$, may then be expressed as a norm of the $\overrightarrow{AB}$ vector in the HSP graph (Equation.5.2):

$$R_{a,\mathrm{A-B}} = \left\|\overrightarrow{AB}\right\| = \sqrt[2]{4\left(\delta_{D,A} - \delta_{D,B}\right)^2 + \left(\delta_{P,A} - \delta_{P,B}\right)^2 + \left(\delta_{H,A} - \delta_{H,B}\right)^2} \qquad \text{Equation 5.2}$$

Behavioral changes that relate to chemical affinities, such as solubility, swelling, or adsorption, translate into a critical threshold in terms of chemical distance: R_0. For instance, solvents whose chemical distance with CNCs, $R_{a,\mathrm{CNC\text{-}solv}}$ (Equation 5.3), was smaller than $R_{0,CNC}$ = 7.8 $MPa^{1/2}$ were found to adsorb significantly on CNC surfaces, thus preventing their sedimentation [45] by providing solvation-induced colloidal stability [46]. This may add to the electrostatic stabilization experienced by CNCs in highly dielectric solvents. A combination of electrostatic and solvation-induced stabilization was found to be necessary to reach sufficient colloidal stability for CNC particles [46].

$$R_{a,\mathrm{CNC-solv}} = \sqrt[2]{4\left(18.1 - \delta_{D,solv}\right)^2 + \left(20.4 - \delta_{P,solv}\right)^2 + \left(15.3 - \delta_{H,solv}\right)^2} \qquad \text{Equation 5.3}$$

Only a few solvents such as water, formamide, N-methylformamide, and dimethylsulfoxide may offer this level of stabilization. DMF is not part of this shortlist for our CNCs, as the relatively

rheological properties achieved in DMF-casted systems compared to water-casted ones [49] suggest a poorer dispersion of CNCs in DMF.

Literature reports HSP values of ~ {18.5; 8.0; 7.0} $MPa^{1/2}$ for PLA with a solvent solubility radius of $R_{0,PLA} \approx 8$ $MPa^{1/2}$ [50]. PBAT stands at ~ {18.0; 5.6; 8.4} $MPa^{1/2}$ for a solvent solubility radius of $R_{0,PBAT} \approx 4.5$ $MPa^{1/2}$ [50]. Figure 5.1a and b are HSP graphs in 3D and, for greater readability, its 2D projection alongside the parameters δ_P and δ_H. They show the HSP coordinates of CNCs (grey circle), PLA (blue circle), and PBAT (red circle), as well as their respective spheres of radius R_0 (dotted lines in Figure 5.1 b). The lack of superposition between the three domains highlights the lack of solvents that could simultaneously offer a good CNC dispersion and sufficient dissolution for both PLA and PBAT.

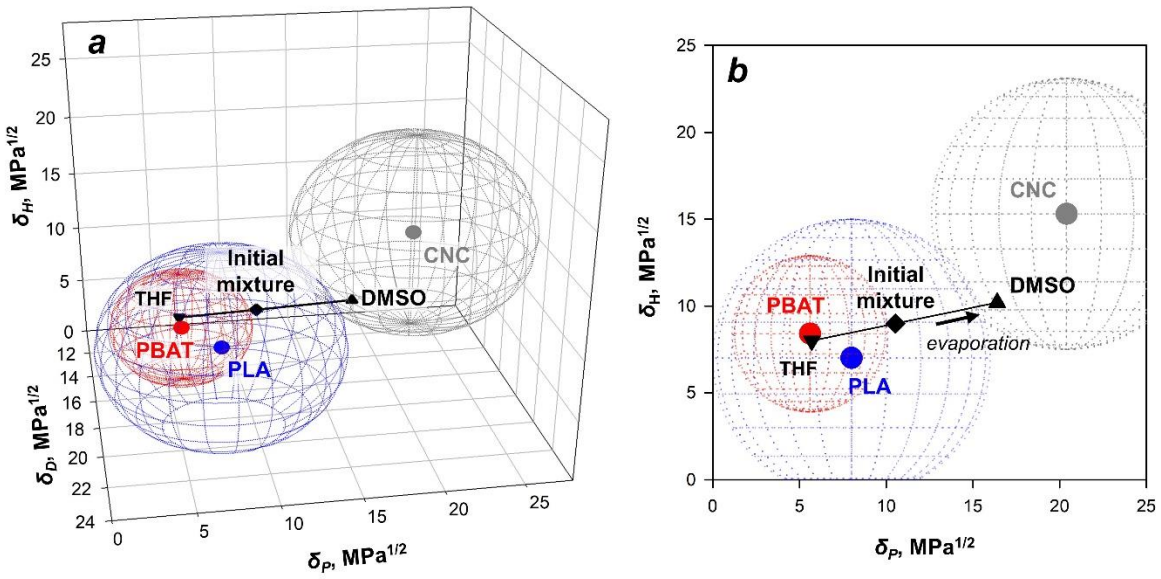

Figure 5.1 HSP graph for CNCs (grey circle), PLA (blue circle), and PBAT (red circle) (a) and its projection in the δ_P-δ_H plane (b). The spheres delimited by their respective HSP radii, R_0, are materialized by dotted lines. DMSO (black triangle up) was selected to disperse CNCs, and THF (black triangle down) to solubilize PLA and PBAT. The two media are then blended in a ratio that corresponds to the black diamond. Upon evaporation, and since THF has a lower boiling point than DMSO, the HSP of the mixture get closer to those of DMSO, following the black line.

Hence, we decided to use a binary mixture: one solvent should offer a good dispersion of the CNCs, while the other should provide an easy dissolution to the polymers. In Figure 5.1b, CNCs and PLA spheres slightly overlap: DMSO (black triangle up) is the solvent that is the closest to this

overlapping area: it is good for CNCs and, while it may not dissolve PLA at room temperature, it may do so under moderate heating. The PBAT sphere is included in that of PLA. THF (black triangle down) is good for both polymers and was selected. Blending the CNC/DMSO suspension with the PLA/THF or PBAT/THF solution in the ratio investigated in this work leads to a mixture (black diamond) in which the polymers remain soluble (thanks to heating in the case of PBAT). However, when CNCs lose their solvation-induced stabilization, solvent-casting should be done fast enough to prevent re-agglomeration [46]. This is favored by the low boiling point of THF; as this solvent evaporates first during the drying process, the composition of the mixture evolves towards DMSO (following the black line) in a sense that is thermodynamically favorable to CNC particles and unfavorable to the polymers.

Note that Equation 5.2 can also be used to calculate the HSP distances between PLA, PBAT, and CNCs: $R_{a,\text{PLA-PBAT}} \approx 3.0$ MPa$^{1/2}$, $R_{a,\text{CNC-PLA}} \approx 14.9$ MPa$^{1/2}$, and $R_{a,\text{CNC-PBAT}} \approx 16.3$ MPa$^{1/2}$. This highlights the relatively close chemical affinity between PLA and PBAT. It also predicts a rather poor chemical affinity between CNCs and both polymers, which is consistent with the difficulties that have been reported to disperse pristine CNCs in these matrices [16], [21].

5.3.3 Sample preparation

A solution mixing method in THF and DMSO medium was used to prepare the nanocomposites. The A-PLA, SC-PLA, and PBAT were first dried in a vacuum oven overnight at 55 °C and then dissolved respectively in THF, while CNCs were dispersed in DMSO. The desired amount of CNCs was dispersed in 70 mL of DMSO using a water bath sonicator (FS30 100 Watts Ultrasonic Cleaner, Fisher Scientific, Pittsburg, PA) for 120 min at room temperature. Neat polymers were dissolved in 85 mL of THF using a magnetic stirrer for 150 min at 63 °C until complete dissolution. In order to minimize the effect of THF evaporation, the level of liquid was kept constant over time by adding adequate amounts of THF at regular intervals. Afterward, the neat polymer solutions (based on PLA or PBAT) were added to the CNC suspension and the stirring process was continued for another 120 min to ensure good mixing between the two media despite their rather high viscosity. Then, the mixtures were poured into a petri dish and dried in a vacuum oven set at 70 °C for 4 days. While the nanocomposites containing low molecular weight PLA (SC-PLA) or PBAT could be ground into powder using a coffee grinder, the high molecular weight PLA (A-PLA) had to be chopped to very small pieces using scissors. Then, the ground and chopped nanocomposites

were put in the vacuum oven for another 4 days in an effort to get rid of any remaining traces of DMSO and THF. The CNC content in the nanocomposites was varied from 0 (i.e. neat polymer for comparison purposes), 1, 2, and 3 wt%, and the nanocomposites are named based on the CNC content on a weight percentage basis. For example, A-PLA/3CNC refers to the nanocomposites based on the amorphous (high molecular weight) PLA with 3 wt% of CNCs, calculated with respect to the total weight of the nanocomposite. Prior to microscopy and rheology analysis, the chopped and powder samples were compression molded using a hydraulic press under a nitrogen atmosphere to make disk shape specimens (1.2 mm thick disks of 25 mm diameter). The samples were first heated to 170 °C for 4 min. Then, pressure forces of 1, 2, and 3 tons were progressively applied for 90 s each. The samples were finally cooled to ambient temperature under atmospheric pressure. The overall compression molding process took roughly 10 min.

5.3.4 Characterization

5.3.4.1 **Microscopy analysis**

5.3.4.1.1 Atomic force microscopy (AFM)

Rheological sample disks were cut and microtomed using an Ultracut FC microtome (LEICA) equipped with a liquid nitrogen cryo-chamber and a diamond knife. An AFM (MultiMode Nanoscope IIIa with extender, Digital Instruments) was used to characterize the prepared samples in air at room temperature without any additional preparation. The AFM machine was equipped with a scanning probe microscope Dimension 3100 with a Nano-scope IVa controller from Veeco Instruments. Silicon tips (ACTA-W AppNano) with a tip radius of less than 10 nm were used in this study. The instrument is located in the materials characterization laboratory (LCM) of the chemistry department of Université de Montréal. The tapping phase mode at a scan rate of 1 Hz was used to determine the morphologies of the nanocomposites because of the differences in the modulus of the polymer matrices with that of the CNCs. Sampling was made every 9 nm horizontally (512 times during the analysis of a 5×5 μm^2 area) for surface characterization. The Software Nanoscope Analysis 1.5 (Brucker, Santa Barbara, CA, USA.) was used to process the AFM images (512×512 pixels).

5.3.4.2 **Fourier transform infrared analysis**

Fourier transform infrared (FTIR) measurements were performed in order to investigate the chemical composition and the possible interactions between the PLA and PBAT matrices with the solvents (DMSO/THF). FTIR spectra of the samples were collected in the absorbance mode at room temperature using a Nicolet 380 FTIR spectrophotometer. The samples were analyzed in the wavenumber range of 600 to 4000 cm^{-1}.

5.3.4.3 **Elemental analysis**

A sample was selected, cut, and microtomed under liquid nitrogen using a cryo-microtome (LEICA-Jung RM 2165). Then, the sample surface was coated with a 15 nm thick chromium layer. The qualitative determination of the composition of neat polymers prepared from solvent casting was done via energy dispersive X-ray spectroscopy (EDS) using a JEOL JSM-840A scanning electron microscope (Oxford Instruments, Abingdon-on-Thames) operating at 15 kV.

5.3.4.4 **Rheometry**

The rheological properties of neat A-PLA, SC-PLA, PBAT, and their respective nanocomposites were measured using a stress/strain-controlled MCR 302 rheometer (Anton Paar, Austria). A parallel plate flow geometry was used with a gap of 1 mm and a diameter of 25 mm. Small amplitude oscillatory shear (SAOS) experiments were conducted at 170 °C under a nitrogen atmosphere to avoid oxidation of the samples. Strain sweep tests were conducted at a frequency of 1 rad/s to find the linear viscoelastic region (LVE) and its limit. Time-sweep experiments at a frequency of 1 rad/s and a strain amplitude of 0.001 were conducted during 40 min to verify the thermal stability of the samples within the time necessary to conduct frequency sweep small-amplitude-oscillatory shear (SAOS) experiments. All rheological measurements were repeated up to 3 times to verify reproducibility.

5.4 Result and discussion

5.4.1 Morphology

The morphologies of the various polymer nanocomposites (A-PLA/CNC, SC-PLA/CNC, and PBAT/CNC) with CNC contents of 1, 2, and 3 wt% were analyzed through AFM with a focus on

CNC dispersion and distribution. In the literature, dispersion usually refers to the level of disaggregation of CNC bundles: particles should, in the best cases, be found as single rods of nanosize. Distribution refers to the spatial homogeneity of the dispersion: it is possible to reach a high level of distribution with imperfectly dispersed CNCs. CNC rods or their bundles may hence be agglomerated but well distributed in the polymer matrix. In this section, we will first make the case that we are able to see the CNCs on the AFM images, then use these images to compare the dispersion and the distribution of the CNCs within the various samples. Our reasoning is presented for SC-PLA. Similar analyses were done for A-PLA/CNC and PBAT/CNC samples (results not shown here) and their conclusions are directly presented here.

AFM images, representative of each SC-PLA samples (CNC contents of 1, 2, and 3 wt%) are presented in Figure 5.2. As reported elsewhere [13], [51], the contrast was better in the phase images than in the height images. Signal variations that occur simultaneously on both types of images are attributed to the presence of CNCs: highlighted on the phase images are what we believe to be CNC bundles (white circles) and single CNC rods (white arrows: more obvious at the higher magnification) (Figure 5.2a). The cross-section analysis of these signal variations on the height images (whose location is highlighted by red, blue, and green continuous or dotted lines in SC-PLA with CNC content of 1, 2, and 3 wt%, respectively) gives us height variations ranging from 5 to 15 nm across the samples and reported in Figure 5.2b. The continuous and dotted lines represent measurements done at two different locations on the AFM height images. The height values are in the same range as the diameter of our CNCs [21] and are to be compared with a root mean square average of height deviations, R_q, that is smaller than 5 nm for all samples. Because of tip-convolution in the AFM analysis, it is worth noting that the width of the transverse lines (horizontal distances) cannot be considered as the particle size of CNCs [51]. These features are in agreement with previous AFM reports of CNC dispersion in polymer matrices [13], [27], [39]. CNC density seemingly increases with filler content. While small bundles can be spotted, CNCs are dispersed and distributed rather well overall for all concentrations. It supports the effectiveness of our solution casting protocol based on two solvents.

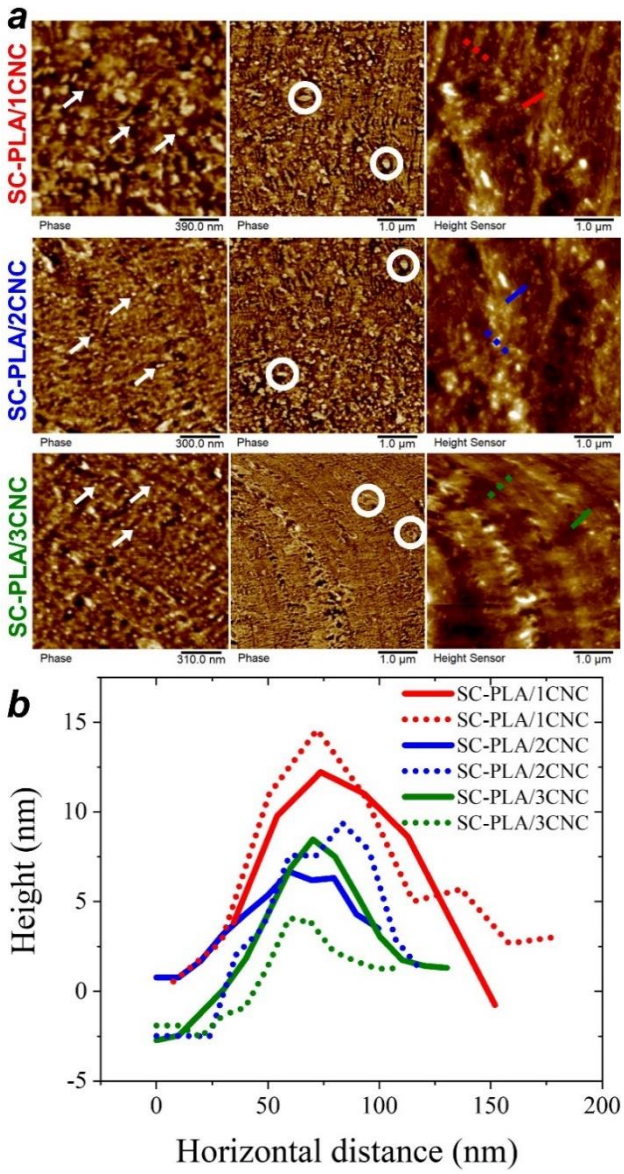

Figure 5.2 (a) AFM phase and height images of SC-PLA nanocomposites with CNC contents of 1, 2, and 3 wt%. Individual rods and bundles are highlighted with white arrows and circles, respectively, on the phase images. The continuous and dotted lines (in green, red, and blue depending on CNC weight content) present on the height images highlight the locations where a cross-section analysis was carried. Their height profiles are displayed in (b), where the line colors (green, red, or blue) and type (continuous or dotted) match those on the height images. The continuous and dotted lines represent measurements done at two different locations on the AFM height images.

Similar analyses were carried out for the PBAT/CNC and A-PLA/CNC nanocomposites (results not shown here). While all nanocomposites displayed a rather good CNC dispersion and distribution, the dispersion appeared to be poorer in A-PLA/CNC (despite an equally good distribution). This may arise from an impoverishment of the nanoparticles mixing as the length of the polymer chains, and the occurrence of their entanglements, increases. Besides the possible effect of molecular weight on mixing, the heterogeneous crystallization that occurred in SC-PLA and PBAT upon drying might also have favored the dispersion of CNCs. Indeed, ordered polymer chains within the evaporating media might act as a sterical barrier preventing CNC re-agglomeration in the later stages of the casting. Our observations substantiate previous findings reported in the literature that using a low molecular weight and crystalline grade PLA favors CNC dispersion by preventing particle-particle agglomeration [52].

Hence, AFM results point towards a homogeneous distribution of the CNCs in all samples and an overall good dispersion. The latter is comparatively better in SC-PLA and PBAT than in A-PLA. It is in agreement with the rheological data that will be presented in the next section.

5.4.2 Rheological analysis

5.4.2.1 Stability analysis and SAOS data

From time-sweep experiments, we observed a 5% loss of the complex viscosity at most for all samples during 40 min. SAOS data (complex viscosity (η^*) and storage modulus (G')) as functions of the frequency (ω) for the neat polymers and their nanocomposites with CNC contents of 1, 2, and 3 wt% are reported in Figures 5.3a-f. The stabilities of the neat polymers and their nanocomposites containing 3 wt% CNCs were further assessed in frequency-sweep using two consecutive tests at a strain of 0.001: from high to low frequencies (filled symbols), and then from low to high (empty symbols) frequencies (Figures 5.3a-f). While both sets of data are superimposed for SC-PLA, SC-PLA/3CNC, PBAT, and PBAT/3CNC (Figures 5.3b, c, e, and f), small decreases of about 4 and 5 % in the complex viscosity and storage modulus, respectively, are observed in the case of neat A-PLA and A-PLA/3CNC (Figures 5.3a and d). These decreases are attributed to some thermal degradation of the amorphous PLA.

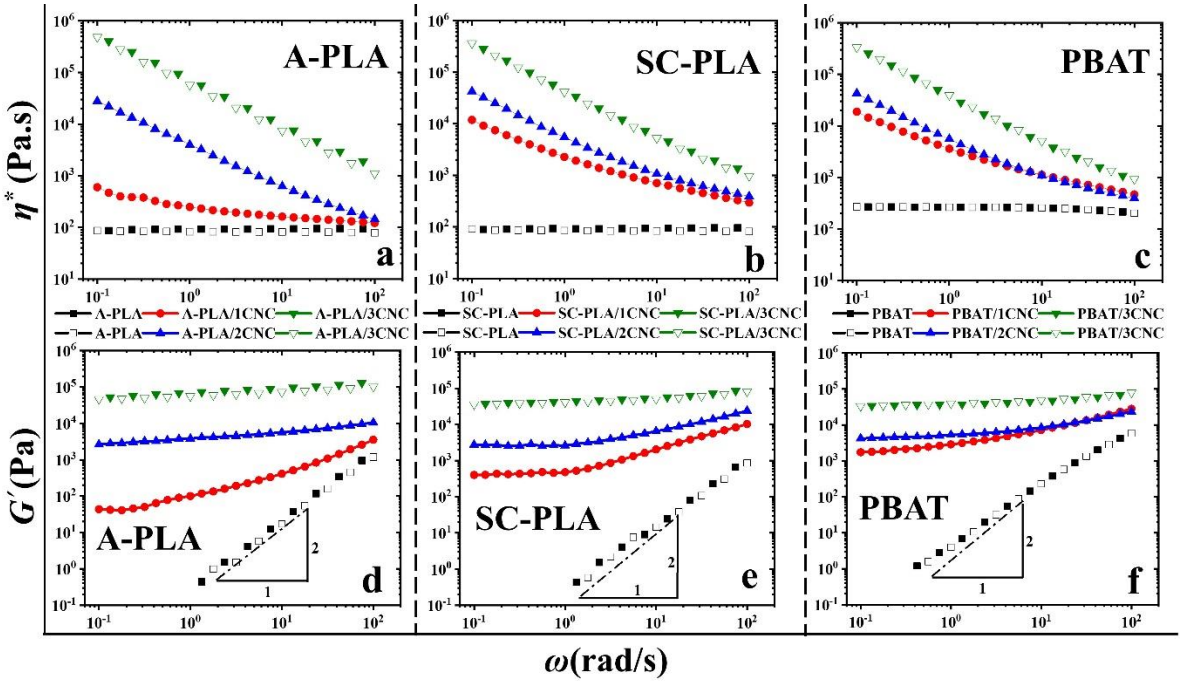

Figure 5.3 Complex viscosity, η^*, (a, b, and c) and storage modulus, G',(d, e, and f) versus frequency, ω, of the A-PLA, SC-PLA, and PBAT nanocomposites at 170 °C (strain = 0.001). Filled and empty symbols represent frequency sweep from high to low and low to high, respectively.

The neat polymers are behaving as second-order fluids with a nearly constant complex viscosity and a storage modulus that is about proportional to the square of the frequency. The behavior for the three different filled systems is quite similar and is typical of that observed for polymer nanocomposites as reported in the literature: the complex viscosity and the storage modulus increase significantly with CNC loading, becoming more shear-thinning and solid-like materials. For all nanocomposites, spectacular increases in the complex viscosity and storage modulus are observed when incorporating only 1 wt% CNCs. It is even more obvious at low frequencies: the complex viscosity increased by 1 order of magnitude for A-PLA, and by 2 orders of magnitude for both SC-PLA and PBAT. Smaller increases for A-PLA/1CNC (Figure 5.3a) could be an indication that CNCs are not so well dispersed compared to the SC-PLA and in PBAT nanocomposites (Figures 5.3b and c), which is coherent with the insights provided by the AFM analyses. As mentioned previously, this is probably due to molecular weight effects: with their shorter polymer chains, SC-PLA and PBAT have a better ability to penetrate amidst CNC agglomerates, which in turn leads to a better dispersion [52]. With increasing CNC content up to 3 wt%, the complex

viscosity and storage modulus increase dramatically to almost 10^6 Pa.s and 10^5 Pa, respectively, for the three systems. Bagheriasl et al. [21] investigated the rheological behavior of PLA 3251 (identical to our SC-PLA) with the same CNCs as investigated in this work but prepared using DMF casting. A content of 6 wt% CNCs was required to observe the improvement observed here for 3 wt%. In a recent study, Vatansever et al. [52] investigated the same A-PLA and SC-PLA. Both required up to 10 wt% CNCs (different from that of this work) to achieve a similar increase in the rheological properties as reported in Figures 5.3a, b, d, and e for 3 wt% CNCs.

All these results confirm the efficiency and the pertinence of our protocol to select the best solvents based on the HSP theory and disperse the CNCs in PLA and PBAT: the improvements at CNC contents are an indication of a better dispersion on CNCs in PLA with respect to results reported in the literature. As mentioned in the introduction, no comparison with the literature can be performed in the case of PBAT since we are, to our knowledge, the first authors to report results for a solution casted PBAT/CNC nanocomposite using pristine CNCs (no surface modification). We note, however, that the improvements in rheological properties are quite similar to those for PLA/CNC systems.

5.4.2.2 **Effect of solvent on SAOS data**

As evidenced by Figures 5.3a and b, both neat PLAs (A-PLA and SC-PLA) prepared from solution casting have a similar complex viscosity of around 100 Pa.s at low frequencies. This is surprising given their difference of molecular weight. In their molten state and at a given temperature, A-PLA (190 kg/mol) is indeed expected to be considerably more viscous than SC-PLA (55 kg/mol). Figures 5.4a and b show the effect of the solution casting preparation method on the complex viscosity of the neat polymers comparatively to that of their as-received granules. For the granules, the complex viscosities of A-PLA (5000 Pa.s) and SC-PLA (400 Pa.s) are coherent with their different molecular weights. It is only in the solution casted samples that a similar viscosity value of about 100 Pa.s is observed (Figure 5.4a). On the other hand, the complex viscosity of neat PBAT prepared from solution casting, which stands at ~300 Pa.s, is almost the same as for the granules of PBAT (Figure 5.4a). These results for both PLAs are attributed to the effect of solvent traces (DMSO and THF). It is more drastic for A-PLA but negligible for PBAT. As the boiling point of DMSO (~180 °C) is higher than that of THF (~66 °C), it is more likely that this is due to traces of DMSO in the dried samples. To clarify this, we performed a solution casting of neat A-PLA with

THF alone and with a mixture of THF/DMSO (Figure 5.4b). Using THF, the decrease in complex viscosity was around one order of magnitude with respect to the value for the A-PLA granules, and incorporation of DMSO made this situation more severe with a decrease close to two orders of magnitude (Figures 5.4a and b). Although from its low boiling point one would expect all THF to be removed during the long drying stage, it is a good solvent for PLA and this strong chemical affinity with PLA chains (with a HSP distance, $R_{a,\text{PLA-THF}}$, of 4.2 $MPa^{1/2}$, when compared to a HSP sphere radius of $R_{0,\text{PLA}} \approx 8$ $MPa^{1/2}$ for PLA) could explain the difficulty of removing all traces in the drying process.

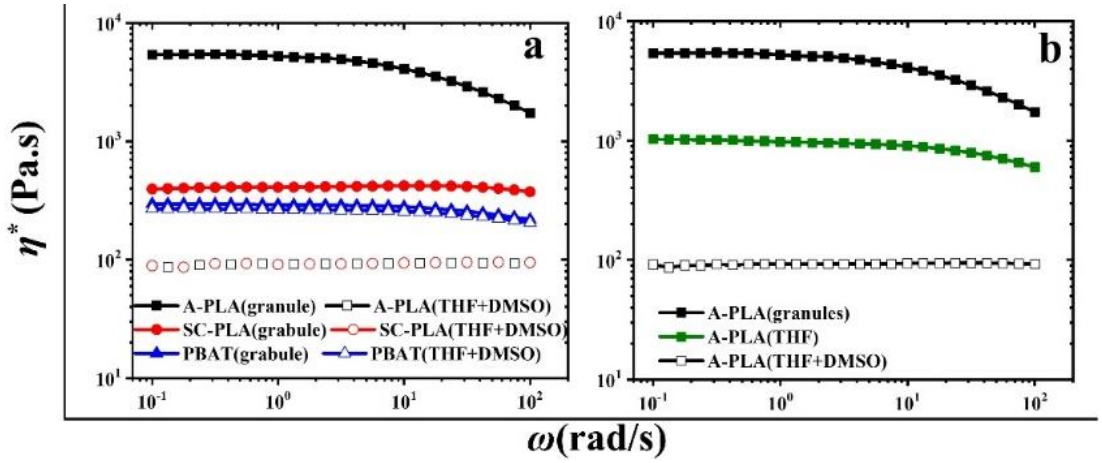

Figure 5.4 (a) Effect of the solution casting method on the complex viscosity, η^*, of the neat A-PLA, SC-PLA, and PBAT; filled symbols: granules of polymers as received and open symbols: polymers from solution casting and (b) effect of THF and DMSO on the complex viscosity, η^*, of the neat A-PLA

To confirm the presence of DMSO in the PLA matrices and its absence in PBAT, an elemental analysis, through energy dispersive X-ray spectroscopy (EDS), was carried out on neat PLA and PBAT samples casted in mixtures of THF and DMSO. EDS may notably detect the atomic content in terms of C, O, and S atoms. Excluding hydrogen, PLA (repeating $C_3H_4O_2$ units) has a theoretical C/O/S atomic composition of ~60/40/0 atomic At.%. PBAT ranges between roughly 75/25/0 and 72/28/0 At.% depending on the ratio of $C_{12}H_{12}O_4$ and $C_{10}H_{16}O_4$ units. Experimentally, A-PLA had a C/O/S composition of ~56.2/43.3/0.5 At.%, SC-PLA stood at ~54.9/44.7/0.4 At.%, and PBAT at ~64.7/35.3/0 At.%. In the absence of CNCs, which are slightly sulfated, polymer matrices should be totally sulfur-free. The sulfur content, detected in the PLAs, may hence be attributed to DMSO

traces. Atomic ratio of 0.4 and 0.5 At.% roughly translates into a DMSO ($SO(CH_3)_2$) content that ranges between 2 and 2.5 wt% in the PLAs (a more precise estimation by weight would require the determination of the hydrogen content). The significant quantity of DMSO was obtained despite 8 days of drying in a vacuum oven at 70°C and is coherent with the significant plasticizing effect observed on the complex viscosity of these matrices (Figures 5.3 and 5.4 a and b). It is remarkable that, under the same drying protocol, DMSO could be fully evaporated in PBAT. We attribute this both to the lower-molecular weight of PBAT and to the fact that the drying process was conducted at a temperature of 70 °C that matches the crystallization point of PBAT; hence, crystallization of PBAT chains may have favored solvent removal in PBAT samples. SC-PLA crystallizes at higher temperatures (closer to 100-110 °C) [35]. It is worth noting that, while all samples are richer than expected in oxygen, the deviation is smaller for A-PLA (~3 At.%), than for SC-PLA (~5 At.%) and PBAT (~7-10 At.%). This remains true even once corrected by the small influence of DMSO traces on the oxygen over carbon ratio. THF (C_4H_8O), with an oxygen of 20 At.% (excluding hydrogens) cannot be held responsible for the enrichment in O. However, this observation is coherent with the ranking of the various polymers in terms of molecular weights: they have hydroxyl-rich end-groups, which should slightly increase the overall oxygen ratio. The effect is expected to be stronger for short polymer chains (PBAT or SC-PLA) than for their longer counterparts (A-PLA) that have fewer end groups per weight of matrices.

Elemental analysis is unable to detect THF traces in the matrices due to its lack of distinctive elements. Figure 5.5 reports the normalized Fourier-transform infrared spectroscopy (FTIR) spectra of the neat A-PLA prepared via the various protocols. A-PLA was chosen because it was the most affected by the solution casting. The spectra intensities were normalized to 1 with respect to the main PLA peak (~1082 cm^{-1}) to facilitate the comparison. The main difference between the spectrum of A-PLA granules and those of the polymer prepared from THF or THF/DMSO lies in the 2850-3000 cm^{-1} wavenumber region. A-PLA from granules shows small peaks at ~2850, ~2918, ~2952, and ~2995 cm^{-1} that can be attributed to the presence of CH and CH_3 bonds in the polymer chains. The two first peaks (~2850 and ~2918 cm^{-1}) are accentuated significantly in samples cast from THF and THF+DMSO with nearly double and triple intensities with respect both to the last peaks (~2952 and ~2995 cm^{-1}) and to the main PLA peak (~1082 cm^{-1}). Since THF and DMSO's main peaks in the area are doublets that show at ~2865-2975 cm^{-1} and ~2905-2990 cm^{-1}, respectively, the shift in relative intensities cannot, hence, directly be attributed to the presence of

THF and DMSO. However, it seems that traces of solvent from solution casting alter the interaction patterns of CH and CH_3 groups in PLA. Similarly, to what was observed in the frequency sweep (Figure 5.4 b), the influence of solution casting is visible in A-PLA casted with THF, and further accentuated in samples casted with THF+DMSO.

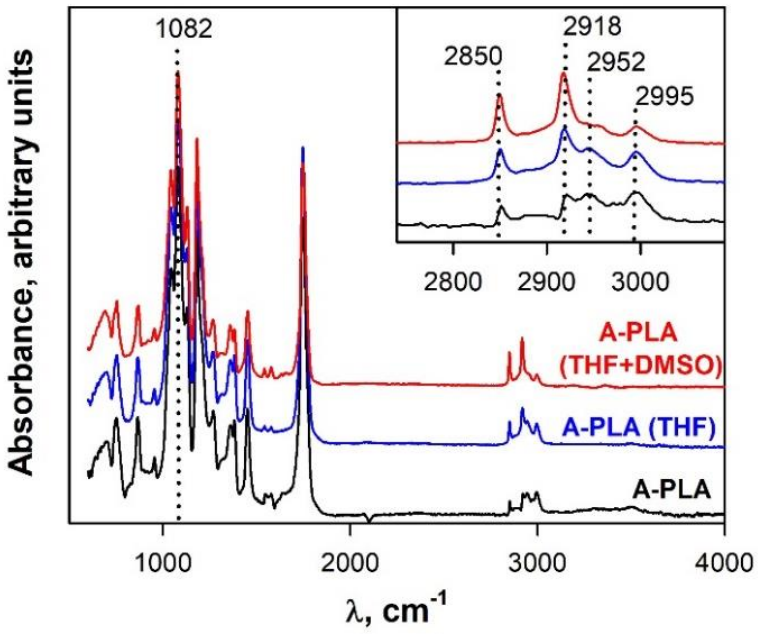

Figure 5.5 FTIR of granules and solution casted samples of neat A-PLA

5.4.2.3 **Linear viscoelastic region and apparent yield stress**

Strain-sweep tests were conducted to determine the range of the linear viscoelasticity (LVE) region, and the results are presented in Figures 5.6a-c. The maximum strain amplitude, γ_{max}^{0}, is obtained by drawing the horizontal (small dotted) and the straight (small dashed) lines in the LVE and non-LVE region (above the yielding point), respectively, and finding the intercept of those lines (circles) as shown in Figures 5.6a-c and reported in Table 5.1 [22]. The figure highlights how the maximum strain amplitude decreases significantly with increasing CNC content in all the nanocomposites. The values of the maximum strain amplitude decrease from 0.09 to 0.003, 0.08 to 0.02, and 0.04 to 0.01 in the A-PLA, SC-PLA, and PBAT, respectively. The shortening of the LVE region is an indication that the network structure formed in the nanocomposites can be easily broken by strain. We note that for the three neat polymers, the LVE region was observed up to an

imposed strain amplitude of 1. Our results confirm those reported for other polymer nanocomposite systems in the literature [22], [53]–[55].

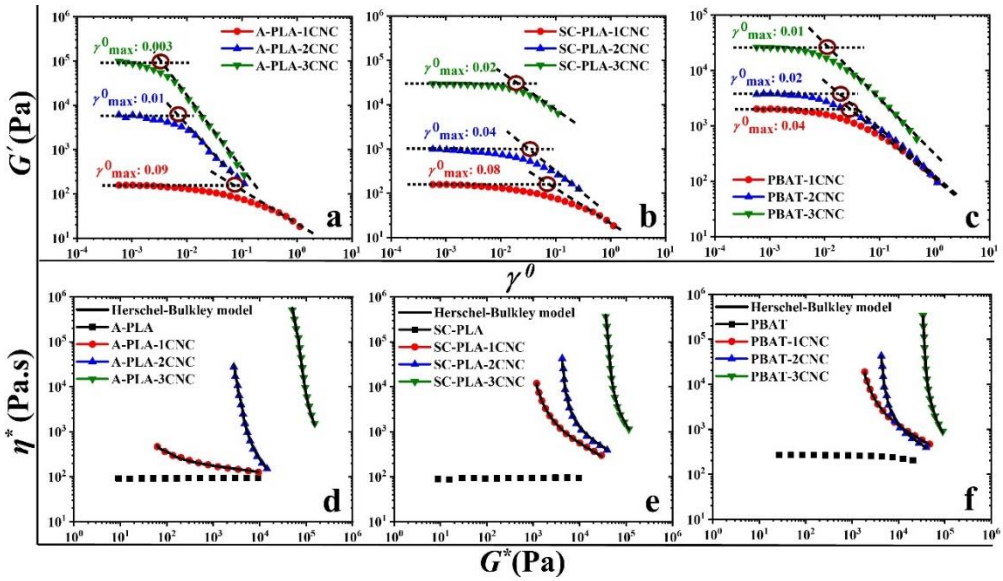

Figure 5.6 (a, b, and c) Strain sweeps and (d, e, and f) complex viscosity, η^*, versus the complex modulus, G^*, for A-PLA, SC-PLA, and PBAT containing CNC with different concentrations. The circles in (a, b, and c) highlight the intersections between the straight dotted lines that characterize the LVE region and inclined dashed lines of the high strain region. The continuous lines in (d, e, and f) are the fits of the modified Herschel–Bulkley model (Equation 5.4)

Table 5.1 Yield stress, melt flow index, and percolation threshold of the nanocomposites

Material		Max. strain amplitude	Yield stress and melt flow index			Percolation threshold
Matrix	Sample	γ^0_{max} [a]	$\sigma_0 = G^*_0 \gamma^0_{max}$ [b]	k	n	$m_c G$ [c]
		. . .	Pa	Pa.s^n	…	wt%
A-PLA	A-PLA-1CNC	0.09	2.73	158	0.89	1
	A-PLA -2CNC	0.01	28.0	120	0.52	
	A-PLA -3CNC	0.003	150	450	0.40	
SC-PLA	SC-PLA -1CNC	0.08	68.3	580	0.64	0.3
	SC-PLA -2CNC	0.04	135	600	0.65	
	SC-PLA -3CNC	0.02	724	1150	0.45	
PBAT	PBAT-1CNC	0.04	54.2	720	0.64	0.3
	PBAT-2CNC	0.02	77.2	450	0.65	
	PBAT-3CNC	0.01	294	550	0.40	

(a) Based on the intersection between the lines of storage modulus in LVE and high strain regions. This parameter was used as an input in the modified Herschel–Bulkley model (Equation 5.4)

(b) Modified Herschel–Bulkley model (Equation 5.4, Figures 5.6 d, e, and f)

(c) Based on Equation 5.5

Both the increases in the complex viscosity and the plateau value of the storage modulus at low frequencies are indications of the CNC good dispersion and the formation of an interconnected network. Its strength may be estimated by calculating the apparent yield stress and threshold concentration at which it forms. In all the nanocomposite systems, η^* tends toward infinity at low G^* suggesting the presence of an apparent yield stress that can be estimated by fitting the data of Figures 5.6d-f using the modified Hershel-Bulkley model written as:

$$\eta^* = \frac{\sigma_0}{\gamma_{max}^0 \omega} + k\left(\gamma_{max}^0 \omega\right)^{n-1} \qquad \text{Equation 5.4}$$

In this modified Herschel-Bulkley model (Equation 5.4), σ_0 is the apparent yield stress, γ_{max}^0 is the maximum strain amplitude of the LVE region, k is a parameter, and n is the flow index. σ_0, k, and n obtained by fitting the Herschel-Bulkley model to the complex viscosity data are reported in Table 5.1. As shown in Figures 5.6d-f the model gives very good fits of the data for all the nanocomposite systems (root mean square deviation (RMDS) ~ 0.003 Pa.s). It is worth noting that in Equation 5.4 we used the maximum strain amplitude from LVE data whereas most authors used the strain amplitude at which the SAOS data were obtained. The use of the maximum strain amplitude seems to be more appropriate for defining the yield stress.

As reported in Table 5.1, the apparent yield stress increases, and n decreases with increasing CNC content. This behavior is an indication of strong particle-particle and particle-polymer interactions and a decreased mobility of the polymer chains in the nanocomposites [56], [57]. The improved dispersion that is achievable for CNCs in SC-PLA and PBAT, when compared to A-PLA, has an obvious effect on the fitted values of the apparent yield stress and their dependency on CNC content (Table 5.1). Whereas σ_0 increases from 2.73 to 150 Pa in A-PLA, it increases from 68.3 and 54.2 to 724 and 294 Pa in SC-PLA and PBAT, respectively. Bagheriasl et al. [21] obtained a value of

217 Pa for the same SC-PLA/3CNC but from cast films in DMF; this is three times lower than our finding, and after using the strain amplitude (much smaller than the maximum) at which the SAOS data were obtained. It confirms the effectiveness of our solution casting method using two solvents. In another work, Vatanserver et al. [52] could not obtain any apparent yield stress for the A-PLA below 7 wt% CNCs. Finally, we note that the flow index, *n*, as a characteristics of shear thinning, is decreasing with the CNC content for the A-PLA nanocomposites; its value for the SC-PLA and PBAT systems is about constant for 1 and 2 wt% CNCs, but decreases significantly for 3 wt%. However, the variation of the consistency parameter *k* is not coherent, and this stresses the limitation of empirical models such as that of Equation 5.4.

5.4.2.4 **Rheological percolation threshold**

The onset of CNC percolation network corresponds to the concentration at which the rheological properties will dramatically increase. It can be calculated by fitting an empirical power-law model to the data of the storage modulus versus CNC content (Equation 5.5) [57]. The storage modulus was calculated by considering its value at the lowest frequency probed in the frequency sweep tests (0.1 rad/s).

$$G' = \beta_c G \left(\frac{m - m_c G}{m_c G} \right)^{n_2} \qquad \text{for } m > m_c G \qquad \text{Equation 5.5}$$

In this equation $\beta_c G$ and n_2 are power-law constants, *m* is the CNC concentration (wt%) and $m_c G$ is the rheological percolation threshold (wt%) [17], [21], [52], [57]–[59]. By fitting this empirical model to the rheological data plotted in Figure 5.7, percolation thresholds of 1, 0.3, and 0.3 wt% could be calculated for CNC nanocomposites based on A-PLA, SC-PLA, and PBAT, respectively. The quality of the fits for the SC-PLA and PBAT systems wt% is not very good, possibly due to the lack of sufficient data in the low concentration range. These results nevertheless confirm the rheological data and microscopic analysis that CNC dispersion is favored in low molecular weight and crystalline PLA such as SC-PLA [52]. As a comparison, Bagheriasl et al. [21] obtained a value of 0.66 wt% for the percolation threshold of the same SC-PLA/CNC nanocomposites: the only difference with our protocol arises on the fact that they used DMF both to disperse the CNCs and dissolve the polymer, while we used two solvents. The only study on A-PLA/CNC (led with the same amorphous PLA than in this study) was conducted by Vatanserver et al. [52] who reported a

percolating threshold value of 7.8 wt%, considerably larger than the value of 1 wt% obtained in this work. To the best of our knowledge, this work is the first to report apparent yield stress and percolating threshold concentration of CNCs for PBAT. Overall, CNCs have a very similar effect on the rheological properties of SC-PLA and PBAT. This may be related to the similar HSP distances between CNCs and PLA and PBAT, (14.9 $MPa^{1/2}$ compared to16.3 $MPa^{1/2}$). Hence, the chemical affinity between CNCs and the matrices is similar for both systems. However, the lower rheological improvements observed in A-PLA when compared to SC-PLA show clearly that parameters other than chemical affinity could affect the properties although that the HSP parameters for PLA could be affected considerably by its structure.

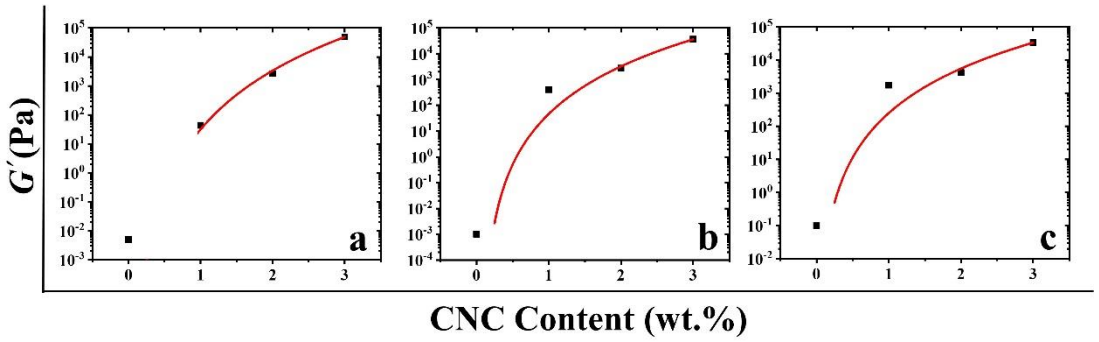

Figure 5.7 Storage modulus of the (a) A-PLA/CNC, (b) SC-PLA/CNC, (c) PBAT/CNC nanocomposites as a function of the CNC loading obtained at 170 °C and ω = 0.1 rad s^{-1}. The lines are the fits of the power-law expression (Equation 5.5).

5.5 Conclusion

A-PLA, SC-PLA, and PBAT respective nanocomposites incorporating CNC were prepared through solvent casting using a protocol based on two solvents. They were selected using a thermodynamic approach relying on the Hansen solubility parameter (HSP) theory in order to optimize the dispersion of the CNCs and the dissolution of the polymers. Both microscopy and rheology analysis were employed to investigate the effectiveness of this approach. AFM micrographs highlighted high degrees of CNC dispersion and distribution in the low molecular weight and crystalline SC-PLA and PBAT. In A-PLA, however, CNCs formed small bundles that were homogeneously distributed in the matrix. This level of dispersion was confirmed through spectacular increases of SAOS data and the maximum strain amplitude that represents the upper

limit of the linear viscoelastic region was found to decrease significantly with increasing CNC content. The complex viscosity and storage modulus increased dramatically upon the addition of 1, 2, and 3 wt% CNCs. The presence of a 3D network was evidenced by the determination of an apparent yield stress by fitting a modified Herschel-Bulkely model to the SAOS data. The percolation threshold concentration, calculated using an empirical power-law model fitted to the rheological data of the storage modulus as a function of CNC concentration, was as low as 1 wt% for A-PLA and 0.3 wt% for both SC-PLA and PBAT. Finally, the effect of solvent traces on the rheological and morphological properties of A-PLA, SC-PLA, and PBAT was investigated. The small amount of solvents significantly decreased the complex viscosity of SC-PLA and A-PLA by 1 and 2 orders of magnitude, respectively. This was not observed in PBAT and it is suggested that the crystallization of PBAT at the drying temperature (70 °C) may have favored the removal of solvent traces in PBAT. The rheological properties and morphological analysis investigated in this article highlight the effectiveness of solvent selection on the dispersion and distribution of CNCs, which in turn contributes to the formation of 3D networks in the A-PLA, SC-PLA, and PBAT matrices.

5.6 Acknowledgments

Financial support from the Natural Science and Engineering Research Council (NSERC) of Canada is gratefully acknowledged. The authors are also grateful to FPInnovations for providing the CNCs. The Fond de Recherche du Québec - Nature et Technologies (FRQNT) kindly provided a scholarship to C. Bruel. The authors also wish to acknowledge the help of Dr. Helia Sojoudiasli and Mr. Matthieu Gauthier for the material preparation and processing. Finally, we wish to thank Mr. Jed Randall from NatureWorks for providing one of the PLA samples.

5.7 References

[1] A. L. Andrady and M. A. Neal, “Applications and societal benefits of plastics,” *Philos. Trans. R. Soc. B Biol. Sci.*, vol. 364, no. 1526, pp. 1977–1984, Jul. 2009, doi: 10.1098/rstb.2008.0304.

[2] Y. Tokiwa, B. Calabia, C. Ugwu, and S. Aiba, “Biodegradability of Plastics,” *Int. J. Mol. Sci.*, vol. 10, no. 9, pp. 3722–3742, Aug. 2009, doi: 10.3390/ijms10093722.

[3] M. Rujnić-Sokele and A. Pilipović, “Challenges and opportunities of biodegradable plastics: A mini review,” *Waste Manag. Res.*, vol. 35, no. 2, pp. 132–140, 2017, doi: 10.1177/0734242X16683272.

[4] M. Nofar, D. Sacligil, P. J. Carreau, M. R. Kamal, and M.-C. Heuzey, “Poly (lactic acid) blends: Processing, properties and applications,” *Int. J. Biol. Macromol.*, vol. 125, pp. 307–360, 2018, doi: 10.1016/j.ijbiomac.2018.12.002.

[5] F. V. Ferreira, L. S. Cividanes, R. F. Gouveia, and L. M. F. Lona, “An overview on properties and applications of poly(butylene adipate- co -terephthalate)-PBAT based composites,” *Polym. Eng. Sci.*, vol. 59, no. s2, pp. E7–E15, Mar. 2019, doi: 10.1002/pen.24770.

[6] Y. Tokiwa and B. P. Calabia, “Biodegradability and biodegradation of poly(lactide),” *Appl. Microbiol. Biotechnol.*, vol. 72, no. 2, pp. 244–251, Sep. 2006, doi: 10.1007/s00253-006-0488-1.

[7] J.-M. Raquez, Y. Habibi, M. Murariu, and P. Dubois, “Polylactide (PLA)-based nanocomposites,” *Prog. Polym. Sci.*, vol. 38, no. 10–11, pp. 1504–1542, Oct. 2013, doi: 10.1016/j.progpolymsci.2013.05.014.

[8] J. Jian, Z. Xiangbin, and H. Xianbo, “An overview on synthesis, properties and applications of poly(butylene-adipate-co-terephthalate)–PBAT,” *Adv. Ind. Eng. Polym. Res.*, vol. 3, no. 1, pp. 19–26, Jan. 2020, doi: 10.1016/j.aiepr.2020.01.001.

[9] I. F. Pinheiro *et al.*, “Mechanical, rheological and degradation properties of PBAT nanocomposites reinforced by functionalized cellulose nanocrystals,” *Eur. Polym. J.*, vol. 97, pp. 356–365, 2017, doi: 10.1016/j.eurpolymj.2017.10.026.

[10] A. Dufresne, “Cellulose nanomaterials as green nanoreinforcements for polymer nanocomposites,” *Philos. Trans. R. Soc. A*, vol. 376, no. 2112, p. 20170040, Feb. 2018, doi: 10.1098/rsta.2017.0040.

[11] K. Oksman *et al.*, “Review of the recent developments in cellulose nanocomposite processing,” *Compos. Part A Appl. Sci. Manuf.*, vol. 83, pp. 2–18, Apr. 2016, doi: 10.1016/j.compositesa.2015.10.041.

[12] C. Miao and W. Y. Hamad, “Critical insights into the reinforcement potential of cellulose nanocrystals in polymer nanocomposites,” *Curr. Opin. Solid State Mater. Sci.*, vol. 23, no. 4, p. 100761, Aug. 2019, doi: 10.1016/j.cossms.2019.06.005.

[13] V. Heshmati, M. R. Kamal, and B. D. Favis, “Tuning the localization of finely dispersed cellulose nanocrystal in poly (lactic acid)/bio-polyamide11 blends,” *J. Polym. Sci. Part B Polym. Phys.*, vol. 56, no. 7, pp. 576–587, 2018, doi: 10.1002/polb.24563.

[14] F. Rol, M. N. Belgacem, A. Gandini, and J. Bras, “Recent advances in surface-modified cellulose nanofibrils,” *Progress in Polymer Science*, vol. 88. pp. 241–264, Jan. 2019, doi: 10.1016/j.progpolymsci.2018.09.002.

[15] C. Wu, X. Zhang, X. Wang, Q. Gao, and X. Li, “Surface modification of cellulose nanocrystal using succinic anhydride and its effects on poly(butylene succinate) based composites,” *Cellulose*, vol. 26, no. 5, pp. 3167–3181, Mar. 2019, doi: 10.1007/s10570-019-02292-5.

[16] C. L. Morelli, M. N. Belgacem, M. C. Branciforti, M. C. B. Salon, J. Bras, and R. E. S. Bretas, “Nanocomposites of PBAT and cellulose nanocrystals modified by in situ polymerization and melt extrusion,” *Polym. Eng. Sci.*, vol. 56, no. 12, pp. 1339–1348, 2016, doi: 10.1002/pen.24367.

[17] A. Gupta, W. Simmons, G. T. Schueneman, D. Hylton, and E. A. Mintz, “Rheological and thermo-mechanical properties of poly(lactic acid)/lignin-coated cellulose nanocrystal composites,” *ACS Sustain. Chem. Eng.*, vol. 5, no. 2, pp. 1711–1720, Feb. 2017, doi: 10.1021/acssuschemeng.6b02458.

[18] A. Dufresne, “Cellulose nanomaterial reinforced polymer nanocomposites,” *Curr. Opin. Colloid Interface Sci.*, vol. 29, pp. 1–8, May 2017, doi: 10.1016/j.cocis.2017.01.004.

[19] F. V. Ferreira *et al.*, “How do cellulose nanocrystals affect the overall properties of biodegradable polymer nanocomposites: A comprehensive review,” *Eur. Polym. J.*, vol. 108, pp. 274–285, Nov. 2018, doi: 10.1016/j.eurpolymj.2018.08.045.

[20] C. L. Morelli, N. Belgacem, R. E. S. Bretas, and J. Bras, “Melt extruded nanocomposites of polybutylene adipate- co -terephthalate (PBAT) with phenylbutyl isocyanate modified cellulose nanocrystals,” *J. Appl. Polym. Sci.*, vol. 133, no. 34, Sep. 2016, doi: 10.1002/app.43678.

[21] D. Bagheriasl, P. J. Carreau, B. Riedl, C. Dubois, and W. Y. Hamad, “Shear rheology of polylactide (PLA)–cellulose nanocrystal (CNC) nanocomposites,” *Cellulose*, vol. 23, no. 3, pp. 1885–1897, 2016, doi: 10.1007/s10570-016-0914-1.

[22] M. R. Kamal and V. Khoshkava, “Effect of cellulose nanocrystals (CNC) on rheological and mechanical properties and crystallization behavior of PLA/CNC nanocomposites,” *Carbohydr. Polym.*, vol. 123, pp. 105–114, 2015, doi: 10.1016/j.carbpol.2015.01.012.

[23] G. Da Silva Gois *et al.*, “Soil biodegradation of PLA/CNW nanocomposites modified with ethylene oxide derivatives,” *Mater. Res.*, vol. 20, pp. 899–904, 2017, doi: 10.1590/1980-5373-MR-2016-0960.

[24] A. P. Mathew, K. Oksman, and M. Sain, “Mechanical properties of biodegradable composites from poly lactic acid (PLA) and microcrystalline cellulose (MCC),” *J. Appl. Polym. Sci.*, vol. 97, no. 5, pp. 2014–2025, Sep. 2005, doi: 10.1002/app.21779.

[25] I. F. Pinheiro, F. V. Ferreira, G. F. Alves, A. Rodolfo, A. R. Morales, and L. H. I. Mei, “Biodegradable PBAT-Based Nanocomposites Reinforced with Functionalized Cellulose Nanocrystals from Pseudobombax munguba: Rheological, Thermal, Mechanical and Biodegradability Properties,” *J. Polym. Environ.*, vol. 27, no. 4, pp. 757–766, Apr. 2019, doi: 10.1007/s10924-019-01389-z.

[26] S. Mohanty and • S K Nayak, “Biodegradable Nanocomposites of Poly(butylene adipate-co-terephthalate) (PBAT) and Organically Modified Layered Silicates,” *Springer*, vol. 20, no. 1, pp. 195–207, Mar. 2012, doi: 10.1007/s10924-011-0408-z.

[27] V. Khoshkava and M. R. Kamal, “Effect of cellulose nanocrystals (CNC) particle morphology on dispersion and rheological and mechanical properties of polypropylene/CNC nanocomposites,” *ACS Appl. Mater. Interfaces*, vol. 6, no. 11, pp. 8146–8157, 2014, doi: 10.1021/am500577e.

[28] E. Vatansever, D. Arslan, and M. Nofar, “Polylactide cellulose-based nanocomposites,” *Int. J. Biol. Macromol.*, vol. 137, pp. 912–938, Sep. 2019, doi: 10.1016/j.ijbiomac.2019.06.205.

[29] F. Safdari, D. Bagheriasl, P. J. Carreau, M. C. Heuzey, and M. R. Kamal, “Rheological, Mechanical, and thermal properties of polylactide/cellulose nanofiber biocomposites,” *Polym. Compos.*, vol. 39, no. 5, pp. 1752–1762, May 2018, doi: 10.1002/pc.24127.

[30] J. Trifol *et al.*, “A comparison of partially acetylated nanocellulose, nanocrystalline cellulose, and nanoclay as fillers for high-performance polylactide nanocomposites,” *J. Appl. Polym. Sci.*, vol. 133, no. 14, Apr. 2016, doi: 10.1002/app.43257.

[31] N. Pal, P. Dubey, P. Gopinath, and K. Pal, “Combined effect of cellulose nanocrystal and reduced graphene oxide into poly-lactic acid matrix nanocomposite as a scaffold and its anti-bacterial activity,” *Int. J. Biol. Macromol.*, vol. 95, pp. 94–105, Feb. 2017, doi: 10.1016/j.ijbiomac.2016.11.041.

[32] C. L. Morelli, M. N. Belgacem, M. C. Branciforti, R. E. S. Bretas, A. Crisci, and J. Bras, “Supramolecular aromatic interactions to enhance biodegradable film properties through incorporation of functionalized cellulose nanocrystals,” *Compos. Part A Appl. Sci. Manuf.*, vol. 83, pp. 80–88, Apr. 2016, doi: 10.1016/j.compositesa.2015.10.038.

[33] T. Mukherjee *et al.*, “Chemically imaging the interaction of acetylated nanocrystalline cellulose (NCC) with a polylactic acid (PLA) polymer matrix,” *Cellulose*, vol. 24, no. 4, pp. 1717–1729, Apr. 2017, doi: 10.1007/s10570-017-1217-x.

[34] D. Bagheriasl and P. J. Carreau, “Polymer–Cellulose Nanocrystal (CNC) Nanocomposites,” in *Processing of Polymer Nanocomposites*, München: Carl Hanser Verlag GmbH & Co. KG, 2019, pp. 371–393.

[35] D. Bagheriasl, P. J. Carreau, B. Riedl, and C. Dubois, “Enhanced properties of polylactide by incorporating cellulose nanocrystals,” *Polym. Compos.*, vol. 39, no. 8, pp. 2685–2694, 2018, doi: 10.1002/pc.24259.

[36] F. V. Ferreira *et al.*, “Cellulose nanocrystal-based poly(butylene adipate-co-terephthalate) nanocomposites covered with antimicrobial silver thin films,” *Polym. Eng. Sci.*, vol. 59, no. s2, pp. E356–E365, Feb. 2019, doi: 10.1002/pen.25066.

[37] D. Bagheriasl, F. Safdari, P. J. Carreau, C. Dubois, and B. Riedl, “Development of cellulose nanocrystal-reinforced polylactide: A comparative study on different preparation methods,” *Polym. Compos.*, vol. 40, pp. E342–E349, Jan. 2019, doi: 10.1002/pc.24676.

[38] A. L. Goffin *et al.*, “From interfacial ring-opening polymerization to melt processing of cellulose nanowhisker-filled polylactide-based nanocomposites,” *Biomacromolecules*, vol. 12, no. 7, pp. 2456–2465, Jul. 2011, doi: 10.1021/bm200581h.

[39] V. Heshmati, M. R. Kamal, and B. D. Favis, “Cellulose nanocrystal in poly(lactic acid)/polyamide11 blends: Preparation, morphology and co-continuity,” *Eur. Polym. J.*, vol. 98, pp. 11–20, 2018, doi: 10.1016/j.eurpolymj.2017.10.027.

[40] A. Arias, M.-C. Heuzey, M. A. Huneault, G. Ausias, and A. Bendahou, “Enhanced dispersion of cellulose nanocrystals in melt-processed polylactide-based nanocomposites,” *Cellulose*, vol. 22, no. 1, pp. 483–498, Feb. 2015, doi: 10.1007/s10570-014-0476-z.

[41] J. Shojaeiarani, D. S. Bajwa, and N. M. Stark, “Spin-coating: A new approach for improving dispersion of cellulose nanocrystals and mechanical properties of poly (lactic acid) composites,” *Carbohydr. Polym.*, vol. 190, pp. 139–147, Jun. 2018, doi: 10.1016/j.carbpol.2018.02.069.

[42] W. Y. Hamad and T. Q. Hu, “Structure-process-yield interrelations in nanocrystalline cellulose extraction,” *Can. J. Chem. Eng.*, vol. 88, no. 3, pp. 392–402, Jun. 2010, doi: 10.1002/cjce.20298.

[43] C. M. Hansen, “The Three Dimensional Solubility Parameter and Solvent Diffusion Coefficient,” *J. Paint Technol.*, vol. 39, pp. 104–117, 1967, Accessed: Aug. 29, 2020. [Online]. Available: https://www.hansen-solubility.com/contents/HSP1967-OCR.pdf.

[44] C. Bruel, Q. Beuguel, J. R. Tavares, P. J. Carreau, and M.-C. Heuzey, “The apparent structural hydrophobicity of cellulose nanocrystals,” *J. Sci. Technol. For. Prod. Process.*, vol. 7, no. 4, pp. 13–23, 2018.

[45] C. Bruel, J. R. Tavares, P. J. Carreau, and M. C. Heuzey, “The structural amphiphilicity of cellulose nanocrystals characterized from their cohesion parameters,” *Carbohydr. Polym.*, vol. 205, pp. 184–191, 2019, doi: 10.1016/j.carbpol.2018.10.026.

[46] C. Bruel, T. S. Davies, P. J. Carreau, J. R. Tavares, and M.-C. Heuzey, “Self-assembly behaviors of colloidal cellulose nanocrystals: A tale of stabilization mechanisms,” *J. Colloid Interface Sci.*, vol. 574, pp. 399–409, Aug. 2020, doi: 10.1016/j.jcis.2020.04.049.

[47] C. Bruel, J. R. Tavares, P. J. Carreau, and M. Heuzey, “Impact of Colloidal Stability on Cellulose Nanocrystals Self-Ordering in Thin Films,” *TechConnect Briefs*, no. 1, pp. 61–64, 2019.

[48] C. M. Hansen, *Hansen Solubility Parameters*. Boca Raton: CRC Press, 2007.

[49] Q. Beuguel, D. Bagheriasl, C. Bruel, J. R. Tavares, P. J. Carreau, and M.-C. Heuzey, “Comportement rhéologique à l’état fondu de nanocomposites à base de nanocristaux de cellulose (CNCs),” *Rhéologie*, vol. 34, pp. 10–16, 2018.

[50] S. Abbott, C. M. Hansen, and H. Yamamoto, *Hansen solubility parameters in practice software, ebook, datasets. http://www.hansen-solubility.com. Accessed 03 July 2018*.

[51] V. Khoshkava and M. R. Kamal, "Effect of surface energy on dispersion and mechanical properties of polymer/nanocrystalline cellulose nanocomposites," *Biomacromolecules*, vol. 14, no. 9, pp. 3155–3163, 2013, doi: 10.1021/bm400784j.

[52] E. Vatansever, D. Arslan, D. S. Sarul, Y. Kahraman, and M. Nofar, "Effects of molecular weight and crystallizability of polylactide on the cellulose nanocrystal dispersion quality in their nanocomposites," *Int. J. Biol. Macromol.*, vol. 154, pp. 276–290, Mar. 2020, doi: 10.1016/j.ijbiomac.2020.03.115.

[53] G. Galgali, C. Ramesh, and A. Lele, "Rheological study on the kinetics of hybrid formation in polypropylene nanocomposites," *Macromolecules*, vol. 34, no. 4, pp. 852–858, Feb. 2001, doi: 10.1021/ma000565f.

[54] R. Krishnamoorti and E. P. Giannelis, "Rheology of end-tethered polymer layered silicate nanocomposites," *Macromolecules*, vol. 30, no. 14, pp. 4097–4102, Jul. 1997, doi: 10.1021/ma960550a.

[55] M. J. Solomon, A. S. Almusallam, K. F. Seefeldt, A. Somwangthanaroj, and P. Varadan, "Rheology of polypropylene/clay hybrid materials," *Macromolecules*, vol. 34, no. 6, pp. 1864–1872, Mar. 2001, doi: 10.1021/ma001122e.

[56] J. Jeddi, O. Yousefzade, A. Babaei, S. Ghanbar, and A. Rostami, "Morphology, microstructure and rheological properties of SAN (styrene-acrylonitrile)/EPDM (ethylene-propylene-diene monomer) nanocomposites: Investigating the role of organoclay type and order of mixing," *Mater. Chem. Phys.*, vol. 187, pp. 191–202, Feb. 2017, doi: 10.1016/j.matchemphys.2016.12.001.

[57] S. Abbasi, P. J. Carreau, A. Derdouri, and M. Moan, "Rheological properties and percolation in suspensions of multiwalled carbon nanotubes in polycarbonate," *Rheol. Acta*, vol. 48, no. 9, pp. 943–959, Jul. 2009, doi: 10.1007/s00397-009-0375-7.

[58] G. Hu, C. Zhao, S. Zhang, M. Yang, and Z. Wang, "Low percolation thresholds of electrical conductivity and rheology in poly(ethylene terephthalate) through the networks of multi-walled

carbon nanotubes," *Polymer (Guildf).*, vol. 47, no. 1, pp. 480–488, Jan. 2006, doi: 10.1016/j.polymer.2005.11.028.

[59] F. Du, R. C. Scogna, W. Zhou, S. Brand, J. E. Fischer, and K. I. Winey, "Nanotube networks in polymer nanocomposites: Rheology and electrical conductivity," *Macromolecules*, vol. 37, no. 24, pp. 9048–9055, Nov. 2004, doi: 10.1021/ma049164g.

CHAPTER 6 ARTICLE 2: MORPHOLOGICAL AND RHEOLOGICAL PROPERTIES OF PLA, PBAT, AND PLA/PBAT BLEND NANOCOMPOSITES CONTAINING CNCS[2]

Mojtaba Mohammadi [1], Marie-Claude Heuzey [1], Pierre J. Carreau [1,*] and Aurélie Taguet [2]

1) *Center for High Performance Polymer and Composite systems (CREPEC), Department of Chemical Engineering, École Polytechnique de Montréal, Montreal, QC H3T 1J4, Canada*

2) *Polymers Composites and Hybrids (PCH), IMT Mines Ales, 30319 Ales, France*

6.1 Abstract

Morphological and rheological properties of poly(lactic acid), PLA (semicrystalline and amorphous), and poly(butylene adipate-co-terephthalate), PBAT, and their blends (75 wt%/25 wt%; PLA/PBAT) were investigated in the presence of cellulose nanocrystals (CNCs) prepared from solution casting followed by melt mixing. For the solution casting step, the CNCs were either incorporated into the matrix, the dispersed phase, or both. The dispersion and distribution of the CNCs in the neat polymers and localization in their blends were analyzed via scanning electron microscopy (SEM) and atomic force microscopy (AFM). The highly dispersed CNCs in the solution cast nanocomposites were agglomerated after melt mixing. In the blends with 1 wt% CNCs, the nanoparticles were mostly localized on the surface of the PBAT droplets irrespective of their initial localization. The rheological behavior of the single polymer matrix nanocomposites and their blends was determined in dynamic and transient shear flow in the molten state. Upon melt mixing the complex viscosity and storage modulus of the solution cast nanocomposites decreased markedly due to re-agglomeration of the CNCs. Under shearing at 0.1 s^{-1}, a significant droplet coalescence was observed in the neat blends, but was prevented by the presence of the CNCs at the interface in the blend nanocomposites.

---

[2] Published in Nanomaterials, *11*(4), 857. (2021)

Keywords: cellulose nanocrystals**;** PLA; PBAT; CNC localization; blends; nanocomposites; rheology; morphology

6.2 Introduction

Over recent years, poly(lactic acid) (PLA) has received remarkable attention mainly because it is a bio-based, biodegradable under specific conditions, biocompatible, and non-toxic polymer [1]. However, PLA suffers from serious drawbacks such as low melt strength, low and slow crystallization rate, poor processability, low toughness, low service temperature, and high brittleness [2]. Polymer blending is one of the most commonly used and practical approaches to improve the properties of PLA [3], [4]. One of the most promising polymers to blend with PLA is poly(butylene adipate-co-terephthalate) (PBAT) with high flexibility and ductility features [5]. Jalali Dil et al. [6] investigated the morphology, miscibility and co-continuity development of a PLA/PBAT blend. They showed that the co-continuity region of the PLA/PBAT blend starts at a PBAT volume fraction between 30 and 40% [6]. Different studies revealed a low interfacial tension of around 1 mN/m for the PLA/PBAT system [7].

The final performance of polymer blends can be increased by introducing nanoparticles as reinforcements [8], [9]. The localization of nano-inclusions at the interface, in the matrix, or dispersed phase can have a significant effect on the blend properties [8], [10]. These localizations are affected by thermodynamics [11] and processing parameters such as the sequence of mixing [12], [13], the viscosity of polymer components [13], [14] as well as the quality of the particle dispersion and nature of the particles [15].

Different localizations have been investigated through the incorporation of different nanoparticles in PLA/PBAT blends such as nano-silica [13], [16], carbon nanotube [12,17,18], graphene [17], [18], and nano-clay [17], [19]–[22]. Jalali Dil et al. [16] investigated the droplet/matrix and co-continuous morphology of PLA/PBAT (70/30 and 50/50, respectively) in the presence of nano-silica. They reported that adding 1 wt% nano-silica decreased the droplet size from 1.7 to 1 µm and by increasing the amount of nano-silica the droplet-like morphology changed to a co-continuous state. Nofar et al. [21] investigated properties of 75/25 (wt%) PLA/PBAT blends containing an organo-modified nano-clay (Cloisite 30B). Similarly to thermodynamics predictions, the organoclay was located at the interface of the two phases, was found to act as a barrier against the

coalescence of droplets and stabilized the blend morphology under shear flow. Salehiyan et al. [23] also investigated the effects of selective localization of 1 wt% of carbon nanotubes, nano-silica, nano-clays, and graphene oxides on the morphology development and rheological properties of melt-processed PLA/PBAT blend nanocomposites.

One of the most promising nanoparticles is cellulose nanocrystal (CNCs), which is based on one of the most abundant resources in the environment and has the advantages of being non-toxic, biocompatible, and biodegradable. CNC has been used to increase the properties of various polymers, in particular PLA and PBAT. In our research group, solution casting methods were used to improve the morphology, rheological and mechanical properties of PLA/CNC and PBAT/CNC nanocomposites [24]–[28]. Bagheriasl et al. [24] used dimethylformamide (DMF) to prepare PLA/CNC nanocomposite and for the first time obtained a high degree of dispersion of pristine CNCs in PLA and reached a rheological percolation threshold at 0.66 wt% CNCs. Mohammadi et al. [28], based on a thermodynamics analysis, also identified that dimethyl sulfoxide (DMSO) and tetrahydrofuran (THF) were the best solvents for the dispersion of the CNCs and dissolution of semicrystalline PLA (scPLA) and amorphous PLA (aPLA)) as well as PBAT. They obtained the lowest rheological percolation threshold of 0.3 wt% CNCs in scPLA and PBAT and 1 wt% in aPLA [28]. They also showed that the complex viscosity dramatically decreased by one to two orders of magnitude for PLA due to the presence of residual solvent, but residual solvent did not affect PBAT, probably due to crystallization of the latter at the drying temperature (70 °C) [28].

There are many pieces of research on PLA blends containing CNCs. It can be categorized as PLA/poly-hydroxybutyrate (PHB)/freeze-dried-CNC [29]–[31], PLA/ polybutylene succinate (PBS)/CNC [32], [33], PLA/poly-vinyl alcohol (PVAc)/CNC [34], and PLA/natural rubber (NR)/CNC [35], [36]. However, none of these reports a very good dispersion of CNCs as shown by transmission electron microscopy (TEM) or atomic force microscopy (AFM) images. In a recent study, Sarul et al. [37] investigated the preparation of PLA/PBAT/CNC blend nanocomposites through solution casting followed by melt mixing via a twin-screw extruder. However, the authors did not report on the CNC dispersion in the neat polymers. Their analysis of the effect of the localization of CNCs was based on expectations from thermodynamics considerations and they did not present a microscopic analysis to localize the CNCs and confirm their thermodynamics analysis. They did not present a strong explanation on the rheological analysis section (with no information about the rheological properties of the single polymer matrices before and after melt

mixing). Heshmati et al. [38] reported a very good dispersion of spray-dried CNCs in PLA/PA11 blends, prepared through a combination of solvent casting and melting methods. They also prepared a masterbatch of both PLA/CNC and PA11/CNC and diluted them via melt mixing. They showed that irrespective of the preparing method the spray dried CNCs preferred to remain in the PA11 phase, which was the thermodynamically favorable phase. Heshmati et al. [39] also showed that using poly(ethylene oxide) (PEO) as a polymer carrier for CNCs in the blend of PLA/PA11 resulted in the localization of the CNCs in PLA, which was not the thermodynamically favorable phase for the CNCs.

The goal of this work is to investigate the effect of melt mixing on rheology and morphological properties of highly dispersed CNCs of solution cast PLA-based nanocomposites. Droplet coalescence during processing is avoided by controlling the localization of CNCs in PLA/PBAT blends. The blend composition was chosen as 75 wt% PLA and 25 wt% PBAT in order to have an emulsion-type (droplets) morphology while the concentration of PBAT is large enough to significantly affect the rheological properties of the blends.

6.3 Materials and Methods

6.3.1 Materials

Ingeo 4060D and 3251D were used as the amorphous PLA (aPLA) and the semicrystalline PLA (scPLA), respectively. They were purchased from NatureWorks LLC (Minnetonka, MN, USA). The PBAT (Ecoflex® FBX 7011) was purchased from BASF (Montreal, Canada). The aPLA has a weight average molecular weight of 190 kg/mol and a D-lactide content of 12 mol%, and scPLA has a weight average molecular weight of 55 kg/mol and a D-lactide content of 1.4 mol%. The PBAT has a weight average molecular weight of 24.4 kg/mol, a density of 1.23 g/cm^3, and a melt flow index (MFI) of 2 g/10 min. Freeze-dried CNCs were kindly provided by FP Innovations (Pointe-Claire, QC, Canada) with width, length, and aspect ratio of 16 ± 3, 90 ± 17 nm, and 6 ± 2, respectively [24]. Information on CNC preparation can be found elsewhere [40]. These CNCs were neutralized using sodium hydroxide (NaOH) before freeze-drying. N,N-dimethylformamide (DMF), anhydrous 99.8 %, was purchased from Sigma-Aldrich Canada Co. (Oakville, ON, Canada).

6.3.2 Single Polymer Matrix and Blend Nanocomposites Preparation

6.3.2.1 Single Polymer Matrix Nanocomposites Preparation

DMF was used to disperse and dissolve the CNCs and the neat polymers using a water bath sonicator and magnetic stirrer, respectively. After complete dispersion and dissolution of CNCs and neat polymers, they were further mixed using a magnetic stirrer. Then, the mixtures were poured into a petri dish and dried in an oven in two steps under air circulation and vacuum (the details and step by step preparation method is presented in the supplementary materials (SM)). The weight percentage of CNC within the nanocomposites was 0 (i.e., neat polymers for a comparison purposes), 1, and 3. The CNC content was reported based on weight percentage basis. In this regard, aPLA/3CNC denotes a nanocomposite made of the amorphous (high molecular weight) PLA containing 3 wt% CNCs, calculated as a percentage of total weight of the nanocomposites. The effect of melt mixing using a DDRV501 Brabender (C. W. Brabender Instruments Inc., South Hackensack, NJ, USA) was also investigated on previously dried single polymer matrix nanocomposites, operating at 180 °C, 100 rpm for 7 min under a nitrogen atmosphere. The term "+IMM" is used in the nomenclature to identify the effect of melt mixing on the samples from solution casting.

6.3.2.2 Blend Nanocomposites Preparation

Blend nanocomposites containing 75 wt% PLA and 25 wt % PBAT and, overall, 1 wt % CNCs were prepared from the nanocomposites as described above using the internal mixer (at 180 °C, 100 rpm for 7 min under a nitrogen atmosphere) and the detailed formulations are provided in Table 6.1. The schematic preparation method is provided in the SM (Figure 6.S1). In the first two mixing strategies, granules of the neat complementary polymer (dried overnight at 55 °C) were added to the polymer nanocomposites in the internal mixer. In the third strategy both PLA and PBAT nanocomposites containing 1 wt% prepared from solution casting were melt mixed in the internal mixer. For example, (PLA-1CNC)/PBAT (mixing strategy 1) represents the blend nanocomposites containing 1 wt% CNCs based on the whole blend for which the CNCs were initially localized in the matrix (PLA). Similarly, PLA/(PBAT-1CNC) and PLA/PBAT/1CNC refer to the blend nanocomposites when the CNCs were initially localized in the dispersed (PBAT) phase or both phases, respectively. Three different neat blends were prepared for comparison purposes:

neat PLA/PBAT blends from the granules (melt mixing), neat blends from solution casting, and neat blends from solution casting followed by the internal melt mixing.

A hydraulic press was used to prepare the rheological disk shape with 1.2 mm thickness and 25 mm in diameter. The compression molding process continued for 10 min at 180 °C under a nitrogen atmosphere including 4 min of heating and 6 min of progressive increasing pressure force from 1 to 3 tons. The rheological disk shapes were used for microscopy analysis.

Table 6.1 Mixing sequences to prepare the blend nanocomposites and final composition.

Notation	Mixing Steps	Real Final Composition, wt% Poly (lactic acid)/ poly (butylene adipate-co-terephthalate)/cellulose nanocrystals (PLA/PBAT/CNC)
PLA/PBAT granules	Mixing the neat PLA and PBAT granules using the internal mixer to prepare neat blends	75/25/0
PLA/PBAT	Mixing the neat PLA and PBAT granules using the solution casting to prepare neat blends	75/25/0
PLA/PBAT (+IMM)	Mixing the neat PLA and PBAT from solution casting followed by melt mixing via the internal mixer to prepare neat blends	75/25/0
(PLA-1CNC)/PBAT (Mixing strategy 1)	Mixing PLA/1.4CNC with PBAT granules via the internal mixer. CNCs were initially mixed with PLA	74.95/25/1.05
PLA/(PBAT-1CNC) (Mixing strategy 2)	Mixing PBAT/4CNC with PLA granules via the internal mixer CNCs were initially mixed with the PBAT	75/24/1.0
PLA/PBAT/1CNC (Mixing strategy 3)	Mixing PLA/1CNC and PBAT/1CNC. via the internal mixer CNCs were initially mixed with both PLA and PBAT	74.25/24.75/1.0

6.3.3 Characterization

6.3.3.1 **Scanning Electron Microscope (SEM)**

In order to determine the morphology and the localization of cellulose nanocrystals, the blends and blend nanocomposites were fractured in liquid nitrogen. A chromium-coated layer of 15 nm thickness was then applied to the samples. The morphology was observed under SEM (JSM 7600F, JEOL, Akishima, Tokyo 196-8558, JAPAN) at a voltage of 5 kV. The blend nanocomposites were

also observed (after cryofracture of a thickness of about 20 nm) using an environmental scanning electron microscope Quanta 200 FEG from FEI company, SEM operating at 3 kV.

The volume-average radius (R_v) of the dispersed phase domains was defined as follows (Equation 6.1):

$$R_v = \frac{\sum_i n_i R_i^4}{\sum_i n_i R_i^3} \quad \text{Equation 6.1}$$

where n_i is the number of dispersed domains with radii R_i counted from SEM images [41], for at least 250–350 PBAT droplets, using the ImageJ software (version 1.52a Wayne Rasband, National Institutes of Health, Bethesda, Maryland, USA). As the samples were fractured in liquid nitrogen, no correction was applied to account for the fact that the observation plane might not cut the particles through their equator. In the samples with dispersed elongated droplets, an equivalent radius (R_{eq}) of an oval was used and calculated as follows (Equations 6.2- 6.4) [42]:

$$R_{eq} = \frac{3.1A^{0.625}}{P^{0.25}} \quad \text{Equation 6.2}$$

$$with \quad A = \frac{\pi ab}{4} \quad \text{Equation 6.3}$$

$$p \sim 2\pi \sqrt{\left(\frac{1}{2}\left(\left(\frac{a}{2}\right)^2 + \left(\frac{b}{2}\right)^2\right)\right)} \quad \text{Equation 6.4}$$

where A and P are the cross-section area and perimeter of the ovals, respectively, and a and b are major and minor dimensions of the flat ovals, respectively [42]. Using Equations (6.1)– (6.4), the equivalent volume-average radius ($R_{v\text{-}eq}$) was calculated for the samples with elongated droplets.

6.3.3.2 **Atomic Force Microscopy (AFM)**

Samples were cut and microtomed using an Ultracut FC microtome (Leica, Jung RM 2165, Concord, Ontario, Canada) equipped with a liquid nitrogen cryo-chamber and a glass knife. AFM images were acquired in the air at room temperature without any additional preparation using tapping mode on a Dimension ICON AFM (Bruker/Santa Barbara, CA, USA). Intermittent contact imaging (i.e., “tapping mode”) was performed at a scan rate of 0.8 Hz using etched silicon cantilevers (ACTA from AppNano, Mountain View, California, USA) with a resonance frequency of around 300 kHz, a spring constant of ≈ 42 N/m, and a tip radius of <10 nm. All images were acquired with a medium tip oscillation damping (20%–30%).

6.3.3.3 **Rheometry**

The rheological properties of the neat aPLA, scPLA, PBAT, and their respective neat blends and nanocomposites were measured using a stress/strain-controlled MCR 302 rheometer (Anton Paar, Graz, Austria). A parallel plate flow geometry was used with a gap of 1 mm and a diameter of 25 mm. All rheological experiments were conducted at 180 °C under a nitrogen atmosphere to avoid oxidation of the samples. Strain sweep tests were conducted at a frequency of 1 rad/s to find the linear viscoelastic region (LVE) and all small amplitude oscillatory shear (SAOS) tests were conducted at a strain amplitude of 0.001. Time-sweep experiments at a frequency of 1 rad/s were carried out for 40 min to verify the thermal stability of the samples within the time necessary to conduct the frequency sweep experiments, all done from 628 rad/s to 0.05 rad/s. The structural recovery of the nanocomposites was investigated, following consecutive stress-growth experiments at a shear rate of 5 s^{-1}, via time sweep experiments at 1 rad/s for 1800 s, and frequency sweep experiments. For the blend nanocomposites, stress-growth experiments were carried out at a shear rate of 0.1 s^{-1}, selected to investigate coalescence of droplets in the blends (at that low shear rate, no droplet break-up is expected, as the capillary number, Ca, should be smaller than 1 [43]). Also, coalescence in PLA/PBAT/CNC blend nanocomposites was analyzed through SAOS time sweep experiments at a frequency of 1 rad/s for 1 h. Almost all rheological measurements were repeated up to three times to verify reproducibility.

6.4 Results and Discussion

6.4.1 Neat PLA and BPAT Nanocomposites

6.4.1.1 **Dispersion of CNCs in PLA and PBAT Matrices**

Figure 6.1 shows SEM micrographs of scPLA/1CNC and aPLA/1CNC nanocomposites from solution casting before melt mixing (Figure 6.1a,c) and after melt mixing (Figure 6.1b,d). Solution casting leads to a good dispersion and distribution of the CNCs in both PLAs (Figure 6.1a,c), more likely as small bundles than individual CNC nanorods. Comparing Figure 6.1a,b and Figure 6.1c,d, it is obvious that melt mixing leads to the agglomeration of CNCs (circles in Figure 6.1b,d). The agglomeration of CNCs is more important in the high molecular weight PLA (aPLA) and an agglomerate of around 8–10 μm is seen in Figure 6.1d after melt mixing. The agglomeration of the

dispersed CNCs during melt mixing could be due to the de-sulfation of CNCs at higher temperatures [44]. Another contributing phenomenon may be the intrinsic poor affinity of CNCs with the polymer matrices. The Hansen solubility parameters (HSP) and the HSP distances of PLA, PBAT, CNCs, and DMF, and their relative energy differences (RED) were calculated at room and processing temperatures (detailed information is presented in SM). According to the calculated HSP distances between CNCs and the polymers compared to the HSP radius of CNC, (Table 6.S1), at room and processing temperatures the RED is more than 1, which indeed represents a rather poor chemical affinity between CNCs and both polymers. This is in contrast to the high affinity of CNCs with DMF (RED < 1). As a result, the dispersed CNCs, which are in a metastable state after the removal of the solvent, may have a tendency to re-agglomerate during melt mixing. After solvent removal, in quiescent melt conditions, the high viscosity of the polymer matrices retards re-agglomeration since the Brownian motion is very slow [45]. However, in the internal mixer frequent CNC collisions may favor re-agglomeration. Our observations substantiate previous findings reported in the literature that while solution casting leads to a high level of dispersion and distribution, melt mixing following solution casting results in agglomeration of CNCs in the matrix [28,29,48]. These observations are in agreement with the rheological data presented in the next section.

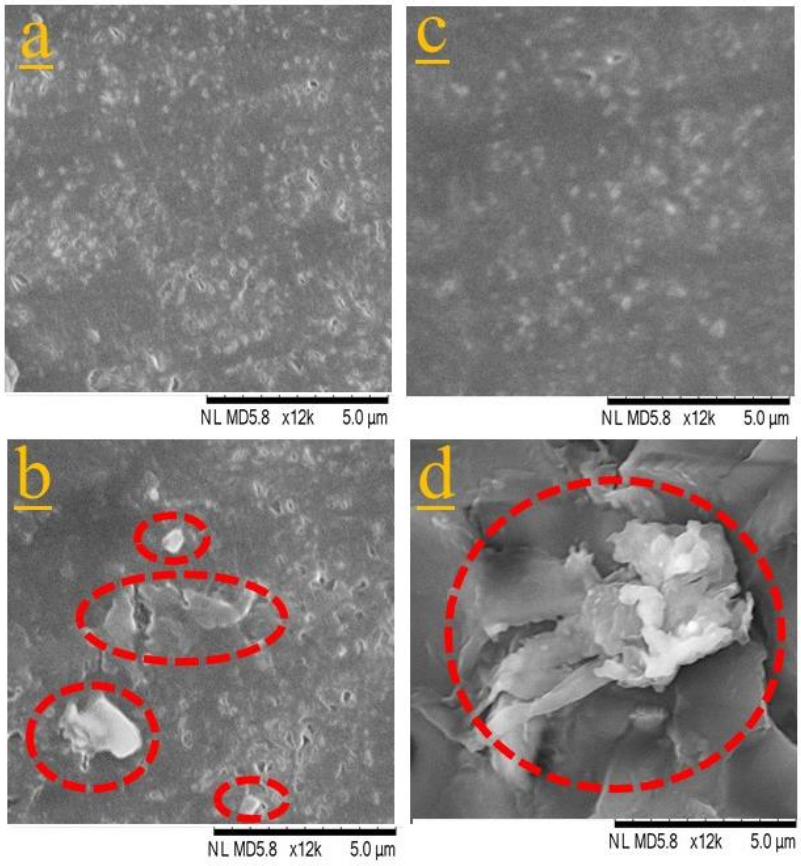

Figure 6.1 Scanning electron microscopy (SEM) images showing the dispersion and distribution of CNCs in (a,c) scPLA/1CNC and aPLA/1CNC nanocomposites, respectively, prepared from solution casting, in (b,d) after melt mixing for scPLA/1CNC and aPLA/1CNC nanocomposites, respectively.

6.4.1.2 **Rheology of Single Polymer Matrix Nanocomposites**

Rheological analysis is another practical method to investigate the dispersion quality of nanoparticles in polymer nanocomposites [30,49,50]. Figures 6.2 and 6.3 present the complex viscosity and storage modulus of the neat polymers and nanocomposites from solution casting (Figure 6.2) and the effect of melt mixing, +IMM, (Figure 6.3), respectively, as functions of angular frequency and CNC content. In Figure 6.2, the complex viscosities of the neat PLA (scPLA or aPLA) and PBAT exhibit a very broad Newtonian plateau at low frequencies. The storage modulus of the neat polymers also reveals a terminal zone with a slope of 2 at low frequencies, which is a characteristic of homogeneous molten polymers. For these samples prepared directly from solution casting, there are significant increases of the complex viscosity and storage modulus with the

addition of CNCs (obviously more important for the 3 wt% CNC than for the 1 wt% CNC sample) as expected for the whole frequency range compared to the neat aPLA, scPLA and PBAT, also prepared from solution casting. What is more, the sudden upturn in the complex viscosity and the occurrence of a plateau in the storage modulus in the low frequency region for the 1 and 3 wt% CNC samples are characteristics of a network formation of the cellulose nanocrystals. These improvements in rheological properties are in accordance with the microscopic analysis of scPLA/1CNC nanocomposite sample prepared from solution casting (Figure 6.1a). We note that the relative increases in the rheological properties of the aPLA/CNC samples are less significant than for the scPLA/CNC nanocomposites, as expected for a lower degree of nanoparticle dispersion in the more viscous PLA (Figure 6.1b). We observe a decrease in the complex viscosity of both neat PLAs compared to the PLA prepared from the granules (empty squares in Figures 6.2 and 6.3) mainly due to traces of solvent left in the samples after drying. For the neat PBAT, the effect of residual solvent is almost negligible, due to the crystallization of PBAT at the drying temperature (60–80 °C) that facilitated the solvent evaporation as explained in our previous work [28], in which more significant effects of residual solvents have been reported for the same polymers but using different solvents. The effect of the remaining solvent is also less visible on scPLA as compared to aPLA and this could be attributed to the higher viscosity of aPLA, which may hinder solvent removal during drying.

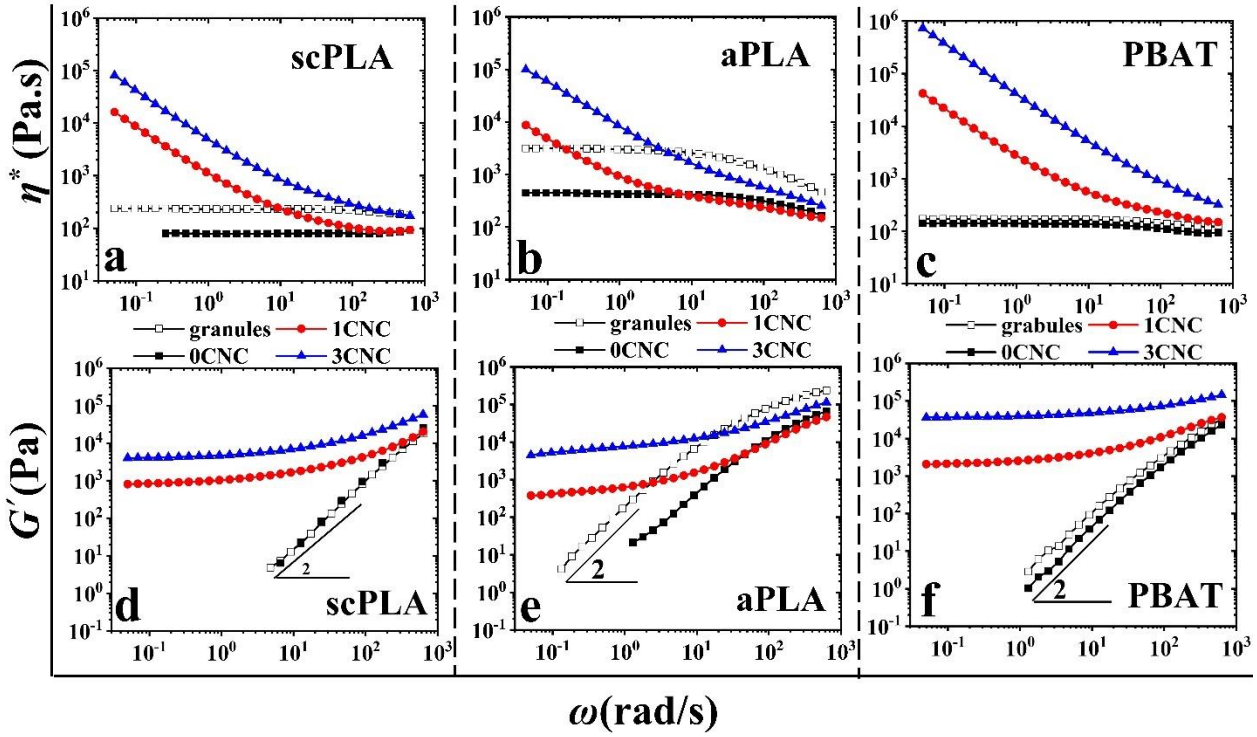

Figure 6.2 Complex viscosity (a–c) and storage modulus (d–f) of the neat polymers (0 CNC) and nanocomposites (1 and 3 CNC) prepared from solution casting (filled symbols) as functions of angular frequency and CNC content. Empty symbols are small amplitude oscillatory shear (SAOS) data of neat polymer samples prepared directly from granules using compression molding.

Figure 6.3 shows the effect of melt mixing (+IMM) on the complex viscosity and storage modulus of samples prepared from solution casting. When compared to Figure 6.2, there are considerable decreases of the SAOS properties due to the agglomeration of the CNCs and, although the addition of 1 and 3 wt% CNCs could slightly improve the complex viscosity and storage modulus of scPLA and PBAT, there is a decrease in the rheological properties of aPLA nanocomposites with respect to the neat aPLA. This is clearly seen in the 1 wt% sample, indicative of the degradation of the aPLA during melt mixing and possibly due to the presence of more remaining solvent in aPLA. A similar lack of rheological enhancements in SAOS have been reported for other polymer nanocomposites containing CNCs [28,51,52].

Overall, such a decrease in viscoelastic properties is a clear indication of the disruption of the CNC dispersion when the samples were melt blended in the internal mixer. In other words, as there was

no CNC surface treatment or compatibilizer, the dispersed cellulose nanocrystals dramatically tended to re-agglomerate mostly due to the low chemical affinity of CNCs with both polymers and possible de-sulfation of CNCs at higher temperatures during the melting process, as discussed in the previous section. The SEM images of Figure 6.1b,d confirm the drastic effect of melt mixing on the CNC dispersion in the scPLA/1CNC and aPLA/1CNC nanocomposites, respectively.

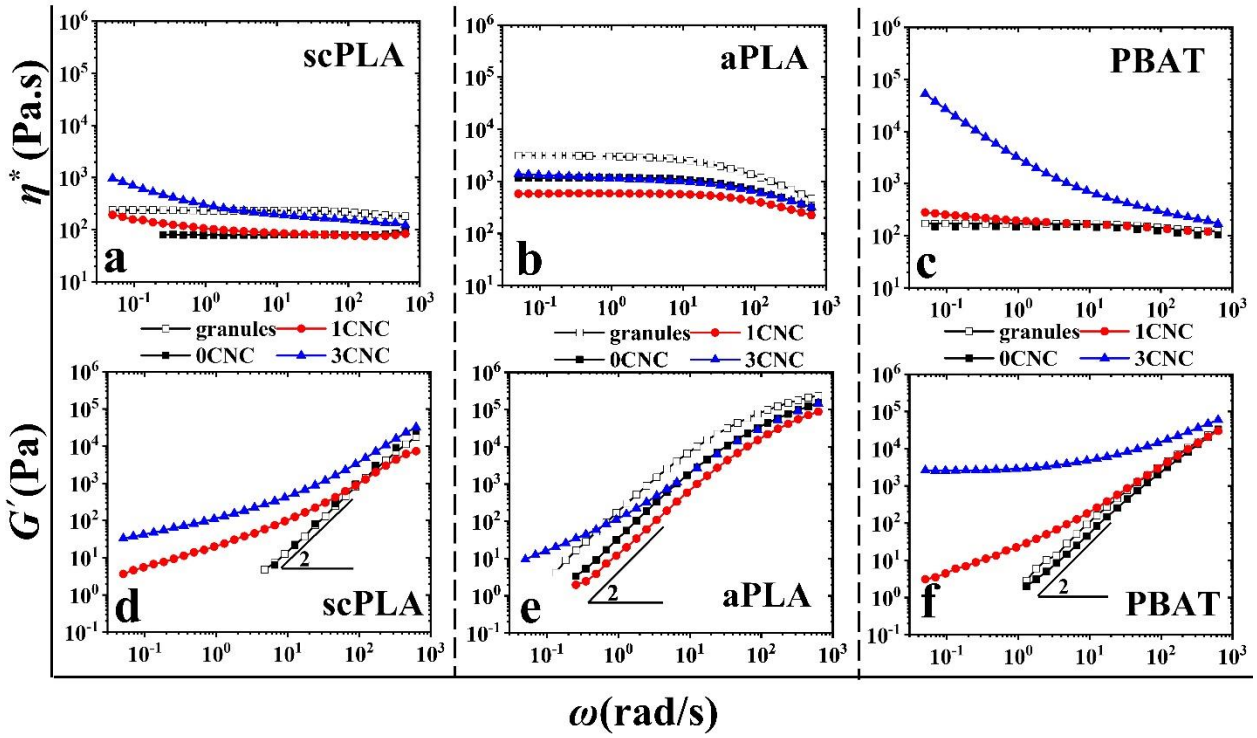

Figure 6.3 Effect of melt mixing (+IMM) on the complex viscosity (a–c) and storage modulus (d–f) of the neat polymers (0 CNC) and nanocomposites (1 and 3 CNC) prepared from solution casting +IMM (filled symbols) as functions of angular frequency and CNC content. Empty symbols are SAOS data of the neat polymer samples prepared directly from granules using compression molding.

Figure 6.4 presents the stress growth coefficient, $\eta+$, of the neat PBAT and its nanocomposites containing 1 and 3 wt% CNCs in a stress growth (start-up) experiments at an imposed shear rate of 5 s^{-1} for the first 20 s of the test that lasted 480 s ($\eta+$ was about constant for $t \geq 20$ s). The solid and dash lines represent the PBAT/CNC nanocomposites prepared from solution casting followed or not by melt mixing, respectively. At this low applied shear rate, the neat PBAT does not show any overshoot for the sample before and after melt mixing as there is no network formed in absence

of CNCs. On the other hand, the observation of overshoots (mainly in solution cast samples) in the transient viscosity versus time is assigned to the network of cellulose nanocrystals in the matrix of PBAT. Melt mixing (dashed lines in Figure 6.4) results in a severe decrease in the intensity of the overshoot due to the re-agglomeration of CNCs during melt mixing. For the higher concentration CNC sample, the overshoot also becomes larger, revealing a stronger CNC network. Bagheriasl et al. [24] showed similar behavior for the nanocomposites of PLA/CNC (same grade of scPLA in this paper) prepared from solution casting. Similar results were obtained for scPLA/CNC and aPLA/CNC nanocomposites and are presented in SM (Figure 6.S3a,b). Due to the startup flow experiments, the CNC networks in scPLA, aPLA, and PBAT were destroyed and the rebuild-up of these networks was investigated through SAOS time sweep experiments for 1800 s and the result are presented in the SM (Figure 6.S4). There is no structural build-up for all neat polymers before and after melt mixing, as expected. On the other hand, the structural build-up is clear for all single polymer matrix nanocomposites especially the ones from solution casting with a larger CNC content. SAOS frequency sweep tests were also conducted after stress growth experiments and the results are presented in SM (Figures 6.S5 and 6.S6 for the samples from solution casting and solution casting followed by melt mixing, respectively). The structural recovery after time sweep tests may not be completed and there are significant differences between SAOS data before and after stress growth experiments (mostly for solution cast samples).

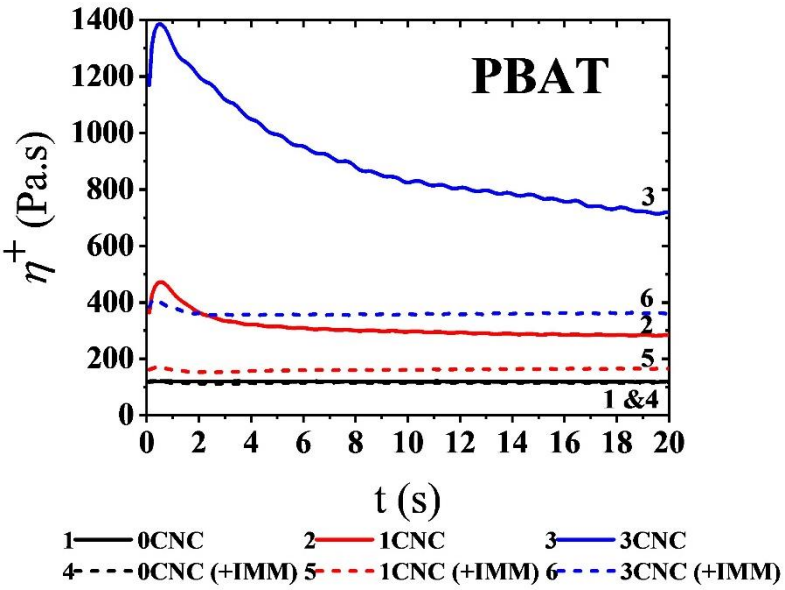

Figure 6.4 Variations of the shear stress growth coefficient, η^+, of the PBAT/CNC nanocomposites as functions of time for an imposed shear rate of 5 s^{-1}. Solid and dashed lines represent the samples prepared from solution casting and solution casting followed by melt mixing, respectively.

6.4.2 PLA/PBAT Blend Nanocomposites

6.4.2.1 Morphology of Blend Nanocomposites

Based on the values of the surface energies of PLA, PBAT, and CNC and related interfacial tensions (details are presented in SM) between the PLA/PBAT/CNC components (Table 6.S2), the wetting coefficient (Equation S6) is calculated as 6.67 (i.e., $\omega \gg 1$), which predicts that the thermodynamic equilibrium localization of CNC particles should be in the PBAT phase. The interfacial tension between both PLA and PBAT was also obtained from the best fits of the linear viscoelastic data using the Palierne model (Equations S9 and S10) of the neat blends prepared both from granules and from solution casting followed by melt mixing. The results are presented in Figure 6.S2. The respective interfacial tensions were found to be 1.2 (aPLA/PBAT (granules)), 0.8 (scPLA/PBAT (granules)), 1.8 (aPLA/PBAT (+IMM)), and 1.3 mN/m (scPLA/PBAT (+IMM)). These values are quite different than those calculated by the harmonic-mean equation as explained in SM (Table 6.S2 and Figure 6.S2). The lower calculated interfacial tension for scPLA/PBAT compared to aPLA/PBAT confirms the better compatibility between the semicrystalline PLA and PBAT, as expected from the HSP parameters (details are presented in SM). The 50% increase in the interfacial tension for the samples prepared from solution casting followed by melt mixing could be due to the fact that the Palierne model predictions are not very sensitive as shown by the predictions using the interfacial tension obtained for the blends prepared from granules and given the dashed lines in Figures 6.S2c,d. Overall, using the interfacial tensions (Figure 6.S2) calculated from the best fits of the Palierne model predictions of the SAOS data, the wetting parameter is calculated to be between 0 and 1, which predicts that the localization of CNCs should be at the interface of the PLA and PBAT, in contrast to the localization in PBAT predicted from the thermodynamics analysis.

Figure 6.5 shows the SEM micrographs of cryo-fractured neat blends PLA (scPLA and aPLA)/PBAT prepared from solution casting (a,c) and solution casting followed by melt mixing

(b,d). It is obvious that melt mixing has a substantial effect on the morphology of the neat blends, and the samples are more homogenous with finer morphologies. The volume average radius (R_v) of the dispersed phase after melt mixing decreases from around 10–30 µm for aPLA/PBAT (observed from different SEM images at different locations) to 2.8 µm and from 2.1 to 0.9 µm for scPLA/PBAT, respectively. These decreases in the volume average radius of the dispersed phase after melt mixing are due to the higher deformation rate and better mixing via the internal mixer, compared to low mixing efficiency using a magnetic stirrer in solution casting. The finer morphology obtained for scPLA/PBAT is explained by the viscosity ratio closer to 1 [46] as can be deduced from Figures 6.2 and 6.3. In most publications we examined, there was no clear attention paid to the difference between the morphology of blends from solution casting and melt mixing [47].

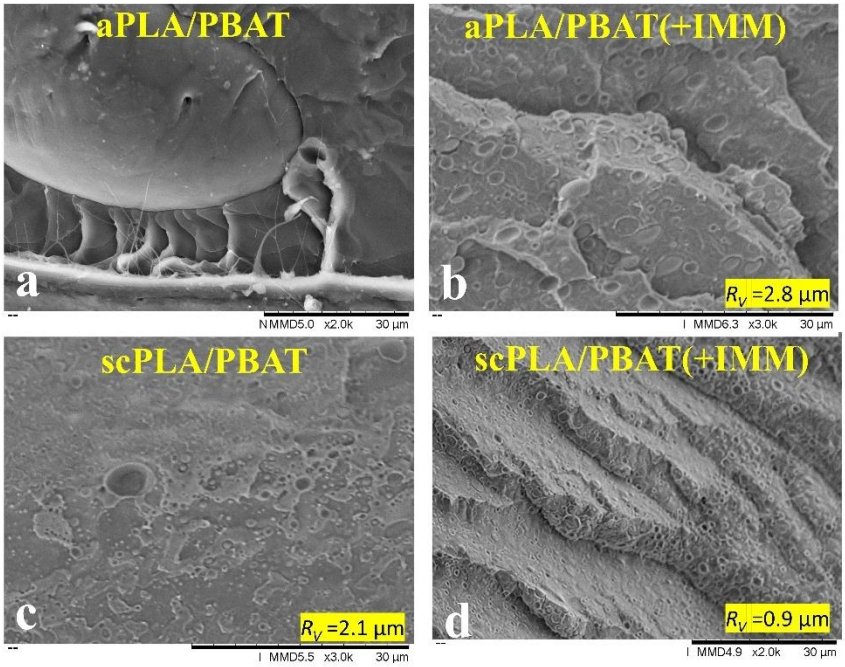

Figure 6.5 SEM images showing the morphologies of the neat blends from solution casting (a,c) and solution casting followed by melt mixing (b,d); (+IMM).

Figure 6.6 presents the effect of the addition of CNCs on the morphology of PLA (scPLA and aPLA)/PBAT blends. It should be noted that the localization of the CNCs cannot be seen as the magnification level is too low. Adding CNCs to the aPLA/PBAT blend results in a decrease of the volume average radius of the dispersed phase no matter if the CNCs were initially localized in the

matrix, dispersed, or both phases (Figure 6.6a–c). By adding CNCs to the aPLA/PBAT blend, R_v decreases from 2.8 (Figure 6.5b) to 1.6, 1.2, and 2 µm for (aPLA-1CNC)/PBAT (Figure 6.6a), aPLA/(PBAT-1CNC) (Figure 6.6b), and aPLA/PBAT/1CNC (Figure 6.6c), respectively. The lowest R_v is obtained when the CNCs were initially dispersed in PBAT ($\eta_{PBAT} < \eta_{PLA}$). Then, the CNCs in PBAT increased the viscosity of PBAT, which comes close to that of PLA, favoring the breakup of the dispersed droplets during mixing [48].

In the case of scPLA/PBAT, when the CNCs were initially localized in PBAT the R_v values, 0.8 µm, (Figure 6.6e) are almost the same as the neat scPLA/PBAT, 0.9 µm, (Figure 6.5d). It is also worth mentioning that in the scPLA/PBAT/CNC blend nanocomposites the size of PBAT droplets varies between 0.5 to 5 µm, which shows a high polydispersity. In the other cases when CNCs were initially localized in the matrix or both phases, elongated PBAT droplets are observed and equivalent volume average radius, $R_{v\text{-}eq}$, values of 1.3 and 1.4 µm are calculated for (scPLA-1CNC)/PBAT and scPLA/(PBAT-1CNC), respectively. It seems that the dispersed droplet-type morphology tends to be converted into a co-continuous one and this transformation could have a substantial effect on the final properties of the blend nanocomposites.

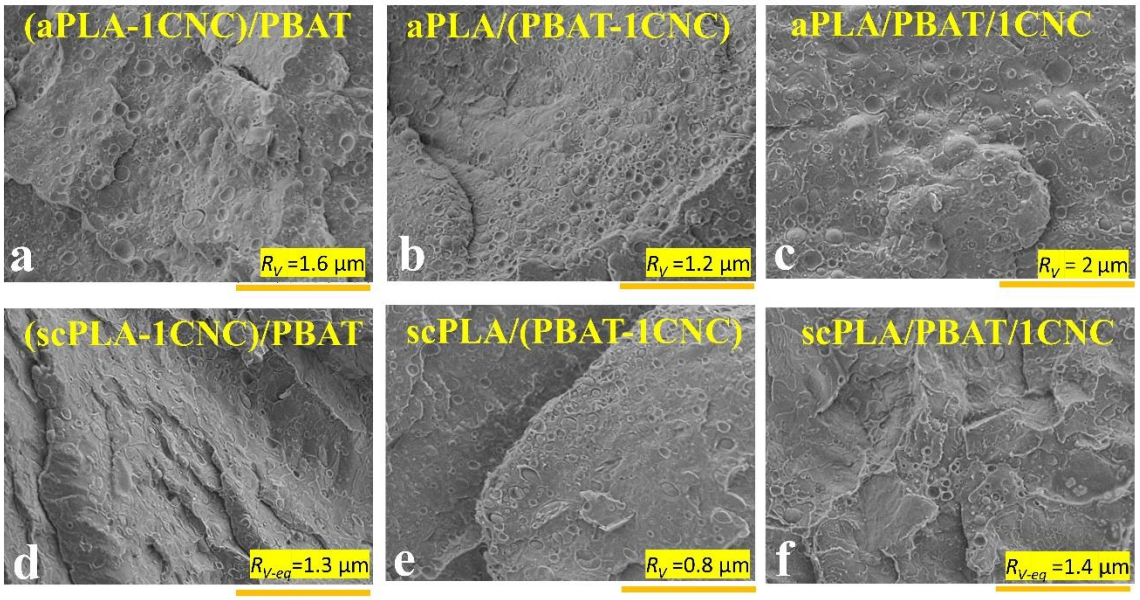

Figure 6.6 SEM images showing the morphologies of aPLA/PBAT/CNC (a–c) and scPLA/PBAT/CNC (d–f) blend nanocomposites. CNCs were initially (during the solution casting step) localized in the matrix (a,d), dispersed (b,e), and both phases (c,f). The scale bars are 30 µm.

To better localize the CNCs after melt mixing, SEM and AFM analyses were done at higher magnification and SEM and AFM phase images of aPLA/PBAT and scPLA/PBAT blend nanocomposites are presented in Figure 6.7a–e and Figure 6.7f–j, respectively. As reported elsewhere [38], [39], the CNCs particles appear as white dots (arrows) and also rods (circles) in these images. The cellulose nanocrystals in the aPLA/PBAT blend nanocomposites have migrated from the PLA phase, when CNCs were initially added to aPLA (Figure 6.7a,d) or both phases (Figure 6.7c,e), to the surface of the PBAT droplets (circles and arrows). This migration is clearer in the AFM images (Figure 6.7d,e) with a higher magnification. For the samples for which the CNCs were initially incorporated in the PBAT phase, it is difficult to tell from the SEM images if the CNCs are in the PBAT or aPLA phase, but as the thermodynamically favorable phase is PBAT the CNCs are most probably localized in the PBAT phase. For the scPLA/PBAT blend nanocomposites, it is difficult to identify the localization of CNCs through SEM images (Figure 6.7f–h). However, the AFM images (Figure 6.7i,j) clearly show the localization of CNCs at the interface of scPLA and PBAT droplets when the CNCs were initially added to the matrix or both phases. The CNCs are indicated by circles and arrows. All the findings in the SEM and AFM analyses are in accordance with the rheological properties which will be discussed in the next section.

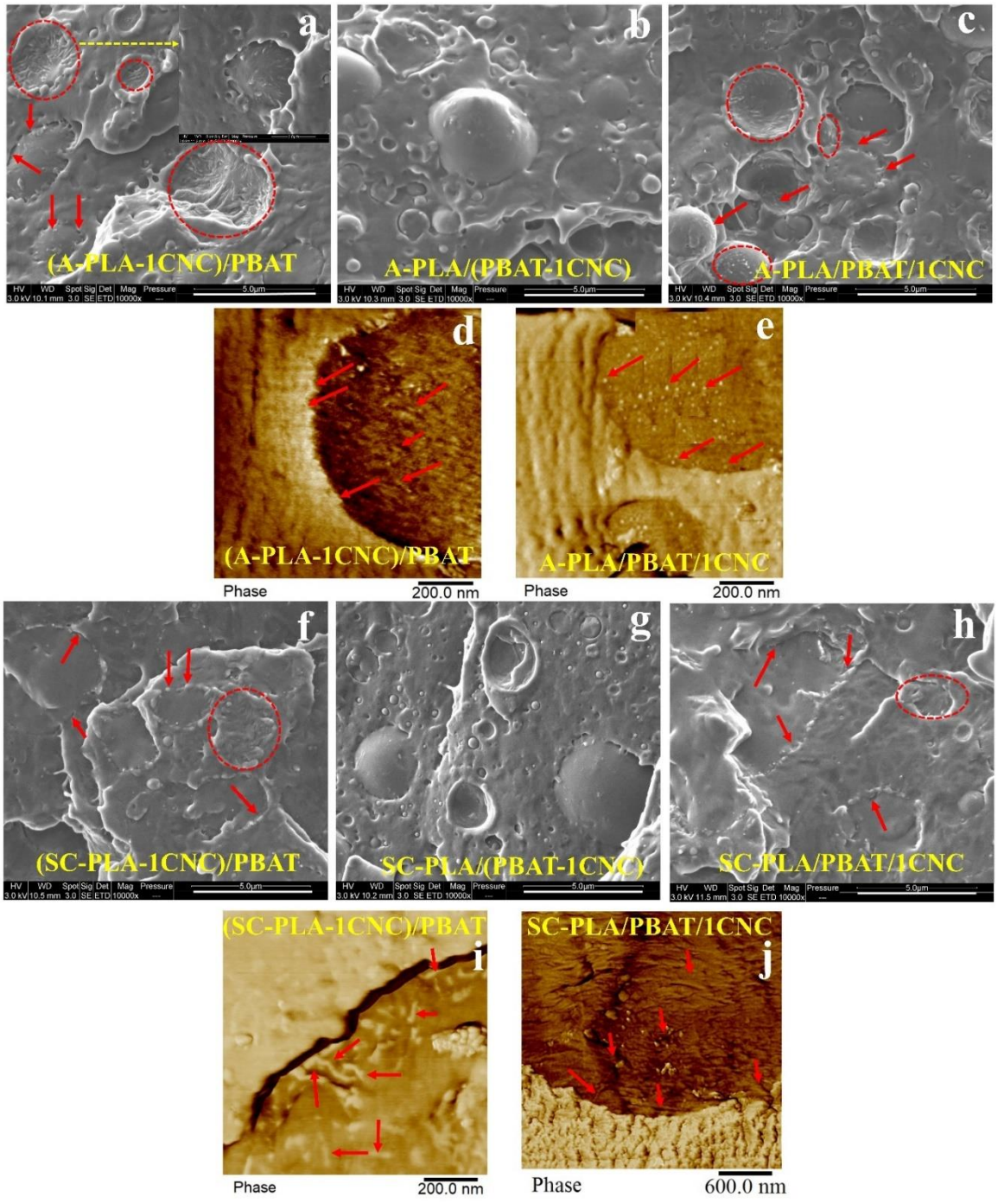

Figure 6.7 SEM (a–c,f–h) and AFM (d,e,i,j) images showing the localization of CNCs in the aPLA/PBAT/CNC (a–e) and scPLA/PBAT/CNC (f–i) blend nanocomposites. The CNCs were initially localized in the matrix (a,d,f,i), dispersed (b,g), and both phases (c,e,h,i) during the solution casting step.

6.4.2.2 **SAOS Behavior of PLA/PBAT/CNC Nanocomposites**

Figure 6.8 reports the complex viscosity (a,b) and storage modulus (c,d) of aPLA or scPLA/PBAT blends, from granules (empty squares), solution casting (half filled-half empty), and solution casting followed by melt mixing (filled squares), and their blend nanocomposites (circles, upward and downward triangles) after melt mixing. It is clear from Figure 6.8 that melt mixing (filled squares) increases the complex viscosity and storage modulus of the neat blend of aPLA or scPLA/PBAT prepared from solution casting (half filled-half empty squares). This is mainly because the morphology is finer (Figure 6.5b,d) and some residual solvent (DMF) has evaporated during melt mixing. However, it is still far from the complex viscosity of aPLA or scPLA/PBAT blends prepared from granules (empty squares), due to remaining solvent in the samples as discussed in a previous section. Adding CNCs to the PBAT during the solution casting step to prepare PLA/(PBAT-1CNC) blend nanocomposites results in an increase in the complex viscosity and storage modulus of the blend nanocomposites (upward triangles). These rheological results are in agreement with the SEM images of the blend nanocomposites when CNCs were introduced to the blends through PBAT; finer matrix-droplet morphologies are obtained, which in turn increase the rheological properties of the blend nanocomposites (Figure 6.6b,e). On the other hand, the addition of CNCs to the aPLA or scPLA during the solution casting step to prepare (PLA-1CNC)/PBAT (circles) and PLA/PBAT/1CNC (downward triangles) blend nanocomposites results in a slight increase and a sharp upturn in the complex viscosities at low frequencies of aPLA/PBAT/CNC and scPLA/PBAT/CNC blend nanocomposites, respectively (Figure 6.8a,b). Significant slope reductions in the storage modulus at low frequencies are observed mainly for scPLA/PBAT/CNC (Figure 6.8d). The SEM and AFM images of Figure 6.7 show that for (aPLA-1CNC)/PBAT and aPLA/PBAT/1CNC blend nanocomposites, there is a portion of cellulose nanocrystals that migrated to the thermodynamically stable phase (PBAT) and some CNCs are at the interface between the matrix and droplets. Moreover, in the scPLA/PBAT blend nanocomposites, when CNCs were initially incorporated into the matrix or in both phases, the complex viscosity results indicate a transition from a viscoelastic liquid to a solid behavior. This suggests that the CNCs form a 3D network in the blend, probably because enough CNC particles remain in the matrix. In the case of the (aPLA-1CNC)/PBAT blend nanocomposite, the observed finer morphology (Figure 6.8a) may explain the slightly larger values for the complex viscosity and storage modulus for that blend nanocomposite (Figure 6.8a,c). On the other hand, we see an

almost identical rheological behavior for (scPLA-1CNC)/PBAT and scPLA/PBAT/1CNC (Figure 6.8b,d), in agreement with the SEM images of Figure 6d,f and Figure 7f,h, which show almost the same morphologies.

The droplet relaxation phenomenon can be analyzed using plots of the imaginary component of the complex viscosity (η'') versus its real component (η') in the form of Cole-Cole plots [49], as presented in Figure 6.9 for the PLA/PBAT/CNC blend nanocomposites. The left and right arcs in the Cole-Cole plots are the characteristics of the relaxation phenomena for the polymer chains and the droplets, respectively [49]. As seen from Figure 6.9, when CNCs were introduced to the nanocomposites through the PBAT phase (PLA/(PBAT-1CNC)), we have a matrix-droplet morphology with complete relaxation of the PBAT droplets. However, introducing 1 wt% of CNCs through PLA ((PLA-1CNC)/PBAT) or both phases (PLA/PBAT/1CNC) diminishes the arc of the Cole-Cole plots related to the relaxation of the dispersed phase and retards the relaxation of the droplets due to the network of CNCs formed through co-continuity of the phases or localization at the interface. Compared to the SEM images it could be concluded that the selective localization (at the interface) of CNCs in the PLA/PBAT/CNC blend nanocomposites retards the relaxation of PBAT droplets.

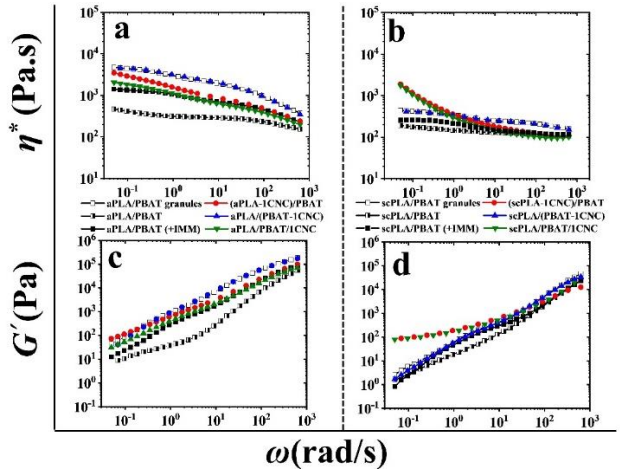

Figure 6.8 Complex viscosity (a,b) and storage modulus (c,d) versus angular frequency of aPLA or scPLA/PBAT/CNC blend nanocomposites. Empty, half filled-half empty, and filled black squares are for neat blends from granules, solution casting, and melt mixing of solution casted samples, respectively. Circles, upward, and downward triangles represent the blend nanocomposites when CNCs were initially localized in the matrix, dispersed, and both phases, respectively.

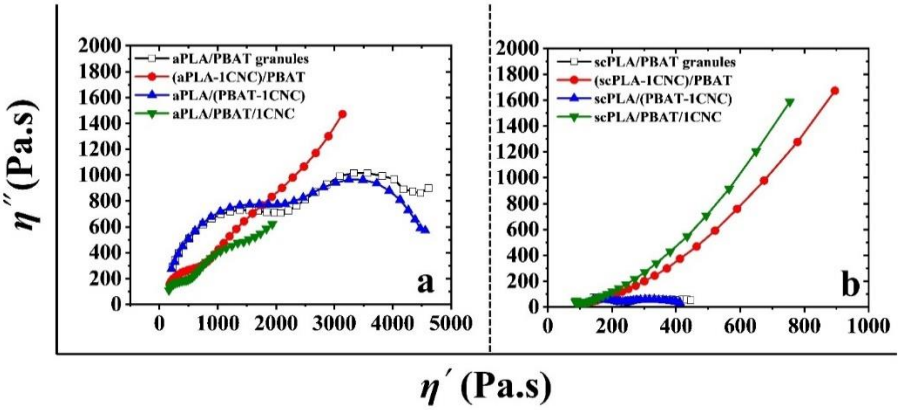

Figure 6.9 Cole-Cole plots of (a): aPLA/PBAT/CNC and (b): scPLA/PBAT/CNC blend nanocomposites.

6.4.2.3 **Stress Growth Behavior and Coalescence**

Figure 6.10 presents the stress growth data for PLA/PBAT blends and PLA/PBAT/CNC blend nanocomposites containing 1 wt% CNCs. The experiments were carried out at 0.1 s^{-1} with a total shearing time of 2400 s. According to this figure, the more or less rapid decreases in the transient viscosity with time are an indication of coalescence of the PBAT droplets. In addition to coalescence, thermal degradation of PLA (mostly aPLA) could also contribute to the decrease in the transient viscosity over longer times. According to time-sweep experiments during 40 min, aPLA and scPLA showed a 10% drop in their transient viscosity within 20–25 min and around 35 min, respectively, while PBAT was stable. In the blend nanocomposites based on both PLAs, the transient viscosity drop is not as significant as those in the neat blends (Figure 6.10a,b). This decrease is clearer for the neat scPLA/PBAT in Figure 6.10b. This may be due to the viscosity ratio of the dispersed PBAT to the PLA matrix, which is around 1 and 0.1 in the scPLA/PBAT and aPLA/PBAT blends (Figure 6.3), respectively. The 10-fold larger viscosity ratio of the scPLA/PBAT blend could have a critical effect on more rapid coalescence.

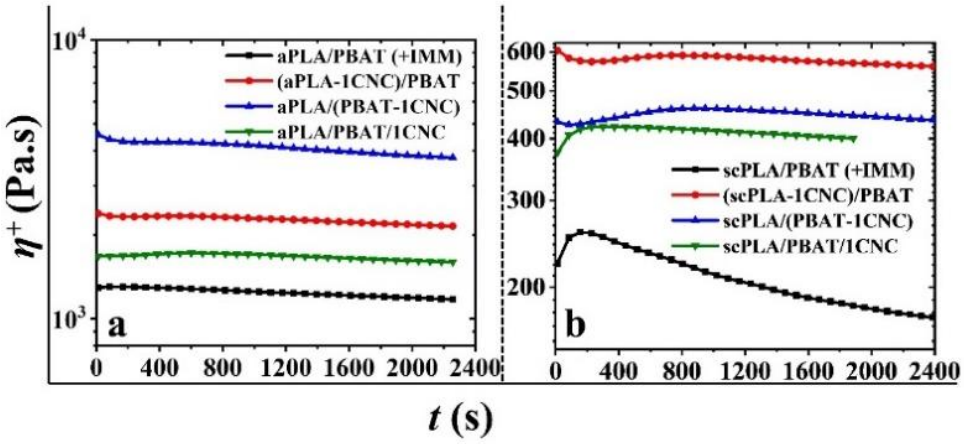

Figure 6.10 Stress growth coefficient (η+) as a function of time (t) for PLA/PBAT blends and PLA/PBAT/CNC blend nanocomposites containing 1 wt% CNCs; (a,b) are data for the amorphous and semicrystalline PLA blends, respectively.

In order to have a better understanding of the effect of shearing on the properties of the neat blends and their nanocomposites, the morphology of the neat scPLA/PBAT blend and scPLA/PBAT/CNC blend nanocomposites containing 1 wt% CNCs have been investigated and the results are shown in Figure 6.11 for samples before and after the stress growth experiments. As seen from Figure 6.11a,b, a significant droplet coalescence occurred for the neat scPLA/PBAT blend during shearing, and the volume average radius increases from 0.9 to 1.0–3.0 μm (Table 6.2). In contrast, Figures 6.11c–h show no or minor morphological changes after shearing for the blend nanocomposites, and no matter the initial localization of CNCs, the morphologies are uniform and, as presented in previous parts, the cellulose nanocrystals stayed in the dispersed phase or at the interface of the phases, before and after shearing (see Table 6.2). This suggests that the cellulose nanocrystals in the dispersed phase or at the interface between the two polymers served as a droplet coalescence barrier during shearing. To confirm the absence of coalescence in the PLA/PBAT nanocomposites, time sweep experiments were conducted at a frequency of 1 rad/s for 1 h, and the results are presented in the SM (Figure 6.S7).

Table 6.2 Volume average or equivalent average of PBAT droplet radius, R_v, before and after shearing at a rate of 0.1 s^{-1} during 2400 s.

	Non-Sheared, R_v or $R_{v\text{-}eq}$	**Sheared at 0.1 s^{-1}, R_v or $R_{v\text{-}eq}$**
scPLA/PBAT	0.90 μm	1.0–3.0 μm
(scPLA-1CNC)/PBAT	PBAT droplets are slightly elongated. 1.3 μm	PBAT droplets are slightly elongated. 1.4 μm
scPLA/(PBAT-1CNC)	0.8	0.8 μm
scPLA/PBAT/1CNC	PBAT droplets are slightly elongated. 1.4 μm	PBAT droplets are slightly elongated. 1.4 μm

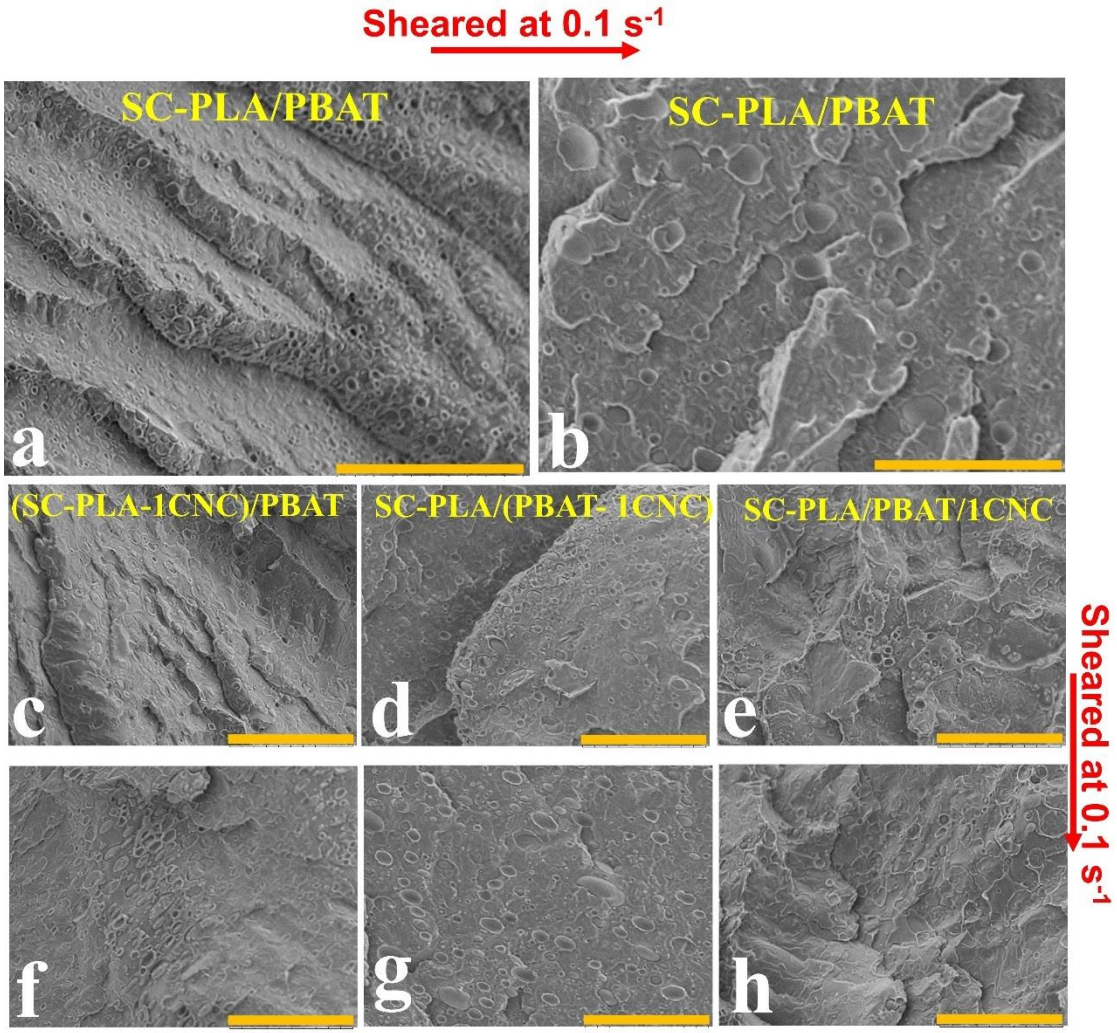

Figure 6.11SEM images showing the dispersed PBAT phase in the scPLA matrix after (a) molding (i.e., non-sheared) and (b) sheared at a rate of 0.1 s^{-1} (c–h) the PBAT droplet morphological stability in presence of 1 wt% CNCs: (c–e) non-sheared and (f–h) sheared at a rate of 0.1 s^{-1}. The scale bars are 30 μm.

6.5 Conclusions

In this work, the localization of CNCs in PLA (amorphous and semicrystalline)/PBAT blends through solution casting and melt mixing methods and its effect on the rheology and morphology as well as on morphological stability under shear were studied in detail. PLA/CNC or PBAT/CNC neat nanocomposites obtained from solution casting exhibit a high level of CNC dispersion in each polymer. The effect of the melt mixing on the single polymer matrix nanocomposites was also investigated, showing a significant re-agglomeration of the CNCs. For preparing the blend nanocomposites, the CNCs were initially localized in the matrix, dispersed, or with both phases during the solution casting step, and the final localization of CNCs were studied after melt mixing. In most cases, it was shown that the incorporation of CNCs decreased the PBAT droplet size and created a finer morphology in the blend nanocomposites. When CNCs were initially dispersed, in PLA or both phases, they tended to be localized at the interface of the PLA and PBAT phases, which was favorable for stabilization of the blend morphology under shear flow. When CNCs were introduced to the blend nanocomposites through the PBAT phase, a matrix-droplet morphology was obtained with a complete relaxation of the PBAT droplets. However, introducing 1 wt% of CNCs, through PLA or both phases, retarded the relaxation of the droplets due to the network formation of CNCs. Applying a shear rate of 0.1 s^{-1} induced a pronounced droplet coalescence in the neat PLA/PBAT blend, whereas adding 1 wt % CNCs significantly prevented PBAT droplet coalescence. In this context, it could be noted that when solvents are used in the preparation method, the choice of solvent and the possibly remaining solvent in the prepared samples have a great effect on the rheological and morphological properties, but it should still be considered a proper method for the dispersion of unmodified CNCs in hydrophobic polymers.

6.6 Author Contributions:

Conceptualization, M.M.; Formal analysis, M.M., M.C.H., P.J.C. and A.T.; Funding acquisition, P.J.C.; Investigation, M.M.; Methodology, M.M.; Project administration, P.J.C.; Resources, M.C.H. and P.J.C.; Software, M.M.; Supervision, M.C.H. and P.J.C.; Validation, M.M., M.C.H., P.J.C. and A.T.; Visualization, M.C.H. and P.J.C.; Writing—original draft, M.M.; Writing—review & editing, M.M., M.C.H., P.J.C. and A.T.

6.7 Funding:

Natural Science and Engineering Research Council (NSERC) of Canada.

6.8 Institutional Review Board Statement:

Not applicable.

6.9 Informed Consent Statement:

Not applicable.

6.10 Data Availability Statement:

Not applicable.

6.11 Acknowledgments:

Financial support from the Natural Science and Engineering Research Council (NSERC) of Canada is gratefully acknowledged. The authors are also grateful to FPInnovations for providing the CNCs. We wish to thank Jed Randall from NatureWorks for providing one of the PLA samples. The authors also wish to acknowledge the help of Helia Sojoudiasli and Matthieu Gauthier for the material preparation and processing and Patricia Moraille for making the AFM images.

6.12 Conflicts of Interest:

There are no conflicts to declare.

6.13 Supplementary materials

6.13.1 Single polymer matrix and blend nanocomposites preparation

The aPLA, scPLA, and PBAT were first dried in a vacuum oven overnight at 55 °C and then each polymer (about 40 g) was dissolved in 70 mL DMF using a magnetic stirrer for 2 h at 70 °C until complete dissolution. Separately, the desired amount of CNCs (between 0.4–1.6 g based on the final weight percentage of CNCs in the neat and blend nanocomposites) was dispersed in 70 mL of DMF using a water bath sonicator (FS30 100 Watts Ultrasonic Cleaner, Fisher Scientific,

Pittsburg, PA, USA) for 2 h at room temperature. Afterward, the neat polymer solution was added to the CNC suspension and magnetic stirring was continued for another 2 h at 70 °C to ensure a good distribution and dispersion of the nanoparticles despite the rather high viscosity of the solution. Then, the mixtures were poured into a petri dish and dried in an oven in two steps. First, the samples were put in the vacuum oven (0.9 bar) with air circulation set at 60 °C for 2 days. Then, the drying process was completed for another 2 days at 80 °C under vacuum (−0.65 bar). After removing the samples, the nanocomposites containing the low molecular weight PLA (scPLA) could be ground into powder using a coffee grinder, but the high molecular weight PLA (aPLA) and PBAT samples had to be chopped to very small pieces using scissors.

Figure 6.S1 shows blend nanocomposites preparation containing 75 wt% PLA and 25 wt % PBAT and overall, 1 wt % CNCs. In the first two mixing strategies (Figures 6.S1a,b), granules of the neat complementary polymer (dried overnight at 55 °C) were added to the single polymer matrix nanocomposites in the internal mixer. In the third strategy (Figure 6.S1c) both PLA and PBAT nanocomposites containing 1 wt% prepared from solution casting were melt mixed in the internal mixer.

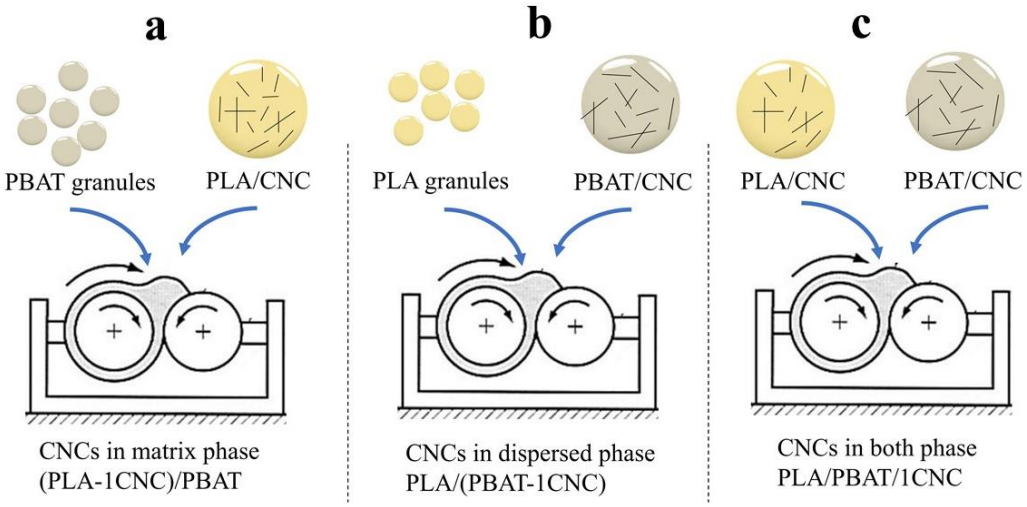

Figure 6.S1 Mixing sequences to prepare the blend nanocomposites. (a) and (b) granules of the neat complementary polymers (PLA and PBAT granules) were added to the neat polymer matrix nanocomposites and (c) PLA and PBAT nanocomposites prepared from solution casting were melt mixed in the internal mixer. All single polymer matrix nanocomposites prepared initially from solution casting.

6.13.2 Hansen solubility parameters (HSP) for PLA, PBAT, and CNCs

In our research group, the Hansen solubility parameter (HSP) theory [50] was used to determine the chemical affinity of CNCs [51], [52] and predict both their level of colloidal stability and behavior upon solvent casting [53], [54]. The HSP theory is based on cohesive energy density. The total cohesion parameter, δ_T, is the square root of the cohesive energy density and is split into three components, dispersive (δ_D), dipole-dipole (δ_P) and hydrogen-bonding (δ_H) (and other Lewis acid/base) interactions. δ_T is expressed as follows, with units of $MPa^{1/2}$:

$$\delta_T^2 = \delta_D^2 + \delta_P^2 + \delta_H^2 \qquad \text{Equation S1}$$

The chemical distance $R_{a,\mathrm{A-B}}$ between two substances A $\{\delta_{D,\mathrm{A}}; \delta_{P,\mathrm{A}}; \delta_{H,\mathrm{A}}\}$ and B $\{\delta_{D,\mathrm{B}}; \delta_{P,\mathrm{B}}; \delta_{H,\mathrm{B}}\}$ may then be expressed as the norm of the $vector\ \overrightarrow{AB}$ in the HSP graph:

$$R_{a,\mathrm{A-B}} = \left\|\overrightarrow{AB}\right\| = \sqrt[2]{4\left(\delta_{D,A} - \delta_{D,B}\right)^2 + \left(\delta_{P,A} - \delta_{P,B}\right)^2 + \left(\delta_{H,A} - \delta_{H,B}\right)^2} \qquad \text{Equation S2}$$

Literature reports HSP values at room temperature of ~ {18.1; 20.4; 15.3} $MPa^{1/2}$ [52], ~ {18.5; 8.0; 7.0} $MPa^{1/2}$ [55], and ~ {18.0; 5.6; 8.4} $MPa^{1/2}$ [55] for CNCs, PLA, and PBAT, respectively, along with solvent solubility radii $R_{0,\mathrm{CNC}}$ = 7.8 $MPa^{1/2}$, $R_{0,\mathrm{PLA}} \approx 8$ $MPa^{1/2}$, and $R_{0,\mathrm{PBAT}} \approx 4.5$ $MPa^{1/2}$ [52], [53], [55]. R_0 is the critical threshold chemical distance for the substance to be dispersed or dissolved in a solvent. Solvents whose chemical distances with CNCs are smaller than 7.8 $MPa^{1/2}$ were found to adsorb significantly on CNC surfaces [52]. Therefore, by defining a sphere of radius R_0, which contains all the good solvents, we can identify a relative energy difference, RED = R_a/R_0. Solvents with RED ≤ 1 are considered as good suspending media. Also, RED ≤ 1 between two materials indicates a good chemical affinity.

A combination of electrostatic and solvation-induced stabilization was found to be necessary to reach sufficient colloidal stability for CNC particles [53] and among the best-suspending media, dimethylformamide (DMF), with HSP values of ~ {17.4; 13.7; 11.3} $MPa^{1/2}$ stands after water, formamide, N-methylformamide, and dimethylsulfoxide (DMSO) [28].

If the temperature rises, then the density decreases and as a result, the HSP values decrease. The effect depends on ΔT, (the change of temperature with respect to 25 °C), and the thermal expansion coefficient, α, which is taken to be 0.0007/K for polymers, CNCs, and DMF [56]. So, dispersive,

dipole-dipole, and hydrogen-bonding (and other Lewis acid/base) interactions in the solubility parameters will change as follows [56]:

$$\delta_D^T = \delta_D \cdot (1 - \Delta T \cdot \alpha \cdot 1.25) \quad \text{Equation S3}$$

$$\delta_P^T = \delta_P \cdot \left(1 - \Delta T \cdot \frac{\alpha}{2}\right) \quad \text{Equation S4}$$

$$\delta_H^T = \delta_H \cdot (1 - \Delta T(0.00122 + \alpha/2) \quad \text{Equation S5}$$

According to Equations S3, S4, and S5, the HSP values at 180 °C decrease to ~ {15.6; 19.2; 11.4} $MPa^{1/2}$ for CNCs, ~ {15.9; 7.5; 5.3} $MPa^{1/2}$ for PLA, ~ {15.5; 5.3; 6.3} $MPa^{1/2}$ for PBAT, and ~ {15.0; 12.9; 8.6} $MPa^{1/2}$ for DMF. Also, Table 6.S1 reports the HSP distances and relative energy differences (RED) between PLA, PBAT, CNCs, and DMF (Equation S2) at 25 and 180 °C.

Table 6.S1 HSP distances and relative energy differences (RED) between PLA, PBAT, CNCs, and DMF.

	25 °C / RED	180 °C / RED
$R_{a,\text{PLA-PBAT}}$	3.0 $MPa^{1/2}$/ ≤1	2.6 $MPa^{1/2}$/ ≤1
$R_{a,\text{CNC-DMF}}$	7.9 $MPa^{1/2}$/ ≤1	6.9 $MPa^{1/2}$/ ≤1
$R_{a,\text{CNC-PLA}}$	14.9 $MPa^{1/2}$/ >1	13.2 $MPa^{1/2}$/ >1
$R_{a,\text{CNC-PBAT}}$	16.3 $MPa^{1/2}$/ >1	14.8 $MPa^{1/2}$/ >1

According to the HSP distances reported in Table 6.S1, the RED values for $R_{a,\text{CNC-PLA}}$ and $R_{a,\text{CNC-PBAT}}$ compared to the HSP radius of CNCs, $R_{0,\text{CNC}}$ = 7.8 $MPa^{1/2}$, are greater than 1 at 25 and 180 °C and, hence, they predict a poor chemical affinity between CNCs and both polymers. In contrast, the RED is less or equal to 1 for PLA and PBAT, and CNCs and DMF. This highlights a good chemical affinity between PLA and PBAT, and CNCs and DMF. These results are consistent with the difficulties that have been reported to disperse unmodified CNCs in these matrices [24], [57]. Also, it should be mentioned that the HSP parameters are affected by molecular weight and crystallinity [55], [58]. For the same two polymers of different molecular weights, the HSP radius of low molecular weight is larger than the high molecular weight [59]. Hence, scPLA with a low molecular weight and higher crystallinity compared to aPLA should have a larger HSP radius, R_0. As a result, the RED for scPLA and PBAT with larger R_0 is smaller than that for aPLA and PBAT. So, the chemical affinity between scPLA and PBAT with smaller RED is better than that for aPLA and PBAT, although they are phase separated.

6.13.3 Surface energy and interfacial tension

The Young model can predict the localization of solid particles in polymer blends [10] based on the wetting parameter, ω_a, defined by :

$$\omega_a = \frac{\gamma_{1s} - \gamma_{2s}}{\gamma_{12}} \quad \text{Equation S6}$$

where γ_{1s}, γ_{2s}, and γ_{12} are the interfacial tensions between polymer 1 and solid particles, polymer 2 and solid particles, and polymers 1 and 2, respectively. Thermodynamically, the particles would be localized in phase 2 when $\omega_a > 1$, while phase 1 is the preferred location of the solid particles when $\omega_a < -1$. The solid particles will be thermodynamically localized at the interface when $-1 \leq \omega_a \leq 1$ [13].

The harmonic-mean approach is used to estimate the interfacial tension between PLA and PBAT [60]:

$$\gamma_{ij} = \gamma_i + \gamma_j - 4\left(\frac{\gamma_i^d \gamma_j^d}{\gamma_i^d + \gamma_j^d} + \frac{\gamma_i^p \gamma_j^p}{\gamma_i^p + \gamma_j^p}\right) \quad \text{Equation S7}$$

and the interfacial tension between PLA and CNC, and PBAT and CNC is determined via the geometric-mean equation [60]:

$$\gamma_{ij} = \gamma_i + \gamma_j - 2\left[\sqrt{\gamma_i^d \gamma_j^d} + \sqrt{\gamma_i^p \gamma_j^p}\right] \quad \text{Equation S8}$$

where γ_{ij} is the interfacial tension between components i and j, γ_i is the surface tension of material i and γ_i^d and γ_i^p are the dispersive and polar components, respectively, of the surface tension of the same material. The harmonic mean approach is more accurate for estimating the interfacial tensions between low surface energy materials while the geometric mean equation can predict the interfacial tensions between low and high surface energy materials more accurately [60]. We can obtain the values of the interfacial tensions between the PLA/PBAT/CNC components and the wetting coefficient to estimate the localization preference of CNCs within the blend. The interfacial tensions were calculated based on surface tension values for PLA, PBAT, and CNCs at 25 °C reported in the literature [12], [13], [61]. To obtain the surface tension of the polymer components at the processing temperature (180 °C), a temperature coefficient of 0.06 $mJ \cdot m^{-2} \cdot K^{-1}$ was used to extrapolate the surface tension values at 25 °C [41]. Also, the CNC surface tension was estimated

at 180 °C using a temperature coefficient of −0.2 $mJ \cdot m^{-2} \cdot K^{-1}$ reported in the literature [61]. The surface tension parameters of the blend nanocomposite components at the processing temperature of 180 °C and their estimated interfacial tensions are reported in Table 6.S2. Considering PLA as phase 1 and PBAT as phase 2 and replacing the estimated interfacial tensions in Equation S6, the wetting parameter is calculated as 6.67 (i.e., $\omega \gg 1$), which predicts that the thermodynamic equilibrium localization of CNCs should be in the PBAT phase.

Table 6.S2 Surface energy values of PLA, PBAT, and CNCs as well as the calculated interfacial tensions between CNCs, PLA, and PBAT at 180 °C.

	At 25 °C			**At 180 °C**			**Interfacial tension at 180 °C γ_{12} (mN/m)**		
	γ (mN/m)	**γ^d (mN/m)**	**γ^p (mN/m)**	**γ (mN/m)**	**γ^d (mN/m)**	**γ^p** (mN/m)	**PLA**	**PBAT**	**CNC**
PLA	39.4	33.6	5.8	30.1	25.7	4.4	-	0.06 [a]	3.4 [b]
PBAT	38.4	32.1	6.3	29.1	24.3	4.8	0.06 [a]	-	3.0 [b]
CNCs	68.9	40.9	28	37.9	22.5	15.4	3.4 [b]	3.0 [b]	-

[a] Calculated from the harmonic-mean approach (Equation S7)

[b] Calculated from the geometric-mean approach (Equation S8)

Also, in this work, the emulsion model of Palierne [62] was used to determine the interfacial tension of PLA and PBAT from the SAOS data [62], [63]. This model (Equations S9 & S10) is used for the neat blends prepared from granules and solution casting followed by melt mixing with narrow droplet size distribution. As the average droplet size for the neat blends prepared by solution casting are more than 2 μm with varying droplet size distribution and coarse morphology, the Palierne model is not applicable for the interfacial analysis of those neat blends [64]. The complex modulus of a blend of narrow droplet size distribution ($R_v/R_n \leq 2$, where R_n is the number-average diameter) and constant interfacial tension is expressed by [64]:

$$G_b^*(\omega) = G_m^*(\omega)\frac{1+3\phi H^*(\omega)}{1-2\phi H^*(\omega)} \qquad \text{Equation S9}$$

and

$$H^*(\omega) = \frac{4\left(\frac{\gamma_{12}}{R_v}\right)\left[2G_m^*(\omega)+5G_d^*(\omega)\right]+\left[G_d^*(\omega)-G_m^*(\omega)\right]\left[16G_m^*(\omega)+19G_d^*(\omega)\right]}{40\left(\frac{\gamma_{12}}{R_v}\right)\left[G_m^*(\omega)+G_d^*(\omega)\right]+\left[2G_d^*(\omega)+3G_m^*(\omega)\right]\left[16G_m^*(\omega)+19G_d^*(\omega)\right]} \qquad \text{Equation S10}$$

where ϕ, ω, and γ_{12} are the volume fraction of droplets of volume average radius, R_v, the angular frequency, and the interfacial tension, respectively. $G_b^*(\omega)$, $G_m^*(\omega)$, and $G_d^*(\omega)$ are the complex modulus of the blend, matrix, and dispersed phase, respectively. The interfacial tension was obtained by fitting the data to the model predictions for the neat blends (Figures 6.S2a–d) using MATLAB (MATLAB software package R2019b, the Mathworks, Inc. Massachusetts, USA) and for the values of R_v determined from the SEM images. The storage and loss moduli of the blends can be expressed explicitly in terms of the moduli of both components [64], [65].

$$G_b^{'} = \frac{1}{D}\left[G_m^{'}(B_1B_2 + B_3B_4) - G_m^{''}(B_4B_1 - B_2B_3)\right] \quad \text{Equation S11}$$

$$G_b^{''} = \frac{1}{D}\left[G_m^{'}(B_1B_4 - B_2B_3) + G_m^{''}(B_1B_2 + B_3B_4)\right] \quad \text{Equation S12}$$

where the constants are expressed by:

$$B_1 = C_1 - 2\phi C_3 \quad \text{Equation S13}$$

$$B_2 = C_1 + 3\phi C_3 \quad \text{Equation S14}$$

$$B_3 = C_2 - 2\phi C_4 \quad \text{Equation S15}$$

$$B_4 = C_2 + 3\phi C_4 \quad \text{Equation S16}$$

$$D = (C_2 - 2\phi C_4)^2 + (C_1 - 2\phi C_3)^2 \quad \text{Equation S17}$$

with

$$C_1 = 40\left(\frac{\gamma_{12}}{R_v}\right)\left(G_m^{'} + G_d^{'}\right) + 38\left(G_d^{'2} - G_d^{''2}\right) + 48\left(G_m^{'2} - G_m^{''2}\right) + 89(G_m^{'}G_d^{'} - G_m^{''}G_d^{''})$$

Equation S18

$$C_2 = 40\left(\frac{\gamma_{12}}{R_v}\right)\left(G_m^{''} + G_d^{''}\right) + 98G_m^{'}G_m^{''} + 76G_d^{'}G_d^{''} + 89(G_m^{''}G_d^{'} - G_m^{'}G_d^{''}) \quad \text{Equation S19}$$

$$C_3 = 4\left(\frac{\gamma_{12}}{R_v}\right)\left(2G_m^{'} + 5G_d^{'}\right) - 16\left(G_m^{'2} - G_m^{''2}\right) + 19\left(G_d^{'2} - G_d^{''2}\right) - 3(G_m^{'}G_d^{'} - G_m^{''}G_d^{''})$$

Equation S20

$$C_4 = 4\left(\frac{\gamma_{12}}{R_v}\right)\left(2G_m^{''} + 5G_d^{''}\right) - 32G_m^{'}G_m^{''} + 38G_d^{'}G_d^{''} - 3(G_m^{''}G_d^{'} + G_m^{'}G_d^{''}) \quad \text{Equation S21}$$

Figure 6.S2 shows that the best fits (a–d; solid lines) are quite adequate, and the interfacial tensions were found to be 1.2 mN/m (aPLA/PBAT granules), 0.8 mN/m (scPLA/PBAT granules), 1.8 mN/m

(aPLA/PBAT (+IMM)), and 1.3 mN/m (scPLA/PBAT (+IMM)). These values are quite different than those estimated from the harmonic-mean equation. The lower calculated interfacial tension for scPLA/PBAT compared to aPLA/PBAT confirms the better compatibility between scPLA and PBAT. This better compatibility is expected from the HSP parameters as explained above. Also, the increase in interfacial tension for the samples prepared from solution casting followed by melt mixing could be due to fact that the Palierne model predictions are not always very sensitive to the interfacial tension as shown by Lacroix et al. [22] and demonstrated here by the predictions using the interfacial tension obtained for the blends prepared from granules, given the dashed lines in Figure 6.S2c & d. For both blends, the fits appear to be as good and one may assume that the interfacial tension values obtained for the blends prepared from granules are quite reasonable. Overall, using these interfacial tensions, the wetting parameter is calculated to be between 0 and 1, which predicts that the localization of CNCs should be at the interface of the PLA and PBAT, in contrast to the localization in PBAT predicted from the thermodynamics analysis presented above.

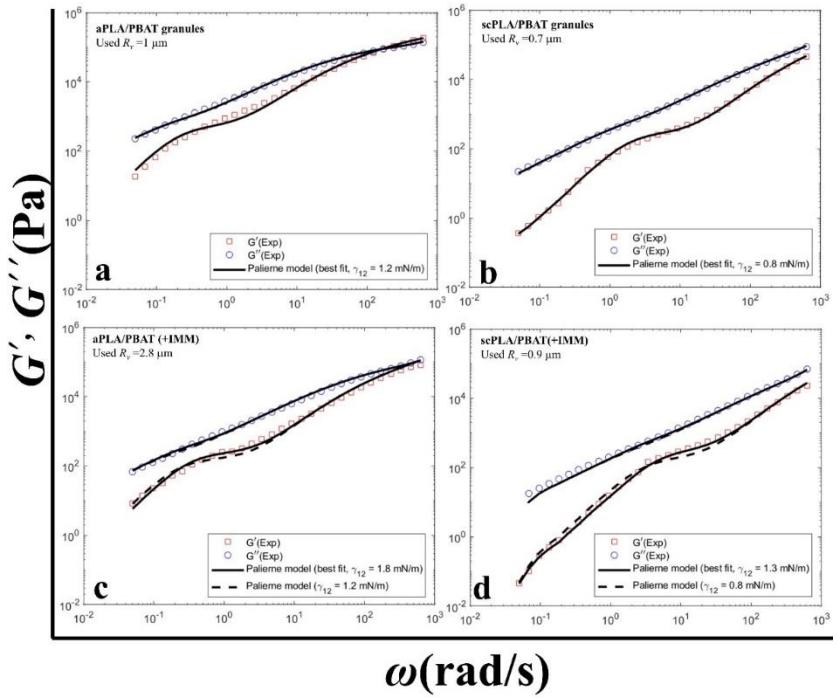

Figure 6.S2 Palierne model predictions; solid lines: best fits of G' and G'' for the blends of aPLA/PBAT and scPLA/PBAT prepared from granules (a & b) and solution casting followed by melt mixing (c & d) and dashed lines: comparison with the data of the 75/25 (wt%) aPLA/PBAT (c) and scPLA/PBAT (d) blends using the interfacial tension obtained from the best fits of the neat blends from granules (a & b).

6.13.4 Additional rheological data of the single polymer matrix and blend nanocomposites

Figure 6.S3 presents the stress growth coefficient, η^+, versus time, t, for scPLA/CNC (Figure 6.S3a) and aPLA/CNC (Figure 6.S3b) nanocomposites for an imposed shear rate 5 s^{-1} for the first 20 s of the test that lasted 480 s (η^+ was about constant for a time longer than 20 s). Solid and dashed lines represent the data for the samples prepared from solution casting and solution casting followed by melt mixing, respectively. Neat scPLA and aPLA do not show any overshoot before and after melt mixing in the absence of CNCs and network formation. On the other hand, the formation of a CNCs network in the matrix of both PLA results in significant overshoots mainly for solution cast samples. Also, melt mixing (dashed lines) results in a severe decrease in the intensity of overshoot due to the re-agglomeration of CNCs during melt mixing.

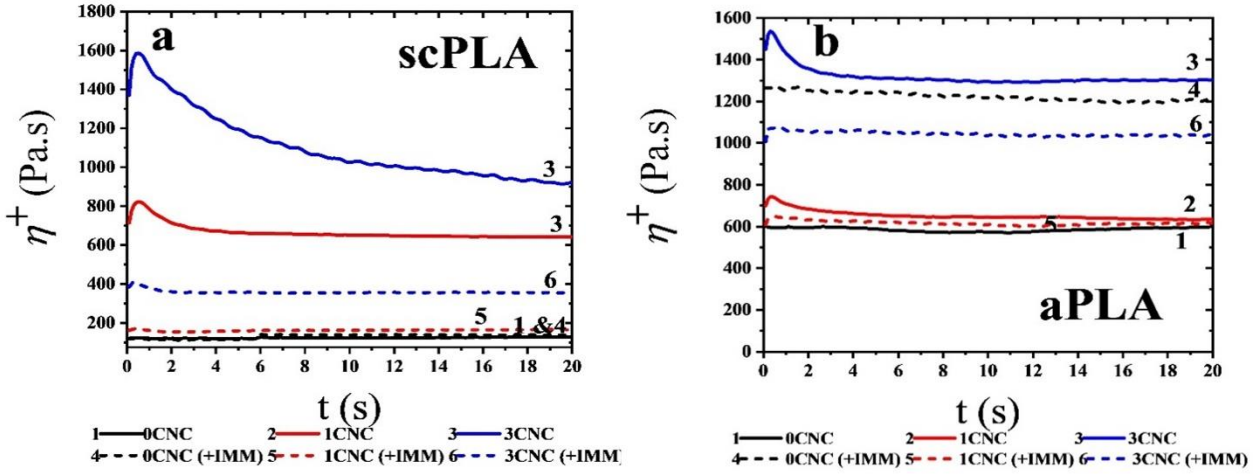

Figure 6.S3 Variations of the shear stress growth coefficient, η+, with time, t, for scPLA/CNC (a) and aPLA/CNC (b) nanocomposites for an imposed shear rate of 5 s^{-1}. The solid and dashed lines represent the samples prepared from solution casting and solution casting followed by melt mixing, respectively.

Due to the startup flow experiments, the CNC networks in scPLA, aPLA, and PBAT were destroyed and the rebuild-up of the networks was investigated through SAOS time sweep experiments for 1800 s. Figure 6.S4 reports the storage modulus versus time as solid and dashed lines for the single polymer matrix nanocomposites prepared from solution casting without melt mixer and followed by melt mixing, respectively. There is no structural build-up for all neat polymers before and after melt mixing, as expected. On the other hand, the structural build-up is

clear for all single polymer matrix nanocomposites, especially the ones from solution casting with a larger CNC content. We note that after 1800 s, *G´* is still evolving as the structure has not attained an equilibrium value. The structural build-up can be affected by both the pre-shear rate, time of the startup flow experiments, and the concentration of CNCs.

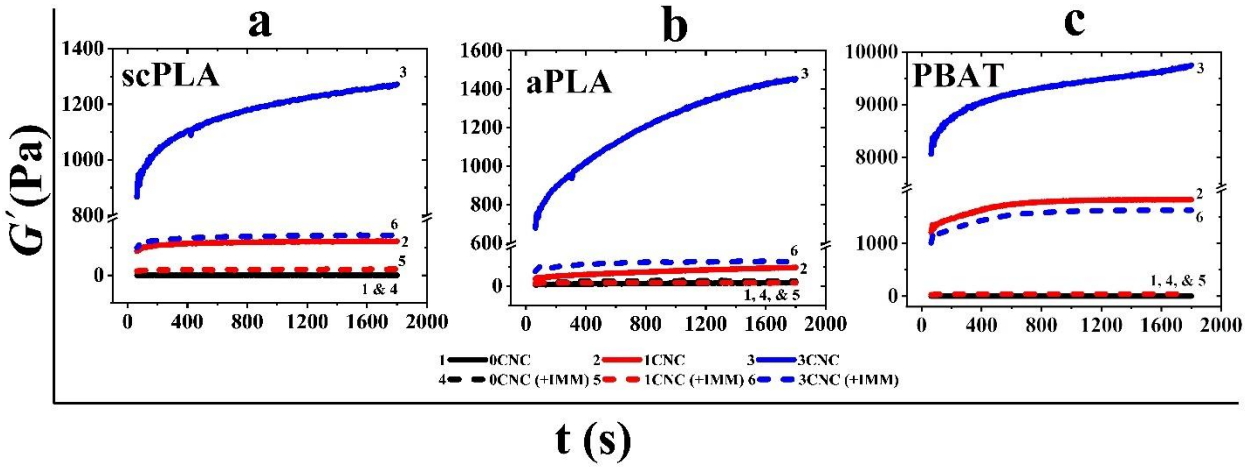

Figure 6.S4 Structure evolution expressed by the storage modulus versus time for scPLA/CNC (a), aPLA/CNC (b), and PBAT/CNC (c) nanocomposites right after the cessation of shear flow. Solid lines are the data of samples from solution casting and dashed lines represent the effect of melt mixing.

The frequency sweep tests were conducted after the stress growth experiments of Figure 6.S3 and the results are presented in Figures 6.S5 and 6.S6 for the samples from solution casting and solution casting followed by melt mixing, respectively. The reductions of the complex viscosity and storage modulus for the samples from solution casting are larger than the ones after melt mixing. Also, the small decrease in the complex viscosity of aPLA/CNC nanocomposites at high frequencies compared to the sample prepared from granules (Figures 6.2 and 6.3 in the main manuscript) could be due to degradation of aPLA in the presence of CNCs. Although the structural recovery after time sweep tests may not be completed, these differences between solution casting and melt mixing could be due to the evaporation of the remaining solvent during melt mixing.

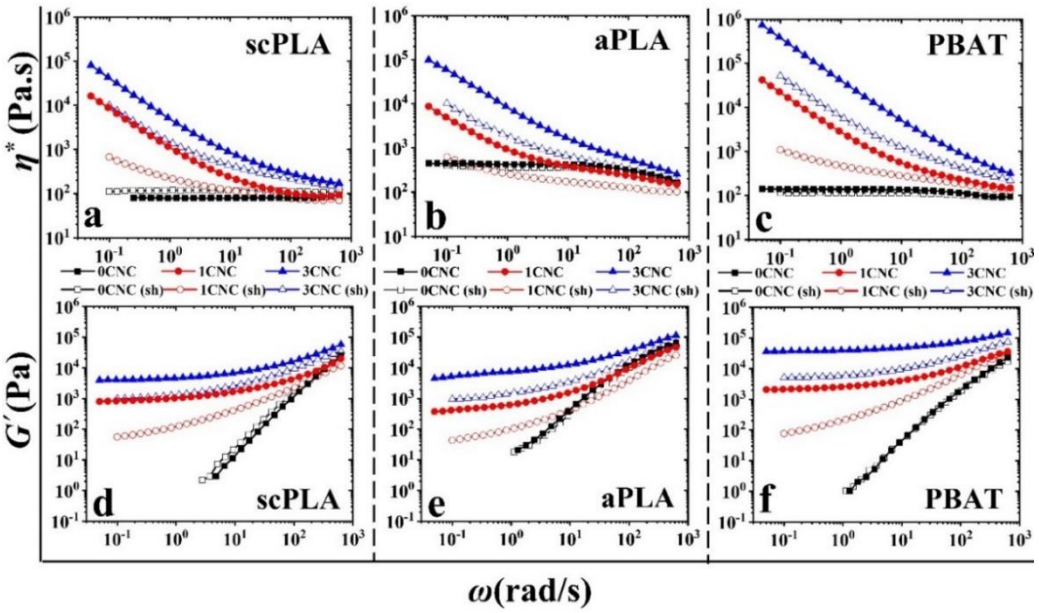

Figure 6.S5 Complex viscosity (a-c) and storage modulus (d-f) versus angular frequency of the neat polymers (0 CNC) and nanocomposites (1 and 3 CNC) from solution casting. Filled and empty symbols are SAOS data before and after stress growth experiments (sh), respectively.

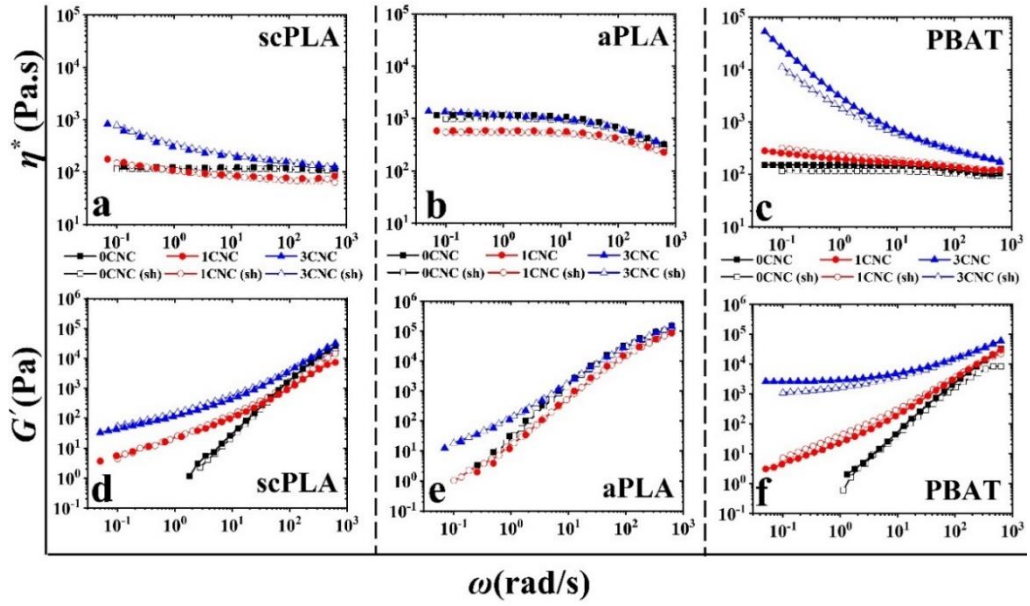

Figure 6.S5 Effect of melt mixing (solvent casting + IMM) on the complex viscosity (a-c) and storage modulus (d-f) of the neat polymers (0 CNC) and nanocomposites (1 and 3 CNC) prepared through solution casting as functions of angular frequency and CNC content. Filled and empty symbols are SAOS data before and after stress growth experiments (sh), respectively.

To confirm the absence of coalescence in the PLA/PBAT nanocomposites, time sweep experiments were conducted at a frequency of 1 rad/s for 1 h, and the results are presented in Figure 6.S7. The initial increases of the complex viscosity could be due to the formation of an extended interconnected network of nanoparticles with time. If we look at the SAOS data (Figure 6.9 in the main manuscript), we observe a solid-like behavior at low frequencies when the CNCs are initially localized in the matrix or both phases, whereas this behavior is not observed when the CNCs are initially in PBAT. So, we can conclude that the proportion of CNCs at the interface between the matrix and droplet results in an interconnected network of nanoparticles over time. Due to PLA degradation and PBAT droplet coalescence, the time to reach a 10% drop in the complex viscosity is about 12 min and 60 min for scPLA/PBAT and aPLA/PBAT, respectively. In the presence of 1 wt% CNCs, when the CNCs were initially localized in the matrix or both phases, the system is stable up to 60 min. On the other hand, localizing CNCs in the dispersed phase (upward triangle) results in a decrease in the complex viscosity. However, this decrease is less than 10% for aPLA/(PBAT-1CNC) and around 10% for scPLA/(PBAT-1CNC) blend nanocomposites. For example, the viscosity of aPLA/(PBAT-1CNC) decreases from 3250 Pa.s to 3000 Pa.s, which is around 9% after 1 h.

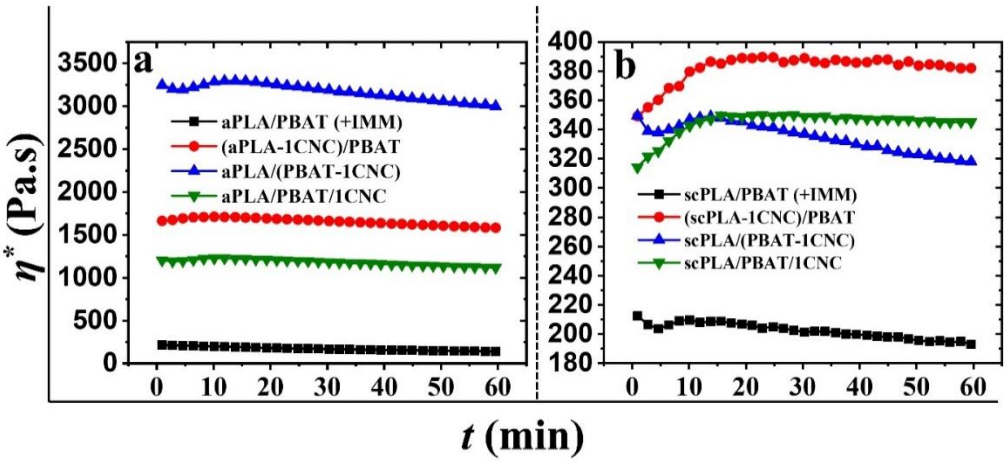

Figure 6.S7 Complex viscosity (η^*) versus time (t) of the neat PLA/PBAT (a: amorphous and b: semicrystalline) and blend nanocomposites reinforced with 1 wt% CNCs during 1 h at a frequency of 1 rad/s and strain amplitude of 0.001.

6.14 References

[1] D. Garlotta, “A literature review of poly(lactic acid),” *J. Polym. Environ.*, vol. 9, no. 2, pp. 63–84, 2001, doi: 10.1023/A:1020200822435.

[2] M. Jamshidian, E. A. Tehrany, M. Imran, M. Jacquot, and S. Desobry, “Poly-Lactic Acid: Production, applications, nanocomposites, and release studies,” *Compr. Rev. Food Sci. Food Saf.*, vol. 9, no. 5, pp. 552–571, 2010, doi: 10.1111/j.1541-4337.2010.00126.x.

[3] M. Wang, Y. Wu, Y. D. Li, and J. B. Zeng, “Progress in Toughening Poly(Lactic Acid) with Renewable Polymers,” *Polymer Reviews*. 2017, doi: 10.1080/15583724.2017.1287726.

[4] M. Nofar, D. Sacligil, P. J. Carreau, M. R. Kamal, and M.-C. Heuzey, “Poly (lactic acid) blends: Processing, properties and applications,” *Int. J. Biol. Macromol.*, vol. 125, pp. 307–360, 2018, doi: 10.1016/j.ijbiomac.2018.12.002.

[5] J. Jian, Z. Xiangbin, and H. Xianbo, “An overview on synthesis, properties and applications of poly(butylene-adipate-co-terephthalate)–PBAT,” *Adv. Ind. Eng. Polym. Res.*, vol. 3, no. 1, pp. 19–26, Jan. 2020, doi: 10.1016/j.aiepr.2020.01.001.

[6] E. Jalali Dil, P. J. Carreau, and B. D. Favis, “Morphology, miscibility and continuity development in poly(lactic acid)/poly(butylene adipate-co-terephthalate) blends,” *Polymer (Guildf).*, vol. 68, pp. 202–212, Jun. 2015, doi: 10.1016/j.polymer.2015.05.012.

[7] M. Nofar, A. Maani, H. Sojoudi, M. C. Heuzey, and P. J. Carreau, “Interfacial and rheological properties of PLA/PBAT and PLA/PBSA blends and their morphological stability under shear flow,” *J. Rheol. (N. Y. N. Y).*, vol. 59, no. 2, pp. 317–333, Mar. 2015, doi: 10.1122/1.4905714.

[8] A. Taguet, P. Cassagnau, and J.-M. Lopez-Cuesta, “Structuration, selective dispersion and compatibilizing effect of (nano)fillers in polymer blends,” *Prog. Polym. Sci.*, vol. 39, no. 8, pp. 1526–1563, Aug. 2014, doi: 10.1016/j.progpolymsci.2014.04.002.

[9] M. Salzano de Luna and G. Filippone, “Effects of nanoparticles on the morphology of immiscible polymer blends – Challenges and opportunities,” *Eur. Polym. J.*, vol. 79, pp. 198–218, Jun. 2016, doi: 10.1016/j.eurpolymj.2016.02.023.

[10] F. Fenouillot, P. Cassagnau, and J.-C. Majesté, “Uneven distribution of nanoparticles in immiscible fluids: Morphology development in polymer blends,” *Polymer (Guildf).*, vol. 50, no. 6, pp. 1333–1350, Mar. 2009, doi: 10.1016/j.polymer.2008.12.029.

[11] Z. Yuan and B. D. Favis, “Coarsening of immiscible co-continuous blends during quiescent annealing,” *AIChE J.*, vol. 51, no. 1, pp. 271–280, Jan. 2005, doi: 10.1002/aic.10281.

[12] E. Jalali Dil, M. Arjmand, I. Otero Navas, U. Sundararaj, and B. D. Favis, “Interface Bridging of Multiwalled Carbon Nanotubes in Polylactic Acid/Poly(butylene adipate- co -terephthalate): Morphology, Rheology, and Electrical Conductivity,” *Macromolecules*, vol. 53, no. 22, pp. 10267–10277, Nov. 2020, doi: 10.1021/acs.macromol.0c01525.

[13] E. Jalali Dil and B. D. Favis, “Localization of micro- and nano-silica particles in heterophase poly(lactic acid)/poly(butylene adipate-co-terephthalate) blends,” *Polymer (Guildf).*, vol. 76, pp. 295–306, Oct. 2015, doi: 10.1016/j.polymer.2015.08.046.

[14] A. Göldel, G. Kasaliwal, and P. Pötschke, “Selective Localization and Migration of Multiwalled Carbon Nanotubes in Blends of Polycarbonate and Poly(styrene-acrylonitrile),” *Macromol. Rapid Commun.*, vol. 30, no. 6, pp. 423–429, Mar. 2009, doi: 10.1002/marc.200800549.

[15] R. Salehiyan and S. Sinha Ray, “Processing of Polymer Blends, Emphasizing: Melt Compounding; Influence of Nanoparticles on Blend Morphology and Rheology; Reactive Processing in Ternary Systems; Morphology–Property Relationships; Performance and Application Challenges; and Opportunities ,” in *Springer Series in Materials Science*, vol. 278, Springer Verlag, 2018, pp. 167–197.

[16] E. Jalali Dil, N. Virgilio, and B. D. Favis, “The effect of the interfacial assembly of nano-silica in poly(lactic acid)/poly(butylene adipate-co-terephthalate) blends on morphology, rheology and mechanical properties,” *Eur. Polym. J.*, vol. 85, pp. 635–646, Dec. 2016, doi: 10.1016/j.eurpolymj.2016.07.022.

[17] S. Girdthep, N. Komrapit, R. Molloy, S. Lumyong, W. Punyodom, and P. Worajittiphon, “Effect of plate-like particles on properties of poly(lactic acid)/poly(butylene adipate-co-terephthalate) blend: A comparative study between modified montmorillonite and graphene

nanoplatelets," *Compos. Sci. Technol.*, vol. 119, pp. 115–123, Nov. 2015, doi: 10.1016/j.compscitech.2015.10.005.

[18] M. S. Garg and D. Srivastava, "Effect of glycidyl methacrylate (GMA) content on thermal and mechanical properties of ternary blend systems based on cardanol-based vinyl ester resin, styrene and glycidyl methacrylate," *Prog. Org. Coatings*, vol. 77, no. 7, pp. 1208–1220, Jul. 2014, doi: 10.1016/j.porgcoat.2014.03.029.

[19] M. Nofar, R. Salehiyan, U. Ciftci, A. Jalali, and A. Durmuş, "Ductility improvements of PLA-based binary and ternary blends with controlled morphology using PBAT, PBSA, and nanoclay," *Compos. Part B Eng.*, vol. 182, p. 107661, Feb. 2020, doi: 10.1016/j.compositesb.2019.107661.

[20] M. Nofar, M.-C. Heuzey, P. J. Carreau, and M. R. Kamal, "Nanoparticle Interactions and Molecular Relaxation in PLA/PBAT/Nanoclay Blends," *Exp. Results*, vol. 1, 2020, doi: 10.1017/exp.2020.54.

[21] M. Nofar, M.-C. Heuzey, P. J. Carreau, and M. R. Kamal, "Effects of nanoclay and its localization on the morphology stabilization of PLA/PBAT blends under shear flow," *Polymer (Guildf).*, vol. 98, pp. 353–364, Aug. 2016, doi: 10.1016/j.polymer.2016.06.044.

[22] S. Adrar, A. Habi, A. Ajji, and Y. Grohens, "Synergistic effects in epoxy functionalized graphene and modified organo-montmorillonite PLA/PBAT blends," *Appl. Clay Sci.*, vol. 157, pp. 65–75, Jun. 2018, doi: 10.1016/j.clay.2018.02.028.

[23] R. Salehiyan, M. Nofar, K. Malkappa, and S. S. Ray, "Effect of nanofillers characteristics and their selective localization on morphology development and rheological properties of melt-processed polylactide/poly(butylene adipate-co-terephthalate) blend composites," *Polym. Eng. Sci.*, p. pen.25505, Sep. 2020, doi: 10.1002/pen.25505.

[24] D. Bagheriasl, P. J. Carreau, B. Riedl, C. Dubois, and W. Y. Hamad, "Shear rheology of polylactide (PLA)–cellulose nanocrystal (CNC) nanocomposites," *Cellulose*, vol. 23, no. 3, pp. 1885–1897, 2016, doi: 10.1007/s10570-016-0914-1.

[25] D. Bagheriasl, P. J. Carreau, B. Riedl, and C. Dubois, "Enhanced properties of polylactide by incorporating cellulose nanocrystals," *Polym. Compos.*, vol. 39, no. 8, pp. 2685–2694, 2018, doi: 10.1002/pc.24259.

[26] D. Bagheriasl, F. Safdari, P. J. Carreau, C. Dubois, and B. Riedl, “Development of cellulose nanocrystal-reinforced polylactide: A comparative study on different preparation methods,” *Polym. Compos.*, vol. 40, pp. E342–E349, Jan. 2019, doi: 10.1002/pc.24676.

[27] D. Bagheriasl and P. J. Carreau, “Polymer–Cellulose Nanocrystal (CNC) Nanocomposites,” in *Processing of Polymer Nanocomposites*, München: Carl Hanser Verlag GmbH & Co. KG, 2019, pp. 371–393.

[28] M. Mohammadi, C. Bruel, M. C. Heuzey, and P. J. Carreau, “CNC dispersion in PLA and PBAT using two solvents: morphological and rheological properties,” *Cellulose*, vol. 27, no. 17, pp. 9877–9892, Sep. 2020, doi: 10.1007/s10570-020-03460-8.

[29] M. P. Arrieta, E. Fortunati, F. Dominici, E. Rayón, J. López, and J. M. Kenny, “PLA-PHB/cellulose based films: Mechanical, barrier and disintegration properties,” *Polym. Degrad. Stab.*, vol. 107, pp. 139–149, 2014, doi: 10.1016/j.polymdegradstab.2014.05.010.

[30] M. P. Arrieta, E. Fortunati, F. Dominici, E. Rayón, J. López, and J. M. Kenny, “Multifunctional PLA-PHB/cellulose nanocrystal films: Processing, structural and thermal properties,” *Carbohydr. Polym.*, vol. 107, no. 1, pp. 16–24, Jul. 2014, doi: 10.1016/j.carbpol.2014.02.044.

[31] M. P. Arrieta, E. Fortunati, F. Dominici, J. López, and J. M. Kenny, “Bionanocomposite films based on plasticized PLA-PHB/cellulose nanocrystal blends,” *Carbohydr. Polym.*, vol. 121, pp. 265–275, May 2015, doi: 10.1016/j.carbpol.2014.12.056.

[32] F. Luzi *et al.*, “Production and characterization of PLA_PBS biodegradable blends reinforced with cellulose nanocrystals extracted from hemp fibres,” *Ind. Crops Prod.*, vol. 93, pp. 276–289, Dec. 2016, doi: 10.1016/j.indcrop.2016.01.045.

[33] X. Zhang and Y. Zhang, “Reinforcement effect of poly(butylene succinate) (PBS)-grafted cellulose nanocrystal on toughened PBS/polylactic acid blends,” *Carbohydr. Polym.*, vol. 140, pp. 374–382, Apr. 2016, doi: 10.1016/j.carbpol.2015.12.073.

[34] M. Pracella, M. M. U. Haque, and D. Puglia, “Morphology and properties tuning of PLA/cellulose nanocrystals bio-nanocomposites by means of reactive functionalization and blending with PVAc,” *Polymer (Guildf).*, vol. 55, no. 16, pp. 3720–3728, Aug. 2014, doi: 10.1016/j.polymer.2014.06.071.

[35] N. Bitinis *et al.*, “Poly(lactic acid)/natural rubber/cellulose nanocrystal bionanocomposites Part I. Processing and morphology,” *Carbohydr. Polym.*, vol. 96, no. 2, pp. 611–620, 2013, doi: 10.1016/j.carbpol.2013.02.068.

[36] N. Bitinis *et al.*, “Poly(lactic acid)/natural rubber/cellulose nanocrystal bionanocomposites. Part II: Properties evaluation,” *Carbohydr. Polym.*, vol. 96, no. 2, pp. 621–627, 2013, doi: 10.1016/j.carbpol.2013.03.091.

[37] D. S. Sarul *et al.*, “Preparation and characterization of PLA/PBAT/CNC blend nanocomposites,” *Colloid Polym. Sci.*, Feb. 2021, doi: 10.1007/s00396-021-04822-9.

[38] V. Heshmati, M. R. Kamal, and B. D. Favis, “Cellulose nanocrystal in poly(lactic acid)/polyamide11 blends: Preparation, morphology and co-continuity,” *Eur. Polym. J.*, vol. 98, pp. 11–20, 2018, doi: 10.1016/j.eurpolymj.2017.10.027.

[39] V. Heshmati, M. R. Kamal, and B. D. Favis, “Tuning the localization of finely dispersed cellulose nanocrystal in poly (lactic acid)/bio-polyamide11 blends,” *J. Polym. Sci. Part B Polym. Phys.*, vol. 56, no. 7, pp. 576–587, 2018, doi: 10.1002/polb.24563.

[40] W. Y. Hamad and T. Q. Hu, “Structure-process-yield interrelations in nanocrystalline cellulose extraction,” *Can. J. Chem. Eng.*, vol. 88, no. 3, pp. 392–402, Jun. 2010, doi: 10.1002/cjce.20298.

[41] D. Wu, L. Yuan, E. Laredo, M. Zhang, and W. Zhou, “Interfacial properties, viscoelasticity, and thermal behaviors of poly(butylene succinate)/polylactide blend,” *Ind. Eng. Chem. Res.*, vol. 51, no. 5, pp. 2290–2298, Feb. 2012, doi: 10.1021/ie2022288.

[42] P. Koch, “Equivalent diameters of rectangular and oval ducts,” *Build. Serv. Eng. Res. Technol.*, vol. 29, no. 4, pp. 341–347, Nov. 2008, doi: 10.1177/0143624408094631.

[43] H. P. Grace, “Dispersion phenomena in high viscosity immiscible fluid systems and application of static mixers as dispersion devices in such systems,” *Chem. Eng. Commun.*, vol. 14, no. 3–6, pp. 225–277, Mar. 1982, doi: 10.1080/00986448208911047.

[44] S. Saha, U. D. Hemraz, and Y. Boluk, “The Effects of High Pressure and High Temperature in Semidilute Aqueous Cellulose Nanocrystal Suspensions,” *Biomacromolecules*, vol. 21, no. 2, pp. 1031–1035, Feb. 2020, doi: 10.1021/acs.biomac.9b01130.

[45] M. Mariano, N. El Kissi, and A. Dufresne, “Structural Reorganization of CNC in Injection-Molded CNC/PBAT Materials under Thermal Annealing,” *Langmuir*, vol. 32, no. 39, pp. 10093–10103, Oct. 2016, doi: 10.1021/acs.langmuir.6b03220.

[46] B. D. Favis and J. P. Chalifoux, “The effect of viscosity ratio on the morphology of polypropylene/polycarbonate blends during processing,” *Polym. Eng. Sci.*, vol. 27, no. 21, pp. 1591–1600, 1987, doi: 10.1002/pen.760272105.

[47] Y. Wang, Z. Ying, W. Xie, and D. Wu, “Cellulose nanofibers reinforced biodegradable polyester blends: Ternary biocomposites with balanced mechanical properties,” *Carbohydr. Polym.*, vol. 233, p. 115845, Apr. 2020, doi: 10.1016/j.carbpol.2020.115845.

[48] B. D. Favis, “Polymer alloys and blends: Recent advances,” *The Canadian Journal of Chemical Engineering*, vol. 69, no. 3. pp. 619–625, 1991, doi: 10.1002/cjce.5450690303.

[49] D. Graebling, R. Muller, and J. F. Palierne, “Linear Viscoelastic Behavior of Some Incompatible Polymer Blends in the Melt. Interpretation of Data with a Model of Emulsion of Viscoelastic Liquids,” *Macromolecules*, vol. 26, no. 2, pp. 320–329, 1993, doi: 10.1021/ma00054a011.

[50] C. M. Hansen, “The Three Dimensional Solubility Parameter and Solvent Diffusion Coefficient,” *J. Paint Technol.*, vol. 39, pp. 104–117, 1967, Accessed: Aug. 29, 2020. [Online]. Available: https://www.hansen-solubility.com/contents/HSP1967-OCR.pdf.

[51] C. Bruel, Q. Beuguel, J. R. Tavares, P. J. Carreau, and M.-C. Heuzey, “The apparent structural hydrophobicity of cellulose nanocrystals,” *J. Sci. Technol. For. Prod. Process.*, vol. 7, no. 4, pp. 13–23, 2018.

[52] C. Bruel, J. R. Tavares, P. J. Carreau, and M. C. Heuzey, “The structural amphiphilicity of cellulose nanocrystals characterized from their cohesion parameters,” *Carbohydr. Polym.*, vol. 205, pp. 184–191, 2019, doi: 10.1016/j.carbpol.2018.10.026.

[53] C. Bruel, T. S. Davies, P. J. Carreau, J. R. Tavares, and M.-C. Heuzey, “Self-assembly behaviors of colloidal cellulose nanocrystals: A tale of stabilization mechanisms,” *J. Colloid Interface Sci.*, vol. 574, pp. 399–409, Aug. 2020, doi: 10.1016/j.jcis.2020.04.049.

[54] C. Bruel, J. R. Tavares, P. J. Carreau, and M. Heuzey, “Impact of Colloidal Stability on Cellulose Nanocrystals Self-Ordering in Thin Films,” *TechConnect Briefs*, no. 1, pp. 61–64, 2019.

[55] S. Abbott, C. M. Hansen, and H. Yamamoto, *Hansen solubility parameters in practice complete with eBook , software and data*. 2013.

[56] “HSP and Temperature | Hansen Solubility Parameters.” https://www.hansen-solubility.com/HSP-science/HSP-T.php (accessed Feb. 23, 2021).

[57] C. L. Morelli, M. N. Belgacem, M. C. Branciforti, M. C. B. Salon, J. Bras, and R. E. S. Bretas, “Nanocomposites of PBAT and cellulose nanocrystals modified by in situ polymerization and melt extrusion,” *Polym. Eng. Sci.*, vol. 56, no. 12, pp. 1339–1348, 2016, doi: 10.1002/pen.24367.

[58] C. M. Hansen, *Hansen Solubility Parameters*. Boca Raton: CRC Press, 2007.

[59] “HSPiP FAQ | Hansen Solubility Parameters.” https://www.hansen-solubility.com/HSPiP/faq.php (accessed Feb. 23, 2021).

[60] S. Wu, *Polymer Interface and Adhesion*. Routledge, 2017.

[61] V. Khoshkava and M. R. Kamal, “Effect of surface energy on dispersion and mechanical properties of polymer/nanocrystalline cellulose nanocomposites,” *Biomacromolecules*, vol. 14, no. 9, pp. 3155–3163, 2013, doi: 10.1021/bm400784j.

[62] J. F. Palierne, “Linear rheology of viscoelastic emulsions with interfacial tension,” *Rheol. Acta*, vol. 29, no. 3, pp. 204–214, May 1990, doi: 10.1007/BF01331356.

[63] S. Wu, *Polymer Interface and Adhesion*. New York ;;Basel: Routledge, 2017.

[64] M. Bousmina and R. Muller, “Linear viscoelasticity in the melt of impact PMMA. Influence of concentration and aggregation of dispersed rubber particles,” *J. Rheol. (N. Y. N. Y).*, vol. 37, no. 4, pp. 663–679, Jul. 1993, doi: 10.1122/1.550389.

[65] C. Lacroix, M. Bousmina, P. J. Carreau, B. D. Favis, and A. Michel, “Properties of PETG/EVA blends: 1. Viscoelastic, morphological and interfacial properties,” *Polymer (Guildf).*, vol. 37, no. 14, pp. 2939–2947, Jul. 1996, doi: 10.1016/0032-3861(96)89389-X.

CHAPTER 7 ARRTICLE 3: MORPHOLOGICAL, THERMAL, AND MECHANICAL PROPERTIES OF CELLULOSE NANOCRYSTAL REINFORCED POLY(LACTIC ACID) AND POLY(BUTYLENE ADIPATE-CO-TEREPHTHALATE): A COMPARATIVE STUDY ON COMMON AND NOVEL SOLVENT CASTING METHODS[3]

Mojtaba Mohammadi, Marie-Claude Heuzey, Pierre J. Carreau

Center for High Performance Polymer and Composite Systems (CREPEC), Department of Chemical Engineering, École Polytechnique de Montréal, Montreal, Québec, H3T 1J4, Canada

7.1 Abstract

The mechanical and thermal properties of semicrystalline (sc) and amorphous (a) poly(lactic acid), PLA, and poly(butylene adipate-co-terephthalate), PBAT, and their nanocomposites containing 1 and 3 wt% CNCs, prepared through solvent casting methods using one (N, N-dimethylformamide (DMF)) or two (dimethyl sulfoxide (DMSO), and tetrahydrofuran (THF)) solvents were analyzed. Differential scanning calorimetry (DSC) showed that the total amount of crystals of the scPLA/CNC nanocomposites increased, whereas it decreased in the PBAT/CNC systems. In both cases, the crystallization temperature increased with CNC content. In tensile experiments, the Young modulus and yield strength of all nanocomposites were found to increase by incorporating CNCs, more significantly for the samples prepared using one solvent. The elongation at break of both PLA nanocomposites increased when prepared via one solvent, while it decreased for the two solvent methods as well as for PBAT nanocomposites prepared by both methods. The impact properties of the samples prepared by the two solvent methods decreased. In contrast, for the one solvent method, incorporating 3 wt% CNCs improved the impact properties by 32 % and 9 % in scPLA and aPLA, respectively, but decreased by 4 % in PBAT nanocomposites. Also, in dynamic mechanical thermal analysis (DMA) the storage modulus of scPLA and PBAT/CNC systems

[3] Submitted to Polymer Composites and is under revision for publication.

increased significantly, especially in the rubbery region (5 to 85 MPa and 105 to 155 MPa, respectively). Using a percolation model, the strength of the percolating CNC was found to be dependent on temperature and affected by traces of solvent mostly in the scPLA nanocomposites.

Keywords: PLA and PBAT/CNC nanocomposites; Solvent effect; Mechanical and thermal properties; DMA modeling

7.2 Introduction

The rod-like nanoparticles known as cellulose nanocrystals (CNCs) that are made by acid hydrolysis of cellulose, are biocompatible and biodegradable materials [1], [2] and have exceptional mechanical properties as well as optical properties and low density [3], [4]. Using CNCs as a reinforcement agent in polymers can improve their mechanical, thermal, and rheological properties when the CNCs are well dispersed and distributed into the polymer matrices. Unmodified CNCs with high polarity can be dispersed in limited hydrophilic polymer matrices [5]–[8], while their dispersion in hydrophobic polymer matrices is still challenging due to the strong hydrogen bonds between CNC particles [9].

Biodegradable polymers such as poly(lactic acid), PLA, and poly(butadiene co-adipate), PBAT, obtained from bio and fossil-based resources, respectively, have gained considerable attention in the last few decades [10], [11]. While PLA possesses mechanical (high modulus (2-16 GPa), high tensile strength (14-117 MPa)) and physical (good clarity) properties, it has significant drawbacks such as low melt strength, hardness, and service temperature, as well as a slow crystallization rate, poor processability, and brittleness. PBAT, on the other hand, has a higher elongation at break (around 700%), with a Young modulus of 20-35 MPa and a tensile strength of 32-36 MPa [11], [12]. Furthermore, it has high manufacturing costs and low thermal and mechanical resistances [10], [11].

Incorporating CNCs as a reinforcing agent in PLA or PBAT could improve the mechanical and thermal properties of these biodegradable polymers throughout a wide temperature range, overcoming these disadvantages in PLA and PBAT [13]–[16]. While melt mixing leads to agglomeration of CNCs as a result of strong inter-particle interactions, [17]–[20] approaches such as in-situ polymerization [21]–[23], compatibilization, and chemical modifications [24]–[27] can be costly and cumbersome. Therefore, solution casting has been considered as an efficient method

for dispersion and distribution of CNCs in the laboratory, but the method is still of limited practice by the industry due to use of expensive and toxic solvents. However, as far as we know except our previous investigation [28] no previous research has investigated an efficient method of selecting the best solvent for dispersion and dissolution of CNCs and polymers. Using a variety of solvents, our group examined the dispersion of CNCs in PLA and PBAT. [16], [20], [28], [29]. Bagheriasl et al. [29] used a solution casting method with dimethylformamide (DMF) as a solvent to prepare PLA/CNC nanocomposites and for the first time obtained a high degree of dispersion of pristine CNCs in PLA. Based on a thermodynamics analysis and solution casting method, Mohammadi et al. [28] determined that dimethyl sulfoxide (DMSO) and tetrahydrofuran (THF) were the best solvents for the dispersion of CNCs and dissolution of scPLA and aPLA as well as PBAT. They achieved the lowest rheological percolation threshold of 0.3 wt% CNCs in scPLA and PBAT and 1 wt% CNCs in aPLA. However, the effect of solution casting on the morphological, thermal, and mechanical properties of these nanocomposites needs to be investigated for samples prepared through common methods.

The presence of CNCs can increase or decrease the degree of crystallinity of semicrystalline polymers. CNCs acting as nuclei in polymer matrices lead to increased crystallinity [15], [16], [19], [26], [30], [31]; otherwise, the mobility of polymer chains decreases, which leads to lower crystalline content [3], [32], [33]. Trifol et al. [34] compared the crystallization behavior of PLA nanocomposites containing CNCs, partially acetylated cellulose nanofibers (CNFs), and nanoclay Cloisite 30B (C30B). The PLA/C30B systems showed faster crystallization than PLA/CNC during isothermal crystallization at 120 °C as a result of providing more nucleating sites (higher aspect ratio of clay platelets compared to nanocellulose-based entities). However, the total crystallinity of PLA/CNC was larger than that of PLA/C30B due to hindered molecular mobility of PLA chains in PLA/C30B, which in turn could impede the crystal's growth and the final crystallinity.

Highly dispersed CNCs in a polymer could increase the Young modulus and tensile strength compared to the neat polymer [3], [33]. The elongation at break, except for systems with a strong interaction at the interface [3], generally decreases compared to the neat polymer [33]. However, there are not unanimous reports on these properties. For example, enhanced Young moduli, unchanged tensile strengths, and decreased strains at break have been observed for many polymer–CNC nanocomposites [16], [17], [26], [35]. Reduced tensile strengths are also reported in some cases [31], [36], [37]. Among different studies on PLA/CNC systems few of them showed

improved mechanical properties using unmodified CNCs with/without other components such as surfactant, compatibilizer, etc. [16]–[18], [32], [38]–[42], On the other hand, few studies have been devoted to PBAT/CNC nanocomposites [15], [43]–[46]. Vatansever et al. [15] did not observe any significant differences in thermal degradation, and mechanical properties of PBAT/CNC prepared from solution casting or dilution of masterbatch through melt mixing. Morelli et al. [43] reported a slight increase in thermal stability and mechanical properties of PBAT reinforced by phenyl butyl isocyanate-modified CNCs prepared through melt-processing using a twin-screw extruder (TSE). In another study using solution casting, Morelli et al. [44] obtained 120 and 40 % improvement in tensile modulus and strength, respectively, when incorporating 10 wt% aromatic isocyanate-grafted CNCs in PBAT. A slight improvement in mechanical properties was reported by Pinherio et al. [45], when they prepared PBAT/octadecyl isocyanate-modified CNCs in an internal melt mixer. Also, Ferreira et al. [46] could achieve an improvement in storage modulus for PBAT/3 wt% unmodified and adipic acid-modified CNCs prepared from solution casting.

Dynamic mechanical thermal analysis (DMA) is another interesting technique to evaluate the thermo-mechanical properties of polymer-CNC nanocomposites. Generally, the storage modulus is increased by incorporating CNCs, and upon a good dispersion of CNCs, the increases are more significant at higher CNC contents [23], [32], [47]–[50]. Using solution casting and DMF as a solvent, Bagheriasl et al. [16] achieved significant improvements in the storage modulus of PLA/CNC both in glassy (74 %) and rubbery (490%) regions by incorporating 6 wt% of unmodified CNCs compared to the neat PLA.

In our previous publications, we presented the effect of CNCs on the morphological and rheological properties of PLA and PBAT nanocomposites prepared from two solvent [28] or one solvent [20] casting methods. It is of interest to whether different methods of solvent casting have considerable effect on mechanical and thermal properties. Therefore, in this work, we investigate the thermal and mechanical properties of PLA/CNC and PBAT/CNC nanocomposites. A mechanical model considering a percolating network is also employed to describe the storage modulus of the nanocomposites at various temperatures. Our overall objective is to develop biodegradable PLA/CNC and PBAT/CNC nanocomposites with significantly improved mechanical and thermal properties.

7.3 Experimental

7.3.1 Materials

Ingeo 4060D (amorphous, aPLA) and 3251D (semi-crystalline, scPLA) were obtained from NatureWorks LLC (Minnetonka, MN, USA). aPLA and scPLA with a D-lactide content of 12 and 1.4 mol%, respectively, had a weight average molecular weight of 190 and 55 kg/mol. Also, PBAT (Ecoflex® FBX 7011) with a weight average molecular weight of 24.4 kg/mol, a density of 1.23 g/cm^{3,} and a melt flow index (MFI) of 2 g/10 min purchased from BASF. Freeze-dried CNCs which were neutralized using sodium hydroxide (NaOH) before freeze-drying kindly provided by FPInnovations (Pointe-Claire, QC, Canada). Their width, length, and aspect ratio are 16 ± 3, 90 ± 17 nm, and 6 ± 2, respectively [29]. The CNC preparation information can be found elsewhere [51]. Dimethyl sulfoxide (DMSO), tetrahydrofuran (THF), and N, N-dimethylformamide (DMF), anhydrous 99.8 %, were purchased from Sigma-Aldrich Canada Co. (Oakville, ON, Canada).

7.3.2 Solvent selection

Solvents such as N, N-dimethylformamide (DMF), dimethyl sulfoxide (DMSO), formic acid, dimethylacetamide (DMAc), pyridine, and a few more solvents [52] have the ability to disperse CNCs. In our previous study [28], we proposed a novel method based on thermodynamics concepts. In that method using Hansen solubility parameter (HSP) theory a binary mixture of DMSO and THF were selected as the best solvents for dispersing CNCs and dissolving PLA or PBAT, respectively. It was shown that in the HSP graph of CNCs, PLA, and PBAT we did not have any superposition of domains which confirm the lack of solvents capable of providing both adequate CNC dispersion and significant PLA and PBAT dissolution [28]. We showed that residual traces of solvents had significant effect on the rheological properties of the nanocomposites. A comprehensive discussion on the morphology and rheological properties can be found in our previous publication [28]. On the other hand, DMF is one of the most used solvents (easier to dry the solvent cast samples and as a consequence less remaining solvent in the final nanocomposites) in preparing polymer or polymer blend nanocomposites [20], [53]. In this work, we will compare the morphological, mechanical and thermal properties of PLA and PBAT nanocomposites prepared using the two solvents method (DMSO and THF) with those of the same nanocomposites prepared using a single solvent (DMF).

7.3.3 Sample preparation

The solution mixing method based on two solvents (THF and DMSO) as described in detail in our previous publication [28] and the one solvent (DMF) method [20] were used to prepare the neat nanocomposites. The aPLA, scPLA, and PBAT were first dried in a vacuum oven overnight at 55 °C. Using two solvents, the neat polymers and CNCs were dissolved and dispersed in THF and DMSO, respectively (Table 1). Using one solvent, both neat polymers and CNCs were dissolved and dispersed in DMF (Table 1). The desired amount of CNCs was dispersed in 70 mL of DMSO (two solvents method) or DMF (one solvent method) using a water bath sonicator (FS30 100 Watts Ultrasonic Cleaner, Fisher Scientific, Pittsburg, PA) for 120 min at room temperature. The neat polymers were dissolved in 85 mL of THF (two solvents method) or DMF (one solvent method) using a magnetic stirrer for 150 min at 63 °C and 120 min at 70 °C, respectively, until complete dissolution. In the two solvents method, the volume of liquid was kept constant throughout time by adding THF at regular intervals to reduce the influence of THF evaporation. Following that, the polymer solutions were added to the CNC suspension, and the sonication process was continued for another 120 minutes to ensure that the two media mixed well despite their high viscosity. Different drying conditions were applied when using two solvents or one solvent. For the two solvent methods, the mixtures were poured into a petri dish and dried in a vacuum oven (-0.65 bar) set at 70 °C for 4 days. After removing the samples, the low molecular weight PLA (scPLA) and PBAT nanocomposites could be ground into powder with a coffee grinder, whereas the high molecular weight PLA (aPLA) required to be chopped into very small pieces with scissors. Then, the ground and chopped nanocomposites were put in the vacuum oven for another 4 days in an effort to get rid of any remaining traces of DMSO and THF. For the one solvent method, first, the samples were put in the vacuum oven (0.9 bar) with air circulation set at 60 °C for 2 days followed by another 2 days at 80 °C under vacuum (-0.65 bar). In both methods, the CNC content in the nanocomposites was varied from 0 (i.e. neat polymers for comparison purposes), 1, and 3 wt%, and the nanocomposites are named based on the CNC content on a weight percentage basis. For example, aPLAs/3CNC refers to the nanocomposites based on the amorphous, high molecular weight PLA with 3 wt% of CNCs, calculated with respect to the total weight of the nanocomposite, which was prepared using one solvent. The ‘s’ or ‘ss’ following the symbols of the polymers stand for nanocomposites prepared by one solvent and two solvents methods, respectively. The chopped and powder samples were compression molded into disc, rectangle, and dog-bone shaped

specimens using a hydraulic press in a nitrogen atmosphere prior to microscopy, rheology, thermal, and mechanical investigation**.** The samples were first heated to 170 °C for 4 min. Then, pressure forces of 1, 2, and 3 tons were progressively applied for 90 s each. The samples were finally cooled to ambient temperature under atmospheric pressure. The overall compression molding process took roughly 10 min. Neat polymer samples from the solution methods and as-received granules were also prepared for comparison.

Table 7.1 Type of solvents for the dispersion of CNCs and the dissolution of polymers

Type of solvents	CNC dispersion	Polymer dissolution
One solvent (s); DMF	DMF	DMF
Two solvents (ss); DMSO and THF	DMSO	THF

7.3.4 Characterization

7.3.4.1 **Microscopy analysis**

7.3.4.1.1 Field emission scanning electron microscopy (FESEM)

Samples were cut and microtomed using an Ultracut FC microtome (LEICA) equipped with a liquid nitrogen cryo-chamber and a diamond knife. Field emission scanning electron microscopy (FESEM) was carried out on microtomed surfaces, coated with gold, using an FE-SEM (JSM 7600F, JEOL USA, Inc.) at a voltage of 3 kV and an LEI detector. Also, the diameter/thickness of the CNCs was calculated using the ImageJ software (version 1.52a Wayne Rasband, National Institutes of Health, USA).

7.3.4.2 **Thermal analysis**

Differential scanning calorimetry (DSC) of the samples was performed using a DSCQ1000 (TA Instruments, New Castle, DE, USA) on 5 mg material samples, under a nitrogen atmosphere. The samples were heated from 25 (PLA) or -40 (PBAT) to 200 °C at a constant rate of 10 °C /min and held at 200 °C for 3 min, then cooled to 25 °C (PLA) or -40 (PBAT) at a constant rate of 5 °C /min. Then the samples were heated in the second run from 25 (PLA) or -40 (PBAT) to 200 °C at a constant rate of 10 °C /min. The glass transition temperature (T_g), melt and cold crystallization (T_c and T_{cc}), and crystal melting (T_m) temperatures of the samples were extensively analyzed. The

following equations were employed to calculate the total crystallinity content of scPLA/CNC and PBAT/CNC nanocomposites;

$$X_c^{heating} = \frac{\Delta H_m - \Delta H_{cc}}{w \times \Delta H_m^\circ} \times 100 \quad \text{Equation 7.1}$$

$$X_c^{cooling} = \frac{\Delta H_c}{w \times \Delta H_m^\circ} \times 100 \quad \text{Equation 7.2}$$

where w, ΔH_m, ΔH_{cc}, ΔH_m°, and ΔH_c are the weight fraction of the polymeric matrix in the nanocomposite, enthalpy of melting, enthalpy of cold crystallization, enthalpy of melting of 100% crystalline polymer (93 J/g [54] and 114 J/g [55] for PLA and PBAT, respectively), and enthalpy of crystallization in cooling runs.

7.3.4.3 **Mechanical analysis**

Instron 3365 was used to investigate the tensile properties of the samples at room temperature according to standard ASTM D638. Tensile specimens, dog bone shaped type V of 1.6 mm thick, were stretched at room temperature at a crosshead speed of 5 mm/min using a load cell of 5 kN. For each sample, a minimum of five specimens were tested.

Dynamic mechanical thermal analysis (DMA) was conducted on compression-molded samples (1.6 mm thick, 12.2 mm wide, and 60.5 mm long) using a DMA 2980 analyzer (TA Instruments). The specimens were tested in the dual cantilever bending mode at an amplitude of 30 μm, a frequency of 1 Hz, and a heating rate of 3 °C /min from 24 to 120 °C. Four replicates for each sample were tested.

Notched Izod impact toughness was measured by using a Ray-Ran Universal Pendulum Impact Tester according to standard ASTM D256. The dimensions of specimens for impact testing were 63.5 ×12.7 ×3.0 mm^3 and a minimum of five specimens were tested.

7.3.4.4 **Modeling of DMA results**

A mechanical model was proposed by Takayanagi et al. [56] to show the relation between the complex modulus of a polymer blend with a matrix-droplet morphology and moduli of the components. Ouali et al. [57] using a modified series-parallel model of Takayanagi predicted the modulus of poly(methyl methacrylate) (PMMA) “reinforced” by poly(styrene-co-butyl acrylate) (PSBA). Bagheriasl et al. [16] extended the approach of Ouali et al. to predict the storage modulus

of scPLA/CNC nanocomposite (same semicrystalline PLA and CNC used in this work) by considering PLA as a soft polymer matrix reinforced by a rigid percolated CNC network. The main reason that other classical models such as the modified Halpin-Tsai and Halpin-Kardos [58] models underpredict the experimental data for a well-dispersed system is that they do not consider the percolation network and are mainly based on the aspect ratio of the filler and the storage moduli of the components. On the other hand, the modified Takayanagi model suggests that the mechanical properties are controlled by the percolating network of the nanoparticles. Following the approach of Bagheriasl et al. [16] the storage modulus (E') of scPLA/CNC and PBAT/CNC nanocomposites can be described by [16]:

$$E' = \frac{(1-2\psi+\psi\varphi_f)E'_m E'_{net}+(1-\varphi_f)\psi {E'_{net}}^2}{(1-\varphi_f)E'_{net}+(\varphi_f-\psi)E'_m} \quad \text{Equation 7.3}$$

where

$$\psi = \varphi_f \left(\frac{\varphi_f-\varphi_c}{1-\varphi_c}\right)^4 \quad \text{for } \varphi_f > \varphi_c \quad \text{Equation 7.4}$$

$$\psi = 0 \quad \text{for } \varphi_f \leq \varphi_c \quad \text{Equation 7.5}$$

E'_m, and E'_{net} are the storage moduli of the polymer matrix and of the percolating CNC network, respectively; E'_{net} , is fitted from the experimental data and assumed to be constant, independent of the volume fraction of CNCs. ψ, φ_f, and φ_c are the volume fraction of the percolating CNC network, CNC volume fraction, and critical volume fraction required for percolation, respectively. φ_c was assumed to be identical to the rheological percolating threshold determined in rheometry [16].

7.4 Results and discussion

7.4.1 Morphology

Figures. 7.1 and 7.2 present the low (left) and high (right) magnification of FESEM images of scPLA, aPLA, and PBAT polymers containing 1 wt% CNCs prepared from two solvents and one solvent methods, respectively. Individual and bundles of few CNCs are seen to be well dispersed and distributed for both methods. The CNCs appear as rod shape particles (some of them indicated by arrows in the higher magnification images (right sections in Figures. 7.1 and 7.2)) in

aPLA/CNC, scPLA/CNC, and PBAT/CNC. Also, the small holes (indicated by circles in the images of PBAT/CNC in Figures. 7.1 and 7.2) are possibly CNCs that were pulled out during microtoming as a result of the soft intrinsic characteristics of the PBAT matrix. The diameter/thickness of the CNC particles based on these images are in the range of 15 to 80 nm calculated from ImageJ software and this confirms the presence of CNC as individual nanoparticles and bundles in the matrix of PLA and PBAT for both methods. The extensive rheological analysis for both methods presented in our previous work confirms these morphological features [20], [29]. It is worthy to mention that based on a thermodynamics analysis [29] the use of DMSO and THF for dispersing CNCs and dissolving polymers, respectively, could result in a better dispersion and distribution of CNCs in hydrophobic PLA and PBAT (clearer from the rheological analysis of our previous publications [20], [29]). However, the effect of remaining solvents from the drying process may significantly affect the final properties of the nanocomposites and this without considering the time needed for drying (8 days for 2 solvents compared to 4 days for one solvent).

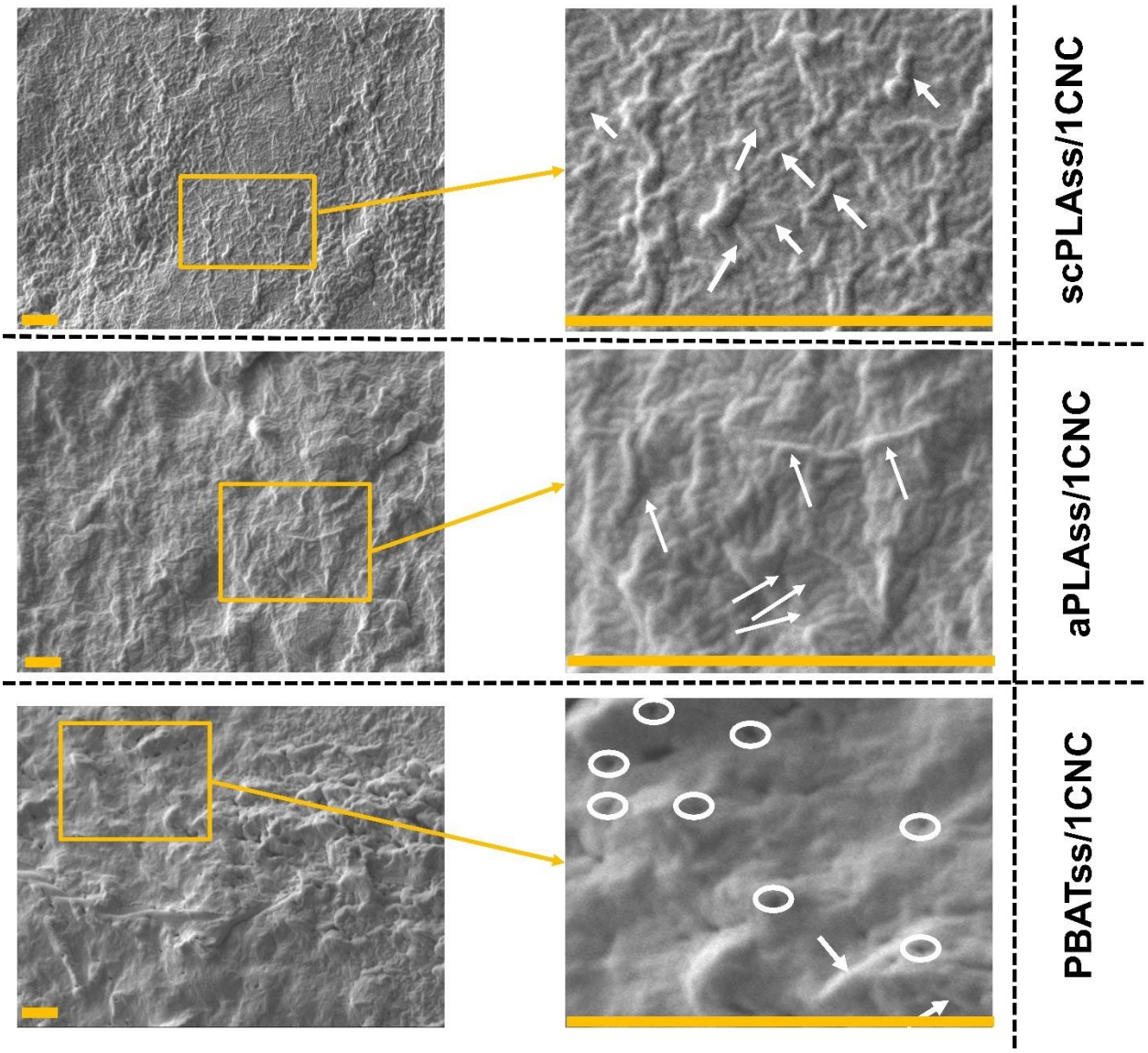

Figure 7.1 Low (left figures) and high (right figures) magnification of FESEM images of scPLA, aPLA, and PBAT containing 1 wt% CNCs prepared from two solvent method. The scale bars are 1 µm.

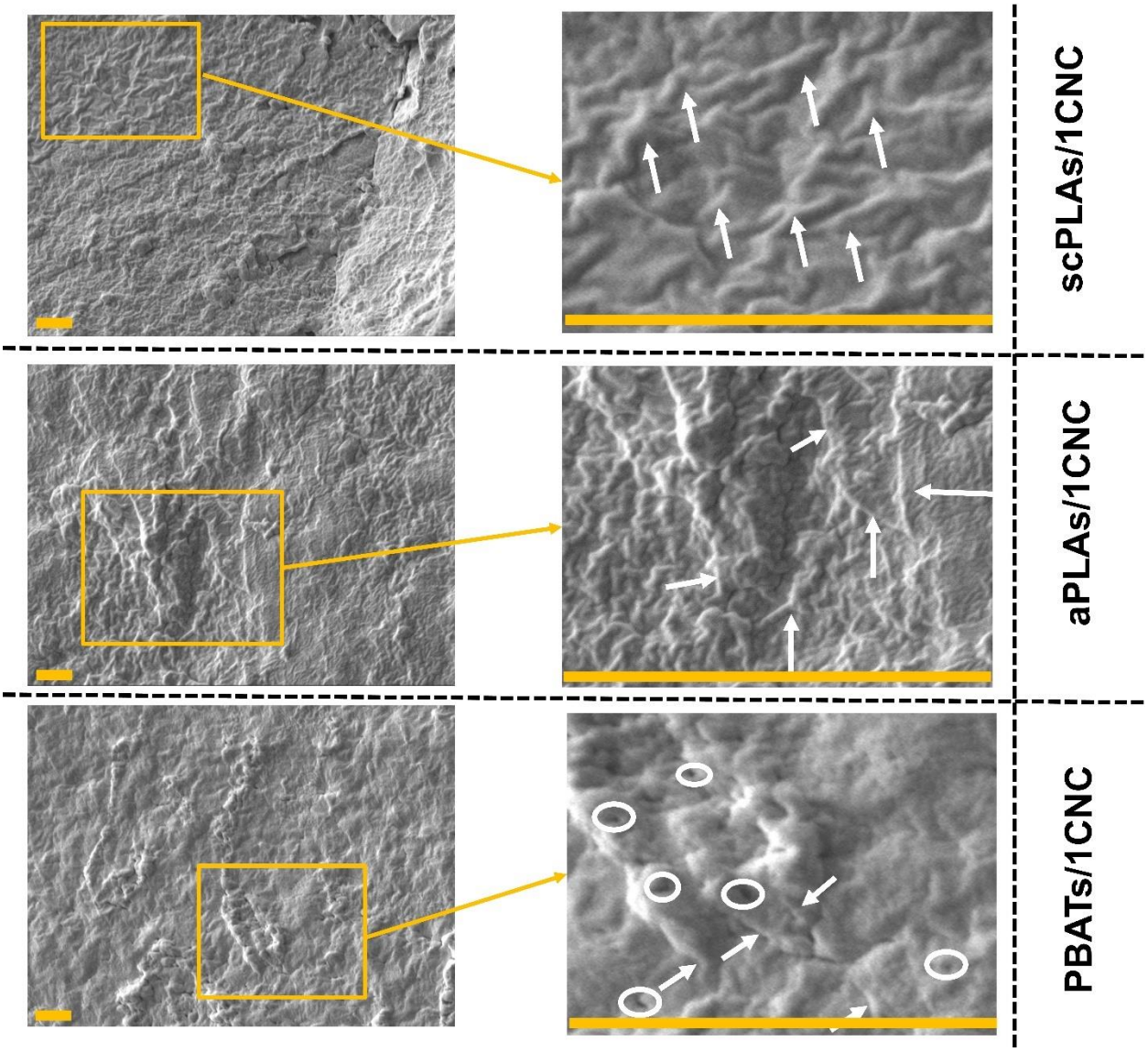

Figure 7.2 Low (left figures) and high (right figures) magnification of SEM images of scPLA, aPLA, and PBAT containing 1 wt% CNCs prepared from one solvent method. The scale bars are 1 µm.

7.4.2 Differential scanning calorimetry (DSC)

Figure. 7. 3 presents the DSC heating and cooling curves of scPLA, aPLA, and PBAT containing 0 (neat polymers), 1 and 3 wt% CNCs prepared from two solvents (solid lines) and one solvent (dashed lines). For both methods, the DSC curves show variations in exothermic values and the position of cold crystallization temperatures. The rearrangement of crystalline structures is different for scPLA and PBAT due to the dissimilar mobility of the polymer chains. Also, in Figure.

7.1a, a few thermograms with multiple peaks in the first heating sequence are observed (mostly for scPLA). This phenomenon could be ascribed to two different crystal structures formed during cooling in processing [59], [60]; the less perfect structure (shish kebab-like) is melting more easily at lower temperatures. On the other hand, for the highly ordered crystalline structures (spherulitic-like structures), a higher melting temperature is observed. What is more, the first heating curves of scPLA do not show cold crystallization because the samples have fully crystallized during the lengthy preparation process. In all the samples the first heating thermograms (left in Figure. 7. 3) do not provide proper information due to the different cooling profiles applied to the samples during processing. The corresponding results of second heating (h_2) and cooling thermograms (glass transition (T_g), melt crystallization (T_c), cold crystallization (T_{cc}), crystalline melting (T_m), and crystallinity (X%)) are reported in Table 7.2.

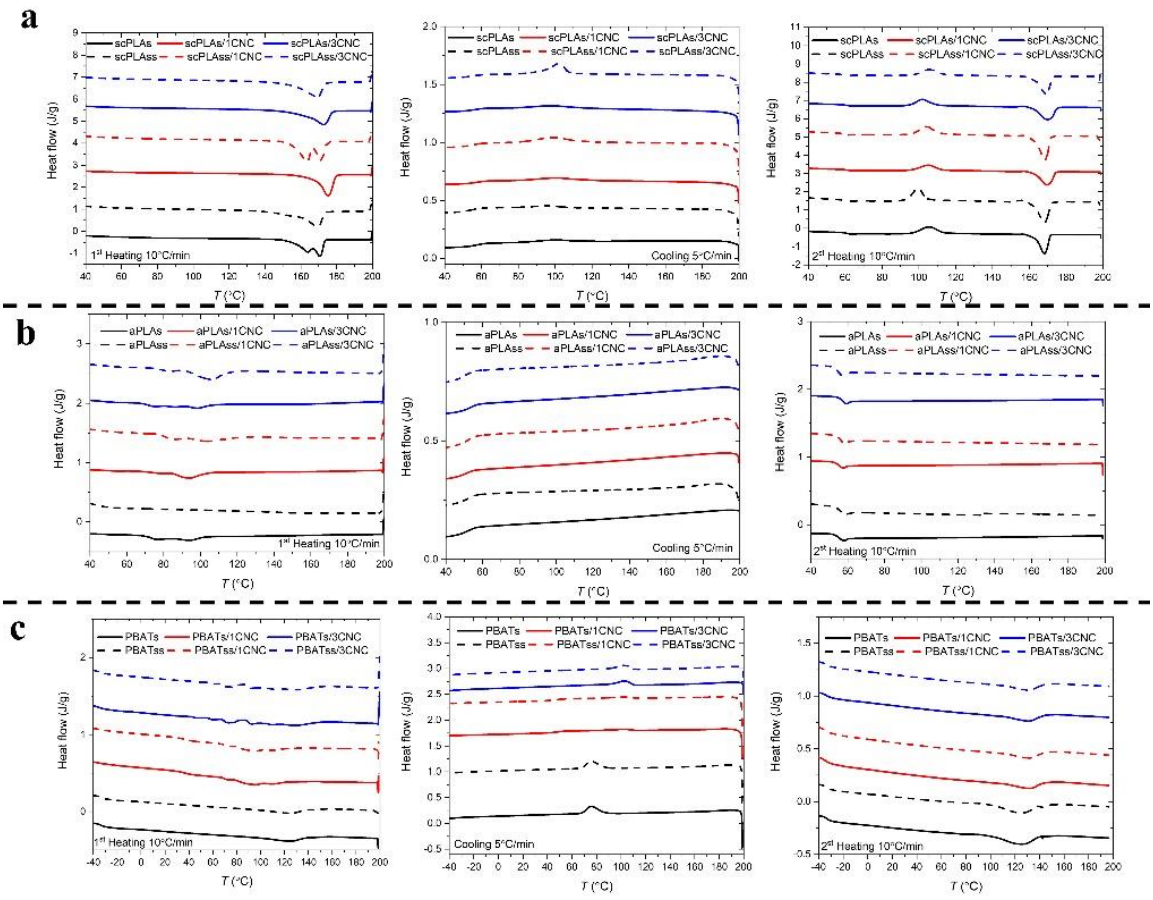

Figure 7.3 DSC thermograms of first heating (left), cooling (middle), and second heating (right) sequences for scPLA (a), aPLA (b), and PBAT systems (c). Solid and dashed lines represent the samples prepared from one solvent and two solvent methods, respectively.

All neat polymers and their nanocomposites show higher T_g values during the second heating cycle ($T_g^{h_2}$) compared to that from the cooling cycles ($T_g^{cooling}$). These differences could be due to the remaining traces of solvents even after the first heating cycle. Compared to aPLA, scPLA exhibits a higher T_g due to chain mobility restriction. In scPLA the macromolecules are arranged in certain patterns that decrease their flexibility and increase the intermolecular forces. Compared to the neat polymers, the crystallization temperatures of scPLA and PBAT/CNC nanocomposites increase as a result of the good dispersion of CNCs using both methods. The scPLA shows a crystallization peak in the second heating cycle and its cold crystallization temperature increases from 98 °C (scPLAs) to 106 °C (scPLAs/3CNC) and from 96 °C (scPLAss) to 102 °C (scPLAss/3CNC) by incorporating 3 wt% CNCs. Also, note the tremendous increases in the cold crystallization temperature of the PBAT nanocomposites observed for both methods when the CNC content is 3 wt% (from around 75 to 103 °C). This can be attributed to the nucleation effect of the CNCs that facilitates the crystallization of scPLA and PBAT [61]. For both methods the melting temperatures of the second heating cycle ($T_m^{h_2}$) of scPLA/CNC and PBAT/CNC are almost the same as that of the neat scPLA (around 170 °C) and that of the neat PBAT (around 128 °C).

The total crystallinity content of the polymer nanocomposites can increase or decrease due to the presence of the nanoparticles, as the nanoparticles play the role of nucleating agents while decreasing the mobility of polymer chains. So, if the former phenomenon is dominant, the total crystallinity content of polymer nanocomposite will increase and vice versa. By adding 1 and 3 wt% CNCs to scPLA, the total crystalline content in the cooling step ($X_c^{cooling}$) calculated from Equation 7.2 increases from 4% (scPLAss) to 15% (scPLAss/3CNC) and from 4% (scPLAs) to 11% (scPLAs/3CNC). So, it is obvious that the CNCs play the role of nucleation agents in scPLA. The more important enhancement in the degree of crystallinity in scPLA prepared from two solvents can be ascribed to the better dispersion of CNCs in scPLA. The more uniform CNCs dispersion in the two solvents method (presented by rheological data published in our previous publications [20], [29] and FESEM images in the previous section), results in higher interfacial interactions between CNCs and PLA chains favoring a higher nucleation effect [62]. Using DMF for preparing PLA/CNC nanocomposites (same scPLA and CNCs used in this work), Bagheriasl et al. [16] reported similar improvement in crystalline content of PLA nanocomposites in cooling cycles and the onset of crystallization temperature. On the other hand, in PBAT, adding 1 and 3

wt% CNCs, the total crystalline content in the cooling step decreases from 19% (PBATss) to 9% (PBATss/3CNCss) and from 18% (PBATs) to 10% (PBATs/3CNC). These reductions can be attributed to the chain mobility restriction. Similar variations in the total crystallinity content of scPLA/CNC and PBAT/CNC calculated in the second heating cycle $X_c^{h_2}$ are observed and details are presented in Table 7.2. As expected, no crystal melting, nor crystallization was detected for the amorphous PLA based systems.

Table 7.2 DSC results for first and second heating and cooling sequences for one and two solvent methods

Samples	Glass transition temperatures (°C)		Crystallization temperatures (°C)		Crystal melting temperatures (°C)	Degree of crystallinity (X%)	
	$T_g^{cooling}$	$T_g^{h_2}$	T_c	T_{c_c}	$T_m^{h_2}$	$X_c^{h_2}$	$X_c^{cooling}$
scPLAss	55	60	96	99	168	22	4
scPLAs	58	61	98	102	168	11	4
scPLAss/1CNC	54	60	99	104	168	23	13
scPLAs/1CNC	59	61	100	105	169	15	9
scPLAss/3CNC	56	59	102	106	169	25	15
scPLAs/3CNC	57	61	106	106	169	18	11
PBATss	-36	-33	75	…	124	12	19
PBATs	-32	-33	76	…	125	13	18
PBATss/1CNC	-35	-35	102	…	128	11	14
PBATs/1CNC	-34	-32	102	…	129	10	14
PBATss/3CNC	-37	-34	103	…	128	9	9
PBATs/3CNC	-34	-33	104	…	129	9	10
aPLAss	52	57	…	…	…	…	…
aPLAs	52	55	…	…	…	…	…
aPLAss/1CNC	51	57	…	…	…	…	…
aPLAs/1CNC	51	55	…	…	…	…	…
aPLAss/3CNC	51	55	…	…	…	…	…
aPLAs/3CNC	54	57	…	…	…	…	…

7.4.3 Tensile and impact properties

Figure. 7. 4 presents the tensile properties (Young's modulus (a), yield strength (b), and elongation at break (c)) of the scPLA (left part of the figure), aPLA (middle part), and PBAT (right part) nanocomposites with those of the neat polymers prepared from both methods. Table 7.3 reports the mean values and standard deviations of the tensile and impact properties of the neat scPLA, aPLA,

PBAT, and their corresponding nanocomposites with 1 and 3 wt% CNCs prepared from both methods. The neat polymers prepared from solution casting (both methods) show almost the same values compared to the neat polymers prepared from as-received granules; small differences could be due to the presence of remaining solvents in the samples prepared by the solution methods. The final mechanical properties of the polymer nanocomposites are affected by the level of dispersion of the nanoparticles, interfacial characteristics, and polymer crystallinity [63], [64]. The well-dispersed CNCs and an interconnected CNC network in scPLA, aPLA, and PBAT result in increases in the Young modulus and tensile strength values compared to the values of the neat polymers prepared from the solution casting methods. By incorporating 3 wt% CNCs the Young modulus increases by 24 %, 15 %, and 40% for the two solvent methods compared to the neat scPLA, aPLA, and PBAT, respectively. Similar enhancements are obtained for the nanocomposites prepared by the one solvent method. Such improvements due to a good dispersion of CNCs were reported in other publications [15], [32], [62]. For the same scPLA/CNC nanocomposites prepared from one solvent (DMF), Bageheriasl et al. [16] could improve the Young modulus of PLA by 12 % by incorporating 3 wt % CNCs and obtained a 23 % improvement using 6 wt% CNCs. The more significant improvement in the Young modulus of PLA (25 % by incorporation of 3 wt% CNC) in this work could be due to the different drying processes used in this work compared to that of Bagheriasl et al [16].

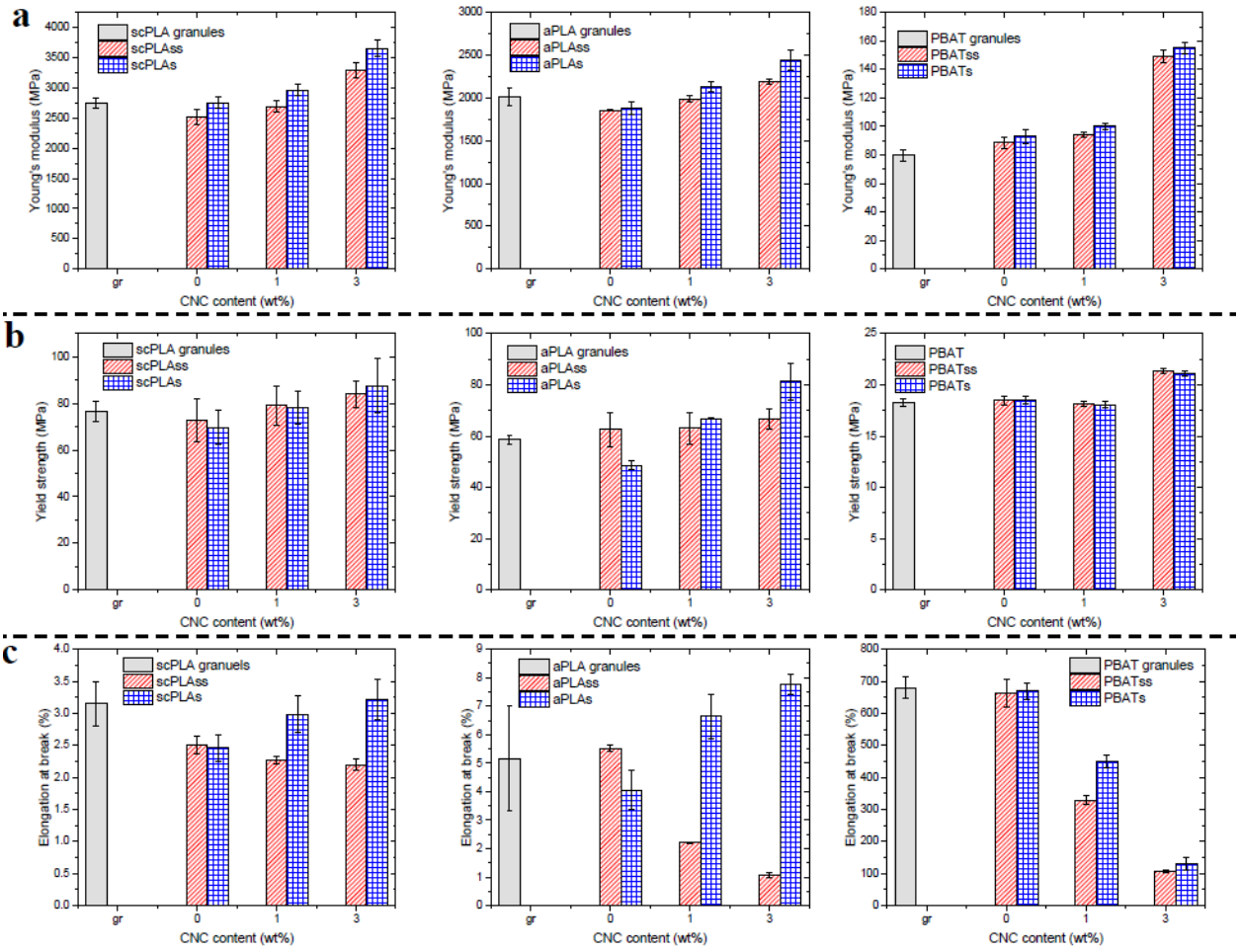

Figure 7.4 Young's modulus (a), yield strength (b), and elongation at break (c) of scPLA (left part), aPLA (middle), and PBAT (right) and its nanocomposites with different CNC contents. "gr" in the x-axis stands for neat polymers prepared from granules.

As illustrated in Table 2 the crystallinity of scPLA is improved by the incorporation of CNCs as the scPLA nanocomposites have undergone annealing through their preparation, which in turn results in enhancements of their Young modulus and tensile strength. It is worthy to mention that, as the samples for mechanical tests were prepared using a press, annealing was occurring, and the data obtained from the second heating are more relevant. The same correlation between crystallinity and mechanical properties (strength) is reported in other publications [65], [66]. Although the crystallinity of PBAT does not increase as shown in Table 2 (after annealing in the first heating cycle), the polymer chain restriction in the presence of CNCs provides enough rigidity to improve the Young modulus and tensile strength of PBAT/CNC nanocomposites. The effect of the remaining solvent is more obvious in the elongation at break. For both PLA nanocomposites

the elongation at break increases when the one solvent method was used, whereas the two solvent method yields a decrease of this value. On the other hand, both methods result in a decrease in the elongation at break of the PBAT nanocomposites due to presence of CNCs as a filler in thermoplastic PBAT and absence of proper adhesion between the filler and PBAT macromolecules. All the nanocomposites prepared by the two solvent methods exhibit a brittle behavior. As shown in Table 3 or Fig. 4, the elongation at break values of the neat scPLA, aPLA, and PBAT that are 5.5, 2.5, and 661 %, respectively, decrease drastically to 2.2 %, 1.1 %, and 105 % when 3 wt% CNCs are incorporated into the polymers. Similar decreases in elongation at break were reported in other investigations on polymer-CNC systems [15], [16], [35], [37]. On the contrary, for the one solvent method the elongation at break increases from 2.5 to 3.2 % and from 4 to 7.8 % in the scPLA and aPLA, respectively, although these polymer systems remain brittle. This increase in elongation at break using one solvent could be due to plasticization effect of traces of solvent. Such an improvement for the elongation at break by adding CNCs was reported in other publications [41], [42]. The elongation at break decreases from 670 to 130 % in the PBAT by the incorporation of 3 wt% CNCs via the one solvent method. A similar reduction in elongation at break for PBAT/CNC was reported by Vatansever et al. [15], who prepared the PBAT/CNC nanocomposites (1, 3, and 5 wt% of CNC) through solution casting and dilution of a masterbatch in TSE.

Table 7.3 Mechanical properties of scPLA, aPLA, and PBAT and their nanocomposites prepared from two solvent and one solvent methods.

sample	Young modulus (MPa)	Yield strength (MPa)	Elongation at break (%)	Impact strength (Jm^{-1})
scPLA granules	2748 ± 84.0	76.0 ± 4.0	3.20 ± 0.3	21.0± 0.2
scPLAss	2516 ± 121	72.0 ± 9.0	2.50 ± 0.2	14.0 ± 1.7
scPLAs	2750 ± 91.0	69.0 ± 7.0	2.50 ± 0.2	20.0 ± 4.2
scPLAss/1CNC	2691 ± 97.0	79.0 ± 8.0	2.20 ± 0.1	9.80 ± 1.3
scPLAs/1CNC	2967 ± 93.0	78.0 ± 7.0	3.00 ± 0.2	22.8 ± 4.9
scPLAss/3CNC	3292 ± 127	84.0 ± 6.0	2.20 ± 0.1	12.7 ± 1.8
scPLAs/3CNC	3659 ± 129	87.0 ± 11	3.20 ± 0.3	26.4 ± 0.90
aPLA granules	2010 ± 100	58.0 ± 2.0	5.00 ± 1.8	27.0 ± 1.0
aPLAss	1857 ± 10.0	62.0 ± 6.0	5.50 ± 0.1	24.3 ± 3.3
aPLAs	1875 ± 72.0	48.0 ± 2.0	4.00 ± 0.7	26.8 ± 1.3
aPLAss/1CNC	1990 ± 43.0	63.0 ± 6.0	2.20 ± 0.1	21.6 ± 3.1
aPLAs/1CNC	2127 ± 61.0	66.0 ± 1.0	6.60 ± 0.7	28.0 ± 0.8
aPLAss/3CNC	2193 ± 26.0	66.0 ± 4.0	1.10 ± 0.1	21.9 ± 2.2
aPLAs/3CNC	2442 ± 123.0	81.0 ± 7.0	7.80 ± 0.3	29.2 ± 1.3
PBAT granules	80.00 ± 4.00	18.3 ± 0.4	680 ± 32	260 ± 5.0

PBATss	88.00 ± 4.00	18.5 ± 0.5	661 ± 42	258 ± 8.0
PBATs	93.00 ± 5.00	18.5 ± 0.4	670 ± 25	260 ± 8.0
PBATss/1CNC	95.00 ± 20.0	18.2 ± 0.3	328 ± 13	215 ± 5.0
PBATs/1CNC	100.0 ± 2.00	18.5 ± 0.3	450 ± 20	225 ± 7.0
PBATss/3CNC	149.0 ± 4.00	21.3 ± 0.3	105 ± 10	247 ± 6.0
PBATs/3CNC	155.0 ± 4.00	21.1 ± 0.3	130 ± 20	250 ± 7.0

Figure 7. 5 presents the impact properties of the scPLA, aPLA, and PBAT nanocomposites compared to the mentioned neat polymers prepared from the two solvent (ss) and one solvent (s) methods. Also, the related data are reported in Table 7.3. Similarly to the elongation at break, all the nanocomposites prepared via the two solvent method exhibit a brittle behavior and we see decreases in the impact strength by incorporating 3 wt% CNCs: from 14.0 to 12.7 Jm^{-1}, 24.3 to 21.9 Jm^{-1}, and 258 to 247 Jm^{-1}, for scPLA, aPLA, and PBAT, respectively. On the other hand, for the one solvent method, incorporating 3 wt% CNCs improves the impact properties by 23 and 10 % in scPLA and aPLA, respectively, but the impact strength of the PBAT nanocomposite decreases by 4%. This is in line with elongation at break data discussed in the previous section.

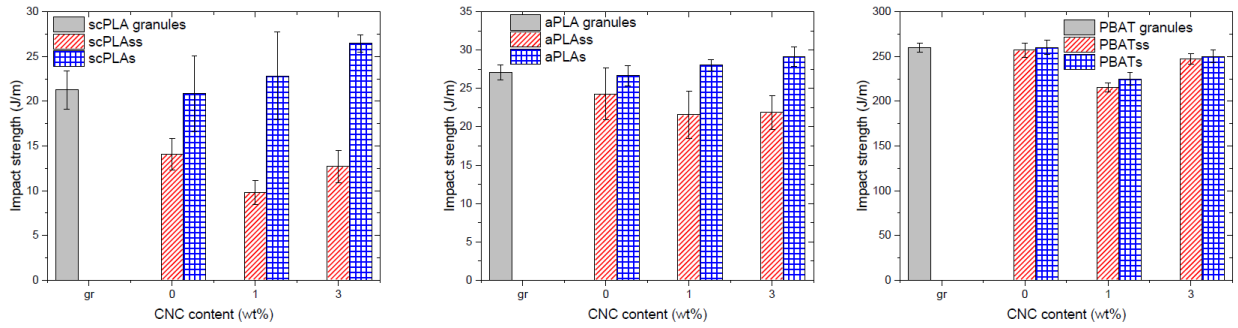

Figure 7.5 Impact strength properties of scPLA (left), aPLA (middle), PBAT (right), and their nanocomposites with different CNC contents. “gr” in the x-axis stands for neat polymer samples prepared from granules as received.

7.4.4 Dynamic mechanical thermal analysis (DMA)

The thermo-mechanical properties of the nanocomposites (storage modulus and tan δ) obtained from dynamic mechanical thermal analysis (DMA) are presented in Figure. 7. 6 over a wide range of temperature. The DMA results for aPLA/CNC nanocomposites are not presented as they were not consistent between replicates, possibly due to the more significant effect of residual solvent on the amorphous PLA. The storage modulus of the scPLA system (left part of Figure. 7. 5a) is

significantly increased by incorporating CNCs, especially at 3 wt%. These increases are much larger for the samples prepared from the one solvent method, possibly due to less residual solvent. Large enhancements of the storage modulus are observed by the incorporation of CNCs in the rubbery region (temperature ≥ 65 ^{o}C), with corresponding shifts in the peak of tan δ and large decreases of the area under the tan δ versus T curves (right part of Figure. 7. 6a). Note the very important increases at higher temperatures in the rubbery region of the storage modulus of scPLA and its nanocomposites due to cold crystallization (see Figure. 7. 3 and Table 7.2). In contrast, the effects of adding CNCs to PBAT are rather marginal on the storage modulus and tan δ versus T curves (Figure. 7. 6b). Key DMA results are summarized in Table 7.4. For the two solvents method, by incorporation 3 wt% CNCs the storage modulus values in the glassy region (30 °C for scPLA and -30 °C for PBAT), increase from 1570 to 1820 MPa and 912 to 1340 MPa for scPLA and PBAT, respectively. In the rubbery region (70 °C for scPLA and 30 °C for PBAT) the corresponding increases are from 5 to 85 MPa and 105 to 155 MPa for scPLA and PBAT, respectively. For the one solvent method, by incorporating 3 wt% CNCs, the storage modulus increases from 1400 to 1760 MPa (scPLA) and 1010 to 1420 MPa (PBAT) in the glassy region and from 30 to 333 MPa (scPLA) and 110 to 170 MPa (PBAT) in the rubbery region. These large enhancements in the rubbery region can extend the applications of PLA and PBAT for products exposed to high temperatures.

The T_g values of the neat polymers and their nanocomposites can be obtained from the characteristic peaks in tan δ versus T (right parts of Figure. 7. 6). We note first that T_g of the neat scPLAss and scPLAs are 65 and 59 ^{o}C, respectively. This difference in T_g of scPLA prepared from one and two solvents confirms the presence of more residual solvent when the two solvents method was used. T_g of the neat PBATs and PBATss is about the same at -13 and -14 ^{o}C, respectively, suggesting less residual solvent when preparing the PBAT systems from cast film methods. T_g of the polymer matrices does not change significantly by the addition of CNCs: T_g of scPLA increases from 65 to 68 °C by incorporating 3 wt% CNCs by the two solvents method. It is about constant at 59 ^{o}C when the one solvent method was used. Also, by adding 3 wt% CNCs to PBAT, the T_g is changed from about -14 to -17 °C for both methods. Another more important characteristic of tan δ is the area under the peak of T_g versus T curves that represents the extent of damping or energy dissipation due to the segmental motion of the polymer chains at T_g. The polymer chains are more

restricted for large contents of CNCs due to more interfacial interactions between the polymer chains and cellulose nanocrystals. This area decreases significantly with the addition of CNCs. In scPLA, the peak of the tan δ curve decreases from 1.78 to 0.62 for the two solvents method and from 1.04 to 0.3 for the one solvent method by incorporating 3 wt% CNCs (Table 7.4).

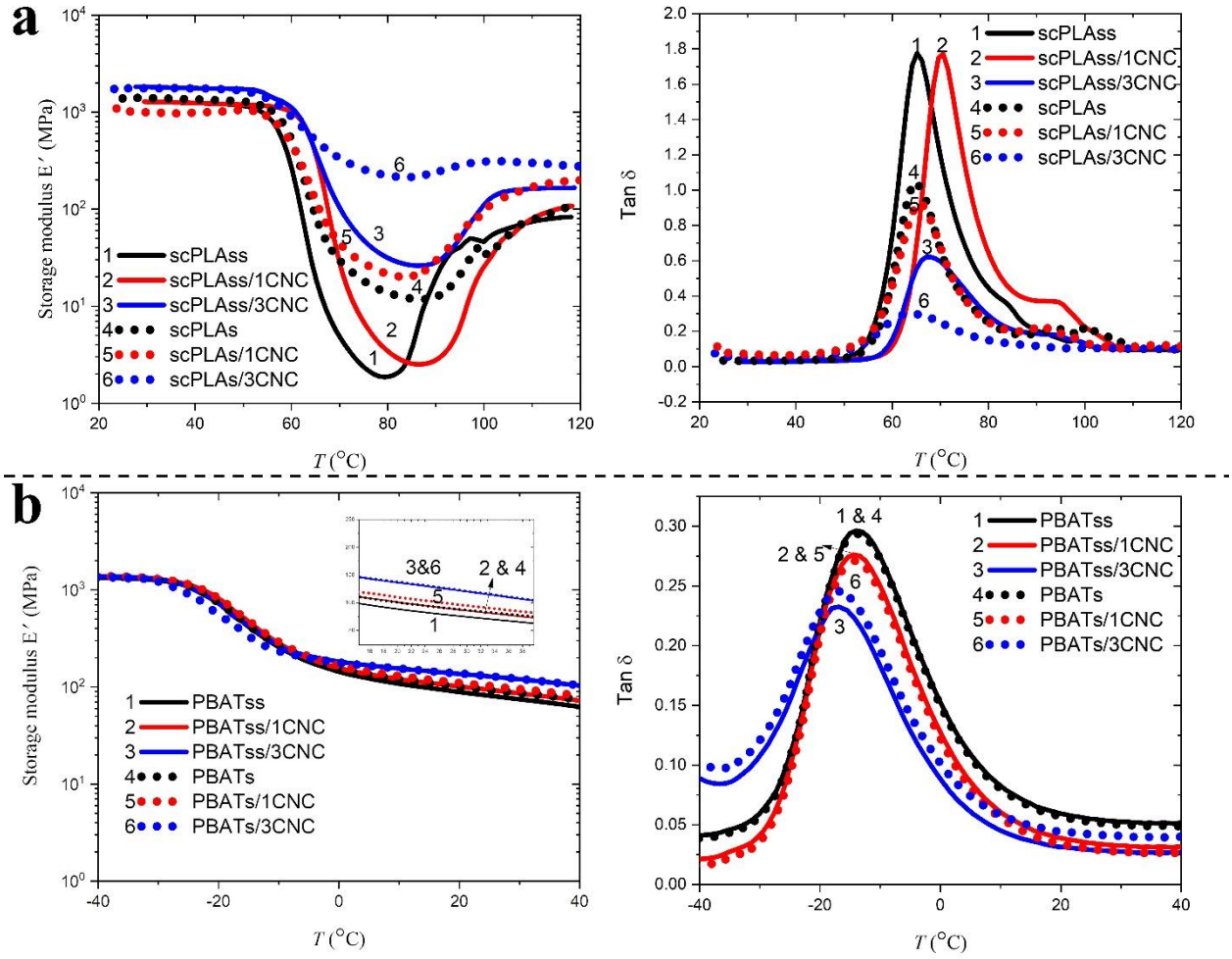

Figure 7.6 DMTA data of scPLA and scPLA/CNC (a) and PBAT and PBAT/CNC (b) over a wide range of temperature: storage modulus (left) and tan δ (right)

Table 7.4 DMTA results for scPLA/CNC and PBAT/CNC prepared from two solvent and one solvent methods.

Samples	Tan δ peak		Storage modulus (MPa)	
	T_g (°C)	**Peak in tan δ curve**	**Glassy region 30 °C**	**Rubbery region 70 °C**
scPLAss	65	1.78	1570	5.0
scPLAs	59	1.04	1400	30

scPLAss/1CNC	66	1.67	1650	8.0
scPLAs/1CNC	58	0.92	1570	45
scPLAss/3CNC	68	0.62	1823	85
scPLAs/3CNC	59	0.30	1760	333
	T_g (°C)	**Peak in tan δ curve**	**Glassy region -30 °C**	**Rubbery region 30 °C**
PBATss	-14	0.30	912	105
PBATs	-13	0.29	1010	110
PBATss/1CNC	-15	0.28	1330	120
PBATs/1CNC	-15	0.26	1210	135
PBATss/3CNC	-17	0.23	1340	155
PBATs/3CNC	-17	0.22	1420	170

The more important decrease of the area under tan δ curves for the one solvent method could be due to the better interactions between scPLA chains and CNCs as a result of less remaining solvent in the system. Also, in PBAT the peak in tan δ changes from 0.30 to almost 0.23 by adding 3 wt% CNCs for both methods. For scPLA/CNC nanocomposites Bagheriasl et al. [16] (same scPLA and CNCs used in this work, but a different drying protocol) reported a 74 and 490% increase of the storage modulus for the glassy (25 °C) and rubbery regions (70 °C), respectively with the addition of 6 wt% CNCs. Also, they reported that the CNC incorporation did not significantly affect T_g, but the area under the peak of T_g significantly decreased. At the same CNC content (3 wt% CNC), the peak of tan δ (damping factor) in this work of ca. 0.3 compares favorably to the value of around 1.5 obtained by Bagheriasl et al. [16].

Figure. 7. 7 presents the predictions of the modified Takayanagi model (Equation 7.3) and the experimental data of the storage modulus of the scPLA/CNC (Figures. 7. 7 a & b) and PBAT/CNC (Figures. 7. 7 c & d) nanocomposites with 1 and 3 wt% CNCs. The modeling of DMA results for aPLA/CNC nanocomposites are not presented as they were inconsistent as mentioned above. As done in the previous section the temperatures of 30 and -30 °C are considered as the glassy regions for scPLA/CNC and PBAT/CNC, respectively, and the temperatures of 70 and 30 °C used for the rubbery regions for scPLA/CNC and PBAT/CNC, respectively. The two adjustable parameters in this model are E'_{net} and φ_c, which are reported in Table 7.5. The predictions from this model are in good agreement with the experimental data of the reduced storage modulus of the polymer-CNC nanocomposites in both the glassy and rubbery regions. According to Table 7.5, for the one solvent method in the glassy region E'_{net} is 62.6 and 73.2 GPa for scPLA/CNC and PBAT/CNC, respectively, and decreases to 18.5 and 20.2 GPa in the rubbery region. For the two solvent method,

E'_{net} changes from 42.3 and 84.9 GPa in the glassy region to 14.2 and 14.5 GPa in the rubbery region for scPLA/CNC and PBAT/CNC, respectively. φ_c is equal to 0.003 and 0.005 for all cases for the two solvent and one solvent methods, respectively. The percolation threshold is quite close to that determined by rheometry. Bagheriasl et al. [16] reported for the one solvent method (DMF) the percolation threshold was identical to that determined in rheometry. For scPLA/CNC in the rubbery region, a better enhancement of the modulus is observed by incorporating CNCs to PLA compared to glassy region (Figure. 7. 6a & b). However, a much lower value for the modulus of the CNC network is obtained from the fits of Equation 7.3, which predicts a much weaker CNC network at higher temperatures. Using predictions of the modified Takayanagi model (Equation 7.3) Bagheriasl et al. [16] reported similar results for the fitting parameters. In their work, the fitting parameter, E'_{net}, was 108 and 2.64 GPa in the glassy (25 °C) and rubbery region (70 °C), respectively, for scPLA/CNC (CNC contents of 1, 3, 4, 6 wt%). Also, they reported the value of 0.0055 for φ_c. The lower value of φ_c in this work for two solvent method could be due to a better dispersion and distribution of CNCs (clearer from rheological data presented in our previous publications [20], [29]), which in turn lead to better interfacial interactions between CNCs and polymer chains.

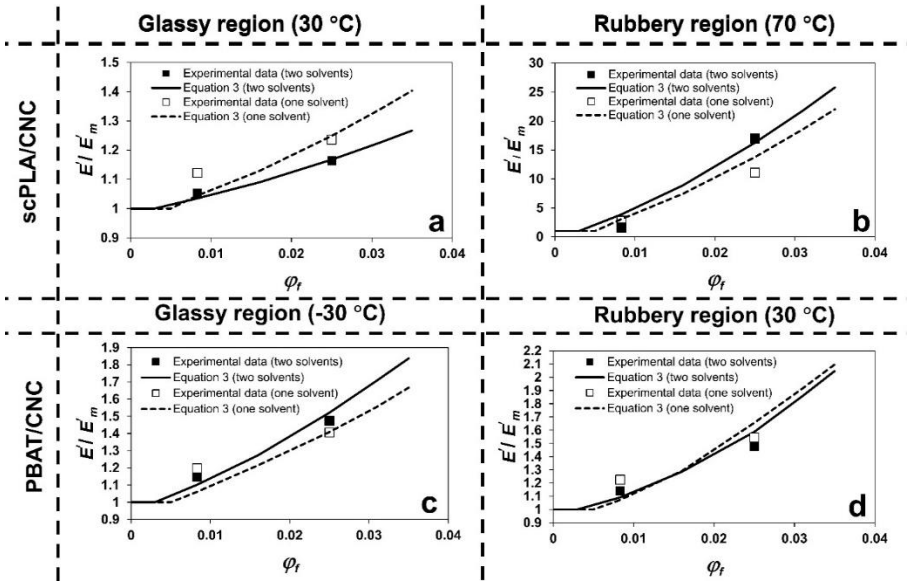

Figure 7.7 Comparison of the predictions of the modified Takayanagi model (Eqs. 3–5) and experimental data of the storage modulus at glassy region (a & c) and rubbery region (b & d). (a & b): scPLA/CNC nanocomposites and (c & d) PBAT/CNC nanocomposites.

Table 7.5 Storage modulus values of the percolating CNC network (E'_{net}) and critical CNC volume fraction (φ_c) for percolation obtained from fitting the modified Takayangi model (Eqs. 3-5) to the reduced storage modulus data, E'/E'_m of scPLA/CNC and PBAT/CNC in both glassy and rubbery regions; E'_m is the storage modulus of the neat matrix reported in Table 7.4.

Samples	Glassy region (Figures. 7a & c)				Rubbery region (Figures. 7b & d)			
	One solvent (s)		Two solvents (ss)		One solvent (s)		Two solvents (ss)	
	E'_{net} (GPa)	φ_c	E'_{net} (GPa)	φ_c	E'_{net} (GPa)	φ_c	E'_{net} (GPa)	φ_c
scPLA/CNC	62.6	0.005	42.3	0.003	18.5	0.005	14.2	0.003
PBAT/CNC	73.2	0.005	84.9	0.003	20.2	0.005	14.5	0.003

7.5 Concluding remarks

In this work, the effect of dispersed CNCs on the morphological, mechanical and thermal properties of PLA (semicrystalline and amorphous) and PBAT prepared from two different solvent casting methods was investigated. The nanocomposites were prepared from two solvent (DMSO and THF) or one solvent (DMF) methods. FESEM images showed a good dispersion and distribution of the CNCs in the matrices prepared from both methods. While for scPLA the total crystallinity content increased during cooling cycles for both preparation methods as a result of the nucleation effect, it decreased in PBAT due to chain mobility restriction. The addition of the CNCs into PLA and PBAT via solution-based preparation methods resulted in significant increases of the Young modulus. The yield strength of all nanocomposites increased for both methods, but it was more significant for the one solvent method as a result of less remaining solvent in the samples. All the nanocomposites prepared via the two solvent methods exhibited a brittle behavior. While the elongation at break values of the neat scPLA, aPLA, and PBAT in the two solvent methods were decreased by incorporating 3 wt% CNCs, in the one solvent method it increased. Small decreases of the impact strength of all the nanocomposites prepared by the two solvent method were observed. In contrast, for the one solvent method, incorporating 3 wt% CNCs improved the impact properties by 23 % and 10 % in scPLA and aPLA, respectively, but the impact properties of PBAT nanocomposites decreased by 4%. In DMA, the storage modulus values in the glassy and rubbery region of the samples prepared by the one and two solvent methods increased. The modified Takayangi model predictions were compared with the storage modulus data of the nanocomposites and an acceptable agreement was observed for both the glassy and rubbery regions. The storage

modulus of the CNC network was found to decrease at higher temperatures suggesting a marked reduction of the strength of the CNC network, due to weaker hydrogen bonds. These results confirm that both solution cast methods lead to a good dispersion of hydrophilic CNCs within PLA and PBAT matrices, but remaining solvent had some negative effects on the mechanical and thermal properties, especially when the two solvent method was used. Nevertheless, as a result of CNC network formation, the mechanical and thermal properties of PLA and PBAT could be improved without the need for compatibilization or modification of the CNCs. Also, in one solvent method the elongation at break and impact properties were improved compared to the two solvent method. So, those improvements in the mechanical and thermal properties could pave the way for applications of PLA and PBAT for packaging and automotive industries.

7.6 Acknowledgments

Financial support from the Natural Science and Engineering Research Council (NSERC) of Canada is gratefully acknowledged. The authors also wish to acknowledge the help of Dr. Helia Sojoudiasli and Mr. Matthieu Gauthier for the material preparation and processing. Finally, we wish to thank Mr. Jed Randall from NatureWorks for providing one of the PLA samples.

7.7 References

[1] A. Blanco, M. C. Monte, C. Campano, A. Balea, N. Merayo, and C. Negro, "Nanocellulose for industrial use: Cellulose nanofibers (CNF), cellulose nanocrystals (CNC), and bacterial cellulose (BC)," in *Handbook of Nanomaterials for Industrial Applications*, Elsevier, 2018, pp. 74–126.

[2] C. Miao and W. Y. Hamad, "Cellulose reinforced polymer composites and nanocomposites: A critical review," *Cellulose*, vol. 20, no. 5. Springer, pp. 2221–2262, Oct. 04, 2013, doi: 10.1007/s10570-013-0007-3.

[3] X. Xu, F. Liu, L. Jiang, J. Y. Zhu, D. Haagenson, and D. P. Wiesenborn, "Cellulose Nanocrystals vs. Cellulose Nanofibrils: A Comparative Study on Their Microstructures and Effects as Polymer Reinforcing Agents," *ACS Appl. Mater. Interfaces*, vol. 5, no. 8, pp. 2999–3009, Apr. 2013, doi: 10.1021/am302624t.

[4] K. Oksman *et al.*, “Review of the recent developments in cellulose nanocomposite processing,” *Compos. Part A Appl. Sci. Manuf.*, vol. 83, pp. 2–18, Apr. 2016, doi: 10.1016/j.compositesa.2015.10.041.

[5] A. Bendahou, H. Kaddami, and A. Dufresne, “Investigation on the effect of cellulosic nanoparticles’ morphology on the properties of natural rubber based nanocomposites,” *Eur. Polym. J.*, vol. 46, no. 4, pp. 609–620, Apr. 2010, doi: 10.1016/j.eurpolymj.2009.12.025.

[6] W. Zhang *et al.*, “High performance poly (vinyl alcohol)/cellulose nanocrystals nanocomposites manufactured by injection molding,” *Cellulose*, vol. 21, no. 1, pp. 485–494, Feb. 2014, doi: 10.1007/s10570-013-0141-y.

[7] W.-I. Park, M. Kang, H.-S. Kim, and H.-J. Jin, “Electrospinning of Poly(ethylene oxide) with Bacterial Cellulose Whiskers,” *Macromol. Symp.*, vol. 249–250, no. 1, pp. 289–294, Apr. 2007, doi: 10.1002/masy.200750347.

[8] T. Abitbol, T. Johnstone, T. M. Quinn, and D. G. Gray, “Reinforcement with cellulose nanocrystals of poly(vinyl alcohol) hydrogels prepared by cyclic freezing and thawing,” *Soft Matter*, vol. 7, no. 6, pp. 2373–2379, Mar. 2011, doi: 10.1039/c0sm01172j.

[9] H. Kargarzadeh *et al.*, “Recent developments on nanocellulose reinforced polymer nanocomposites: A review,” *Polymer*, vol. 132. Elsevier Ltd, pp. 368–393, Dec. 06, 2017, doi: 10.1016/j.polymer.2017.09.043.

[10] M. Nofar, D. Sacligil, P. J. Carreau, M. R. Kamal, and M.-C. Heuzey, “Poly (lactic acid) blends: Processing, properties and applications,” *Int. J. Biol. Macromol.*, vol. 125, pp. 307–360, 2018, doi: 10.1016/j.ijbiomac.2018.12.002.

[11] F. V. Ferreira, L. S. Cividanes, R. F. Gouveia, and L. M. F. Lona, “An overview on properties and applications of poly(butylene adipate- co -terephthalate)-PBAT based composites,” *Polym. Eng. Sci.*, vol. 59, no. s2, pp. E7–E15, Mar. 2019, doi: 10.1002/pen.24770.

[12] J.-M. Raquez, Y. Habibi, M. Murariu, and P. Dubois, “Polylactide (PLA)-based nanocomposites,” *Prog. Polym. Sci.*, vol. 38, no. 10–11, pp. 1504–1542, Oct. 2013, doi: 10.1016/j.progpolymsci.2013.05.014.

[13] M. R. Kamal and V. Khoshkava, “Effect of cellulose nanocrystals (CNC) on rheological and mechanical properties and crystallization behavior of PLA/CNC nanocomposites,” *Carbohydr. Polym.*, vol. 123, pp. 105–114, Jun. 2015, doi: 10.1016/j.carbpol.2015.01.012.

[14] A. L. Goffin *et al.*, “From interfacial ring-opening polymerization to melt processing of cellulose nanowhisker-filled polylactide-based nanocomposites,” *Biomacromolecules*, vol. 12, no. 7, pp. 2456–2465, Jul. 2011, doi: 10.1021/bm200581h.

[15] E. Vatansever *et al.*, “Development of CNC-reinforced PBAT nanocomposites with reduced percolation threshold: a comparative study on the preparation method,” *J. Mater. Sci.*, 2020, doi: 10.1007/s10853-020-05105-4.

[16] D. Bagheriasl, P. J. Carreau, B. Riedl, and C. Dubois, “Enhanced properties of polylactide by incorporating cellulose nanocrystals,” *Polym. Compos.*, vol. 39, no. 8, pp. 2685–2694, 2018, doi: 10.1002/pc.24259.

[17] A. Arias, M.-C. Heuzey, M. A. Huneault, G. Ausias, and A. Bendahou, “Enhanced dispersion of cellulose nanocrystals in melt-processed polylactide-based nanocomposites,” *Cellulose*, vol. 22, no. 1, pp. 483–498, Feb. 2015, doi: 10.1007/s10570-014-0476-z.

[18] D. Bondeson and K. Oksman, “Dispersion and characteristics of surfactant modified cellulose whiskers nanocomposites,” *Compos. Interfaces*, vol. 14, no. 7–9, pp. 617–630, Sep. 2007, doi: 10.1163/156855407782106519.

[19] D. Bagheriasl, F. Safdari, P. J. Carreau, C. Dubois, and B. Riedl, “Development of cellulose nanocrystal-reinforced polylactide: A comparative study on different preparation methods,” *Polym. Compos.*, vol. 40, pp. E342–E349, Jan. 2019, doi: 10.1002/pc.24676.

[20] M. Mohammadi, M.-C. Heuzey, P. J. Carreau, and A. Taguet, “Morphological and Rheological Properties of PLA, PBAT, and PLA/PBAT Blend Nanocomposites Containing CNCs,” *Nanomater. 2021, Vol. 11, Page 857*, vol. 11, no. 4, p. 857, Mar. 2021, doi: 10.3390/nano11040857.

[21] C. Miao and W. Y. Hamad, “In-situ polymerized cellulose nanocrystals (CNC)—poly(L-lactide) (PLLA) nanomaterials and applications in nanocomposite processing,” *Carbohydr. Polym.*, vol. 153, pp. 549–558, Nov. 2016, doi: 10.1016/j.carbpol.2016.08.012.

[22] A. L. Goffin, Y. Habibi, J. M. Raquez, and P. Dubois, “Polyester-grafted cellulose nanowhiskers: A new approach for tuning the microstructure of immiscible polyester blends,” *ACS Appl. Mater. Interfaces*, vol. 4, no. 7, pp. 3364–3371, Jul. 2012, doi: 10.1021/am3008196.

[23] E. L. De Paula *et al.*, “Effect of surface-grafted cellulose nanocrystals on the thermal and mechanical properties of PLLA based nanocomposites,” *Eur. Polym. J.*, vol. 84, pp. 173–187, Nov. 2016, doi: 10.1016/j.eurpolymj.2016.09.019.

[24] H. M. Hassanabadi, A. Alemdar, and D. Rodrigue, “Polypropylene reinforced with nanocrystalline cellulose: Coupling agent optimization,” *J. Appl. Polym. Sci.*, vol. 132, no. 34, p. n/a-n/a, Sep. 2015, doi: 10.1002/app.42438.

[25] A. Pei, Q. Zhou, and L. A. Berglund, “Functionalized cellulose nanocrystals as biobased nucleation agents in poly(l-lactide) (PLLA) - Crystallization and mechanical property effects,” *Compos. Sci. Technol.*, vol. 70, no. 5, pp. 815–821, May 2010, doi: 10.1016/j.compscitech.2010.01.018.

[26] D. Bagheriasl, P. J. Carreau, C. Dubois, and B. Riedl, “Properties of polypropylene and polypropylene/poly(ethylene-co-vinyl alcohol) blend/CNC nanocomposites,” *Compos. Sci. Technol.*, vol. 117, pp. 357–363, Sep. 2015, doi: 10.1016/j.compscitech.2015.07.012.

[27] V. Heshmati, M. R. Kamal, and B. D. Favis, “Tuning the localization of finely dispersed cellulose nanocrystal in poly (lactic acid)/bio-polyamide11 blends,” *J. Polym. Sci. Part B Polym. Phys.*, vol. 56, no. 7, pp. 576–587, 2018, doi: 10.1002/polb.24563.

[28] D. Bagheriasl, P. J. Carreau, B. Riedl, C. Dubois, and W. Y. Hamad, “Shear rheology of polylactide (PLA)–cellulose nanocrystal (CNC) nanocomposites,” *Cellulose*, vol. 23, no. 3, pp. 1885–1897, 2016, doi: 10.1007/s10570-016-0914-1.

[29] M. Mohammadi, C. Bruel, M. C. Heuzey, and P. J. Carreau, “CNC dispersion in PLA and PBAT using two solvents: morphological and rheological properties,” *Cellulose*, vol. 27, no. 17, pp. 9877–9892, Sep. 2020, doi: 10.1007/s10570-020-03460-8.

[30] E. Vatansever, D. Arslan, D. S. Sarul, Y. Kahraman, and M. Nofar, “Effects of molecular weight and crystallizability of polylactide on the cellulose nanocrystal dispersion quality in their nanocomposites,” *Int. J. Biol. Macromol.*, vol. 154, pp. 276–290, Mar. 2020, doi: 10.1016/j.ijbiomac.2020.03.115.

[31] A. Junior de Menezes, G. Siqueira, A. A. S. Curvelo, and A. Dufresne, “Extrusion and characterization of functionalized cellulose whiskers reinforced polyethylene nanocomposites,” *Polymer (Guildf).*, vol. 50, no. 19, pp. 4552–4563, Sep. 2009, doi: 10.1016/j.polymer.2009.07.038.

[32] M. Pracella, M. M. U. Haque, and D. Puglia, “Morphology and properties tuning of PLA/cellulose nanocrystals bio-nanocomposites by means of reactive functionalization and blending with PVAc,” *Polymer (Guildf).*, vol. 55, no. 16, pp. 3720–3728, Aug. 2014, doi: 10.1016/j.polymer.2014.06.071.

[33] J. G. Gwon *et al.*, “Mechanical and thermal properties of toluene diisocyanate-modified cellulose nanocrystal nanocomposites using semi-crystalline poly(lactic acid) as a base matrix,” *RSC Adv.*, vol. 6, no. 77, pp. 73879–73886, Aug. 2016, doi: 10.1039/c6ra10993d.

[34] J. Trifol *et al.*, “A comparison of partially acetylated nanocellulose, nanocrystalline cellulose, and nanoclay as fillers for high-performance polylactide nanocomposites,” *J. Appl. Polym. Sci.*, vol. 133, no. 14, p. n/a-n/a, Apr. 2016, doi: 10.1002/app.43257.

[35] Y. Habibi, A. L. Goffin, N. Schiltz, E. Duquesne, P. Dubois, and A. Dufresne, “Bionanocomposites based on poly(ε-caprolactone)-grafted cellulose nanocrystals by ring-opening polymerization,” *J. Mater. Chem.*, vol. 18, no. 41, pp. 5002–5010, Oct. 2008, doi: 10.1039/b809212e.

[36] G. Siqueira, J. Bras, N. Follain, S. Belbekhouche, S. Marais, and A. Dufresne, “Thermal and mechanical properties of bio-nanocomposites reinforced by Luffa cylindrica cellulose nanocrystals,” *Carbohydr. Polym.*, vol. 91, no. 2, pp. 711–717, Jan. 2013, doi: 10.1016/j.carbpol.2012.08.057.

[37] G. Siqueira, J. Bras, and A. Dufresne, “Cellulose Whiskers versus Microfibrils: Influence of the Nature of the Nanoparticle and its Surface Functionalization on the Thermal and Mechanical Properties of Nanocomposites,” *Biomacromolecules*, vol. 10, no. 2, pp. 425–432, Feb. 2009, doi: 10.1021/bm801193d.

[38] M. Mariano *et al.*, “Preparation of Cellulose Nanocrystal-Reinforced Poly(lactic acid) Nanocomposites through Noncovalent Modification with PLLA-Based Surfactants,” *ACS Omega*, vol. 2, no. 6, pp. 2678–2688, Jun. 2017, doi: 10.1021/acsomega.7b00387.

[39] C. Xiang, Y. L. Joo, and M. W. Frey, “Nanocomposite fibers electrospun from poly(Lactic Acid)/cellulose nanocrystals,” *J. Biobased Mater. Bioenergy*, vol. 3, no. 2, pp. 147–155, Jun. 2009, doi: 10.1166/jbmb.2009.1016.

[40] N. Herrera, A. M. Salaberria, A. P. Mathew, and K. Oksman, “Plasticized polylactic acid nanocomposite films with cellulose and chitin nanocrystals prepared using extrusion and compression molding with two cooling rates: Effects on mechanical, thermal and optical properties,” *Compos. Part A Appl. Sci. Manuf.*, vol. 83, pp. 89–97, Apr. 2016, doi: 10.1016/j.compositesa.2015.05.024.

[41] J. Shojaeiarani, D. S. Bajwa, and N. M. Stark, “Spin-coating: A new approach for improving dispersion of cellulose nanocrystals and mechanical properties of poly (lactic acid) composites,” *Carbohydr. Polym.*, vol. 190, pp. 139–147, Jun. 2018, doi: 10.1016/j.carbpol.2018.02.069.

[42] K. Oksman, A. P. Mathew, D. Bondeson, and I. Kvien, “Manufacturing process of cellulose whiskers/polylactic acid nanocomposites,” *Compos. Sci. Technol.*, vol. 66, no. 15, pp. 2776–2784, Dec. 2006, doi: 10.1016/j.compscitech.2006.03.002.

[43] C. L. Morelli, N. Belgacem, R. E. S. Bretas, and J. Bras, “Melt extruded nanocomposites of polybutylene adipate- co -terephthalate (PBAT) with phenylbutyl isocyanate modified cellulose nanocrystals,” *J. Appl. Polym. Sci.*, vol. 133, no. 34, Sep. 2016, doi: 10.1002/app.43678.

[44] C. L. Morelli, M. N. Belgacem, M. C. Branciforti, R. E. S. Bretas, A. Crisci, and J. Bras, “Supramolecular aromatic interactions to enhance biodegradable film properties through incorporation of functionalized cellulose nanocrystals,” *Compos. Part A Appl. Sci. Manuf.*, vol. 83, pp. 80–88, Apr. 2016, doi: 10.1016/j.compositesa.2015.10.038.

[45] I. F. Pinheiro *et al.*, “Mechanical, rheological and degradation properties of PBAT nanocomposites reinforced by functionalized cellulose nanocrystals,” *Eur. Polym. J.*, vol. 97, pp. 356–365, 2017, doi: 10.1016/j.eurpolymj.2017.10.026.

[46] F. V. Ferreira *et al.*, “Cellulose nanocrystal-based poly(butylene adipate-co-terephthalate) nanocomposites covered with antimicrobial silver thin films,” *Polym. Eng. Sci.*, vol. 59, no. s2, pp. E356–E365, Feb. 2019, doi: 10.1002/pen.25066.

[47] S. Camarero-Espinosa, D. J. Boday, C. Weder, and E. J. Foster, “Cellulose nanocrystal driven crystallization of poly(d, l -lactide) and improvement of the thermomechanical properties,” *J. Appl. Polym. Sci.*, vol. 132, no. 10, p. n/a-n/a, Mar. 2015, doi: 10.1002/app.41607.

[48] J. Shojaeiarani, D. S. Bajwa, and N. M. Stark, “Green esterification: A new approach to improve thermal and mechanical properties of poly(lactic acid) composites reinforced by cellulose nanocrystals,” *J. Appl. Polym. Sci.*, vol. 135, no. 27, p. 46468, Jul. 2018, doi: 10.1002/app.46468.

[49] E. Espino-Pérez, J. Bras, V. Ducruet, A. Guinault, A. Dufresne, and S. Domenek, “Influence of chemical surface modification of cellulose nanowhiskers on thermal, mechanical, and barrier properties of poly(lactide) based bionanocomposites,” *Eur. Polym. J.*, vol. 49, no. 10, pp. 3144–3154, Oct. 2013, doi: 10.1016/j.eurpolymj.2013.07.017.

[50] Y. Habibi, S. Aouadi, J. M. Raquez, and P. Dubois, “Effects of interfacial stereocomplexation in cellulose nanocrystal-filled polylactide nanocomposites,” *Cellulose*, vol. 20, no. 6, pp. 2877–2885, Dec. 2013, doi: 10.1007/s10570-013-0058-5.

[51] W. Y. Hamad and T. Q. Hu, “Structure-process-yield interrelations in nanocrystalline cellulose extraction,” *Can. J. Chem. Eng.*, vol. 88, no. 3, pp. 392–402, Jun. 2010, doi: 10.1002/cjce.20298.

[52] C. Bruel, Q. Beuguel, J. R. Tavares, P. J. Carreau, and M.-C. Heuzey, “The apparent structural hydrophobicity of cellulose nanocrystals,” *J. Sci. Technol. For. Prod. Process.*, vol. 7, no. 4, pp. 13–23, 2018.

[53] E. Vatansever, D. Arslan, and M. Nofar, “Polylactide cellulose-based nanocomposites,” *Int. J. Biol. Macromol.*, vol. 137, pp. 912–938, Sep. 2019, doi: 10.1016/j.ijbiomac.2019.06.205.

[54] J. Ambrosio-Martín, M. J. Fabra, A. Lopez-Rubio, and J. M. Lagaron, “Melt polycondensation to improve the dispersion of bacterial cellulose into polylactide via melt compounding: enhanced barrier and mechanical properties,” *Cellulose*, vol. 22, no. 2, pp. 1201–1226, Apr. 2015, doi: 10.1007/s10570-014-0523-9.

[55] R. Herrera, L. Franco, A. Rodríguez-Galán, and J. Puiggalí, “Characterization and degradation behavior of poly(butylene adipate- *co* -terephthalate)s,” *J. Polym. Sci. Part A Polym. Chem.*, vol. 40, no. 23, pp. 4141–4157, Dec. 2002, doi: 10.1002/pola.10501.

[56] M. Takayanagi, S. Uemura, and S. Minami, “Application of equivalent model method to dynamic rheo-optical properties of crystalline polymer,” *J. Polym. Sci. Part C Polym. Symp.*, vol. 5, no. 1, pp. 113–122, Mar. 2007, doi: 10.1002/polc.5070050111.

[57] N. Ouali, J. Y. Cavaille, and J. Perez, “Elastic, viscoelastic and plastic behavior of multiphase polymer blends,” *Plast. Rubber Compos. Process. Appl.*, vol. 16, no. 1, pp. 55–60, 1991.

[58] T. Gómez-del Río, P. Poza, J. Rodríguez, M. C. García-Gutiérrez, J. J. Hernández, and T. A. Ezquerra, “Influence of single-walled carbon nanotubes on the effective elastic constants of poly(ethylene terephthalate),” *Compos. Sci. Technol.*, vol. 70, no. 2, pp. 284–290, Feb. 2010, doi: 10.1016/j.compscitech.2009.10.019.

[59] M. Yasuniwa, K. Sakamo, Y. Ono, and W. Kawahara, “Melting behavior of poly(l-lactic acid): X-ray and DSC analyses of the melting process,” *Polymer (Guildf).*, vol. 49, no. 7, pp. 1943–1951, Apr. 2008, doi: 10.1016/j.polymer.2008.02.034.

[60] O. Martin and L. Avérous, “Poly(lactic acid): Plasticization and properties of biodegradable multiphase systems,” *Polymer (Guildf).*, vol. 42, no. 14, pp. 6209–6219, Apr. 2001, doi: 10.1016/S0032-3861(01)00086-6.

[61] M. D. Sanchez-Garcia and J. M. Lagaron, “On the use of plant cellulose nanowhiskers to enhance the barrier properties of polylactic acid,” *Cellulose*, vol. 17, no. 5, pp. 987–1004, Jul. 2010, doi: 10.1007/s10570-010-9430-x.

[62] E. Fortunati *et al.*, “Microstructure and nonisothermal cold crystallization of PLA composites based on silver nanoparticles and nanocrystalline cellulose,” in *Polymer Degradation and Stability*, Oct. 2012, vol. 97, no. 10, pp. 2027–2036, doi: 10.1016/j.polymdegradstab.2012.03.027.

[63] B. P. Grady, “Recent Developments Concerning the Dispersion of Carbon Nanotubes in Polymers,” *Macromol. Rapid Commun.*, vol. 31, no. 3, pp. 247–257, Feb. 2010, doi: 10.1002/marc.200900514.

[64] D. R. Paul and L. M. Robeson, “Polymer nanotechnology: Nanocomposites,” *Polymer (Guildf).*, vol. 49, no. 15, pp. 3187–3204, Jul. 2008, doi: 10.1016/j.polymer.2008.04.017.

[65] Q. Shi, C. Zhou, Y. Yue, W. Guo, Y. Wu, and Q. Wu, “Mechanical properties and in vitro degradation of electrospun bio-nanocomposite mats from PLA and cellulose nanocrystals,” *Carbohydr. Polym.*, vol. 90, no. 1, pp. 301–308, Sep. 2012, doi: 10.1016/j.carbpol.2012.05.042.

[66] A. Gupta, W. Simmons, G. T. Schueneman, D. Hylton, and E. A. Mintz, “Rheological and thermo-mechanical properties of poly(lactic acid)/lignin-coated cellulose nanocrystal composites,” *ACS Sustain. Chem. Eng.*, vol. 5, no. 2, pp. 1711–1720, Feb. 2017, doi: 10.1021/acssuschemeng.6b02458.

CHAPTER 8 ARTICLE 4: INTERFACIAL LOCALIZATION OF CNCS IN PLA/PBAT BLENDS AND ITS EFFECT ON RHEOLOGICAL, THERMAL, AND MECHANICAL PROPERTIES[4]

Mojtaba Mohammadi[1], Marie-Claude Heuzey[1], Pierre J. Carreau[1], Aurélie Taguet[2]

[1]*Center for High Performance Polymer and Composite systems (CREPEC), Department of Chemical Engineering, École Polytechnique de Montréal, Montreal, Québec, H3T 1J4, Canada*

[2] *Polymers Composites and Hybrids (PCH), IMT Mines Ales, Ales, France*

8.1 Abstract

In this study the effect of interfacial localization of 1 wt% cellulose nanocrystals (CNCs) was investigated on the morphology, rheology, thermal, and mechanical properties of poly (lactic acid), PLA (semicrystalline (sc) and amorphous (a)) and poly (butylene adipate-co-terephthalate), PBAT, blends (75/25 wt%). Different mixing strategies were adopted using solution casting followed by melt mixing to localize CNCs at the interface of PLA/PBAT blends. Scanning electron microscopy (SEM) and atomic force microscopy (AFM) confirmed this localization. The interfacial localization of CNCs significantly impeded the relaxation of the dispersed PBAT droplets in the PLA/PBAT blends and converted the droplet/matrix morphology of the scPLA/PBAT blend nanocomposites into a co-continuous one resulting in a solid-like rheological behavior. Also, CNCs played the role of nucleating agents in the PLA/PBAT blends and improved the crystallization behavior of scPLA and PBAT. Although Young's modulus and yield strength decreased in the neat PLA/PBAT blends, interfacial localization of CNCs improved these properties (mostly in scPLA/PBAT) to be closer to those values of neat PLAs, accompanied by improved elongation at break from ~3 % (scPLA (+IMM)) to ~ 150 % (scPLA/PBAT/CNC) and impact strength from ~20 J/m (scPLA (+IMM)) to ~95 J/m (scPLA/PBAT/CNC). These improvements were less effective in the aPLA/PBAT/CNC due to less effectiveness of CNC localization at the interface because of

[4] Submitted to Polymer and is under revision for publication.

more residual solvent in aPLA/PBAT/CNC, better affinity of CNCs with solvent compared to polymers and more spherical PBAT dispersed phase compared to that in scPLA/PBAT/CNC blend nanocomposites.

Keywords: PLA/PBAT/CNC nanocomposites; Interfacial localization; rheological properties; Mechanical and thermal properties.

8.2 Introduction

One of the most promising biodegradable polymer blend is poly(lactic acid) (PLA)/ poly(butylene adipate-co-terephthalate) (PBAT) [1], where PBAT allows to give better ductility, toughness, melt strength, and processability to PLA. On the other hand, while adding PBAT to PLA may improve several properties, it may decrease the strength and modulus of the blend. Solid particles in polymer blends can help attaining a balance between toughness and stiffness [2–5]. Polymer blends containing solid particles have distinct morphologies than neat binary blends. The control of the localization of solid particles in the dispersed phase, matrix, or at the interface of the two is the most essential aspect in developing high-performance polymer blend composites. The morphology and mechanical properties are directly affected by this localization [6–8]. Nanoparticles, due to their substantially higher specific surface area, have a significant potential to improve the mechanical and/or electrical properties at much lower particle concentrations than microparticles [7,9–11]. Several researchers have looked into the characteristics of PLA/PBAT blends with nanoparticles including nano clay [12–16], graphene [16,17], carbon nanotube [18–20], nanosilica [5,21], and cellulose nanocrystals (CNCs) [22,23]. It has been reported that the dispersed phase size in polymer blends could decrease when nanoparticles are localized in the matrix. It is explained by an increase of matrix viscosity that facilitates dispersed phase break up phenomenon [7,24,25]. Also, this localization is a well-known method for achieving a good balance of toughness and stiffness [7,26]. When nanoparticles are localized in the dispersed phase, the viscosity and elasticity of the dispersed phase increase, hence stabilizing the morphology of the minor phase [4,27,28]. Higher nanoparticle contents in the dispersed phase could eventually lead to a co-continuous morphology [29–32]. Nanoparticle localization at the interface of polymer blends has gained a lot of interest recently [7,10,24]. It may result in a reduction in the dispersed phase size via two key mechanisms: a) suppression coalescence caused by nanoparticles solid barrier effect and b) compatibilization of the blend. In the former mechanism nanoparticles create a shell around the

dispersed phase, preventing colliding droplets of the dispersed phase from coalescing [33,34]. In the latter mechanism, the interaction of nanoparticles with polymer components, as well as the resulting reduction in the interfacial tension, result in blend compatibilization and a reduction in the dispersed phase size [35–37]. In a recent study, Jalali Dil et al. [5] investigated the droplet/matrix and co-continuous morphology of PLA/PBAT (70/30 and 50/50 wt% respectively) in the presence of nanosilica. They reported that adding 1 wt% nanosilica to the 70/30 wt % of PLA/PBAT blend decreases the droplet size from 1.7 to 1 μm in PLA/PBAT blends by creating a shell around PBAT droplets and acting as a barrier for coalescence. By increasing the amount of nanosilica up to 3 wt% the droplet morphology was converted to a co-continuous one. Upon these morphological changes, the rheological properties of the PLA/PBAT blends were transformed from liquid- to solid-like. On the other hand, adding 3 wt% nanosilica did not change the co-continuous morphology of PLA/PBAT (50/50). In another study conducted by Jalali Dil et al. [20], interfacial localization of 3 wt% MWCNT in the blend of PLA/PBAT (80/20 wt%) converted the dispersed phase morphology to a co-continuous one. Nofar et al. [14] investigated PLA/PBAT blends at a fixed ratio of 75/25 wt% containing Cloisite 30B. They studied the influence of shear flow on the morphology of the blend. Similarly, to thermodynamics predictions, the Cloisite 30B was localized at the interface of the two phases. The Cloisite 30B had a barrier effect on the coalescence of the droplet and stabilized the blend morphology under shear flow. It is worth mentioning that the effect of interfacial localization of nanoparticles on rheological properties of different polymer blend nanocomposites have been investigated in previous studies and they reported similar observations of dramatic increases of the complex viscosity and storage modulus at low frequencies [5,12,14,20,29,38–43]. This improvement depends on the type of nanoparticles, content, state of dispersion, as well as type of components in the blend nanocomposites [8].

Despite prior research on the effect of nanoparticle interfacial localization on the morphology and rheology of polymer blends, few studies focused on the effect of interfacial localization of nanoparticles on the mechanical properties. This is due to the complexity of the subject, which requires a thorough examination of the morphology, rheology, and mechanical characteristics of the system. Jalali Dil et al. [5] demonstrated that 3 wt% nanosilica localized at the interface of PLA/PBAT (70/30 %) blend and converted the matrix-droplet morphology to a co-continuous one. They also proved that the mechanical properties were significantly improved compared to the neat PLA, and they reported an increase from 4.2 ± 1 % (PLA/3wt% nanosilica) to 284 ± 63 %

(PLA/PBAT/3wt% nanosilica) for elongation at break and from 22 ± 5 (PLA/3wt% nanosilica) N/m to 205 ± 31(PLA/PBAT/3wt% nanosilica) N/m for impact strength. In another study on the effect of localization of nanoparticles on mechanical properties, Nofar et al. [23] investigated the system PLA/PBAT/CNC, prepared through solution casting (master batch approach) followed by melt mixing via a twin-screw extruder. They observed that due to the presence of remaining solvent from the solution casting preparation step the expected improved ductility and impact characteristics were not obtained. However, they did not present microscopic analysis.

In our previous study [22], the effect of CNCs on the neat nanocomposites of PLA and PBAT and their blend (PLA/PBAT (75 wt%/25 wt%)) nanocomposites were investigated through morphological and rheological analyses. We observed that in some cases CNCs had a tendency to be localized at the interface of the PLA/PBAT blend [22]. In this work, the effects of interfacial localization of CNCs on the morphology, rheology, thermal, and mechanical properties of the PLA/PBAT(75 wt%/25 wt%) blend are examined. To this aim, at first, the morphology and rheology of PLA/PBAT blends with CNCs localized at the interface are examined. Secondly, thermal and mechanical properties of PLA/PBAT blends with CNCs at the interface are presented and discussed.

8.3 Experimental

8.3.1 Materials

NatureWorks LLC, USA, provided two commercially available grades, respectively amorphous and semi-crystalline linear PLAs, Ingeo 4060D (weight average molecular weight of 190 kg/mol) and 3251D (weight average molecular weight of 55 kg/mol), having D-lactide contents of 12 % and 1.4 %, respectively. Amorphous (a) and semi-crystalline (sc) PLAs are referred as aPLA and scPLA, respectively. PBAT (Ecoflex FBX 7011) was obtained from BASF and has a weight average molecular weight of 24.4 kg/mol and a melt flow index (MFI) of 2 g/10 min. Freeze-dried CNCs with width, length, and aspect ratio of 16 ± 3, 90 ± 17, and 6 ± 2 nm, respectively [44] were kindly provided by FPInnovations (Pointe-Claire, QC, Canada). The CNCs were neutralized using sodium hydroxide (NaOH) before freeze-drying and preparation information can be found elsewhere [45]. N, N-dimethylformamide (DMF), anhydrous 99.8 %, were purchased from Sigma-Aldrich Canada Co. (Oakville, ON, Canada).

8.3.2 Blend nanocomposites preparation

The blend nanocomposites of PLA/PBAT (75/25 wt%) with the incorporation of 1 wt% CNCs were prepared through solution casting followed by melt mixing. Unless otherwise mentioned, PLA in the nomenclature of the neat blends or blend nanocomposites refer to both amorphous (aPLA) and semicrystalline (scPLA). The solution casting process was used to prepare the neat nanocomposites of PLA/CNC, and PBAT/CNC (Figure 1). In the solution casting step, using a water bath sonicator and a magnetic stirrer, DMF was used to disperse and dissolve the CNCs and neat polymers, respectively. The CNCs and neat polymers were further mixed together with a magnetic stirrer after complete dispersion and dissolution. The prepared samples were dried in a vacuum oven in a two-step process [22]. For the first two days, the samples were placed in a vacuum oven (0.9 bar) with air circulation set at 60 °C. The drying process was then finished for another two days at 80 °C under vacuum (-0.65 bar). The weight percent of CNC within the nanocomposites was 1, 1.4, and 4 (PLA/1CNC, PBAT/1CNC, PLA/1.4CNC and PBAT/4CNC). More detailed information on the neat nanocomposites preparation is presented in our previous publication [22].

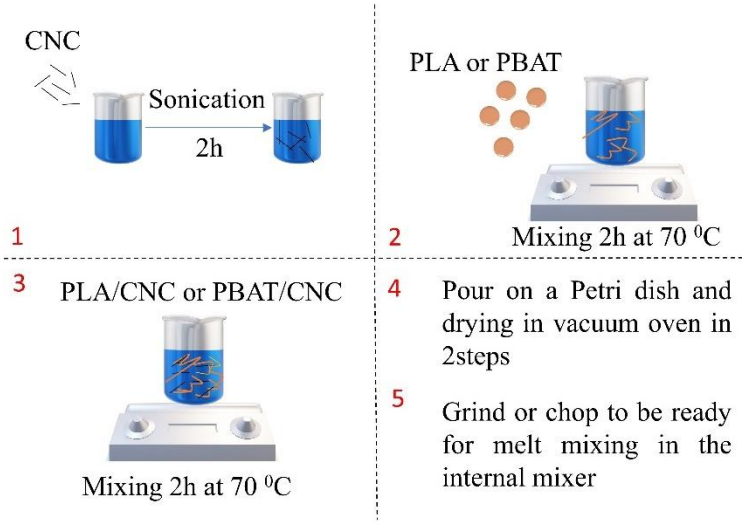

Figure 8.1 PLA/CNC and PBAT/CNC neat nanocomposites preparation method. The CNC content in neat nanocomposites based on their initial localization are 1 wt%; initial localization in both phases, 1.4 wt%; initial localization in the matrix phase and 4 wt%; initial localization in the dispersed phase. Steps 1-5 are from the beginning to end of the process.

The melt blending of neat polymers and their nanocomposites was done in an internal mixer using a DDRV501 Brabender (C. W. Brabender Instruments Inc., South Hackensack, NJ, USA) to prepare final blend nanocomposites of PLA/PBAT containing 1 wt% of CNCs. Prior to melt mixing, all the components were dried overnight at 55 °C. Three mixing strategies were used based on the initial localization of CNCs in PLA, PBAT, or both in the solution casting step. M1) granules of the neat PBAT were added to PLA/1.4CNC nanocomposites, M2) granules of the neat PLAs were added o PBAT/4CNC nanocomposites, and M3) PLA/1CNC and PBAT/1CNC were melt mixed. The melt mixing was performed at 180 °C, 100 rpm for 7 min under a nitrogen atmosphere. The schematic preparation method in the melt mixing step is presented in Figure 2. In this paper based on the initial localization of CNCs, the terms (PLA-1CNC)/PBAT, PLA/(PBAT-1CNC), and PLA/PBAT/1CNC stand for samples prepared from methods M1, M2, and M3, respectively. Also, the neat PLA/PBAT blends and neat PLA from solution casting followed by internal melt mixing were prepared for comparison (PLA/PBAT (+IMM) and PLA (+IMM), respectively).

Before microscopic, rheological, thermal, and mechanical investigations, the samples were compression molded into disc (thickness of 1.2 mm and a diameter of 25 mm), rectangle, and dog-bone-shaped specimens using a hydraulic press in a nitrogen atmosphere. The compression molding process lasted 10 minutes at 180 °C in a nitrogen atmosphere, with 4 minutes of heating and 6 minutes of gradually rising pressure force from 1 to 3 tons. Microscopic analysis was also performed using the rheological discs.

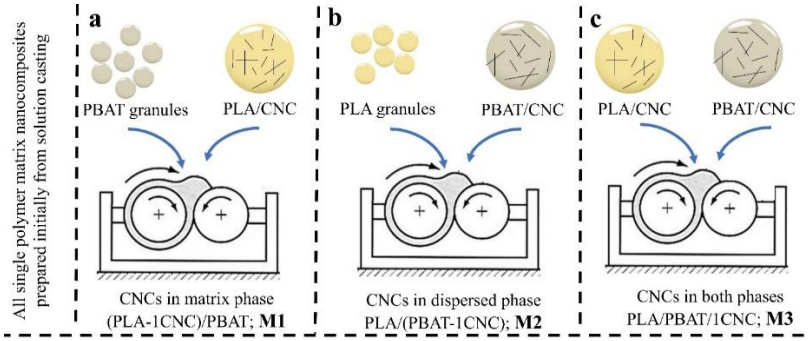

Figure 8.2 Schematics of the preparation method of PLA/PBAT blend nanocomposites containing CNCs. a) M1; (PLA-1CNC)/PBAT): granules of the neat PBAT were added to PLA/1.4CNC nanocomposites, b) M2; PLA/ (PBAT-1CNC): granules of the neat PLAs were added to PBAT/4CNC nanocomposites, and c) M3; PLA/PBAT/1CNC: PLA/1CNC and PBAT/1CNC nanocomposites were melted mixed.

8.3.3 Characterization

8.3.3.1 Scanning Electron Microscope (SEM)

The neat blends (PLA/PBAT) and their blend nanocomposites (PLA/PBAT/CNC) were fractured in liquid nitrogen to assess and compare their morphology before and after adding CNCs. The samples were subsequently covered with a 15 nm thick chromium-coated layer. At a voltage of 5 kV, the morphology was studied using an SEM (JSM 7600F, JEOL, Akishima, Tokyo 196-8558, JAPAN).

8.3.3.2 Atomic Force Microscopy (AFM)

An Ultracut FC microtome (Leica, Jung RM 2165, Concord, Ontario, Canada) with a liquid nitrogen cryo-chamber and a glass knife was used to cut and microtome samples. Using tapping mode on a Dimension ICON AFM (Bruker/Santa Barbara, CA, USA), AFM pictures were collected in the air at ambient temperature without any extra preparation. Using etched silicon cantilevers (ACTA from AppNano, Mountain View, California, USA) with a resonance frequency of roughly 300 kHz, a spring constant of 42 N/m, and a tip radius of <10 nm, intermittent contact imaging (also known as "tapping mode") was conducted at a scan rate of 0.8 Hz. All of the photos were taken using a medium tip oscillation damping (20%–30%).

8.3.3.3 Rheological analysis

A stress/strain-controlled MCR 302 rheometer (Anton Paar, Graz, Austria) with a 25 mm parallel plate flow geometry, and a 1 mm gap was used for the rheological analysis at 180 °C under nitrogen atmosphere. Time-sweep studies at a frequency of 1 rad/s were carried out for 40 minutes to ensure that the thermal stability of the samples was not compromised during the frequency sweep studies, which ranged from 628 rad/s to 0.05 rad/s [22]. Furthermore, strain sweep experiments were performed at a frequency of 1 rad/s on the neat polymers, polymer blend samples, and their nanocomposites to identify the linear viscoelastic area [22]. The results of time and strain sweep were presented in our previous publications [22]. The frequency sweep tests for polymer blends were carried out at a strain of 0.1 %, that is in the linear viscoelastic range.

8.3.3.4 **Thermal analysis**

Differential scanning calorimetry (DSC) was done on 5 mg material samples using a DSCQ1000 (TA Instruments, New Castle, DE, USA) in a nitrogen atmosphere. The blend nanocomposites samples were heated at a constant rate of 10 °C/min from -50 to 200 °C, kept at 200 °C for 3 minutes, and then cooled at a constant rate of 5 °C/min to -50 °C. In the second run, the samples were heated at a steady rate of 10 °C/min from -50 to 200 °C. For the neat PLA initial temperature was started at 25 °C. The glass transition temperature (T_g), melt and cold crystallization temperatures (T_c and $T_{cc,}$ respectively), and crystal melting temperature (T_m) were all thoroughly investigated. The total crystallinity content was calculated using the following equations:

$$X_c^{heating} = \frac{\Delta H_m - \Delta H_{cc}}{w \times \Delta H_m^{\circ}} \times 100 \qquad \text{Equation 8.1}$$

$$X_c^{cooling} = \frac{\Delta H_c}{w \times \Delta H_m^{\circ}} \times 100 \qquad \text{Equation 8.2}$$

where w, ΔH_m, ΔH_{cc}, ΔH_m°, and ΔH_c are the weight fraction of the polymeric matrix in the nanocomposite, enthalpy of melting, enthalpy of cold crystallization, enthalpy of melting of 100% crystalline polymer (93 J/g [46] and 114 J/g [47] for PLA and PBAT, respectively), and enthalpy of crystallization in cooling run.

8.3.3.5 **Mechanical analysis**

The tensile properties of the samples at room temperature were investigated using an Instron 3365 following ASTM D638. Tensile specimens, dog bone-shaped type V with a thickness of 1.6 mm, were stretched at room temperature at a crosshead speed of 5 mm/min using a 5 kN load cell. A minimum of five specimens was tested for each sample. The tensile test was investigated without using an extensometer.

The impact strength of notched Izod was determined using a Ray-Ran Universal Pendulum Impact Tester following ASTM D256. Impact testing specimens were 63.5×12.7×3.0 mm^3 in size, and a minimum of five specimens was tested.

8.4 Result and discussion

8.4.1 Morphology

The thermodynamics equilibrium localization of CNCs in PLA/PBAT blend nanocomposites was determined to be in the PBAT phase in our previous work [22]. This localization was determined using surface energies of the components (PLA, PBAT, and CNCs) in the blend nanocomposites and related interfacial tensions calculated from the harmonic and geometric mean equations as well as using the Palierne model [22]. Figure 3 depicts SEM images of neat PLA/PBAT blends and their blend nanocomposites. The addition of CNCs reduces the PBAT droplet size (volume average radius, R_v) in aPLA/PBAT blend nanocomposites no matter the mixing strategy (Figure 3, first row), but in the scPLA/PBAT blend nanocomposites (Figure 3, second row), the PBAT droplet, R_v, decreases in the M2, while in the M1 and M3 it results in elongated PBAT droplets with a tendency for the scPLA matrix to convert the emulsion-type morphology to a co-continuous structure (more visible for M1). These morphological changes in M1 and M3 are discussed in the next paragraph and presented clearly in Figure 5. More information about the volume average diameter determination of PBAT droplets is given in our previous work [22].

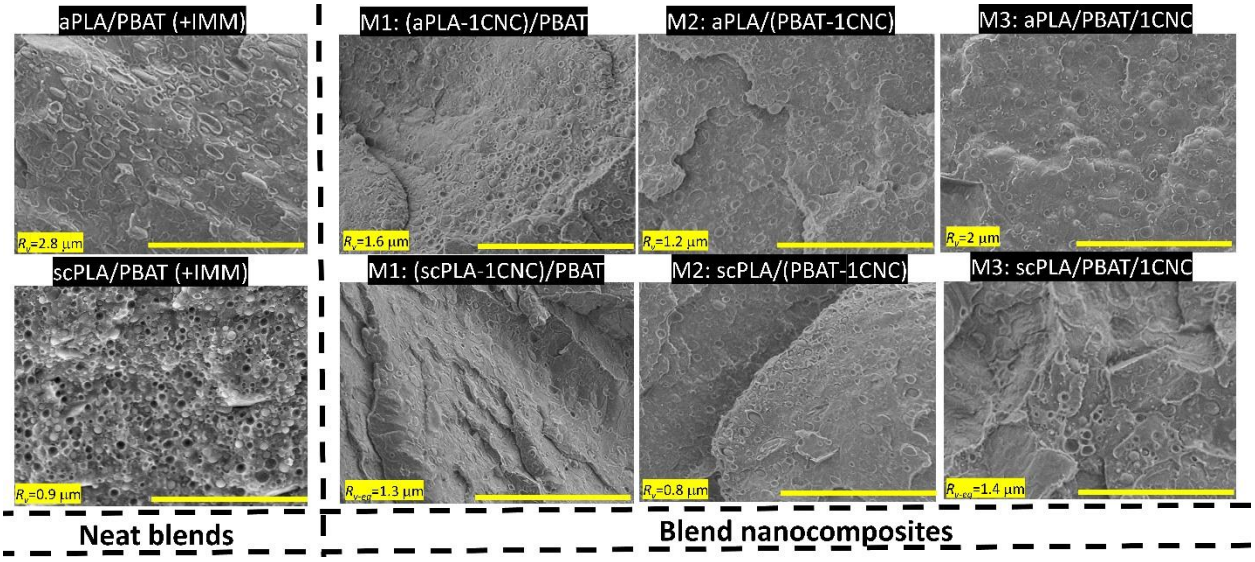

Figure 8.3 SEM images of neat PLA/PBAT blends and their blend nanocomposites. M1, M2, and M3 represent the blend nanocomposites for which CNCs are initially localized in the PLA, PBAT, or both phases, respectively, in the solution casting step. The scale bars are 30 µm.

Changing the mixing strategy can result in varied localizations of CNCs. To assess the localization of the CNCs, AFM analysis (Figure 4) at higher magnifications was done on the aPLA/PBAT/CNC (Figures 4a & b) and scPLA/PBAT/CNC (Figures 4c & d) blend nanocomposites prepared through M1 (Figures 4a & c) and M3 (Figure 4b & d). The CNCs appear as white spots or rods as indicated by arrows in these images [28,48]. The white spots correspond to the transverse sections of CNC particles. Mixing strategy M2 favors the localization of CNCs in the PBAT. When CNCs were initially dispersed in PLA (M1) or both phases (M3), they have a tendency to localize at the PLA/PBAT interface (Figure 4), which was shown in our previous work to be an advantage for droplet coalescence barrier and blend morphological stabilization [22]. In fact, in M1 and M3, CNCs initially localized in the matrix (PLA) phase migrate partly to the interface of PLA/PBAT blends and some to the PBAT phase. The interfacial localization in aPLA/PBAT/CNC results in a size decrease of droplets of PBAT dispersed phase. The decrease in the dispersed phase size caused by nanoparticle interfacial localization has previously been reported in the literature and is attributed to a decrease in coalescence due to the solid shell of nanoparticles surrounding the dispersed phase [5,7,24]. On the other hand, Figure 5 shows the dispersed droplet-type morphology in scPLA/PBAT/CNC prepared through M1 (Figure 5, first row) and M3 (Figure 5, second row) that appears to be converted to a co-continuous morphology as a result of interfacial localization of CNCs in the scPLA/PBAT/CNC (Figures 4c & d), which could have a significant impact on the final mechanical properties of the blend nanocomposites. Selective extraction of each phase is widely used to determine the degree of phase continuity in a polymer mixture [49]. Due to the close solubility properties of the scPLA and PBAT polymers, this approach is not applicable in scPLA/PBAT blend. The most useful tool for the blend nanocomposites of scPLA/PBAT/CNC could be rheological analysis presented later in Figure 6 and with related discussion.

When CNCs are introduced to the blend nanocomposites through the PBAT phase (M2), they remain in the PBAT droplets, and the results are of less interest. As a result, throughout the rest of this article, M1 ((PLA-1CNC)/PBAT) and M3 (PLA/PBAT/1CNC)) will be used as the primary mixing approach to localize CNCs at the PLA/PBAT interface and related rheological, thermal, and mechanical properties will be discussed only for these mixing strategies.

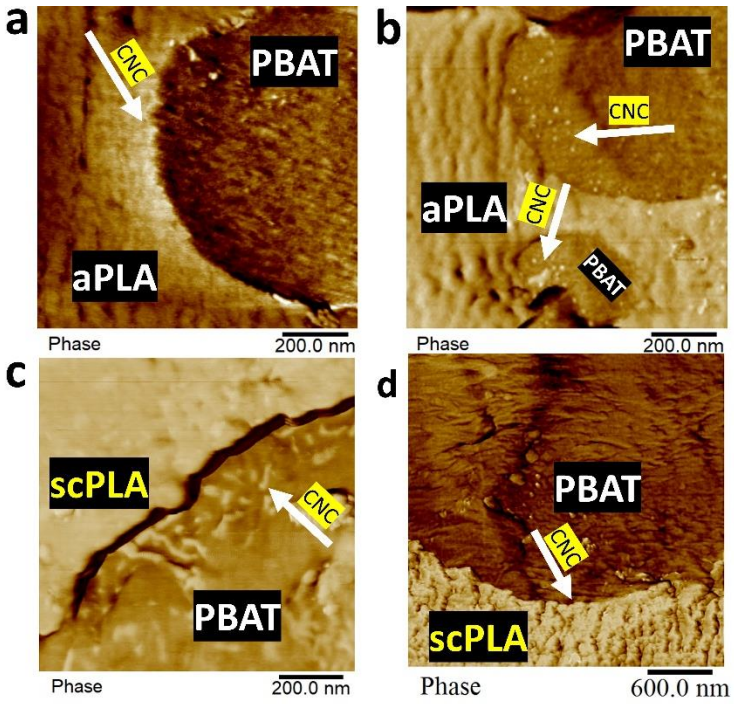

Figure 8.4 Localizations of CNCs at the interface of PLA/PBAT (75/25 wt%) blend nanocomposites: AFM images of blend with 1 wt% of CNCs prepared using M1 (a and c; (PLA-1CNC)/PBAT) and M3 (b and d; PLA/PBAT/1CNC).

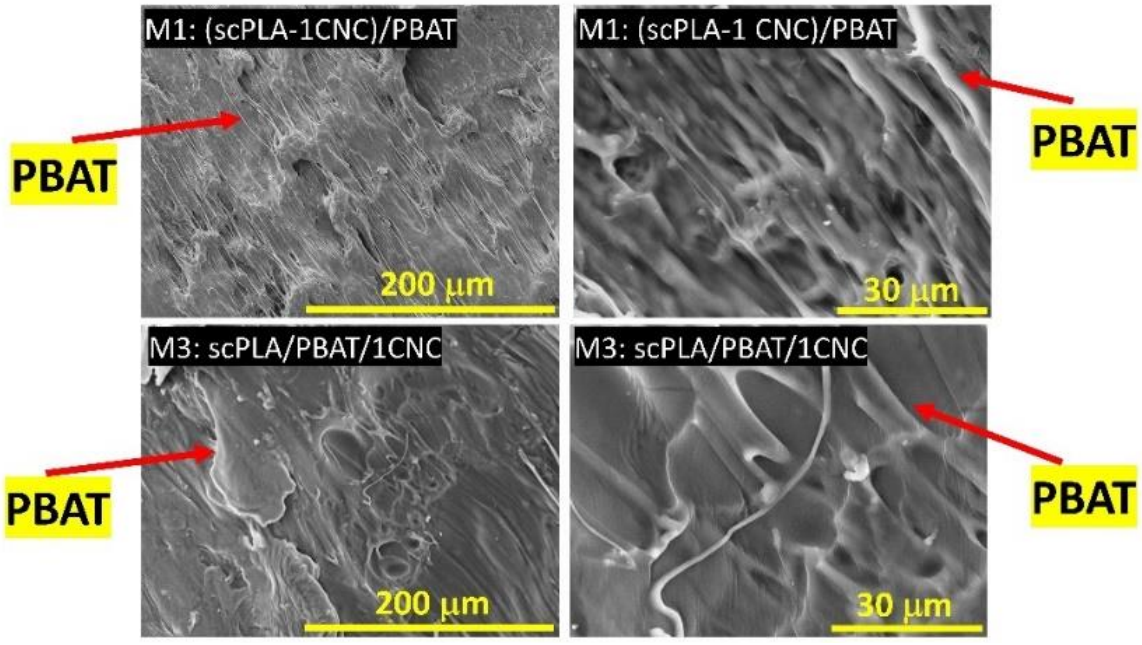

Figure 8.5 SEM images for two magnifications of scPLA/PBAT/CNC prepared from M1 and M3.

8.4.2 Rheological properties

Previous research [50–52] has shown that the rheological properties of PLA/PBAT blends can provide useful information on the morphology of the system. Figure 6 depicts the influence of CNC interfacial localization (M1 and M3) on the rheological parameters (complex viscosity (a & d), storage modulus (b & e), and Cole-Cole plots (c & f)) of a PLA/PBAT (75/25 wt%) blend nanocomposites containing CNCs. When CNCs were added to aPLA or scPLA during the solution casting step (M1), the complex viscosity at low frequencies of scPLA/PBAT/CNC nanocomposites increase sharply, but the corresponding increase for aPLA/PBAT/CNC is only slight (Figures 6a & d). At low frequencies, considerable slope reductions in the storage modulus are also found (Figures 6b & e), primarily for scPLA/PBAT/CNC (Figure 6b). What is more, while Figures 6a & b show identical rheological behavior for scPLA/PBAT/CNC prepared by M1 and M3, slightly higher values of the complex viscosity (Figure 6d) and the storage modulus (Figure 6e) in aPLA/PBAT/CNC observed for M1 could be due to the existence of finer morphology compared to M3 (volume average diameter of 1.6 and 2 μm for M1 and M3, respectively, reported in our previous publication [22]). These results are in accordance with the SEM analysis presented in Figures 3 and 5. The presence of a shoulder in G' and an arc on the right side of the Cole-Cole plots of the neat blend (Figure 6, squares) is an indication of the dispersed phase relaxation and the existence of a matrix-droplet morphology in the sample [53]. Both the shoulder in G' (more obvious for scPLA/PBAT/CNC) and the droplet relaxation arc in the Cole-Cole plots disappear following the interfacial localization of 1 wt% CNCs (Figures 6b, c, e, & f). According to Figure 3 for aPLA/PBAT/CNC (M1 and M3) this interfacial localization does not change the matrix-droplet morphologies. So, disappearance of the second arc of Cole-Cole plots and shoulder in storage modulus of aPLA/PBAT/CNC (M1 and M3, Figures 6e & f) is an indication that the time of relaxation of the PBAT dispersion phase is greatly reduced. This behavior as a result of interfacial localization of nanoparticles in polymer blends has been reported in the literature [5,54,55]. On the other hand, Figure 5 shows that for scPLA/PBAT/CNC blend nanocomposites, the interfacial localization of 1 wt% CNCs change the matrix-droplet morphology to a continuous structure of PBAT in scPLA matrix. Due to the localization of CNC combined with the continuous structure of PBAT, both the shoulder in the storage modulus and relaxation arc in the Cole-Cole plot of scPLA/PBAT/CNC disappears (Figure 6b &c). This is due to the fact that CNCs obstruct the relaxation and mobility of polymer chains near the interface [55]. In addition, the low frequency

data show a plateau in the storage modulus and a considerable upturn in complex viscosity, indicating a transition to gel-like behavior (Figure 6a & b). Similar behavior has been reported by Jalali Dil et al. [5] when 3 wt% of nano silica were localized at the interface of PLA/PBAT blend (70/30 wt%). This behavior is remarkably similar to that reported for bicontinuous interfacial jammed emulsions (Bijels) [56,57]. The creation of a 2D network of solid particles at the interface of the co-continuous emulsion is responsible for the gel-like behavior. Therefore, the flow and deformation of the system is limited by this 2D network of CNCs at the interface and cause a gel-like behavior. These observations confirm a shift from matrix-droplet morphology to a co-continuous one observed in Figure 5 by interfacial localization of CNCs in scPLA/PBAT/CNC.

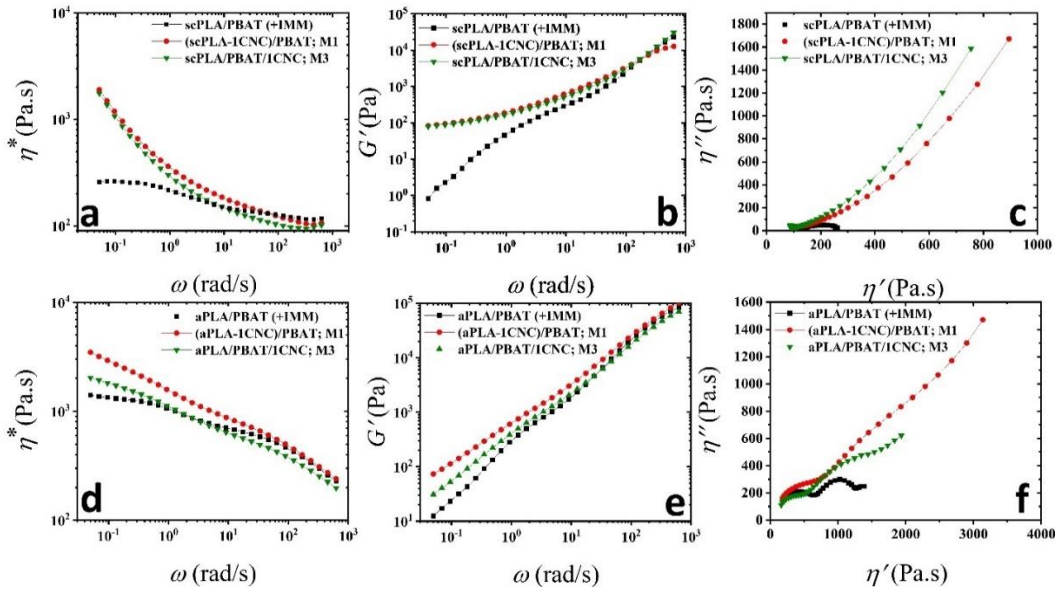

Figure 8.6 The effect of interfacial localization of CNC on (a and d) complex viscosity (b and e) storage modulus, and (c and f) Cole-Cole plots of PLA/PBAT (75/25 wt%) blend nanocomposites.

8.4.3 Differential scanning calorimetry (DSC)

Figures 7a & b show the DSC thermograms of the neat polymers (aPLA (+IMM), scPLA (+IMM), and PBAT (+IMM)). The glass transition temperatures (T_g) of scPLA (+IMM), aPLA (+IMM), and PBAT (+IMM) are 57, 53, -36 °C, respectively, from the cooling cycles, and the crystal melting temperature (T_m) of scPLA (+IMM) and PBAT (+IMM) appear to be at 168 and 128 °C, respectively, from the second heating cycle (Table 1 or Figure 7a & b). Because the presence of

crystalline regions in scPLA (+IMM) hinders the molecular mobility of the amorphous part, a higher T_g is observed when compared to aPLA (+IMM). scPLA (+IMM) shows around 14 and 38 % for the degree of crystallinity in the cooling cycle ($X_c^{cooling}$) and second heating cycle ($X_c^{h_2}$) thermograms (Table 1 and Figure 7a & b). The crystallization behavior of the neat PLA/PBAT (+IMM) blends and their blend nanocomposites (PLA/PBAT/CNC; M1 and M3) were also investigated using DSC and the results of the cooling and second heating cycles are presented in Figures 7c-f and Table 1. Because of the varied cooling profiles applied to the samples during processing, the first heating thermograms do not provide accurate information in all of the samples and are not presented here. By the addition of CNCs, the T_g of scPLA does not change through the cooling and second heating cycles for scPLA/PBAT (+IMM) blends (Table 1). Interestingly, the T_g of aPLA in the neat aPLA/PBAT (+IMM) and its blend nanocomposites increase by about 6 °C from the cooling cycle to the second heating cycle (Table 1) [58]. This could be because the effect of remaining solvent in the melting process is more influential in aPLA/PBAT/CNC compared to scPLA/PBAT/CNC. Therefore, the aPLA/PBAT chains has more free volume in the presence of more residual solvent and exhibits a lower T_g for aPLA in the cooling cycle. Also, Similar to scPLA, the calculated T_g of PBAT (+IMM) (Figure 7a & b; -36 °C) does not change in neat PLA/PBAT blends and their blend nanocomposites (Figure 7c-f).

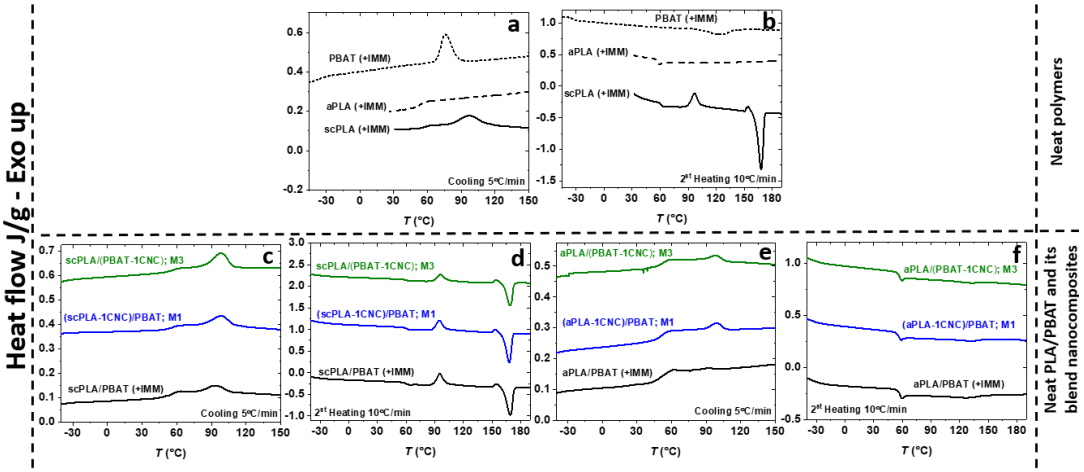

Figure 8.7 DSC thermograms of first cooling (a, c, and e), and second heating (b, d, and f) sequences for a & b) scPLA (+IMM), aPLA (+IMM), and PBAT (+IMM), and c-f) neat PLA/PBAT (+IMM) blends and their blend nanocomposites prepared from M1 ((PLA-1CNC)/PBAT) and M3 (PLA/PBAT/1CNC)).

Table 1 shows that the melt crystallization temperature (T_c) of scPLA/PBAT (+IMM) decreases to 94 °C compared to 96 °C for scPLA (+IMM). Although this decrease is not significant and could be within experimental errors, more importantly, the crystallinity of scPLA (+IMM) in the cooling cycle ($X_c^{cooling}$) decreases from 14 % to 9 % for scPLA/PBAT (+IMM) (similar decreasing effect in the second heating cycle ($X_c^{h_2}$)) (Table 1). Hence, these reductions can be attributed to the effect of PBAT droplets as chain mobility restriction. Similar observation have been reported by Al-Itry et al. [59] for PLA/PBAT blends.

To discuss on the effect of CNC on the crystallization of scPLA, it must be noticed here that scPLA and PBAT crystallized at 75 and 96 °C (Figure 7a). Also, it was proven elsewhere that [59] PBAT decreases the crystallinity and the melt crystalline temperature of PLA [59] and CNC has a tendency to restrict the mobility of PBAT chains and the crystallinity of PBAT in the presence of CNC was decreased [60]. Although cold crystallization temperature (T_{cc}) does not change for scPLA/PBAT/CNC, the melt crystallization temperature (T_c) increases modestly from 94 °C in neat scPLA/PBAT (+IMM) to around 100 °C for both (scPLA-1CNC)/PBAT; M1, and scPLA/PBAT/1CNC; M3. This shows that CNCs in scPLA/PBAT/CNC act as nucleating agents that accelerate the crystallization of the scPLA in the blend nanocomposite. Moreover, the effect of CNCs as a nucleating agent is obvious in the crystallinity of scPLA in the cooling cycle ($X_c^{cooling}$). The $X_c^{cooling}$ increases from 9% in neat scPLA/PBAT (+IMM) to 18% (100 % increase) in both (scPLA-1CNC)/PBAT (M_1) and scPLA/PBAT/1CNC) (M_3) (similar increasing effect in the second heating cycle ($X_c^{h_2}$)) (Table 1). What is more, although crystallization of scPLA and PBAT are at different temperatures (96 and 75 °C, respectively; Figure 7a), Figures 7c & d show scPLA and PBAT crystallized at identical temperatures in the blend nanocomposites, suggesting that the PLA slow crystallization could be promoted by droplets of PBAT in addition to the presence of CNCs as nucleating agents. In other words, scPLA and PBAT crystallized simultaneously, allowing them to enhance each other crystallization and interfacial contacts between matrix and dispersed-phase molecules in a synergistic manner. Therefore, degree of crystallinity obtained for scPLA in Table 1 is affected by possible crystals of PBAT. Finally, the melting temperature of scPLA/PBAT (+IMM) blend nanocomposites are not affected by the addition of CNCs and are around 168 °C (Table 1).

Regarding the DSC of blends based on aPLA, and as mentioned in other articles, CNC do not play any nucleating role for this aPLA [61]. Moreover, PBAT hinders the mobility of PLA chains [59]. Hence, the exothermic peak that are seen in Figure 7e is due to the crystallization of PBAT. The crystallization temperature of PBAT was increased from 81°C for the blend to 100°C for both (aPLA-1CNC)/PBAT; M1, and aPLA/PBAT/1CNC; M3 (Figures 7f & g). Moreover, the calculated degree of crystallinity in PBAT increases from 4% in the neat aPLA/PBAT (+IMM) to around 12% in (aPLA-1CNC)/PBAT; M1, and aPLA/PBAT/1CNC; M3. Also, the melting temperature of around 130 °C in Figure 7f is the PBAT melting temperature in the blends of aPLA/PBAT (+IMM) and their nanocomposites (not affected by the addition of CNCs).

Table 8.1 DSC results for cooling and second heating sequences of neat PLA (+IMM), neat PLA/PBAT (+IMM), and PLA/PBAT blend nanocomposites prepared through M1 and M3.

Samples	Glass transition temperatures (°C)		Melt Crystallization temperatures (°C)	Cold crystallization temperatures (°C)	Crystal melting temperatures (°C)	Degree of crystallinity (X%)	
	$T_g^{cooling}$	$T_g^{h_2}$	T_c	T_{c_c}	$T_m^{h_2}$	$X_c^{cooling}$	$X_c^{h_2}$
scPLA (+IMM)	57	59	96	95	168	14	38
scPLA/PBAT (+IMM)	57	58	94	95	169	9	18
(scPLA-1CNC)/PBAT; M1	57	59	100	96	168	18	25
aPLA/PBAT/1CNC; M3	57	59	99	96	169	18	24
aPLA (+IMM)	53	58	…	…	…	…	
aPLA/PBAT (+IMM)	50	57	…	…	…	…	
(aPLA-1CNC)/PBAT; M1	52	57	…	…	…	…	
aPLA/PBAT/1CNC; M3	53	58	…	…	…	…	

$T_g^{cooling}$: glass transition temperature of the cooling cycle; $T_g^{h_2}$: glass transition temperature of the second heating cycle; T_c: melt crystallization temperature of the cooling cycle; T_{c_c}: cold crystallization temperature of the second heating cycle; $T_m^{h_2}$: crystal meting temperature of the second heating cycle; $X_c^{cooling}$: degree of crystallinity of the cooling cycle; $X_c^{h_2}$: degree of crystallinity of the second heating cycle.

8.4.4 Mechanical properties

Figure 8 reports the mechanical properties of as-received granules of PLA, PLA processed from solution casting followed by melt mixing (PLA (+IMM)), neat PLA/PBAT (+IMM) blends, and PLA/PBAT blend nanocomposites prepared from mixing strategies of M1 ((PLA-1CNC)/PBAT) and M3 (PLA/PBAT/1CNC). In both amorphous and semi-crystalline PLAs, a brittle behavior is obvious from Figure 8 (high Young's modulus and low elongation at break) and the corresponding results are reported in Table 2. As expected, adding PBAT with high elongation at break (~ 700 %) changes the mechanical behavior of PLA from brittle to ductile in the PLA/PBAT (+IMM)

blends. It has been reported in the literature that increasing the content of PBAT has an increasing effect on elongation at break and impact strength of PLA, but decreases the yield strength and modulus [5,62]. Adding 25 wt% PBAT increases the elongation at break from 3 to 95 % in scPLA/PBAT (+IMM) and from 3 to 50 % in aPLA/PBAT (+IMM), respectively, compared to PLA (+IMM). The larger elongation at break for the scPLA/BPAT blend is linked also to the much lower yield strength after adding PBAT to scPLA (that goes from 70 to 43 MPa) compared to aPLA (that goes from 50 to 45 MPa). It means that in the case of scPLA the stress is transferred more easily to the PBAT than in the case of aPLA and this could be due to the better chemical affinity between scPLA and PBAT compared to that between aPLA and PBAT. As briefly discussed in the Supplementary Information of our previous publication [22], we expect scPLA with a low molecular weight and higher crystallinity compared to aPLA to have larger Hansen solubility parameters [63] and a smaller relative energy difference (RED) between scPLA and PBAT. However, the Young modulus and yield strength decrease from 2740 to 1825 MPa and from 70 to 43 MPa in scPLA/PBAT (+IMM) and from 1982 to 1535 MPa and 50 to 45 MPa in aPLA/PBAT (+IMM), respectively, compared to the neat PLAs (+IMM). What is more, the impact strength rises from 20 to 35 J/m in scPLA/PBAT (+IMM) and from 26 to 47 J/m in aPLA/PBAT (+IMM) compared to the neat PLAs (+IMM). As mentioned in the introduction, localization of nanoparticles at the interface can improve the adhesion between phases and, hence, enhance the elongation at break and impact strength of the blend nanocomposites, making a balance between toughness and stiffness. In the morphology and rheology sections, it is shown that mixing strategies 1 and 3 (M1; (PLA-1CNC)/PBAT and M3; (PLA/PBAT/1CNC)) lead to localization of CNCs at the interface of PLA and PBAT phases and this localization is more effective in the semicrystalline scPLA/PBAT/CNC, which exhibits a solid-like behavior in rheology (Figures 6a &b). The interfacial localization of 1 wt% CNCs in the scPLA/PBAT blend nanocomposites increases the elongation at break and impact strength by 52 and 171 % for M1 and 57 and 140 % for M3 compared to the neat scPLA/PBAT (+IMM). A possible phenomenon for the significant improvement in elongation at break and impact properties in scPLA/PBAT (+IMM) blend can be attributed to the tendency of the matrix-droplet morphology in scPLA/PBAT (+IMM) blend to be converted into a co-continuous one in the presence of 1 wt% of CNCs in both M1 and M3 (Figure 5 and 6a, b, & c). This improvement is less effective in the aPLA/PBAT blend nanocomposites with elongation at break and impact strength increasing, respectively, by only 10 % and 23% for

M1 and 6% and 7% for M3 compared to the neat aPLA/PBAT (+IMM). In our previous publications [22,58], it was shown that the effect of traces of solvent after solution casting and drying and even after melt mixing was preventing achieving high performance in the neat polymers and blends. This effect of traces of solvent is more severe in aPLA compared to scPLA and PBAT with lower molecular weight and crystalline structure, which helped in expulsing the solvent out of the samples during the drying process [22,58]. Also, in our previous publication [22], we have shown via the Hansen solubility parameter theory (HSP) that CNCs have a better affinity with DMF (relative energy difference (RED) equal or less than 1) compared to PLA and PBAT (RED more than 1). Therefore, in aPLA/PBAT/CNC that contains more residual solvent, the interactions between CNCs and solvent could be more pronounced compared to the CNC role in promoting interfacial adhesion between aPLA and PBAT. What is more, the addition of PBAT causes a reduction in the Young modulus of both scPLA/PBAT (+IMM) and aPLA/PBAT (+IMM) blends. On the other hand, while the reduction in the Young modulus by adding PBAT to the scPLA (+IMM) is largely recovered by the addition of 1 wt% CNCs, but the Young modulus in aPLA/PBAT/CNC (both M1 and M3) remains at the same level compared to the neat aPLA/PBAT (+IMM) blend. Again, it could be attributed to the presence of more residual solvent in aPLA/PBAT/CNC and also to the difference in molecular weight of scPLA and aPLA.

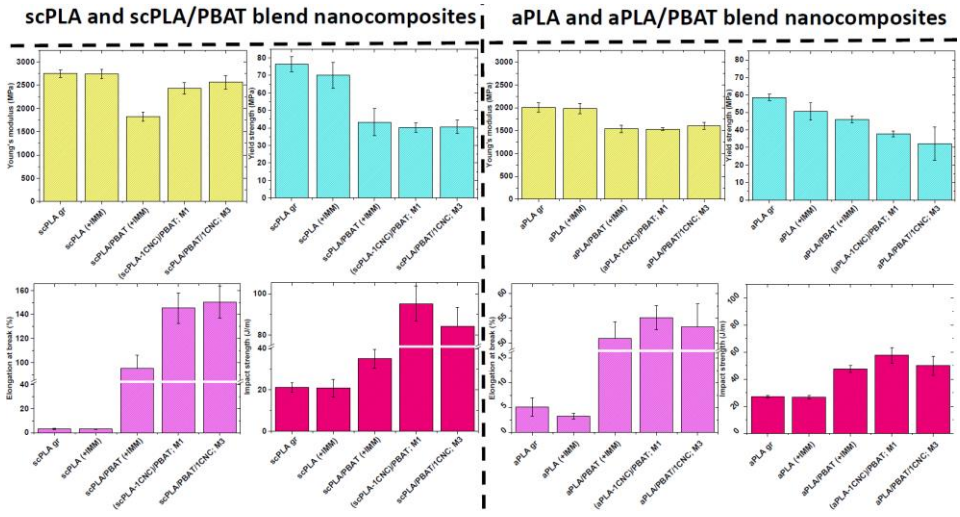

Figure 8.8 Young's modulus, yield strength, elongation at break, and impact strength of granules of PLA, neat PLA (+IMM), neat PLA/PBAT (+IMM) blends, and PLA/PBAT/CNC blend nanocomposites prepared through M1 ((PLA-1CNC)/PBAT) and M3 (PLA/PBAT/1CNC). "gr" in the x-axis stands for neat polymers prepared from granules.

Table 8.2 Mechanical properties of granules of PLA, neat PLA (+IMM), neat PLA/PBAT (+IMM), and PLA/PBAT blend nanocomposites prepared through M1 and M3.

Sample	Young's modulus (MPa)	Yield strength (MPa)	Elongation at break (%)	Impact strength (J m^{-1})
scPLA granules	2748 ± 84	76 ± 4	3.1± 0.3	21 ± 2
scPLA (+IMM)	2740 ± 97	70 ± 7	3.0 ± 0.3	21 ± 4
scPLA/PBAT (+IMM)	1825 ± 101	43 ± 7	95 ± 9	35 ± 5
(scPLA-1CNC)/PBAT; M1	2430 ± 121	40 ± 2	145 ± 12	95 ± 8
scPLA/PBAT/1CNC; M3	2562 ± 146	40 ± 3	150 ± 13	84 ± 9
aPLA granules	2010 ± 100	58 ± 1	5.2 ± 2.0	27 ± 1
aPLA (+IMM)	1982 ± 110	50 ± 4	3.3 ± 0.6	27 ± 1
aPLA/PBAT (+IMM)	1535 ± 83	45 ± 1	50.0 ± 3.0	47 ± 2
(aPLA-1CNC)/PBAT; M1	1530 ± 31	37 ± 1	55.0 ± 2.4	58± 6
aPLA/PBAT/1CNC; M3	1609 ± 76	32 ± 9	53.0 ± 4.7	50± 7

8.5 Conclusion

The influence of interfacial localization of 1 wt% CNCs on the morphology, rheology, thermal, and mechanical properties of scPLA/PBAT and aPLA/PBAT (75wt%/25wt%) blends was investigated. The blend nanocomposites were prepared through solution casting followed by melt mixing using an internal mixer. In the solution casting the CNCs were initially localized in the dispersed phase, matrix, or both phases to prepare neat nanocomposites, and their localization in the blends was studied after melt mixing using SEM and AFM. The initial localization of CNCs in the matrix or both phases resulted in CNCs being mostly localized at the interface after melt mixing. Rheological analysis and especially Cole-Cole plots indicated that for both M1 and M3 morphologies, the PBAT droplet relaxation was delayed. The slower relaxation of the PBAT droplets was also obvious in the storage modulus of scPLA/PBAT/CNC by the presence of a plateau at low frequencies, indicative of a transition from liquid- to solid-like behavior. It is worth mentioning that the initial localization of CNCs in the matrix and dispersed phases, which eventually led to its presence at the interface after melt mixing, converted the matrix-droplet morphology to a co-continuous one in the case of scPLA/PBAT/CNC. Due to this localization at the interface and morphological transformation, considerable improvements in elongation at break and impact properties of scPLA/PBAT were observed using only 1 wt % CNCs. These improvements were less effective in the case of aPLA/PBAT/CNC as a result of more residual solvent in that system and better affinity of CNCs with the solvent. Also, thermal analysis using

DSC revealed the nucleation effect of CNCs and improvements of the crystallization temperature and the degree of crystallinity of scPLA. The interfacial localization of nanoparticles is an effective approach for stabilizing the morphological and improving mechanical characteristics of polymer blends. Moreover, this localization could pave the way for the creation of stable co-continuous structures for blends at low contents of the minor phase.

8.6 Acknowledgments

Financial support from the Natural Science and Engineering Research Council (NSERC) of Canada is gratefully acknowledged. The authors also wish to acknowledge the help of Dr. Helia Sojoudiasli and Mr. Matthieu Gauthier for the material preparation and processing. Finally, we wish to thank Mr. Jed Randall from NatureWorks for providing one of the PLA samples.

8.7 References

[1] M. Nofar, D. Sacligil, P. J. Carreau, M. R. Kamal, and M.-C. Heuzey, “Poly (lactic acid) blends: Processing, properties and applications,” *Int. J. Biol. Macromol.*, vol. 125, pp. 307–360, Mar. 2019, doi: 10.1016/j.ijbiomac.2018.12.002.

[2] Y. Yoo, L. Cui, P. J. Yoon, and D. R. Paul, “Morphology and mechanical properties of rubber toughened amorphous polyamide/MMT nanocomposites,” *Macromolecules*, vol. 43, no. 2, pp. 615–624, Jan. 2010, doi: 10.1021/ma902232g.

[3] H. S. Lee, P. D. Fasulo, W. R. Rodgers, and D. R. Paul, “TPO based nanocomposites. Part 1. Morphology and mechanical properties,” *Polymer (Guildf).*, vol. 46, no. 25, pp. 11673–11689, Nov. 2005, doi: 10.1016/j.polymer.2005.09.068.

[4] M. Kontopoulou, Y. Liu, J. R. Austin, and J. S. Parent, “The dynamics of montmorillonite clay dispersion and morphology development in immiscible ethylene-propylene rubber/polypropylene blends,” *Polymer (Guildf).*, vol. 48, no. 15, pp. 4520–4528, Jul. 2007, doi: 10.1016/j.polymer.2007.05.068.

[5] E. Jalali Dil, N. Virgilio, and B. D. Favis, “The effect of the interfacial assembly of nano-silica in poly(lactic acid)/poly(butylene adipate-co-terephthalate) blends on morphology, rheology and mechanical properties,” *Eur. Polym. J.*, vol. 85, pp. 635–646, Dec. 2016, doi: 10.1016/j.eurpolymj.2016.07.022.

[6] A. Göldel, G. Kasaliwal, and P. Pötschke, “Selective localization and migration of multiwalled carbon nanotubes in blends of polycarbonate and poly(styrene-acrylonitrile),” *Macromol. Rapid Commun.*, vol. 30, no. 6, pp. 423–429, Mar. 2009, doi: 10.1002/marc.200800549.

[7] A. Taguet, P. Cassagnau, and J.-M. Lopez-Cuesta, “Structuration, selective dispersion and compatibilizing effect of (nano)fillers in polymer blends,” *Prog. Polym. Sci.*, vol. 39, no. 8, pp. 1526–1563, Aug. 2014, doi: 10.1016/j.progpolymsci.2014.04.002.

[8] R. Salehiyan, M. Nofar, K. Malkappa, and S. S. Ray, “Effect of nanofillers characteristics and their selective localization on morphology development and rheological properties of melt-processed polylactide/poly(butylene adipate-co-terephthalate) blend composites,” *Polym. Eng. Sci.*, vol. 60, no. 11, pp. 2749–2760, Nov. 2020, doi: 10.1002/pen.25505.

[9] R. Salehiyan, M. Nofar, S. S. Ray, and V. Ojijo, “Kinetically Controlled Localization of Carbon Nanotubes in Polylactide/Poly(vinylidene fluoride) Blend Nanocomposites and Their Influence on Electromagnetic Interference Shielding, Electrical Conductivity, and Rheological Properties,” *J. Phys. Chem. C*, vol. 123, no. 31, pp. 19195–19207, Aug. 2019, doi: 10.1021/acs.jpcc.9b04494.

[10] M. Nofar, R. Salehiyan, and S. S. Ray, “Influence of nanoparticles and their selective localization on the structure and properties of polylactide-based blend nanocomposites,” *Compos. Part B Eng.*, vol. 215, p. 108845, Jun. 2021, doi: 10.1016/j.compositesb.2021.108845.

[11] E. Vatansever, D. Arslan, and M. Nofar, “Polylactide cellulose-based nanocomposites.,” *Int. J. Biol. Macromol.*, vol. 137, pp. 912–938, Sep. 2019, doi: 10.1016/j.ijbiomac.2019.06.205.

[12] M. Nofar, R. Salehiyan, U. Ciftci, A. Jalali, and A. Durmuş, “Ductility improvements of PLA-based binary and ternary blends with controlled morphology using PBAT, PBSA, and nanoclay,” *Compos. Part B Eng.*, vol. 182, p. 107661, Feb. 2020, doi: 10.1016/j.compositesb.2019.107661.

[13] M. Nofar, M.-C. Heuzey, P. J. Carreau, and M. R. Kamal, “Nanoparticle Interactions and Molecular Relaxation in PLA/PBAT/Nanoclay Blends,” *Exp. Results*, vol. 1, p. e47, Oct. 2020, doi: 10.1017/exp.2020.54.

[14] M. Nofar, M.-C. Heuzey, P. J. Carreau, and M. R. Kamal, “Effects of nanoclay and its localization on the morphology stabilization of PLA/PBAT blends under shear flow,” *Polymer (Guildf).*, vol. 98, pp. 353–364, Aug. 2016, doi: 10.1016/j.polymer.2016.06.044.

[15] S. Adrar, A. Habi, A. Ajji, and Y. Grohens, “Synergistic effects in epoxy functionalized graphene and modified organo-montmorillonite PLA/PBAT blends,” *Appl. Clay Sci.*, vol. 157, pp. 65–75, Jun. 2018, doi: 10.1016/j.clay.2018.02.028.

[16] S. Girdthep, N. Komrapit, R. Molloy, S. Lumyong, W. Punyodom, and P. Worajittiphon, “Effect of plate-like particles on properties of poly(lactic acid)/poly(butylene adipate-co-terephthalate) blend: A comparative study between modified montmorillonite and graphene nanoplatelets,” *Compos. Sci. Technol.*, vol. 119, pp. 115–123, Nov. 2015, doi: 10.1016/j.compscitech.2015.10.005.

[17] M. S. Garg and D. Srivastava, “Effect of glycidyl methacrylate (GMA) content on thermal and mechanical properties of ternary blend systems based on cardanol-based vinyl ester resin, styrene and glycidyl methacrylate,” *Prog. Org. Coatings*, vol. 77, no. 7, pp. 1208–1220, Jul. 2014, doi: 10.1016/j.porgcoat.2014.03.029.

[18] S. W. Ko, M. K. Hong, B. J. Park, R. K. Gupta, H. J. Choi, and S. N. Bhattacharya, “Morphological and rheological characterization of multi-walled carbon nanotube/PLA/PBAT blend nanocomposites,” *Polym. Bull.*, vol. 63, no. 1, pp. 125–134, Jul. 2009, doi: 10.1007/s00289-009-0072-9.

[19] J. Urquijo, N. Aranburu, S. Dagréou, G. Guerrica-Echevarría, and J. I. Eguiazábal, “CNT-induced morphology and its effect on properties in PLA/PBAT-based nanocomposites,” *Eur. Polym. J.*, vol. 93, pp. 545–555, Aug. 2017, doi: 10.1016/j.eurpolymj.2017.06.035.

[20] E. Jalali Dil, M. Arjmand, I. Otero Navas, U. Sundararaj, and B. D. Favis, “Interface Bridging of Multiwalled Carbon Nanotubes in Polylactic Acid/Poly(butylene adipate- co -terephthalate): Morphology, Rheology, and Electrical Conductivity,” *Macromolecules*, vol. 53, no. 22, pp. 10267–10277, Nov. 2020, doi: 10.1021/acs.macromol.0c01525.

[21] E. Jalali Dil and B. D. Favis, “Localization of micro- and nano-silica particles in heterophase poly(lactic acid)/poly(butylene adipate-co-terephthalate) blends,” *Polymer (Guildf).*, vol. 76, pp. 295–306, Oct. 2015, doi: 10.1016/j.polymer.2015.08.046.

[22] M. Mohammadi, M.-C. Heuzey, P. J. Carreau, and A. Taguet, “Morphological and Rheological Properties of PLA, PBAT, and PLA/PBAT Blend Nanocomposites Containing CNCs,” *Nanomaterials*, vol. 11, no. 4, p. 857, Mar. 2021, doi: 10.3390/nano11040857.

[23] D. S. Sarul *et al.*, “Preparation and characterization of PLA/PBAT/CNC blend nanocomposites,” *Colloid Polym. Sci.*, vol. 299, no. 6, pp. 987–998, Jun. 2021, doi: 10.1007/s00396-021-04822-9.

[24] F. Fenouillot, P. Cassagnau, and J.-C. Majesté, “Uneven distribution of nanoparticles in immiscible fluids: Morphology development in polymer blends,” *Polymer (Guildf).*, vol. 50, no. 6, pp. 1333–1350, Mar. 2009, doi: 10.1016/j.polymer.2008.12.029.

[25] J. Huitric, J. Ville, P. Médéric, M. Moan, and T. Aubry, “Rheological, morphological and structural properties of PE/PA/nanoclay ternary blends: Effect of clay weight fraction,” *J. Rheol. (N. Y. N. Y).*, vol. 53, no. 5, pp. 1101–1119, Sep. 2009, doi: 10.1122/1.3153551.

[26] M. Bailly and M. Kontopoulou, “Preparation and characterization of thermoplastic olefin/nanosilica composites using a silane-grafted polypropylene matrix,” *Polymer (Guildf).*, vol. 50, no. 11, pp. 2472–2480, May 2009, doi: 10.1016/j.polymer.2009.03.034.

[27] J. S. Hong, H. Namkung, K. H. Ahn, S. J. Lee, and C. Kim, “The role of organically modified layered silicate in the breakup and coalescence of droplets in PBT/PE blends,” *Polymer (Guildf).*, vol. 47, no. 11, pp. 3967–3975, May 2006, doi: 10.1016/j.polymer.2006.03.077.

[28] V. Heshmati, M. R. Kamal, and B. D. Favis, “Cellulose nanocrystal in poly(lactic acid)/polyamide11 blends: Preparation, morphology and co-continuity,” *Eur. Polym. J.*, vol. 98, pp. 11–20, 2018, doi: 10.1016/j.eurpolymj.2017.10.027.

[29] G. Filippone, N. T. Dintcheva, F. P. La Mantia, and D. Acierno, “Using organoclay to promote morphology refinement and co-continuity in high-density polyethylene/polyamide 6 blends – Effect of filler content and polymer matrix composition,” *Polymer (Guildf).*, vol. 51, no. 17, pp. 3956–3965, Aug. 2010, doi: 10.1016/j.polymer.2010.06.044.

[30] G. Filippone, N. T. Dintcheva, D. Acierno, and F. P. La Mantia, “The role of organoclay in promoting co-continuous morphology in high-density poly(ethylene)/poly(amide) 6 blends,” *Polymer (Guildf).*, vol. 49, no. 5, pp. 1312–1322, Mar. 2008, doi: 10.1016/j.polymer.2008.01.045.

[31] A. Nuzzo, E. Bilotti, T. Peijs, D. Acierno, and G. Filippone, “Nanoparticle-induced co-continuity in immiscible polymer blends - A comparative study on bio-based PLA-PA11 blends filled with organoclay, sepiolite, and carbon nanotubes,” *Polymer (Guildf).*, vol. 55, no. 19, pp. 4908–4919, Sep. 2014, doi: 10.1016/j.polymer.2014.07.036.

[32] G. Wu, B. Li, and J. Jiang, “Carbon black self-networking induced co-continuity of immiscible polymer blends,” *Polymer (Guildf).*, vol. 51, no. 9, pp. 2077–2083, Apr. 2010, doi: 10.1016/j.polymer.2010.03.007.

[33] L. Elias, F. Fenouillot, J. C. Majesté, G. Martin, and P. Cassagnau, “Migration of nanosilica particles in polymer blends,” *J. Polym. Sci. Part B Polym. Phys.*, vol. 46, no. 18, pp. 1976–1983, Sep. 2008, doi: 10.1002/polb.21534.

[34] A. C. Baudouin, J. Devaux, and C. Bailly, “Localization of carbon nanotubes at the interface in blends of polyamide and ethylene-acrylate copolymer,” *Polymer (Guildf).*, vol. 51, no. 6, pp. 1341–1354, Mar. 2010, doi: 10.1016/j.polymer.2010.01.050.

[35] L. Elias, F. Fenouillot, J. C. Majeste, and P. Cassagnau, “Morphology and rheology of immiscible polymer blends filled with silica nanoparticles,” *Polymer (Guildf).*, vol. 48, no. 20, pp. 6029–6040, Sep. 2007, doi: 10.1016/j.polymer.2007.07.061.

[36] L. Elias, F. Fenouillot, J. C. Majesté, P. Alcouffe, and P. Cassagnau, “Immiscible polymer blends stabilized with nano-silica particles: Rheology and effective interfacial tension,” *Polymer (Guildf).*, vol. 49, no. 20, pp. 4378–4385, Sep. 2008, doi: 10.1016/j.polymer.2008.07.018.

[37] R. Salehiyan, Y. Yoo, W. J. Choi, and K. Hyun, “Characterization of Morphologies of Compatibilized Polypropylene/Polystyrene Blends with Nanoparticles via Nonlinear Rheological Properties from FT-Rheology,” *Macromolecules*, vol. 47, no. 12, pp. 4066–4076, Jun. 2014, doi: 10.1021/ma500700e.

[38] Z. Shakouri, H. Nazockdast, and H. Sadeghi Ghari, “Effect of the geometry of cellulose nanocrystals on morphology and mechanical performance of dynamically vulcanized PLA/PU blend,” *Cellulose*, vol. 27, no. 1, pp. 215–231, Jan. 2020, doi: 10.1007/s10570-019-02775-5.

[39] M. Shahlari and S. Lee, “Mechanical and morphological properties of poly(butylene

adipate-co-terephthalate) and poly(lactic acid) blended with organically modified silicate layers," *Polym. Eng. Sci.*, vol. 52, no. 7, pp. 1420–1428, Jul. 2012, doi: 10.1002/pen.23082.

[40] D. Wu *et al.*, "Selective Localization of Nanofillers: Effect on Morphology and Crystallization of PLA/PCL Blends," *Macromol. Chem. Phys.*, vol. 212, no. 6, pp. 613–626, Mar. 2011, doi: 10.1002/macp.201000579.

[41] M. R. Aghjeh, V. Asadi, P. Mehdijabbar, H. A. Khonakdar, and S. H. Jafari, "Application of linear rheology in determination of nanoclay localization in PLA/EVA/Clay nanocomposites: Correlation with microstructure and thermal properties," *Compos. Part B Eng.*, vol. 86, pp. 273–284, Feb. 2016, doi: 10.1016/j.compositesb.2015.09.064.

[42] X. Zhao, H. Wang, Z. Fu, and Y. Li, "Enhanced Interfacial Adhesion by Reactive Carbon Nanotubes: New Route to High-Performance Immiscible Polymer Blend Nanocomposites with Simultaneously Enhanced Toughness, Tensile Strength, and Electrical Conductivity," *ACS Appl. Mater. Interfaces*, vol. 10, no. 10, pp. 8411–8416, Mar. 2018, doi: 10.1021/acsami.8b01704.

[43] Z. Shakouri and H. Nazockdast, "Microstructural development and mechanical performance of PLA/TPU blends containing geometrically different cellulose nanocrystals," *Cellulose*, vol. 25, no. 12, pp. 7167–7188, Dec. 2018, doi: 10.1007/s10570-018-2061-3.

[44] D. Bagheriasl, P. J. Carreau, B. Riedl, C. Dubois, and W. Y. Hamad, "Shear rheology of polylactide (PLA)–cellulose nanocrystal (CNC) nanocomposites," *Cellulose*, vol. 23, no. 3, pp. 1885–1897, 2016, doi: 10.1007/s10570-016-0914-1.

[45] W. Y. Hamad and T. Q. Hu, "Structure-process-yield interrelations in nanocrystalline cellulose extraction," *Can. J. Chem. Eng.*, vol. 88, no. 3, pp. 392–402, Jun. 2010, doi: 10.1002/cjce.20298.

[46] J. Ambrosio-Martín, M. J. Fabra, A. Lopez-Rubio, and J. M. Lagaron, "Melt polycondensation to improve the dispersion of bacterial cellulose into polylactide via melt compounding: enhanced barrier and mechanical properties," *Cellulose*, vol. 22, no. 2, pp. 1201–1226, Apr. 2015, doi: 10.1007/s10570-014-0523-9.

[47] R. Herrera, L. Franco, A. Rodríguez-Galán, and J. Puiggalí, "Characterization and degradation behavior of poly(butylene adipate- *co* -terephthalate)s," *J. Polym. Sci. Part A*

Polym. Chem., vol. 40, no. 23, pp. 4141–4157, Dec. 2002, doi: 10.1002/pola.10501.

[48] V. Heshmati, M. R. Kamal, and B. D. Favis, "Tuning the localization of finely dispersed cellulose nanocrystal in poly (lactic acid)/bio-polyamide11 blends," *J. Polym. Sci. Part B Polym. Phys.*, vol. 56, no. 7, pp. 576–587, 2018, doi: 10.1002/polb.24563.

[49] P. Pötschke and D. R. Paul, "Formation of Co-continuous Structures in Melt-Mixed Immiscible Polymer Blends," *J. Macromol. Sci. Part C Polym. Rev.*, vol. 43, no. 1, pp. 87–141, Jan. 2003, doi: 10.1081/MC-120018022.

[50] M. Nofar, A. Maani, H. Sojoudi, M. C. Heuzey, and P. J. Carreau, "Interfacial and rheological properties of PLA/PBAT and PLA/PBSA blends and their morphological stability under shear flow," *J. Rheol. (N. Y. N. Y).*, vol. 59, no. 2, pp. 317–333, Mar. 2015, doi: 10.1122/1.4905714.

[51] E. Jalali Dil, P. J. Carreau, and B. D. Favis, "Morphology, miscibility and continuity development in poly(lactic acid)/poly(butylene adipate-co-terephthalate) blends," *Polymer (Guildf).*, vol. 68, pp. 202–212, Jun. 2015, doi: 10.1016/j.polymer.2015.05.012.

[52] S. Y. Gu, K. Zhang, J. Ren, and H. Zhan, "Melt rheology of polylactide/poly(butylene adipate-co-terephthalate) blends," *Carbohydr. Polym.*, vol. 74, no. 1, pp. 79–85, Oct. 2008, doi: 10.1016/j.carbpol.2008.01.017.

[53] D. Graebling, R. Muller, and J. F. Palierne, "Linear Viscoelastic Behavior of Some Incompatible Polymer Blends in the Melt. Interpretation of Data with a Model of Emulsion of Viscoelastic Liquids," *Macromolecules*, vol. 26, no. 2, pp. 320–329, 1993, doi: 10.1021/ma00054a011.

[54] S. Vandebril, J. Vermant, and P. Moldenaers, "Efficiently suppressing coalescence in polymer blends using nanoparticles: Role of interfacial rheology," *Soft Matter*, vol. 6, no. 14, pp. 3353–3362, Jul. 2010, doi: 10.1039/b927299b.

[55] G. Filippone, G. Romeo, and D. Acierno, "Role of interface rheology in altering the onset of co-continuity in nanoparticle-filled polymer blends," *Macromol. Mater. Eng.*, vol. 296, no. 7, pp. 658–665, Jul. 2011, doi: 10.1002/mame.201000343.

[56] L. Bai, J. W. Fruehwirth, X. Cheng, and C. W. Macosko, "Dynamics and rheology of nonpolar bijels," *Soft Matter*, vol. 11, no. 26, pp. 5282–5293, Jun. 2015, doi:

10.1039/C5SM00994D.

[57] R. Altobelli, M. Salzano De Luna, and G. Filippone, “Interfacial crowding of nanoplatelets in co-continuous polymer blends: Assembly, elasticity and structure of the interfacial nanoparticle network,” *Soft Matter*, vol. 13, no. 37, pp. 6465–6473, Sep. 2017, doi: 10.1039/c7sm01119a.

[58] M. Mohammadi, C. Bruel, M. C. Heuzey, and P. J. Carreau, “CNC dispersion in PLA and PBAT using two solvents: morphological and rheological properties,” *Cellulose*, vol. 27, no. 17, pp. 9877–9892, Sep. 2020, doi: 10.1007/s10570-020-03460-8.

[59] R. Al-Itry, “Blends based on poly(lactic acid) : structure/rheology/processing relationship,” 2012.

[60] E. Vatansever *et al.*, “Development of CNC-reinforced PBAT nanocomposites with reduced percolation threshold: a comparative study on the preparation method,” *J. Mater. Sci.*, vol. 55, no. 32, pp. 15523–15537, Nov. 2020, doi: 10.1007/s10853-020-05105-4.

[61] E. Vatansever, D. Arslan, D. S. Sarul, Y. Kahraman, and M. Nofar, “Effects of molecular weight and crystallizability of polylactide on the cellulose nanocrystal dispersion quality in their nanocomposites,” *Int. J. Biol. Macromol.*, vol. 154, pp. 276–290, Mar. 2020, doi: 10.1016/j.ijbiomac.2020.03.115.

[62] P. Pötschke and D. R. Paul, “Formation of Co-continuous Structures in Melt-Mixed Immiscible Polymer Blends,” *J. Macromol. Sci. Part C Polym. Rev.*, vol. 43, no. 1, pp. 87–141, Jan. 2003, doi: 10.1081/MC-120018022.

[63] “HSPiP FAQ | Hansen Solubility Parameters.” https://www.hansen-solubility.com/HSPiP/faq.php (accessed Feb. 23, 2021).

CHAPTER 9 GENERAL DISCUSSION

How can we disperse a hydrophilic filler in hydrophobic polymer matrices? It is the main question that we can answer from different perspectives. First, it is possible to use different compatibilizers and see their effects on improving the dispersion of fillers in polymer matrices. Second, functionalizing filler particles is another way to enhance interactions between the filler and polymer matrices. Third, the reduction of the surface energy of the filler and polymers could lead to lower filler agglomeration. All these methods are costly, time-consuming, and difficult to control. However, we were investigating an appropriate method to disperse CNCs without any modifications or use of compatibilizers. When CNCs are introduced into hydrophobic matrices, they form agglomerates as large as a few tens of microns due to their high hydrophilicity and strong inter-particle interactions. Therefore, a simple solution casting method with a polar solvent (i.e. N,N- dimethylformamide (DMF) or dimethyl sulfoxide (DMSO)) could favor a good dispersion of hydrophilic CNCs within hydrophobic matrices without the need of CNC modification or use of any compatibilizer. The quality of the CNC dispersion and the interfacial tension between polymer components and CNCs will determine how well these polymer nanocomposites and their blend nanocomposites perform. As CNCs are strongly hydrophilic, their dispersion and distribution in polymer matrices such as polypropylene (PP), polyethylene (PE), polystyrene (PS), polyethylene terephthalate (PET), and biodegradable polymers including PLA and PBAT are a challenging issue. So, in this study, we started our work by using a proper method that can help us to disperse unmodified CNCs and dissolve polymers. In most previous works, researchers [96], [110], [112], [123], [218], [276] used common solvents based on experience or trying different solvents to choose the best one among them. So, we used a thermodynamics approach based on the Hansen solubility parameter (HSP) theory in order to optimize the dispersion of the CNCs and the dissolution of the polymers. This can be extended to all polymers, nanomaterials, and solvents to select the proper solvents to achieve a desirable goal [62], [277]. Therefore, using this method of selecting the best solvents for dispersion (dimethyl sulfoxide (DMSO)) and dissolution (tetrahydrofuran (THF)) of CNCs and PLA or PBAT, respectively, we achieved strongly interconnected networks of CNCs in the matrices of PLA and PBAT. It is worth mentioning that in the HSP theory we used the polar sphere of CNC, and the solvents were selected based on that.

So, using the non-polar sphere of CNC could introduce other solvents which can provide better dispersion of CNCs. Although compared to N, N-dimethylformamide (DMF), DMSO is less toxic, the problem with utilizing DMSO to disperse CNCs is that it has a high boiling temperature, around 190 °C, and its evaporation needs a longer time and higher temperatures. Therefore, it could lead to the degradation of PLA or PBAT. Although using this method resulted in the best one in dispersing CNCs, traces of remaining solvents paused an obstacle of using the melt blending mostly due to severe re-agglomeration of CNCs which leads to degradation of polymers in the presence of remaining solvent. So, preparing neat nanocomposites from solution casting using DMF was used as a solvent for both dispersing and dissolution of CNCs and polymers.

It is worth mentioning, to the best of our knowledge, only a few studies were conducted on PLA/PBAT/CNC blend nanocomposites [218], [278] and none of them presented a comprehensive investigation on the morphological, rheological, thermal, and mechanical properties. Although direct melt mixing is a practical way of preparing polymer blend nanocomposites, agglomeration of CNCs makes an obstacle to achieving highly dispersive CNCs in the blend nanocomposites. Therefore, a solution casting followed by melt mixing was adopted in this work with localizing the CNCs in each or both phases during the solution casting step, and the final localization was investigated after melt mixing. What is more, the idea of preparing the blend nanocomposites directly from solution casting and melt blending after drying was tried in this work. However, it was not possible to control the localization of CNCs during the solution casting step and the result was less interesting compared to the reported results in this work. As we used a solution casting step, the problem of remaining solvent still existed. Through different localizations, we could obtain a finer morphology in the blend nanocomposites and each mixing strategy resulted in different localization of CNCs in the blend nanocomposites. Interfacial localization of CNCs was achieved in this work.

Although the stabilization of the morphology and rheological properties should be presented in every work conducted in polymer blend nanocomposites, previous studies conducted in polymer blends using CNCs did not pay attention to this issue [110], [112], [218]. The coalescence during processing (i.e., under shear flow) could be minimized by controlling the CNCs localization in the PLA/PBAT blends. As a result, it acts as a morphological stabilizer as well as a droplet coalescence barrier. This is accomplished while the localized CNCs help in enhancing rheological and mechanical properties.

CHAPTER 10 CONCLUSIONS, ORIGINAL CONTRIBUTIONS AND RECOMMENDATIONS

10.1 Conclusions

In this Ph.D. work, performance characteristics of semicrystalline (sc) and amorphous (a) PLAs from the morphological, rheological, thermal, and mechanical points of view were improved through blending with PBAT and incorporation of unmodified CNCs. All the samples were prepared through the combination of solution casting and melt mixing.

A novel solution casting method was developed based on the two solvents (one to disperse CNCs and the other to dissolute polymers) according to the thermodynamics analysis using the Hansen solubility parameter (HSP) theory. DMSO and THF were selected as the best solvents for the dispersion and dissolution of CNCs and polymers, respectively. Microscopic (AFM) and rheological (SAOS) analyses confirmed the effectiveness of this method compared to solution casting using a single solvent, DMF. Although this novel method was resulted in highly disperse CNCs in the matrix of PLAs and PBAT, the decreases by one or two orders of the complex viscosity of solvent cast neat nanocomposites (scPLA/CNC and aPLA/CNC, respectively) confirmed the effect of remaining solvents in the samples, which also impeded the ultimate improvement of the mechanical and thermal properties. These effects on the mechanical and thermal properties of neat nanocomposites were further investigated and compared the results obtained with the one solvent (DMF) method. Overall, we could improve the mechanical and thermal properties of PLAs and PBAT without the need for compatibilization or modification of the CNCs. Also, in terms of remaining solvents, the one solvent method was more effective than the two solvents one for achieving improved mechanical and thermal properties, but a higher quality of the dispersion and distribution of CNCs when using two solvents resulted in better rheological properties.

The effect of melt mixing on the morphological and rheological properties of solvent cast PLAs/CNC was investigated. Rheological SAOS properties were shown to considerably decrease due to the agglomeration of the CNCs. As there was no CNC surface treatment or compatibilizer, the dispersed cellulose nanocrystals dramatically tended to re-agglomerate mostly due to the low chemical affinity of CNCs with both polymers and possible desulfation of CNCs at higher temperatures during the melting process.

To achieve ultimate improvements in performance characteristics of PLAs, PBAT was blended with PLAs to remedy the brittleness characteristics of PLAs and with the addition of CNCs. The reduction of the elastic modulus as a result of the incorporation of PBAT was compensated by the addition of CNCs, which made a balance between stiffness and toughness in the blend nanocomposites of PLA/PBAT/CNC. Also, we studied the effect of localization of CNCs in PLAs/PBAT blends through solution casting and melt mixing on the rheology, morphology, mechanical, and thermal properties as well as on their morphological stability under shear flow. We aim at obtaining properties comparable to commercial polyethylene terephthalate (PET) and polypropylene (PP). Figure 10.1 displays the elastic modulus and elongation at break for some conventional and biodegradable plastics. As can be seen, PET and PP have modulus of elasticity of around 2800 and 1800 MPa, respectively, and elongation at break of around 200 and 580 %, respectively [275].

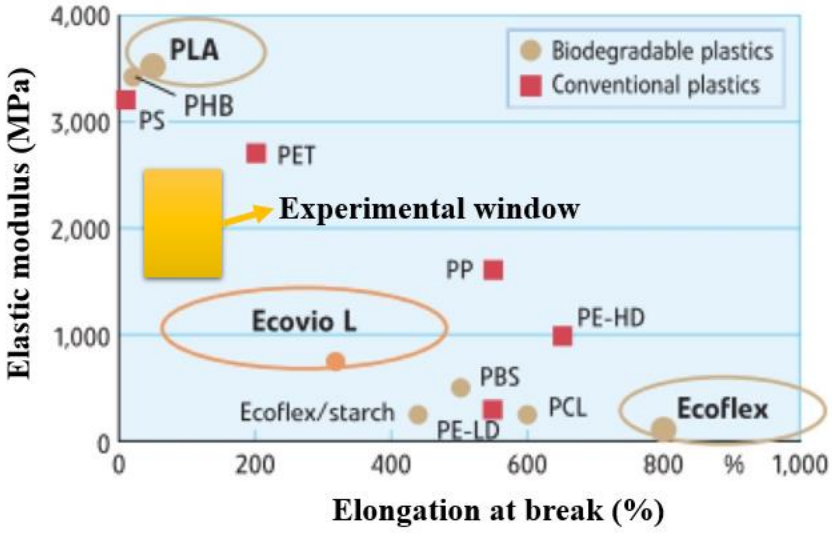

Figure 10.1 Modulus versus elongation at break for biodegradable and commodity polymers [275]. The rectangular box shows the experimental window for the results obtained in this work for the elastic (Young) modulus and elongation at break of scPLA/PBAT and aPLA/PBAT blends with localized CNCs at the interface. The minimum and maximum width and length of the box correspond to the values of scPLA/PBAT/CNC and aPLA/PBAT/CNC, respectively (see Table 8.2).

When CNCs were dispersed in PLAs or both phases during the solution casting step, they tended to be localized at the PLAs/PBAT interface. Interestingly, interfacial localization of CNCs in the

scPLA/PBAT/CNC blend nanocomposites converted the matrix-droplet morphology to a co-continuous one. By this interfacial localization in scPLA/PBAT/CNC, we could obtain values up to 2562 MPa and 150 % in the elastic (Young) modulus and elongation at break, respectively (experimental window in Figure 10.1). These values are very close to the reported values for conventional PET. However, in term of elongation at break we are still far from the value of 580 % for conventional PP. The improvements were less for aPLA/PBAT blend nanocomposites due to the less effectiveness of CNC localization at the interface and lower interfacial adhesion between aPLA and PBAT phases.

10.2 Original contributions

Several major scientific contributions of this work are listed below.

In the first part of this research study:

- We investigated the solvent casting (using a new protocol based on two solvents) of pristine CNC reinforced nanocomposites of PLA (2 different grades; amorphous and semicrystalline) and PBAT in order to produce fully biodegradable materials. Thermodynamics analysis relying on the Hansen solubility parameter (HSP) theory identified dimethyl sulfoxide/tetrahydrofuran (DMSO/THF) as an optimal solvent system to incorporate CNCs into PLA and PBAT because it can both dissolve the PLA or PBAT and distribute the CNCs. It led us to propose a methodology that relies on two solvents: one to disperse the CNCs, and the other to dissolve the polymers.
- Microscopy and rheological analysis employed to investigate the effectiveness of this approach and the results showed the effectiveness of solvent selection on the dispersion and distribution of CNCs, which in turn contributes to the formation of 3D networks in the aPLA, scPLA, and PBAT matrices and the presence of a 3D network was investigated by the determination of the apparent yield stress by fitting a modified Herschel-Bulkely model to the SAOS data.
- The percolation threshold concentration calculated using an empirical power-law model fitted to the rheological data of the storage modulus as a function of CNC concentration presented the lowest percolation threshold in all matrices compared to the literature data.

- The effect of solvent traces on the rheological and morphological properties of aPLA, scPLA, and PBAT showed that a small amount of solvents significantly decreased the complex viscosity of scPLA and aPLA. This was not observed in PBAT, and it is suggested that the crystallization of PBAT at the drying temperature (70 °C) may have favored the removal of solvent traces in PBAT.
- The effect of two solvents method is compared with one solvent method (using DMF for dispersing and dissolving CNCs and polymers, respectively) to see the effect of small traces of solvents left in the samples on mechanical and thermal properties of PLA/CNC and PBAT/CNC nanocomposites. As a result of CNC network formation, the mechanical and thermal properties of PLA and PBAT improved without the need for compatibilization or modification of the CNCs. Also, in one solvent method, the mechanical properties particularly elongation at break and impact properties improved compared to the two solvents method.
- The modified Takayangi model predictions compared with the storage modulus data of the nanocomposites and an acceptable agreement observed for both the glassy and rubbery regions. Other classical models such as the modified Halpin-Tsai and Halpin-Kardos models underpredict the experimental data for a well-dispersed system because they do not consider the percolated network and are mainly based on the aspect ratio of the filler and the storage moduli of the components.

In PLA/PBAT polymer blends containing 1 wt% CNCs:

- The localization of CNCs in PLA (amorphous and semicrystalline)/PBAT blends through solution casting followed by melt mixing methods and its effect on the rheology and morphology as well as on their morphological stability under shear were studied in detail.
- The effect of melt mixing investigated on rheology and morphological properties of highly dispersed CNCs of solution cast PLA-based nanocomposites and the results showed a significant re-agglomeration of the CNCs due to the possible desulfation of CNCs at higher temperatures and the intrinsic poor affinity of CNCs (regarding HSP parameters) with the polymer matrices.
- It was shown that the incorporation of CNCs in most cases decreased the PBAT droplet size and created a finer morphology in the blend nanocomposites and initial localization of

CNCs in the matrix (PLA) or both phases in the solution casting step, resulted in interfacial localization of CNCs after melt mixing. On the other hand, when CNCs were introduced to the blend nanocomposites through the PBAT phase, a matrix-droplet morphology was obtained.

- The relationship between stress growth and coalescence was investigated and it showed that the localization of CNCs at the interface minimized the coalescence during processing. This suggests that the cellulose nanocrystals in the dispersed phase or at the interface between the two polymers served as a droplet coalescence barrier during shearing. Therefore, droplet morphology of PLA/PBAT blends were stabilized in the presence of CNCs under shear flows.
- The influence of interfacial assembly of CNCs investigated on the thermal, and mechanical properties of PLA/PBAT blends. Localization of CNCs at the interface converted the matrix-droplet morphology to a co-continuous one in scPLA/PBAT blend nanocomposites. An improvement observed in elongation at break and impact properties of scPLA/PBAT blend nanocomposites. These improvements were less effective in the case of aPLA/PBAT blend nanocomposites. For the thermal properties, CNCs acted as a nucleation agent and improved the crystallization temperature and degree of crystallinity of PLA and PBAT.

10.3 Recommendations

The following recommendations for future work are suggested based on the findings of this dissertation:

- Optimize the drying process of samples prepared by solution casting to eliminate traces of solvents like DMSO with a high boiling point.
- Extend the application of the protocol based on two solvents to other polymers to investigate the effectiveness of the proposed method in this thesis.
- It would be interesting to modified CNCs using a solvent-free esterification method as a green technology and incorporate that in the PLA/PBAT blend through melt processing. The morphology, rheological and mechanical properties of modified CNCs nanocomposites should then be compared to unmodified systems.

- The automotive and packaging industries could benefit from polymer-CNC nanocomposites. As a result, polymer-CNC films and injection-molded products can be made via film blowing and injection molding, respectively, and their physical and mechanical qualities can be determined.
- It would be interesting to investigate other nanoparticles with different geometry in the blend of PLA/PBAT.
- Studying the localization of CNCs in the blend of PLA/PBAT using a twin-screw extruder would be interesting since it would reveal the effect of the processing method.
- As the two solvent method is more effective than one solvent method for the dispersion and distribution of CNCs, it would be interesting to prepare blends of PLA/PBAT containing CNCs using the two solvent method and compare the outcome with the results of this thesis. However, we would need to prepare the blend nanocomposite without a trace of solvent like DMSO.
- In this study, the matrix-droplet morphology was considered for the effect of CNCs localization on morphological, rheological, mechanical, and thermal properties. It would be interesting to use co-continuous morphology (50/50 wt% of PLA/PBAT blend) and investigated the effect of CNCs localization on mentioned properties.
- It would be interesting to investigate the migration mechanism of CNCs in the blends of PLA/PBAT.
- It would be interesting to investigate the extensional viscosity of PLA/CNC nanocomposites, and PLA/PBAT/CNC blend nanocomposites to examine the potential of PLA based nanocomposites to perform in industrial processes such as injection molding and blow molding.

REFERENCES

[1] T. P. Haider, C. Völker, J. Kramm, K. Landfester, and F. R. Wurm, "Plastics of the Future? The Impact of Biodegradable Polymers on the Environment and on Society," *Angewandte Chemie - International Edition*, vol. 58, no. 1. Wiley-VCH Verlag, pp. 50–62, Jan. 02, 2019, doi: 10.1002/anie.201805766.

[2] O. World, E. Day, and N. Communications, "The future of plastic editorial," *Nat. Commun.*, vol. 9, no. 1, pp. 1–3, 2018, doi: 10.1038/s41467-018-04565-2.

[3] M. Rujnić-Sokele and A. Pilipović, "Challenges and opportunities of biodegradable plastics: A mini review," *Waste Manag. Res.*, vol. 35, no. 2, pp. 132–140, 2017, doi: 10.1177/0734242X16683272.

[4] I. Vroman and L. Tighzert, "Biodegradable polymers," *Materials*, vol. 2, no. 2. pp. 307–344, 2009, doi: 10.3390/ma2020307.

[5] M. Nofar, D. Sacligil, P. J. Carreau, M. R. Kamal, and M.-C. Heuzey, "Poly (lactic acid) blends: Processing, properties and applications," *Int. J. Biol. Macromol.*, vol. 125, pp. 307–360, Mar. 2019, doi: 10.1016/j.ijbiomac.2018.12.002.

[6] R. Auras, B. Harte, and S. Selke, "An Overview of Polylactides as Packaging Materials," *Macromol. Biosci.*, vol. 4, no. 9, pp. 835–864, Sep. 2004, doi: 10.1002/mabi.200400043.

[7] F. V. Ferreira, L. S. Cividanes, R. F. Gouveia, and L. M. F. Lona, "An overview on properties and applications of poly(butylene adipate- co -terephthalate)-PBAT based composites," *Polym. Eng. Sci.*, vol. 59, no. s2, pp. E7–E15, Mar. 2019, doi: 10.1002/pen.24770.

[8] J. Jian, Z. Xiangbin, and H. Xianbo, "An overview on synthesis, properties and applications of poly(butylene-adipate-co-terephthalate)–PBAT," *Adv. Ind. Eng. Polym. Res.*, vol. 3, no. 1, pp. 19–26, Jan. 2020, doi: 10.1016/j.aiepr.2020.01.001.

[9] K. Hamad, M. Kaseem, Y. G. Ko, and F. Deri, "Biodegradable polymer blends and composites: An overview," *Polymer Science - Series A*, vol. 56, no. 6. Maik Nauka-Interperiodica Publishing, pp. 812–829, Nov. 06, 2014, doi: 10.1134/S0965545X14060054.

[10] J. Li, L. Lai, L. Wu, S. J. Severtson, and W. J. Wang, "Enhancement of Water Vapor Barrier

Properties of Biodegradable Poly(butylene adipate- co-terephthalate) Films with Highly Oriented Organomontmorillonite," *ACS Sustain. Chem. Eng.*, vol. 6, no. 5, pp. 6654–6662, May 2018, doi: 10.1021/acssuschemeng.8b00430.

[11] M. Mohammadi, C. Bruel, M. C. Heuzey, and P. J. Carreau, "CNC dispersion in PLA and PBAT using two solvents: morphological and rheological properties," *Cellulose*, vol. 27, no. 17, pp. 9877–9892, Sep. 2020, doi: 10.1007/s10570-020-03460-8.

[12] I. F. Pinheiro, F. V. Ferreira, G. F. Alves, A. Rodolfo, A. R. Morales, and L. H. I. Mei, "Biodegradable PBAT-Based Nanocomposites Reinforced with Functionalized Cellulose Nanocrystals from Pseudobombax munguba: Rheological, Thermal, Mechanical and Biodegradability Properties," *J. Polym. Environ.*, vol. 27, no. 4, pp. 757–766, Apr. 2019, doi: 10.1007/s10924-019-01389-z.

[13] E. Vatansever, D. Arslan, and M. Nofar, "Polylactide cellulose-based nanocomposites.," *Int. J. Biol. Macromol.*, vol. 137, pp. 912–938, Sep. 2019, doi: 10.1016/j.ijbiomac.2019.06.205.

[14] C. L. Morelli, M. N. Belgacem, M. C. Branciforti, M. C. B. Salon, J. Bras, and R. E. S. Bretas, "Nanocomposites of PBAT and cellulose nanocrystals modified by in situ polymerization and melt extrusion," *Polym. Eng. Sci.*, vol. 56, no. 12, pp. 1339–1348, 2016, doi: 10.1002/pen.24367.

[15] I. F. Pinheiro, F. V. Ferreira, G. F. Alves, A. Rodolfo, A. R. Morales, and L. H. I. Mei, "Biodegradable PBAT-Based Nanocomposites Reinforced with Functionalized Cellulose Nanocrystals from Pseudobombax munguba: Rheological, Thermal, Mechanical and Biodegradability Properties," *J. Polym. Environ.*, vol. 27, no. 4, pp. 757–766, Apr. 2019, doi: 10.1007/s10924-019-01389-z.

[16] I. F. Pinheiro *et al.*, "Mechanical, rheological and degradation properties of PBAT nanocomposites reinforced by functionalized cellulose nanocrystals," *Eur. Polym. J.*, vol. 97, pp. 356–365, 2017, doi: 10.1016/j.eurpolymj.2017.10.026.

[17] H. Kargarzadeh *et al.*, "Advances in cellulose nanomaterials," *Cellulose*, vol. 25, no. 4, pp. 2151–2189, Apr. 2018, doi: 10.1007/s10570-018-1723-5.

[18] M. Nofar, R. Salehiyan, and S. S. Ray, "Influence of nanoparticles and their selective localization on the structure and properties of polylactide-based blend nanocomposites,"

Compos. Part B Eng., vol. 215, p. 108845, Jun. 2021, doi: 10.1016/j.compositesb.2021.108845.

[19] M. Nofar, A. Maani, H. Sojoudi, M. C. Heuzey, and P. J. Carreau, "Interfacial and rheological properties of PLA/PBAT and PLA/PBSA blends and their morphological stability under shear flow," *J. Rheol. (N. Y. N. Y).*, vol. 59, no. 2, pp. 317–333, Mar. 2015, doi: 10.1122/1.4905714.

[20] G. E. Luckachan and C. K. S. Pillai, "Biodegradable Polymers- A Review on Recent Trends and Emerging Perspectives," *J. Polym. Environ.*, vol. 19, no. 3, pp. 637–676, Sep. 2011, doi: 10.1007/s10924-011-0317-1.

[21] "Market – European Bioplastics e.V." https://www.european-bioplastics.org/market/ (accessed May 01, 2021).

[22] K. Van De Velde and P. Kiekens, "Biopolymers: Overview of several properties and consequences on their applications," *Polym. Test.*, vol. 21, no. 4, pp. 433–442, Jan. 2002, doi: 10.1016/S0142-9418(01)00107-6.

[23] T. Casalini, F. Rossi, A. Castrovinci, and G. Perale, "A Perspective on Polylactic Acid-Based Polymers Use for Nanoparticles Synthesis and Applications," *Frontiers in Bioengineering and Biotechnology*, vol. 7. Frontiers Media S.A., p. 259, Oct. 11, 2019, doi: 10.3389/fbioe.2019.00259.

[24] V. Nagarajan, A. K. Mohanty, and M. Misra, "Perspective on Polylactic Acid (PLA) based Sustainable Materials for Durable Applications: Focus on Toughness and Heat Resistance," *ACS Sustainable Chemistry and Engineering*, vol. 4, no. 6. American Chemical Society, pp. 2899–2916, Jun. 06, 2016, doi: 10.1021/acssuschemeng.6b00321.

[25] K. S. Anderson, K. M. Schreck, and M. A. Hillmyer, "Polymer Reviews Toughening Polylactide Toughening Polylactide," *Polym. Rev.*, vol. 48, no. 1, pp. 85–108, 2008, doi: 10.1080/15583720701834216.

[26] R. M. Rasal, A. V. Janorkar, and D. E. Hirt, "Poly(lactic acid) modifications," *Prog. Polym. Sci.*, vol. 35, no. 3, pp. 338–356, Mar. 2010, doi: 10.1016/j.progpolymsci.2009.12.003.

[27] B. V. M. Rodrigues, A. S. Silva, G. F. S. Melo, L. M. R. Vasconscellos, F. R. Marciano, and A. O. Lobo, "Influence of low contents of superhydrophilic MWCNT on the properties and

cell viability of electrospun poly (butylene adipate-co-terephthalate) fibers," *Mater. Sci. Eng. C*, vol. 59, pp. 782–791, Feb. 2016, doi: 10.1016/j.msec.2015.10.075.

[28] M. K. Thakur, V. K. Thakur, R. K. Gupta, and A. Pappu, "Synthesis and Applications of Biodegradable Soy Based Graft Copolymers: A Review," *ACS Sustainable Chemistry and Engineering*, vol. 4, no. 1. American Chemical Society, pp. 1–17, Jan. 04, 2016, doi: 10.1021/acssuschemeng.5b01327.

[29] R. V. Nonato, P. E. Mantelatto, and C. E. V. Rossell, "Integrated production of biodegradable plastic, sugar and ethanol," *Appl. Microbiol. Biotechnol.*, vol. 57, no. 1–2, pp. 1–5, 2001, doi: 10.1007/s002530100732.

[30] X. Zhang, P. Ma, and Y. Zhang, "Structure and properties of surface-acetylated cellulose nanocrystal/poly(butylene adipate-co-terephthalate) composites," *Polym. Bull.*, vol. 73, no. 7, pp. 2073–2085, Jul. 2016, doi: 10.1007/s00289-015-1594-y.

[31] S. Mondal, "Review on Nanocellulose Polymer Nanocomposites," *Polym. Plast. Technol. Eng.*, vol. 57, no. 13, pp. 1377–1391, Sep. 2018, doi: 10.1080/03602559.2017.1381253.

[32] D. Klemm, D. Schumann, F. Kramer, N. Heßler, D. Koth, and B. Sultanova, "Nanocellulose Materials - Different Cellulose, Different Functionality," *Macromol. Symp.*, vol. 280, no. 1, pp. 60–71, Jun. 2009, doi: 10.1002/masy.200950608.

[33] A. Junior de Menezes, G. Siqueira, A. A. S. Curvelo, and A. Dufresne, "Extrusion and characterization of functionalized cellulose whiskers reinforced polyethylene nanocomposites," *Polymer (Guildf).*, vol. 50, no. 19, pp. 4552–4563, Sep. 2009, doi: 10.1016/j.polymer.2009.07.038.

[34] H. Kargarzadeh *et al.*, "Recent developments in nanocellulose-based biodegradable polymers, thermoplastic polymers, and porous nanocomposites," *Prog. Polym. Sci.*, 2018, doi: 10.1016/j.progpolymsci.2018.07.008.

[35] H. Kargarzadeh *et al.*, "Recent developments on nanocellulose reinforced polymer nanocomposites: A review," *Polymer*. 2017, doi: 10.1016/j.polymer.2017.09.043.

[36] M. Salajková, L. A. Berglund, and Q. Zhou, "Hydrophobic cellulose nanocrystals modified with quaternary ammonium salts," *J. Mater. Chem.*, vol. 22, no. 37, pp. 19798–19805, Aug. 2012, doi: 10.1039/C2JM34355J.

[37] * Suzelei Montanari, Mohamad Roumani, and Laurent Heux, and M. R. Vignon*, "Topochemistry of Carboxylated Cellulose Nanocrystals Resulting from TEMPO-Mediated Oxidation," *Macromolecules*, vol. 38, no. 5, pp. 1665–1671, Mar. 2005, doi: 10.1021/MA048396C.

[38] H. P. S. A. Khalil *et al.*, "Nanocellulose-Based Polymer Nanocomposite: Isolation, Characterization and Applications," in *Nanocellulose Polymer Nanocomposites*, vol. 9781118871904, Hoboken, NJ, USA: John Wiley & Sons, Inc., 2014, pp. 273–309.

[39] L. K. Kian, N. Saba, M. Jawaid, and M. T. H. Sultan, "A review on processing techniques of bast fibers nanocellulose and its polylactic acid (PLA) nanocomposites," *Int. J. Biol. Macromol.*, vol. 121, pp. 1314–1328, Jan. 2019, doi: 10.1016/j.ijbiomac.2018.09.040.

[40] P. MS, H. Y, Z. JO, P. JJ, and R. OJ, "Nanofiber composites of polyvinyl alcohol and cellulose nanocrystals: manufacture and characterization," *Biomacromolecules*, vol. 11, no. 3, pp. 674–681, Mar. 2010, doi: 10.1021/BM901254N.

[41] W. Zhang *et al.*, "High performance poly (vinyl alcohol)/cellulose nanocrystals nanocomposites manufactured by injection molding," *Cellul. 2013 211*, vol. 21, no. 1, pp. 485–494, Dec. 2013, doi: 10.1007/S10570-013-0141-Y.

[42] T. Abitbol, T. Johnstone, T. M. Quinn, and D. G. Gray, "Reinforcement with cellulose nanocrystals of poly(vinyl alcohol) hydrogels prepared by cyclic freezing and thawing," *Soft Matter*, vol. 7, no. 6, pp. 2373–2379, Mar. 2011, doi: 10.1039/C0SM01172J.

[43] W.-I. Park, M. Kang, H.-S. Kim, and H.-J. Jin, "Electrospinning of Poly(ethylene oxide) with Bacterial Cellulose Whiskers," *Macromol. Symp.*, vol. 249–250, no. 1, pp. 289–294, Apr. 2007, doi: 10.1002/MASY.200750347.

[44] G. Siqueira, H. Abdillahi, J. Bras, and A. Dufresne, "High reinforcing capability cellulose nanocrystals extracted from Syngonanthus nitens (Capim Dourado)," *Cellul. 2009 172*, vol. 17, no. 2, pp. 289–298, Nov. 2009, doi: 10.1007/S10570-009-9384-Z.

[45] J. Tang, J. Sisler, N. Grishkewich, and K. C. Tam, "Functionalization of cellulose nanocrystals for advanced applications," *J. Colloid Interface Sci.*, vol. 494, pp. 397–409, May 2017, doi: 10.1016/j.jcis.2017.01.077.

[46] A. Chakrabarty and Y. Teramoto, "Recent Advances in Nanocellulose Composites with

Polymers: A Guide for Choosing Partners and How to Incorporate Them," *Polymers (Basel).*, vol. 10, no. 5, p. 517, May 2018, doi: 10.3390/polym10050517.

[47] E. Lizundia *et al.*, "PLLA-grafted cellulose nanocrystals: Role of the CNC content and grafting on the PLA bionanocomposite film properties," *Carbohydr. Polym.*, vol. 142, pp. 105–113, May 2016, doi: 10.1016/j.carbpol.2016.01.041.

[48] A. L. Goffin *et al.*, "Poly(ε-caprolactone) based nanocomposites reinforced by surface-grafted cellulose nanowhiskers via extrusion processing: Morphology, rheology, and thermo-mechanical properties," *Polymer (Guildf).*, vol. 52, no. 7, pp. 1532–1538, Mar. 2011, doi: 10.1016/J.POLYMER.2011.02.004.

[49] A.-L. Goffin *et al.*, "From Interfacial Ring-Opening Polymerization to Melt Processing of Cellulose Nanowhisker-Filled Polylactide-Based Nanocomposites," *Biomacromolecules*, vol. 12, no. 7, pp. 2456–2465, Jul. 2011, doi: 10.1021/BM200581H.

[50] G. Morandi, L. Heath, and W. Thielemans, "Cellulose Nanocrystals Grafted with Polystyrene Chains through Surface-Initiated Atom Transfer Radical Polymerization (SI-ATRP)," *Langmuir*, vol. 25, no. 14, pp. 8280–8286, Jul. 2009, doi: 10.1021/LA900452A.

[51] M. Hasani, E. D. Cranston, G. Westman, and D. G. Gray, "Cationic surface functionalization of cellulose nanocrystals," *Soft Matter*, vol. 4, no. 11, pp. 2238–2244, Nov. 2008, doi: 10.1039/B806789A.

[52] B. Couturaud, A. Baldo, A. Mas, and J. J. Robin, "Improvement of the interfacial compatibility between cellulose and poly(l-lactide) films by plasma-induced grafting of l-lactide: The evaluation of the adhesive properties using a peel test," *J. Colloid Interface Sci.*, vol. 448, pp. 427–436, Jun. 2015, doi: 10.1016/J.JCIS.2015.02.035.

[53] M. N. Belgacem, P. Bataille, and S. Sapieha, "Effect of corona modification on the mechanical properties of polypropylene/cellulose composites," *J. Appl. Polym. Sci.*, vol. 53, no. 4, pp. 379–385, Jul. 1994, doi: 10.1002/APP.1994.070530401.

[54] T.-W. Kim, S.-Y. Lee, S.-J. Chun, G.-H. Doh, and K.-H. Paik, "Effect of silane coupling on the fundamental properties of wood flour reinforced polypropylene composites:," *http://dx.doi.org/10.1177/0021998310385589*, vol. 45, no. 15, pp. 1595–1605, Nov. 2010, doi: 10.1177/0021998310385589.

[55] H. Kargarzadeh, R. M. Sheltami, I. Ahmad, I. Abdullah, and A. Dufresne, “Cellulose nanocrystal: A promising toughening agent for unsaturated polyester nanocomposite,” *Polymer (Guildf).*, vol. 56, pp. 346–357, Jan. 2015, doi: 10.1016/J.POLYMER.2014.11.054.

[56] L. J. Lee, C. Zeng, X. Cao, X. Han, J. Shen, and G. Xu, “Polymer nanocomposite foams,” *Compos. Sci. Technol.*, vol. 65, no. 15-16 SPEC. ISS., pp. 2344–2363, Dec. 2005, doi: 10.1016/j.compscitech.2005.06.016.

[57] A. Dufresne, “Cellulose nanomaterials as green nanoreinforcements for polymer nanocomposites,” *Philos. Trans. R. Soc. A*, vol. 376, no. 2112, p. 20170040, Feb. 2018, doi: 10.1098/rsta.2017.0040.

[58] D. Bagheriasl and P. J. Carreau, “Polymer–Cellulose Nanocrystal (CNC) Nanocomposites,” in *Processing of Polymer Nanocomposites*, München: Carl Hanser Verlag GmbH & Co. KG, 2019, pp. 371–393.

[59] A. Dufresne, “Cellulose nanomaterial reinforced polymer nanocomposites,” *Curr. Opin. Colloid Interface Sci.*, vol. 29, pp. 1–8, May 2017, doi: 10.1016/j.cocis.2017.01.004.

[60] F. V. Ferreira *et al.*, “Influence of carbon nanotube concentration and sonication temperature on mechanical properties of HDPE/CNT nanocomposites,” *Fullerenes Nanotub. Carbon Nanostructures*, vol. 25, no. 9, pp. 531–539, Sep. 2017, doi: 10.1080/1536383X.2017.1359553.

[61] “2019, Nofar, Polylactide cellulose-based nanocomposites _ Elsevier Enhanced Reader.”

[62] C. Bruel, Q. Beuguel, J. R. Tavares, P. J. Carreau, and M.-C. Heuzey, “The apparent structural hydrophobicity of cellulose nanocrystals,” *J. Sci. Technol. For. Prod. Process.*, vol. 7, no. 4, pp. 13–23, 2018.

[63] F. V. Ferreira *et al.*, “How do cellulose nanocrystals affect the overall properties of biodegradable polymer nanocomposites: A comprehensive review,” *Eur. Polym. J.*, vol. 108, pp. 274–285, Nov. 2018, doi: 10.1016/j.eurpolymj.2018.08.045.

[64] H. Kargarzadeh *et al.*, “Advances in cellulose nanomaterials,” *Cellulose*, vol. 25, no. 4. Springer Netherlands, pp. 2151–2189, Apr. 01, 2018, doi: 10.1007/s10570-018-1723-5.

[65] G. Siqueira, J. Bras, and A. Dufresne, “Cellulosic Bionanocomposites: A Review of

Preparation, Properties and Applications," *Polymers (Basel).*, vol. 2, no. 4, pp. 728–765, Dec. 2010, doi: 10.3390/polym2040728.

[66] H. M. Ng, L. T. Sin, S. T. Bee, T. T. Tee, and A. R. Rahmat, "Review of Nanocellulose Polymer Composite Characteristics and Challenges," *Polymer - Plastics Technology and Engineering*, vol. 56, no. 7. Taylor and Francis Inc., pp. 687–731, May 03, 2017, doi: 10.1080/03602559.2016.1233277.

[67] C. Miao and W. Y. Hamad, "Cellulose reinforced polymer composites and nanocomposites: a critical review," *Cellulose*, vol. 20, no. 5, pp. 2221–2262, Oct. 2013, doi: 10.1007/s10570-013-0007-3.

[68] H. M. Ng, L. T. Sin, S. T. Bee, T. T. Tee, and A. R. Rahmat, "Review of Nanocellulose Polymer Composite Characteristics and Challenges," *Polymer - Plastics Technology and Engineering*, vol. 56, no. 7. Taylor and Francis Inc., pp. 687–731, May 03, 2017, doi: 10.1080/03602559.2016.1233277.

[69] C. Miao and W. Y. Hamad, "Cellulose reinforced polymer composites and nanocomposites: A critical review," *Cellulose*, vol. 20, no. 5. Springer, pp. 2221–2262, Oct. 04, 2013, doi: 10.1007/s10570-013-0007-3.

[70] M. R. Kamal and V. Khoshkava, "Effect of cellulose nanocrystals (CNC) on rheological and mechanical properties and crystallization behavior of PLA/CNC nanocomposites," *Carbohydr. Polym.*, vol. 123, pp. 105–114, 2015, doi: 10.1016/j.carbpol.2015.01.012.

[71] X. Zhang, P. Ma, and Y. Zhang, "Structure and properties of surface-acetylated cellulose nanocrystal/poly(butylene adipate-co-terephthalate) composites," *Polym. Bull.*, vol. 73, no. 7, pp. 2073–2085, Jul. 2016, doi: 10.1007/s00289-015-1594-y.

[72] C. L. Morelli, N. Belgacem, R. E. S. Bretas, and J. Bras, "Melt extruded nanocomposites of polybutylene adipate- co -terephthalate (PBAT) with phenylbutyl isocyanate modified cellulose nanocrystals," *J. Appl. Polym. Sci.*, vol. 133, no. 34, Sep. 2016, doi: 10.1002/app.43678.

[73] D. Bondeson and K. Oksman, "Dispersion and characteristics of surfactant modified cellulose whiskers nanocomposites," *Compos. Interfaces*, vol. 14, no. 7–9, pp. 617–630, Sep. 2007, doi: 10.1163/156855407782106519.

[74] A. L. Goffin *et al.*, “From interfacial ring-opening polymerization to melt processing of cellulose nanowhisker-filled polylactide-based nanocomposites,” *Biomacromolecules*, vol. 12, no. 7, pp. 2456–2465, Jul. 2011, doi: 10.1021/bm200581h.

[75] J. M. Raquez *et al.*, “Surface-modification of cellulose nanowhiskers and their use as nanoreinforcers into polylactide: A sustainably-integrated approach,” *Compos. Sci. Technol.*, vol. 72, no. 5, pp. 544–549, Mar. 2012, doi: 10.1016/j.compscitech.2011.11.017.

[76] E. Robles, I. Urruzola, J. Labidi, and L. Serrano, “Surface-modified nano-cellulose as reinforcement in poly(lactic acid) to conform new composites,” *Ind. Crops Prod.*, vol. 71, pp. 44–53, Sep. 2015, doi: 10.1016/j.indcrop.2015.03.075.

[77] S. Spinella *et al.*, “Polylactide/cellulose nanocrystal nanocomposites: Efficient routes for nanofiber modification and effects of nanofiber chemistry on PLA reinforcement,” *Polymer (Guildf).*, vol. 65, pp. 9–17, May 2015, doi: 10.1016/j.polymer.2015.02.048.

[78] P. Dhar, S. M. Bhasney, A. Kumar, and V. Katiyar, “Acid functionalized cellulose nanocrystals and its effect on mechanical, thermal, crystallization and surfaces properties of poly (lactic acid) bionanocomposites films: A comprehensive study,” *Polymer (Guildf).*, vol. 101, pp. 75–92, Sep. 2016, doi: 10.1016/j.polymer.2016.08.028.

[79] S. Spinella, C. Samuel, J. M. Raquez, S. A. McCallum, R. Gross, and P. Dubois, “Green and Efficient Synthesis of Dispersible Cellulose Nanocrystals in Biobased Polyesters for Engineering Applications,” *ACS Sustain. Chem. Eng.*, vol. 4, no. 5, pp. 2517–2527, May 2016, doi: 10.1021/acssuschemeng.5b01611.

[80] D. Bagheriasl, F. Safdari, P. J. Carreau, C. Dubois, and B. Riedl, “Development of cellulose nanocrystal-reinforced polylactide: A comparative study on different preparation methods,” *Polym. Compos.*, vol. 40, pp. E342–E349, Jan. 2019, doi: 10.1002/pc.24676.

[81] V. Khoshkava and M. R. Kamal, “Effect of surface energy on dispersion and mechanical properties of polymer/nanocrystalline cellulose nanocomposites,” *Biomacromolecules*, vol. 14, no. 9, pp. 3155–3163, 2013, doi: 10.1021/bm400784j.

[82] A. Arias, M.-C. Heuzey, M. A. Huneault, G. Ausias, and A. Bendahou, “Enhanced dispersion of cellulose nanocrystals in melt-processed polylactide-based nanocomposites,” *Cellulose*, vol. 22, no. 1, pp. 483–498, Feb. 2015, doi: 10.1007/s10570-014-0476-z.

[83] M. R. Kamal and V. Khoshkava, “Effect of cellulose nanocrystals (CNC) on rheological and mechanical properties and crystallization behavior of PLA/CNC nanocomposites,” *Carbohydr. Polym.*, 2015, doi: 10.1016/j.carbpol.2015.01.012.

[84] C. Miao and W. Y. Hamad, “In-situ polymerized cellulose nanocrystals (CNC)—poly(L-lactide) (PLLA) nanomaterials and applications in nanocomposite processing,” *Carbohydr. Polym.*, vol. 153, pp. 549–558, Nov. 2016, doi: 10.1016/j.carbpol.2016.08.012.

[85] A. Gupta, W. Simmons, G. T. Schueneman, D. Hylton, and E. A. Mintz, “Rheological and thermo-mechanical properties of poly(lactic acid)/lignin-coated cellulose nanocrystal composites,” *ACS Sustain. Chem. Eng.*, vol. 5, no. 2, pp. 1711–1720, Feb. 2017, doi: 10.1021/acssuschemeng.6b02458.

[86] J. Trifol *et al.*, “A comparison of partially acetylated nanocellulose, nanocrystalline cellulose, and nanoclay as fillers for high-performance polylactide nanocomposites,” *J. Appl. Polym. Sci.*, vol. 133, no. 14, Apr. 2016, doi: 10.1002/app.43257.

[87] S. Qian and K. Sheng, “PLA toughened by bamboo cellulose nanowhiskers: Role of silane compatibilization on the PLA bionanocomposite properties,” *Compos. Sci. Technol.*, vol. 148, pp. 59–69, Aug. 2017, doi: 10.1016/j.compscitech.2017.05.020.

[88] M. K. M. Haafiz, A. Hassan, Z. Zakaria, I. M. Inuwa, M. S. Islam, and M. Jawaid, “Properties of polylactic acid composites reinforced with oil palm biomass microcrystalline cellulose,” *Carbohydr. Polym.*, vol. 98, no. 1, pp. 139–145, 2013, doi: 10.1016/j.carbpol.2013.05.069.

[89] N. Pal, P. Dubey, P. Gopinath, and K. Pal, “Combined effect of cellulose nanocrystal and reduced graphene oxide into poly-lactic acid matrix nanocomposite as a scaffold and its anti-bacterial activity,” *Int. J. Biol. Macromol.*, vol. 95, pp. 94–105, Feb. 2017, doi: 10.1016/j.ijbiomac.2016.11.041.

[90] T. Mukherjee *et al.*, “Chemically imaging the interaction of acetylated nanocrystalline cellulose (NCC) with a polylactic acid (PLA) polymer matrix,” *Cellulose*, vol. 24, no. 4, pp. 1717–1729, Apr. 2017, doi: 10.1007/s10570-017-1217-x.

[91] M. D. Sanchez-Garcia and J. M. Lagaron, “On the use of plant cellulose nanowhiskers to enhance the barrier properties of polylactic acid,” *Cellulose*, vol. 17, no. 5, pp. 987–1004,

Jul. 2010, doi: 10.1007/s10570-010-9430-x.

[92] K. M. Z. Hossain *et al.*, "Physico-chemical and mechanical properties of nanocomposites prepared using cellulose nanowhiskers and poly(lactic acid)," *J. Mater. Sci.*, vol. 47, no. 6, pp. 2675–2686, Mar. 2012, doi: 10.1007/s10853-011-6093-4.

[93] T. Mukherjee, M. Sani, N. Kao, R. K. Gupta, N. Quazi, and S. Bhattacharya, "Improved dispersion of cellulose microcrystals in polylactic acid (PLA) based composites applying surface acetylation," *Chem. Eng. Sci.*, vol. 101, pp. 655–662, Sep. 2013, doi: 10.1016/j.ces.2013.07.032.

[94] N. Pal, P. Dubey, P. Gopinath, and K. Pal, "Combined effect of cellulose nanocrystal and reduced graphene oxide into poly-lactic acid matrix nanocomposite as a scaffold and its anti-bacterial activity," *Int. J. Biol. Macromol.*, vol. 95, pp. 94–105, Feb. 2017, doi: 10.1016/j.ijbiomac.2016.11.041.

[95] D. Bagheriasl, P. J. Carreau, B. Riedl, and C. Dubois, "Enhanced properties of polylactide by incorporating cellulose nanocrystals," *Polym. Compos.*, vol. 39, no. 8, pp. 2685–2694, 2018, doi: 10.1002/pc.24259.

[96] E. Vatansever, D. Arslan, D. S. Sarul, Y. Kahraman, and M. Nofar, "Effects of molecular weight and crystallizability of polylactide on the cellulose nanocrystal dispersion quality in their nanocomposites," *Int. J. Biol. Macromol.*, vol. 154, pp. 276–290, Mar. 2020, doi: 10.1016/j.ijbiomac.2020.03.115.

[97] C. L. Morelli, M. N. Belgacem, M. C. Branciforti, R. E. S. Bretas, A. Crisci, and J. Bras, "Supramolecular aromatic interactions to enhance biodegradable film properties through incorporation of functionalized cellulose nanocrystals," *Compos. Part A Appl. Sci. Manuf.*, vol. 83, pp. 80–88, Apr. 2016, doi: 10.1016/j.compositesa.2015.10.038.

[98] F. V. Ferreira *et al.*, "Cellulose nanocrystal-based poly(butylene adipate-co-terephthalate) nanocomposites covered with antimicrobial silver thin films," *Polym. Eng. Sci.*, vol. 59, no. s2, pp. E356–E365, Feb. 2019, doi: 10.1002/pen.25066.

[99] K. Oksman, A. P. Mathew, D. Bondeson, and I. Kvien, "Manufacturing process of cellulose whiskers/polylactic acid nanocomposites," *Compos. Sci. Technol.*, vol. 66, no. 15, pp. 2776–2784, Dec. 2006, doi: 10.1016/j.compscitech.2006.03.002.

[100] A. P. Mathew, A. Chakraborty, K. Oksman, and M. Sain, “The structure and mechanical properties of cellulose nanocomposites prepared by twin screw extrusion,” in *ACS Symposium Series*, 2006, vol. 938, pp. 114–131, doi: 10.1021/bk-2006-0938.ch009.

[101] N. Herrera, A. M. Salaberria, A. P. Mathew, and K. Oksman, “Plasticized polylactic acid nanocomposite films with cellulose and chitin nanocrystals prepared using extrusion and compression molding with two cooling rates: Effects on mechanical, thermal and optical properties,” *Compos. Part A Appl. Sci. Manuf.*, vol. 83, pp. 89–97, Apr. 2016, doi: 10.1016/j.compositesa.2015.05.024.

[102] E. Sullivan, R. Moon, and K. Kalaitzidou, “Processing and Characterization of Cellulose Nanocrystals/Polylactic Acid Nanocomposite Films,” *Materials (Basel).*, vol. 8, no. 12, pp. 8106–8116, Dec. 2015, doi: 10.3390/ma8125447.

[103] D. Bondeson and K. Oksman, “Polylactic acid/cellulose whisker nanocomposites modified by polyvinyl alcohol,” *Compos. Part A Appl. Sci. Manuf.*, vol. 38, no. 12, pp. 2486–2492, Dec. 2007, doi: 10.1016/j.compositesa.2007.08.001.

[104] D. Bagheriasl, F. Safdari, P. J. Carreau, C. Dubois, and B. Riedl, “Development of Cellulose Nanocrystal-Reinforced Polylactide: A Comparative Study on Different Preparation Methods,” *Wiley Online Libr.*, vol. 40, pp. E342–E349, Jan. 2017, doi: 10.1002/pc.24676.

[105] E. Vatansever *et al.*, “Development of CNC-reinforced PBAT nanocomposites with reduced percolation threshold: a comparative study on the preparation method,” *J. Mater. Sci.*, vol. 55, no. 32, pp. 15523–15537, Nov. 2020, doi: 10.1007/s10853-020-05105-4.

[106] D. Arslan *et al.*, “Effect of preparation method on the properties of polylactide/cellulose nanocrystal nanocomposites,” *Polym. Compos.*, 2020, doi: 10.1002/pc.25701.

[107] J. Shojaeiarani, D. S. Bajwa, and N. M. Stark, “Spin-coating: A new approach for improving dispersion of cellulose nanocrystals and mechanical properties of poly (lactic acid) composites,” *Carbohydr. Polym.*, vol. 190, pp. 139–147, Jun. 2018, doi: 10.1016/j.carbpol.2018.02.069.

[108] A. L. Goffin *et al.*, “From interfacial ring-opening polymerization to melt processing of cellulose nanowhisker-filled polylactide-based nanocomposites,” *Biomacromolecules*, vol. 12, no. 7, pp. 2456–2465, Jul. 2011, doi: 10.1021/bm200581h.

[109] N. Bitinis *et al.*, “Poly(lactic acid)/natural rubber/cellulose nanocrystal bionanocomposites Part I. Processing and morphology,” *Carbohydr. Polym.*, vol. 96, no. 2, pp. 611–620, Jul. 2013, doi: 10.1016/j.carbpol.2013.02.068.

[110] V. Heshmati, M. R. Kamal, and B. D. Favis, “Cellulose nanocrystal in poly(lactic acid)/polyamide11 blends: Preparation, morphology and co-continuity,” *Eur. Polym. J.*, vol. 98, pp. 11–20, 2018, doi: 10.1016/j.eurpolymj.2017.10.027.

[111] V. Heshmati, M. R. Kamal, and B. D. Favis, “Tuning the localization of finely dispersed cellulose nanocrystal in poly (lactic acid)/bio-polyamide11 blends,” *J. Polym. Sci. Part B Polym. Phys.*, vol. 56, no. 7, pp. 576–587, 2018, doi: 10.1002/polb.24563.

[112] V. Heshmati, M. R. Kamal, and B. D. Favis, “Tuning the localization of finely dispersed cellulose nanocrystal in poly (lactic acid)/bio-polyamide11 blends,” *J. Polym. Sci. Part B Polym. Phys.*, vol. 56, no. 7, pp. 576–587, Apr. 2018, doi: 10.1002/polb.24563.

[113] M. Mariano *et al.*, “Preparation of Cellulose Nanocrystal-Reinforced Poly(lactic acid) Nanocomposites through Noncovalent Modification with PLLA-Based Surfactants,” *ACS Omega*, vol. 2, no. 6, pp. 2678–2688, Jun. 2017, doi: 10.1021/acsomega.7b00387.

[114] M. Pracella, M. M. U. Haque, and D. Puglia, “Morphology and properties tuning of PLA/cellulose nanocrystals bio-nanocomposites by means of reactive functionalization and blending with PVAc,” *Polymer (Guildf).*, vol. 55, no. 16, pp. 3720–3728, Aug. 2014, doi: 10.1016/j.polymer.2014.06.071.

[115] Y. C. Ching *et al.*, “Rheological properties of cellulose nanocrystal-embedded polymer composites: a review,” *Cellulose*, vol. 23, no. 2. Springer Netherlands, pp. 1011–1030, Apr. 01, 2016, doi: 10.1007/s10570-016-0868-3.

[116] V. Khoshkava and M. R. Kamal, “Effect of cellulose nanocrystals (CNC) particle morphology on dispersion and rheological and mechanical properties of polypropylene/CNC nanocomposites,” *ACS Appl. Mater. Interfaces*, 2014, doi: 10.1021/am500577e.

[117] X. Zhang, P. Ma, and Y. Zhang, “Structure and properties of surface-acetylated cellulose nanocrystal/poly(butylene adipate-co-terephthalate) composites,” *Polym. Bull.*, vol. 73, no. 7, pp. 2073–2085, Jul. 2016, doi: 10.1007/s00289-015-1594-y.

[118] I. F. Pinheiro *et al.*, “Mechanical, rheological and degradation properties of PBAT nanocomposites reinforced by functionalized cellulose nanocrystals,” *Eur. Polym. J.*, vol. 97, pp. 356–365, Dec. 2017, doi: 10.1016/j.eurpolymj.2017.10.026.

[119] K. Ben Azouz, E. C. Ramires, W. Van Den Fonteyne, N. El Kissi, and A. Dufresne, “Simple method for the melt extrusion of a cellulose nanocrystal reinforced hydrophobic polymer,” *ACS Macro Lett.*, vol. 1, no. 1, pp. 236–240, 2012, doi: 10.1021/mz2001737.

[120] M. Wang and R. J. Hill, “Anomalous bulk viscosity of polymer-nanocomposite melts,” *Soft Matter*, vol. 5, no. 20, pp. 3940–3953, Oct. 2009, doi: 10.1039/b905686f.

[121] J. T. Kalathi, G. S. Grest, and S. K. Kumar, “Universal viscosity behavior of polymer nanocomposites,” *Phys. Rev. Lett.*, vol. 109, no. 19, Nov. 2012, doi: 10.1103/PhysRevLett.109.198301.

[122] M. Mariano, N. El Kissi, and A. Dufresne, “Structural Reorganization of CNC in Injection-Molded CNC/PBAT Materials under Thermal Annealing,” *Langmuir*, vol. 32, no. 39, pp. 10093–10103, Oct. 2016, doi: 10.1021/acs.langmuir.6b03220.

[123] D. Bagheriasl, P. J. Carreau, B. Riedl, C. Dubois, and W. Y. Hamad, “Shear rheology of polylactide (PLA)–cellulose nanocrystal (CNC) nanocomposites,” *Cellulose*, vol. 23, no. 3, pp. 1885–1897, 2016, doi: 10.1007/s10570-016-0914-1.

[124] A. Gupta, W. Simmons, G. T. Schueneman, D. Hylton, and E. A. Mintz, “Rheological and thermo-mechanical properties of poly(lactic acid)/lignin-coated cellulose nanocrystal composites,” *ACS Sustain. Chem. Eng.*, vol. 5, no. 2, 2017, doi: 10.1021/acssuschemeng.6b02458.

[125] C. Xu, J. Chen, D. Wu, Y. Chen, Q. Lv, and M. Wang, “Polylactide/acetylated nanocrystalline cellulose composites prepared by a continuous route: A phase interface-property relation study,” *Carbohydr. Polym.*, vol. 146, pp. 58–66, Aug. 2016, doi: 10.1016/j.carbpol.2016.03.058.

[126] C. Zhang, M. R. Salick, T. M. Cordie, T. Ellingham, Y. Dan, and L. S. Turng, “Incorporation of poly(ethylene glycol) grafted cellulose nanocrystals in poly(lactic acid) electrospun nanocomposite fibers as potential scaffolds for bone tissue engineering,” *Mater. Sci. Eng. C*, vol. 49, pp. 463–471, Apr. 2015, doi: 10.1016/j.msec.2015.01.024.

[127] G. Hu, C. Zhao, S. Zhang, M. Yang, and Z. Wang, “Low percolation thresholds of electrical conductivity and rheology in poly(ethylene terephthalate) through the networks of multi-walled carbon nanotubes,” *Polymer (Guildf).*, vol. 47, no. 1, pp. 480–488, Jan. 2006, doi: 10.1016/j.polymer.2005.11.028.

[128] F. Du, R. C. Scogna, W. Zhou, S. Brand, J. E. Fischer, and K. I. Winey, “Nanotube networks in polymer nanocomposites: Rheology and electrical conductivity,” *Macromolecules*, vol. 37, no. 24, pp. 9048–9055, Nov. 2004, doi: 10.1021/ma049164g.

[129] S. Abbasi, P. J. Carreau, A. Derdouri, and M. Moan, “Rheological properties and percolation in suspensions of multiwalled carbon nanotubes in polycarbonate,” *Rheol. Acta*, vol. 48, no. 9, pp. 943–959, Jul. 2009, doi: 10.1007/s00397-009-0375-7.

[130] A. Gupta, W. Simmons, G. T. Schueneman, D. Hylton, and E. A. Mintz, “Rheological and thermo-mechanical properties of poly(lactic acid)/lignin-coated cellulose nanocrystal composites,” *ACS Sustain. Chem. Eng.*, vol. 5, no. 2, pp. 1711–1720, Feb. 2017, doi: 10.1021/acssuschemeng.6b02458.

[131] F. Ferreira, W. Franceschi, … B. M.-A. S., and undefined 2017, “Dodecylamine functionalization of carbon nanotubes to improve dispersion, thermal and mechanical properties of polyethylene based nanocomposites,” *Elsevier*, Accessed: May 04, 2021. [Online]. Available: https://www.sciencedirect.com/science/article/pii/S0169433217307584?casa_token=TkmNWrWRkwsAAAAA:AX_ASeXpOSLhrDcnbi8_b8oY1izHPhEk9xw10szIX9IgdpbfBjVHFwKJ8ElFFslxMOPUhtqvfdEf.

[132] J. Chen, N. Li, Y. Wei, B. Han, and W. Yan, “Influence of carbon sources on nitriding process, microstructures and mechanical properties of Si3N4 bonded SiC refractories,” *J. Eur. Ceram. Soc.*, vol. 37, no. 4, pp. 1821–1829, Apr. 2017, doi: 10.1016/j.jeurceramsoc.2016.12.005.

[133] J. Chen, D. Wu, K. C. Tam, K. Pan, and Z. Zheng, “Effect of surface modification of cellulose nanocrystal on nonisothermal crystallization of poly(β-hydroxybutyrate) composites,” *Carbohydr. Polym.*, vol. 157, pp. 1821–1829, Feb. 2017, doi: 10.1016/j.carbpol.2016.11.071.

[134] S. Gårdebjer *et al.*, “Solid-state NMR to quantify surface coverage and chain length of lactic acid modified cellulose nanocrystals, used as fillers in biodegradable composites,” *Compos. Sci. Technol.*, vol. 107, pp. 1–9, Feb. 2015, doi: 10.1016/j.compscitech.2014.11.014.

[135] E. Fortunati *et al.*, “Multifunctional bionanocomposite films of poly(lactic acid), cellulose nanocrystals and silver nanoparticles,” *Carbohydr. Polym.*, vol. 87, no. 2, pp. 1596–1605, Jan. 2012, doi: 10.1016/j.carbpol.2011.09.066.

[136] A. Pei, Q. Zhou, and L. A. Berglund, “Functionalized cellulose nanocrystals as biobased nucleation agents in poly(l-lactide) (PLLA) - Crystallization and mechanical property effects,” *Compos. Sci. Technol.*, vol. 70, no. 5, pp. 815–821, May 2010, doi: 10.1016/j.compscitech.2010.01.018.

[137] N. Hameed, Q. Guo, F. H. Tay, and S. G. Kazarian, “Blends of cellulose and poly(3-hydroxybutyrate-co-3-hydroxyvalerate) prepared from the ionic liquid 1-butyl-3-methylimidazolium chloride,” *Carbohydr. Polym.*, vol. 86, no. 1, pp. 94–104, Aug. 2011, doi: 10.1016/j.carbpol.2011.04.016.

[138] E. Espino-Pérez, J. Bras, V. Ducruet, A. Guinault, A. Dufresne, and S. Domenek, “Influence of chemical surface modification of cellulose nanowhiskers on thermal, mechanical, and barrier properties of poly(lactide) based bionanocomposites,” *Eur. Polym. J.*, vol. 49, no. 10, pp. 3144–3154, Oct. 2013, doi: 10.1016/j.eurpolymj.2013.07.017.

[139] J. G. Gwon *et al.*, “Mechanical and thermal properties of toluene diisocyanate-modified cellulose nanocrystal nanocomposites using semi-crystalline poly(lactic acid) as a base matrix,” *RSC Adv.*, vol. 6, no. 77, pp. 73879–73886, Aug. 2016, doi: 10.1039/c6ra10993d.

[140] E. Fortunati *et al.*, “Microstructure and nonisothermal cold crystallization of PLA composites based on silver nanoparticles and nanocrystalline cellulose,” in *Polymer Degradation and Stability*, Oct. 2012, vol. 97, no. 10, pp. 2027–2036, doi: 10.1016/j.polymdegradstab.2012.03.027.

[141] S. Gazzotti *et al.*, “Polylactide/cellulose nanocrystals: The in situ polymerization approach to improved nanocomposites,” *Eur. Polym. J.*, vol. 94, pp. 173–184, Sep. 2017, doi: 10.1016/j.eurpolymj.2017.07.014.

[142] H. Wu, S. Nagarajan, L. Zhou, Y. Duan, and J. Zhang, “Synthesis and characterization of

cellulose nanocrystal-graft-poly(D-lactide) and its nanocomposite with poly(L-lactide)," *Polymer (Guildf).*, vol. 103, pp. 365–375, Oct. 2016, doi: 10.1016/j.polymer.2016.09.070.

[143] M. D. Sanchez-Garcia and J. M. Lagaron, "On the use of plant cellulose nanowhiskers to enhance the barrier properties of polylactic acid," *Cellulose*, vol. 17, no. 5, pp. 987–1004, Jul. 2010, doi: 10.1007/s10570-010-9430-x.

[144] W. Yang, F. Dominici, E. Fortunati, J. M. Kenny, and D. Puglia, "Melt free radical grafting of glycidyl methacrylate (GMA) onto fully biodegradable poly(lactic) acid films: Effect of cellulose nanocrystals and a masterbatch process," *RSC Adv.*, vol. 5, no. 41, pp. 32350–32357, Apr. 2015, doi: 10.1039/c5ra00894h.

[145] E. Lizundia, J. L. Vilas, and L. M. León, "Crystallization, structural relaxation and thermal degradation in Poly(l-lactide)/cellulose nanocrystal renewable nanocomposites," *Carbohydr. Polym.*, vol. 123, pp. 256–265, Jun. 2015, doi: 10.1016/j.carbpol.2015.01.054.

[146] V. P. Martino, R. A. Ruseckaite, and A. Jiménez, "Thermal and mechanical characterization of plasticized poly (L-lactide-co-D,L-lactide) films for food packaging," in *Journal of Thermal Analysis and Calorimetry*, Dec. 2006, vol. 86, no. 3, pp. 707–712, doi: 10.1007/s10973-006-7897-3.

[147] W. A. Ribeiro Neto *et al.*, "Poly (butylene adipate-co-terephthalate)/hydroxyapatite composite structures for bone tissue recovery," *Polym. Degrad. Stab.*, vol. 120, pp. 61–69, Jun. 2015, doi: 10.1016/j.polymdegradstab.2015.06.009.

[148] V. P. Martino, R. A. Ruseckaite, and A. Jiménez, "Thermal and mechanical characterization of plasticized poly (L-lactide-co-D,L-lactide) films for food packaging," in *Journal of Thermal Analysis and Calorimetry*, Dec. 2006, vol. 86, no. 3, pp. 707–712, doi: 10.1007/s10973-006-7897-3.

[149] L. Jiang, E. Morelius, J. Zhang, M. Wolcott, and J. Holbery, "Study of the poly(3-hydroxybutyrate-co-3-hydroxyvalerate)/cellulose nanowhisker composites prepared by solution casting and melt processing," *J. Compos. Mater.*, vol. 42, no. 24, pp. 2629–2645, Dec. 2008, doi: 10.1177/0021998308096327.

[150] J. C. H. Affdl and J. L. Kardos, "The Halpin-Tsai equations: A review," *Polym. Eng. Sci.*, vol. 16, no. 5, pp. 344–352, May 1976, doi: 10.1002/pen.760160512.

[151] Y. Aitomäki and K. Oksman, “Reinforcing efficiency of nanocellulose in polymers,” *React. Funct. Polym.*, vol. 85, pp. 151–156, Dec. 2014, doi: 10.1016/j.reactfunctpolym.2014.08.010.

[152] T. Schilling, M. A. Miller, and P. Van Der Schoot, “Percolation in suspensions of hard nanoparticles: From spheres to needles,” *EPL*, vol. 111, no. 5, p. 56004, Sep. 2015, doi: 10.1209/0295-5075/111/56004.

[153] J. Andersons, E. Spārniņš, and R. Joffe, “Stiffness and strength of flax fiber/polymer matrix composites,” *Polym. Compos.*, vol. 27, no. 2, pp. 221–229, Apr. 2006, doi: 10.1002/pc.20184.

[154] E. Fortunati *et al.*, “Multifunctional bionanocomposite films of poly(lactic acid), cellulose nanocrystals and silver nanoparticles,” *Carbohydr. Polym.*, vol. 87, no. 2, pp. 1596–1605, Jan. 2012, doi: 10.1016/j.carbpol.2011.09.066.

[155] P. J. Flory, *Principles of Polymer Chemistry - - Google Books*. Cornell University Press, Ithaca, 1953.

[156] C. W. Macosko, “Morphology development and control in immiscible polymer blends,” in *Macromolecular Symposia*, 2000, vol. 149, pp. 171–184, doi: 10.1002/1521-3900(200001)149:1<171::AID-MASY171>3.0.CO;2-8.

[157] D. Wei, H. Wang, H. Xiao, A. Zheng, and Y. Yang, “Morphology and mechanical properties of poly(butylene adipate-co-terephthalate)/potato starch blends in the presence of synthesized reactive compatibilizer or modified poly(butylene adipate-co-terephthalate),” *Carbohydr. Polym.*, vol. 123, pp. 275–282, Jun. 2015, doi: 10.1016/j.carbpol.2015.01.058.

[158] U. Sundararaj, C. W. Macosko, A. Nakayama, and T. Inoue, “Milligrams to kilograms: An evaluation of mixers for reactive polymer blending,” *Polym. Eng. Sci.*, vol. 35, no. 1, pp. 100–114, 1995, doi: 10.1002/pen.760350113.

[159] B. D. Favis, “Polymer alloys and blends: Recent advances,” *The Canadian Journal of Chemical Engineering*, vol. 69, no. 3. pp. 619–625, 1991, doi: 10.1002/cjce.5450690303.

[160] S. Wu, *Polymer Interface and Adhesion*. Routledge, 2017.

[161] D. Y. Kwok and A. W. Neumann, “Contact angle measurement and contact angle

interpretation," *Adv. Colloid Interface Sci.*, vol. 81, no. 3, pp. 167–249, Sep. 1999, doi: 10.1016/S0001-8686(98)00087-6.

[162] C. Bruel, S. Queffeulou, T. Darlow, N. Virgilio, J. R. Tavares, and G. S. Patience, "Experimental methods in chemical engineering: Contact angles," *Can. J. Chem. Eng.*, vol. 97, no. 4, pp. 832–842, Apr. 2019, doi: 10.1002/cjce.23408.

[163] D. Y. Kwok, L. K. Cheung, C. B. Park, and A. W. Neumann, "Study on the surface tensions of polymer melts using axisymmetric drop shape analysis," *Polym. Eng. Sci.*, vol. 38, no. 5, pp. 757–764, May 1998, doi: 10.1002/pen.10241.

[164] R. J. Roe, "Surface tension of polymer liquids," *J. Phys. Chem.*, vol. 72, no. 6, pp. 2013–2017, 1968, doi: 10.1021/j100852a025.

[165] N. R. Demarquette and M. R. Kamal, "Interfacial tension in polymer melts. I: An improved pendant drop apparatus," *Polym. Eng. Sci.*, vol. 34, no. 24, pp. 1823–1833, Dec. 1994, doi: 10.1002/pen.760342407.

[166] L. A. Girifalco and R. J. Good, "A theory for the estimation of surface and interfacial energies. I. Derivation and application to interfacial tension," *J. Phys. Chem.*, vol. 61, no. 7, pp. 904–909, 1957, doi: 10.1021/j150553a013.

[167] S. Wu, "Calculation of interfacial tension in polymer systems," *J. Polym. Sci. Part C Polym. Symp.*, vol. 34, no. 1, pp. 19–30, Mar. 2007, doi: 10.1002/polc.5070340105.

[168] J. F. Palierne, "Linear rheology of viscoelastic emulsions with interfacial tension," *Rheol. Acta*, vol. 29, no. 3, pp. 204–214, May 1990, doi: 10.1007/BF01331356.

[169] M. Bousmina and R. Muller, "Linear viscoelasticity in the melt of impact PMMA. Influence of concentration and aggregation of dispersed rubber particles," *J. Rheol. (N. Y. N. Y).*, vol. 37, no. 4, pp. 663–679, Jul. 1993, doi: 10.1122/1.550389.

[170] E. Manias and L. A. Utracki, "Thermodynamics of polymer blends," in *Polymer Blends Handbook*, Springer Netherlands, 2014, pp. 171–289.

[171] S. Shokoohi and A. Arefazar, "A review on ternary immiscible polymer blends: Morphology and effective parameters," *Polymers for Advanced Technologies*, vol. 20, no. 5. pp. 433–447, 2009, doi: 10.1002/pat.1310.

[172] R. Cardinaels and P. Moldenaers, “Morphology Development in Immiscible Polymer Blends,” in *Polymer Morphology*, Hoboken, NJ, USA: John Wiley & Sons, Inc, 2016, pp. 348–373.

[173] C. E. Scott and C. W. Macosko, “Morphology development during the initial stages of polymer-polymer blending,” *Polymer (Guildf).*, vol. 36, no. 3, pp. 461–470, Jan. 1995, doi: 10.1016/0032-3861(95)91554-K.

[174] U. Sundararaj, “Phase morphology development in polymer blends: Processing and experimental aspects,” in *Micro- and Nanostructured Multiphase Polymer Blend Systems: Phase Morphology and Interfaces*, CRC Press, 2005, pp. 133–164.

[175] U. Sundararaj, C. W. Macosko, R. J. Rolando, and H. T. Chan, “Morphology development in polymer blends,” *Polym. Eng. Sci.*, vol. 32, no. 24, pp. 1814–1823, Dec. 1992, doi: 10.1002/pen.760322404.

[176] M.-B. Coltelli, I. Della Maggiore, M. Bertoldo, F. Signori, S. Bronco, and F. Ciardelli, “Poly(lactic acid) properties as a consequence of poly(butylene adipate- *co* -terephthalate) blending and acetyl tributyl citrate plasticization,” *J. Appl. Polym. Sci.*, vol. 110, no. 2, pp. 1250–1262, Oct. 2008, doi: 10.1002/app.28512.

[177] S. Y. Gu, K. Zhang, J. Ren, and H. Zhan, “Melt rheology of polylactide/poly(butylene adipate-co-terephthalate) blends,” *Carbohydr. Polym.*, vol. 74, no. 1, pp. 79–85, Oct. 2008, doi: 10.1016/j.carbpol.2008.01.017.

[178] L. Jiang, M. P. Wolcott, and J. Zhang, “Study of biodegradable polylactide/poly(butylene adipate-co-terephthalate) blends,” *Biomacromolecules*, vol. 7, no. 1, pp. 199–207, Jan. 2006, doi: 10.1021/bm050581q.

[179] K. Li, J. Peng, L.-S. Turng, and H.-X. Huang, “Dynamic rheological behavior and morphology of polylactide/poly(butylenes adipate-co-terephthalate) blends with various composition ratios,” *Adv. Polym. Technol.*, vol. 30, no. 2, pp. 150–157, Jun. 2011, doi: 10.1002/adv.20212.

[180] H. Xiao, W. Lu, and J.-T. Yeh, “Crystallization behavior of fully biodegradable poly(lactic acid)/poly(butylene adipate- *co* -terephthalate) blends,” *J. Appl. Polym. Sci.*, vol. 112, no. 6, pp. 3754–3763, Jun. 2009, doi: 10.1002/app.29800.

[181] J.-T. Yeh, C.-H. Tsou, C.-Y. Huang, K.-N. Chen, C.-S. Wu, and W.-L. Chai, “Compatible and crystallization properties of poly(lactic acid)/poly(butylene adipate-co-terephthalate) blends,” *J. Appl. Polym. Sci.*, vol. 116, no. 2, p. n/a-n/a, Apr. 2009, doi: 10.1002/app.30907.

[182] S. Lin, W. Guo, C. Chen, J. Ma, and B. Wang, “Mechanical properties and morphology of biodegradable poly(lactic acid)/poly(butylene adipate-co-terephthalate) blends compatibilized by transesterification,” *Mater. Des.*, vol. 36, pp. 604–608, Apr. 2012, doi: 10.1016/j.matdes.2011.11.036.

[183] M. Shahlari and S. Lee, “Mechanical and morphological properties of poly(butylene adipate-co-terephthalate) and poly(lactic acid) blended with organically modified silicate layers,” *Polym. Eng. Sci.*, vol. 52, no. 7, pp. 1420–1428, Jul. 2012, doi: 10.1002/pen.23082.

[184] L. Jiang, B. Liu, and J. Zhang, “Properties of poly(lactic acid)/poly(butylene adipate-co-terephthalate)/ nanoparticle ternary composites,” *Ind. Eng. Chem. Res.*, vol. 48, no. 16, pp. 7594–7602, Aug. 2009, doi: 10.1021/ie900576f.

[185] R. Al-Itry, K. Lamnawar, and A. Maazouz, “Rheological, morphological, and interfacial properties of compatibilized PLA/PBAT blends,” *Rheol. Acta*, vol. 53, no. 7, pp. 501–517, May 2014, doi: 10.1007/s00397-014-0774-2.

[186] M. Nofar, M. C. Heuzey, P. J. Carreau, M. R. Kamal, and J. Randall, “Coalescence in PLA-PBAT blends under shear flow: Effects of blend preparation and PLA molecular weight,” *J. Rheol. (N. Y. N. Y).*, vol. 60, no. 4, pp. 637–648, 2016, doi: 10.1122/1.4953446.

[187] M. Nofar, M.-C. Heuzey, P. J. Carreau, and M. R. Kamal, “Effects of nanoclay and its localization on the morphology stabilization of PLA/PBAT blends under shear flow,” *Polymer (Guildf).*, vol. 98, pp. 353–364, Aug. 2016, doi: 10.1016/j.polymer.2016.06.044.

[188] E. Jalali Dil, N. Virgilio, and B. D. Favis, “The effect of the interfacial assembly of nano-silica in poly(lactic acid)/poly(butylene adipate-co-terephthalate) blends on morphology, rheology and mechanical properties,” *Eur. Polym. J.*, vol. 85, pp. 635–646, Dec. 2016, doi: 10.1016/j.eurpolymj.2016.07.022.

[189] E. Jalali Dil and B. D. Favis, “Localization of micro- and nano-silica particles in heterophase poly(lactic acid)/poly(butylene adipate-co-terephthalate) blends,” *Polymer (Guildf).*, vol. 76, pp. 295–306, Oct. 2015, doi: 10.1016/j.polymer.2015.08.046.

[190] E. Jalali Dil, M. Arjmand, I. Otero Navas, U. Sundararaj, and B. D. Favis, “Interface Bridging of Multiwalled Carbon Nanotubes in Polylactic Acid/Poly(butylene adipate- co -terephthalate): Morphology, Rheology, and Electrical Conductivity,” *Macromolecules*, vol. 53, no. 22, pp. 10267–10277, Nov. 2020, doi: 10.1021/acs.macromol.0c01525.

[191] E. Jalali Dil, P. J. Carreau, and B. D. Favis, “Morphology, miscibility and continuity development in poly(lactic acid)/poly(butylene adipate-co-terephthalate) blends,” *Polymer (Guildf).*, vol. 68, pp. 202–212, Jun. 2015, doi: 10.1016/j.polymer.2015.05.012.

[192] L. Jiang, M. P. Wolcott, and J. Zhang, “Study of biodegradable polylactide/poly(butylene adipate-co-terephthalate) blends,” *Biomacromolecules*, vol. 7, no. 1, pp. 199–207, Jan. 2006, doi: 10.1021/bm050581q.

[193] M. Nofar *et al.*, “Mechanical and bead foaming behavior of PLA-PBAT and PLA-PBSA blends with different morphologies,” *Eur. Polym. J.*, vol. 90, no. March, pp. 231–244, 2017, doi: 10.1016/j.eurpolymj.2017.03.031.

[194] Y. Deng, C. Yu, P. Wongwiwattana, and N. L. Thomas, “Optimising Ductility of Poly(Lactic Acid)/Poly(Butylene Adipate-co-Terephthalate) Blends Through Co-continuous Phase Morphology,” *J. Polym. Environ.*, vol. 26, no. 9, pp. 3802–3816, Sep. 2018, doi: 10.1007/s10924-018-1256-x.

[195] S. Lee, Y. Lee, and J. W. Lee, “Effect of ultrasound on the properties of biodegradable polymer blends of poly(lactic acid) with poly(butylene adipate-co-terephthalate),” *Macromol. Res.*, vol. 15, no. 1, pp. 44–50, 2007, doi: 10.1007/BF03218751.

[196] M. B. Coltelli, I. Della Maggiore, M. Bertoldo, F. Signori, S. Bronco, and F. Ciardelli, “Poly(lactic acid) properties as a consequence of poly(butylene adipate-co-terephthalate) blending and acetyl tributyl citrate plasticization,” *J. Appl. Polym. Sci.*, vol. 110, no. 2, pp. 1250–1262, Oct. 2008, doi: 10.1002/app.28512.

[197] R. Al-Itry, K. Lamnawar, and A. Maazouz, “Reactive extrusion of PLA, PBAT with a multi-functional epoxide: Physico-chemical and rheological properties,” *Eur. Polym. J.*, vol. 58, pp. 90–102, Sep. 2014, doi: 10.1016/j.eurpolymj.2014.06.013.

[198] R. Al-Itry, K. Lamnawar, A. Maazouz, N. Billon, and C. Combeaud, “Effect of the simultaneous biaxial stretching on the structural and mechanical properties of PLA, PBAT

and their blends at rubbery state," *Eur. Polym. J.*, vol. 68, pp. 288–301, Jul. 2015, doi: 10.1016/j.eurpolymj.2015.05.001.

[199] R. Al-Itry, K. Lamnawar, and A. Maazouz, "Improvement of thermal stability, rheological and mechanical properties of PLA, PBAT and their blends by reactive extrusion with functionalized epoxy," in *Polymer Degradation and Stability*, Oct. 2012, vol. 97, no. 10, pp. 1898–1914, doi: 10.1016/j.polymdegradstab.2012.06.028.

[200] W. Dong, B. Zou, Y. Yan, P. Ma, and M. Chen, "Effect of chain-extenders on the properties and hydrolytic degradation behavior of the poly(lactide)/ poly(butylene adipate-co-terephthalate) blends," *Int. J. Mol. Sci.*, vol. 14, no. 10, pp. 20189–20203, Oct. 2013, doi: 10.3390/ijms141020189.

[201] W. Dong *et al.*, "Influence of phthalic anhydride and bioxazoline on the mechanical and morphological properties of biodegradable poly(lactic acid)/poly[(butylene adipate)- *co* -terephthalate] blends," *Polym. Int.*, vol. 62, no. 12, pp. 1783–1790, Dec. 2013, doi: 10.1002/pi.4568.

[202] X. Zhang *et al.*, "Spontaneous atherosclerosis in aged lipoprotein lipase-deficient mice with severe hypertriglyceridemia on a normal chow diet," *Circ. Res.*, vol. 102, no. 2, pp. 250–256, Feb. 2008, doi: 10.1161/CIRCRESAHA.107.156554.

[203] M. Nishida, H. Ichihara, H. Watanabe, N. Fukuda, and H. Ito, "Improvement of dynamic tensile properties of Poly(lactic acid)/Poly(butylene adipate-co-terephthalate) polymer alloys using a crosslinking agent and observation of fracture surfaces," *Int. J. Impact Eng.*, vol. 79, pp. 117–125, May 2015, doi: 10.1016/j.ijimpeng.2014.11.010.

[204] M. B. Coltelli, S. Bronco, and C. Chinea, "The effect of free radical reactions on structure and properties of poly(lactic acid) (PLA) based blends," *Polym. Degrad. Stab.*, vol. 95, no. 3, pp. 332–341, Mar. 2010, doi: 10.1016/j.polymdegradstab.2009.11.015.

[205] N. Zhang, C. Zeng, L. Wang, and J. Ren, "Preparation and Properties of Biodegradable Poly(lactic acid)/Poly(butylene adipate-co-terephthalate) Blend with Epoxy-Functional Styrene Acrylic Copolymer as Reactive Agent," *J. Polym. Environ.*, vol. 21, no. 1, pp. 286–292, Mar. 2013, doi: 10.1007/s10924-012-0448-z.

[206] P. Ma *et al.*, "In-situ compatibilization of poly(lactic acid) and poly(butylene adipate-co-

terephthalate) blends by using dicumyl peroxide as a free-radical initiator," *Polym. Degrad. Stab.*, vol. 102, no. 1, pp. 145–151, Apr. 2014, doi: 10.1016/j.polymdegradstab.2014.01.025.

[207] K. Sirisinha and W. Somboon, "Melt characteristics, mechanical, and thermal properties of blown film from modified blends of poly(butylene adipate-co-terephthalate) and poly(lactide)," *J. Appl. Polym. Sci.*, vol. 124, no. 6, p. n/a-n/a, Jun. 2011, doi: 10.1002/app.35604.

[208] A. Taguet, P. Cassagnau, and J.-M. Lopez-Cuesta, "Structuration, selective dispersion and compatibilizing effect of (nano)fillers in polymer blends," *Prog. Polym. Sci.*, vol. 39, no. 8, pp. 1526–1563, Aug. 2014, doi: 10.1016/j.progpolymsci.2014.04.002.

[209] A. Taguet, "Rheological characterization of compatibilized polymer blends," in *Compatibilization of Polymer Blends*, Elsevier, 2020, pp. 453–487.

[210] M. Nofar, R. Salehiyan, U. Ciftci, A. Jalali, and A. Durmuş, "Ductility improvements of PLA-based binary and ternary blends with controlled morphology using PBAT, PBSA, and nanoclay," *Compos. Part B Eng.*, vol. 182, p. 107661, Feb. 2020, doi: 10.1016/j.compositesb.2019.107661.

[211] M. Nofar, M.-C. Heuzey, P. J. Carreau, and M. R. Kamal, "Nanoparticle Interactions and Molecular Relaxation in PLA/PBAT/Nanoclay Blends," *Exp. Results*, vol. 1, p. e47, Oct. 2020, doi: 10.1017/exp.2020.54.

[212] S. Adrar, A. Habi, A. Ajji, and Y. Grohens, "Synergistic effects in epoxy functionalized graphene and modified organo-montmorillonite PLA/PBAT blends," *Appl. Clay Sci.*, vol. 157, pp. 65–75, Jun. 2018, doi: 10.1016/j.clay.2018.02.028.

[213] S. Girdthep, N. Komrapit, R. Molloy, S. Lumyong, W. Punyodom, and P. Worajittiphon, "Effect of plate-like particles on properties of poly(lactic acid)/poly(butylene adipate-co-terephthalate) blend: A comparative study between modified montmorillonite and graphene nanoplatelets," *Compos. Sci. Technol.*, vol. 119, pp. 115–123, Nov. 2015, doi: 10.1016/j.compscitech.2015.10.005.

[214] M. S. Garg and D. Srivastava, "Effect of glycidyl methacrylate (GMA) content on thermal and mechanical properties of ternary blend systems based on cardanol-based vinyl ester resin, styrene and glycidyl methacrylate," *Prog. Org. Coatings*, vol. 77, no. 7, pp. 1208–

1220, Jul. 2014, doi: 10.1016/j.porgcoat.2014.03.029.

[215] S. W. Ko, M. K. Hong, B. J. Park, R. K. Gupta, H. J. Choi, and S. N. Bhattacharya, "Morphological and rheological characterization of multi-walled carbon nanotube/PLA/PBAT blend nanocomposites," *Polym. Bull.*, vol. 63, no. 1, pp. 125–134, Jul. 2009, doi: 10.1007/s00289-009-0072-9.

[216] J. Urquijo, N. Aranburu, S. Dagréou, G. Guerrica-Echevarría, and J. I. Eguiazábal, "CNT-induced morphology and its effect on properties in PLA/PBAT-based nanocomposites," *Eur. Polym. J.*, vol. 93, pp. 545–555, Aug. 2017, doi: 10.1016/j.eurpolymj.2017.06.035.

[217] P. Ma, L. Jiang, M. Yu, W. Dong, and M. Chen, "Green Antibacterial Nanocomposites from Poly(lactide)/Poly(butylene adipate-co-terephthalate)/Nanocrystal Cellulose-Silver Nanohybrids," *ACS Sustain. Chem. Eng.*, vol. 4, no. 12, pp. 6417–6426, Dec. 2016, doi: 10.1021/acssuschemeng.6b01106.

[218] D. S. Sarul *et al.*, "Preparation and characterization of PLA/PBAT/CNC blend nanocomposites," *Colloid Polym. Sci.*, vol. 299, no. 6, pp. 987–998, Jun. 2021, doi: 10.1007/s00396-021-04822-9.

[219] S. Ray and R. Salehiyan, *Nanostructured Immiscible Polymer Blends: Migration and Interface*. 2019.

[220] F. Fenouillot, P. Cassagnau, and J.-C. Majesté, "Uneven distribution of nanoparticles in immiscible fluids: Morphology development in polymer blends," *Polymer (Guildf).*, vol. 50, no. 6, pp. 1333–1350, Mar. 2009, doi: 10.1016/j.polymer.2008.12.029.

[221] L. Elias, F. Fenouillot, J. C. Majeste, and P. Cassagnau, "Morphology and rheology of immiscible polymer blends filled with silica nanoparticles," *Polymer (Guildf).*, vol. 48, no. 20, pp. 6029–6040, Sep. 2007, doi: 10.1016/j.polymer.2007.07.061.

[222] E. Jalali Dil, M. Arjmand, Y. Li, U. Sundararaj, and B. D. Favis, "Assembling copper nanowires at the interface and in discrete phases in PLA-based polymer blends," *Eur. Polym. J.*, vol. 85, pp. 187–197, Dec. 2016, doi: 10.1016/j.eurpolymj.2016.09.053.

[223] L. Elias, F. Fenouillot, J. C. Majesté, G. Martin, and P. Cassagnau, "Migration of nanosilica particles in polymer blends," *J. Polym. Sci. Part B Polym. Phys.*, vol. 46, no. 18, pp. 1976–1983, Sep. 2008, doi: 10.1002/polb.21534.

[224] R. Salehiyan, M. Nofar, K. Malkappa, and S. S. Ray, “Effect of nanofillers characteristics and their selective localization on morphology development and rheological properties of melt-processed polylactide/poly(butylene adipate-co-terephthalate) blend composites,” *Polym. Eng. Sci.*, vol. 60, no. 11, pp. 2749–2760, Nov. 2020, doi: 10.1002/pen.25505.

[225] R. Salehiyan and S. S. Ray, “Tuning the Conductivity of Nanocomposites through Nanoparticle Migration and Interface Crossing in Immiscible Polymer Blends: A Review on Fundamental Understanding,” *Macromol. Mater. Eng.*, vol. 304, no. 2, p. 1800431, Feb. 2019, doi: 10.1002/mame.201800431.

[226] M. Kontopoulou, Y. Liu, J. R. Austin, and J. S. Parent, “The dynamics of montmorillonite clay dispersion and morphology development in immiscible ethylene-propylene rubber/polypropylene blends,” *Polymer (Guildf).*, vol. 48, no. 15, pp. 4520–4528, Jul. 2007, doi: 10.1016/j.polymer.2007.05.068.

[227] A. Göldel, G. Kasaliwal, and P. Pötschke, “Selective Localization and Migration of Multiwalled Carbon Nanotubes in Blends of Polycarbonate and Poly(styrene-acrylonitrile),” *Macromol. Rapid Commun.*, vol. 30, no. 6, pp. 423–429, Mar. 2009, doi: 10.1002/marc.200800549.

[228] A. C. Baudouin, C. Bailly, and J. Devaux, “Interface localization of carbon nanotubes in blends of two copolymers,” *Polym. Degrad. Stab.*, vol. 95, no. 3, pp. 389–398, Mar. 2010, doi: 10.1016/j.polymdegradstab.2009.11.007.

[229] A. C. Baudouin, J. Devaux, and C. Bailly, “Localization of carbon nanotubes at the interface in blends of polyamide and ethylene-acrylate copolymer,” *Polymer (Guildf).*, vol. 51, no. 6, pp. 1341–1354, Mar. 2010, doi: 10.1016/j.polymer.2010.01.050.

[230] J. K. Yuan, S. H. Yao, A. Sylvestre, and J. Bai, “Biphasic polymer blends containing carbon nanotubes: Heterogeneous nanotube distribution and its influence on the dielectric properties,” *J. Phys. Chem. C*, vol. 116, no. 2, pp. 2051–2058, Jan. 2012, doi: 10.1021/jp210872w.

[231] A. Katada, Y. F. Buys, Y. Tominaga, S. Asai, and M. Sumita, “Relationship between electrical resistivity and particle dispersion state for carbon black filled poly (ethylene-co-vinyl acetate)/poly (L-lactic acid) blend,” *Colloid Polym. Sci.*, vol. 284, no. 2, pp. 134–141,

Nov. 2005, doi: 10.1007/s00396-005-1348-8.

[232] M. Gültner, A. Göldel, and P. Pötschke, “Tuning the localization of functionalized MWCNTs in SAN/PC blends by a reactive component,” *Compos. Sci. Technol.*, vol. 72, no. 1, pp. 41–48, Dec. 2011, doi: 10.1016/j.compscitech.2011.09.013.

[233] L. Elias, F. Fenouillot, J. C. Majesté, P. Alcouffe, and P. Cassagnau, “Immiscible polymer blends stabilized with nano-silica particles: Rheology and effective interfacial tension,” *Polymer (Guildf).*, vol. 49, no. 20, pp. 4378–4385, Sep. 2008, doi: 10.1016/j.polymer.2008.07.018.

[234] R. Cardinaud and T. McNally, “Localization of MWCNTs in PET/LDPE blends,” *Eur. Polym. J.*, vol. 49, no. 6, pp. 1287–1297, Jun. 2013, doi: 10.1016/j.eurpolymj.2013.01.007.

[235] A. Göldel, G. R. Kasaliwal, P. Pötschke, and G. Heinrich, “The kinetics of CNT transfer between immiscible blend phases during melt mixing,” *Polymer (Guildf).*, vol. 53, no. 2, pp. 411–421, Jan. 2012, doi: 10.1016/j.polymer.2011.11.039.

[236] A. Göldel, A. Marmur, G. R. Kasaliwal, P. Pötschke, and G. Heinrich, “Shape-dependent localization of carbon nanotubes and carbon black in an immiscible polymer blend during melt mixing,” *Macromolecules*, vol. 44, no. 15, pp. 6094–6102, Aug. 2011, doi: 10.1021/ma200793a.

[237] J. R. Austin and M. Kontopoulou, “Effect of organoclay content on the rheology, morphology, and physical properties of polyolefin elastomers and their blends with polypropylene,” *Polym. Eng. Sci.*, vol. 46, no. 11, pp. 1491–1501, Nov. 2006, doi: 10.1002/pen.20622.

[238] M. H. Al-Saleh and U. Sundararaj, “An innovative method to reduce percolation threshold of carbon black filled immiscible polymer blends,” *Compos. Part A Appl. Sci. Manuf.*, vol. 39, no. 2, pp. 284–293, Feb. 2008, doi: 10.1016/j.compositesa.2007.10.010.

[239] J. Huang, C. Mao, Y. Zhu, W. Jiang, and X. Yang, “Control of carbon nanotubes at the interface of a co-continuous immiscible polymer blend to fabricate conductive composites with ultralow percolation thresholds,” *Carbon N. Y.*, vol. 73, pp. 267–274, Jul. 2014, doi: 10.1016/j.carbon.2014.02.063.

[240] D. Wu *et al.*, “Selective Localization of Nanofillers: Effect on Morphology and

Crystallization of PLA/PCL Blends," *Macromol. Chem. Phys.*, vol. 212, no. 6, pp. 613–626, Mar. 2011, doi: 10.1002/macp.201000579.

[241] X. Zhao *et al.*, "Effect of the selective localization of carbon nanotubes in polystyrene/poly(vinylidene fluoride) blends on their dielectric, thermal, and mechanical properties," *Mater. Des.*, vol. 56, pp. 807–815, Apr. 2014, doi: 10.1016/j.matdes.2013.11.073.

[242] T. W. Lee and Y. G. Jeong, "Enhanced electrical conductivity, mechanical modulus, and thermal stability of immiscible polylactide/polypropylene blends by the selective localization of multi-walled carbon nanotubes," *Compos. Sci. Technol.*, vol. 103, pp. 78–84, Oct. 2014, doi: 10.1016/j.compscitech.2014.08.019.

[243] E. Jalali, D. Département, D. E. Génie, C. École, and P. De Montréal, "LOCALIZATION OF SOLID MICRO AND NANO-INCLUSIONS IN HETEROPHASE BIOPLASTIC BLENDS."

[244] E. Jalali Dil and B. D. Favis, "Localization of micro and nano- silica particles in a high interfacial tension poly(lactic acid)/low density polyethylene system," *Polymer (Guildf).*, vol. 77, pp. 156–166, Oct. 2015, doi: 10.1016/j.polymer.2015.08.063.

[245] S. H. Lee, M. Bailly, and M. Kontopoulou, "Morphology and Properties of Poly(propylene)/Ethylene-Octene Copolymer Blends Containing Nanosilica," *Macromol. Mater. Eng.*, vol. 297, no. 1, pp. 95–103, Jan. 2012, doi: 10.1002/mame.201100147.

[246] M. Bailly and M. Kontopoulou, "Preparation and characterization of thermoplastic olefin/nanosilica composites using a silane-grafted polypropylene matrix," *Polymer (Guildf).*, vol. 50, no. 11, pp. 2472–2480, May 2009, doi: 10.1016/j.polymer.2009.03.034.

[247] A. Göldel, A. Marmur, G. R. Kasaliwal, P. Pötschke, and G. Heinrich, "Shape-dependent localization of carbon nanotubes and carbon black in an immiscible polymer blend during melt mixing," *Macromolecules*, vol. 44, no. 15, pp. 6094–6102, Aug. 2011, doi: 10.1021/ma200793a.

[248] R. Salehiyan, M. Nofar, S. S. Ray, and V. Ojijo, "Kinetically Controlled Localization of Carbon Nanotubes in Polylactide/Poly(vinylidene fluoride) Blend Nanocomposites and Their Influence on Electromagnetic Interference Shielding, Electrical Conductivity, and

Rheological Properties," *J. Phys. Chem. C*, vol. 123, no. 31, pp. 19195–19207, Aug. 2019, doi: 10.1021/acs.jpcc.9b04494.

[249] P. Cassagnau, "Melt rheology of organoclay and fumed silica nanocomposites," *Polymer*, vol. 49, no. 9. Elsevier BV, pp. 2183–2196, Apr. 29, 2008, doi: 10.1016/j.polymer.2007.12.035.

[250] P. Cassagnau and F. Mélis, "Non-linear viscoelastic behaviour and modulus recovery in silica filled polymers," *Polymer (Guildf).*, vol. 44, no. 21, pp. 6607–6615, Sep. 2003, doi: 10.1016/S0032-3861(03)00689-X.

[251] Y. Song and Q. Zheng, "Linear rheology of nanofilled polymers," *J. Rheol. (N. Y. N. Y).*, vol. 59, no. 1, pp. 155–191, Jan. 2015, doi: 10.1122/1.4903312.

[252] H. Nazockdast, "Morphology and Structure of Polymer Blends Containing Nanofillers," in *Encyclopedia of Polymer Blends*, Weinheim, Germany: Wiley-VCH Verlag GmbH & Co. KGaA, 2016, pp. 401–482.

[253] R. Krishnamoorti and T. Chatterjee, "Rheology and Processing of Polymer Nanocomposites," in *Applied Polymer Rheology*, Hoboken, NJ, USA: John Wiley & Sons, Inc., 2011, pp. 153–177.

[254] M. Nofar, R. Salehiyan, and S. Sinha Ray, "Rheology of poly (lactic acid)-based systems," *Polym. Rev.*, vol. 59, no. 3, pp. 465–509, Mar. 2019, doi: 10.1080/15583724.2019.1572185.

[255] R. Salehiyan, M. Nofar, K. Malkappa, and S. S. Ray, "Effect of nanofillers characteristics and their selective localization on morphology development and rheological properties of melt-processed polylactide/poly(butylene adipate-co-terephthalate) blend composites," *Polym. Eng. Sci.*, vol. 60, no. 11, pp. 2749–2760, Sep. 2020, doi: 10.1002/pen.25505.

[256] R. Salehiyan and S. S. Ray, "Tuning the Conductivity of Nanocomposites through Nanoparticle Migration and Interface Crossing in Immiscible Polymer Blends: A Review on Fundamental Understanding," *Macromol. Mater. Eng.*, vol. 304, no. 2, p. 1800431, Feb. 2019, doi: 10.1002/mame.201800431.

[257] I. Otero-Navas, M. Arjmand, and U. Sundararaj, "Carbon nanotube induced double percolation in polymer blends: Morphology, rheology and broadband dielectric properties," *Polymer (Guildf).*, vol. 114, pp. 122–134, Apr. 2017, doi: 10.1016/j.polymer.2017.02.082.

[258] M. Salzano De Luna and G. Filippone, “Effects of nanoparticles on the morphology of immiscible polymer blends - Challenges and opportunities,” *European Polymer Journal*, vol. 79. Elsevier Ltd, pp. 198–218, Jun. 01, 2016, doi: 10.1016/j.eurpolymj.2016.02.023.

[259] C. Gao, S. Zhang, B. Han, H. Sun, G. Wang, and Z. Jiang, “Multi-walled carbon nanotube induced co-continuity of poly(ether ether ketone)/polyimide blends for high performance conductive materials,” *RSC Adv.*, vol. 4, no. 79, pp. 42175–42182, Sep. 2014, doi: 10.1039/c4ra07473d.

[260] A. Nuzzo, E. Bilotti, T. Peijs, D. Acierno, and G. Filippone, “Nanoparticle-induced co-continuity in immiscible polymer blends - A comparative study on bio-based PLA-PA11 blends filled with organoclay, sepiolite, and carbon nanotubes,” *Polymer (Guildf).*, vol. 55, no. 19, pp. 4908–4919, Sep. 2014, doi: 10.1016/j.polymer.2014.07.036.

[261] G. Filippone, N. T. Dintcheva, F. P. La Mantia, and D. Acierno, “Using organoclay to promote morphology refinement and co-continuity in high-density polyethylene/polyamide 6 blends – Effect of filler content and polymer matrix composition,” *Polymer (Guildf).*, vol. 51, no. 17, pp. 3956–3965, Aug. 2010, doi: 10.1016/j.polymer.2010.06.044.

[262] M. Shahlari and S. Lee, “Mechanical and morphological properties of poly(butylene adipate-co-terephthalate) and poly(lactic acid) blended with organically modified silicate layers,” *Polym. Eng. Sci.*, vol. 52, no. 7, pp. 1420–1428, Jul. 2012, doi: 10.1002/pen.23082.

[263] M. R. Aghjeh, V. Asadi, P. Mehdijabbar, H. A. Khonakdar, and S. H. Jafari, “Application of linear rheology in determination of nanoclay localization in PLA/EVA/Clay nanocomposites: Correlation with microstructure and thermal properties,” *Compos. Part B Eng.*, vol. 86, pp. 273–284, Feb. 2016, doi: 10.1016/j.compositesb.2015.09.064.

[264] X. Zhao, H. Wang, Z. Fu, and Y. Li, “Enhanced Interfacial Adhesion by Reactive Carbon Nanotubes: New Route to High-Performance Immiscible Polymer Blend Nanocomposites with Simultaneously Enhanced Toughness, Tensile Strength, and Electrical Conductivity,” *ACS Appl. Mater. Interfaces*, vol. 10, no. 10, pp. 8411–8416, Mar. 2018, doi: 10.1021/acsami.8b01704.

[265] N. Bitinis, R. Verdejo, E. M. Maya, E. Espuche, P. Cassagnau, and M. A. Lopez-Manchado, “Physicochemical properties of organoclay filled polylactic acid/natural rubber blend

bionanocomposites," *Compos. Sci. Technol.*, vol. 72, no. 2, pp. 305–313, Jan. 2012, doi: 10.1016/j.compscitech.2011.11.018.

[266] M. P. Arrieta, E. Fortunati, F. Dominici, E. Rayón, J. López, and J. M. Kenny, "PLA-PHB/cellulose based films: Mechanical, barrier and disintegration properties," *Polym. Degrad. Stab.*, vol. 107, pp. 139–149, 2014, doi: 10.1016/j.polymdegradstab.2014.05.010.

[267] M. P. Arrieta, E. Fortunati, F. Dominici, E. Rayón, J. López, and J. M. Kenny, "Multifunctional PLA-PHB/cellulose nanocrystal films: Processing, structural and thermal properties," *Carbohydr. Polym.*, vol. 107, no. 1, pp. 16–24, Jul. 2014, doi: 10.1016/j.carbpol.2014.02.044.

[268] M. P. Arrieta, E. Fortunati, F. Dominici, J. López, and J. M. Kenny, "Bionanocomposite films based on plasticized PLA-PHB/cellulose nanocrystal blends," *Carbohydr. Polym.*, vol. 121, pp. 265–275, May 2015, doi: 10.1016/j.carbpol.2014.12.056.

[269] F. Luzi *et al.*, "Production and characterization of PLA_PBS biodegradable blends reinforced with cellulose nanocrystals extracted from hemp fibres," *Ind. Crops Prod.*, vol. 93, pp. 276–289, Dec. 2016, doi: 10.1016/j.indcrop.2016.01.045.

[270] X. Zhang and Y. Zhang, "Reinforcement effect of poly(butylene succinate) (PBS)-grafted cellulose nanocrystal on toughened PBS/polylactic acid blends," *Carbohydr. Polym.*, vol. 140, pp. 374–382, Apr. 2016, doi: 10.1016/j.carbpol.2015.12.073.

[271] N. Bitinis *et al.*, "Poly(lactic acid)/natural rubber/cellulose nanocrystal bionanocomposites Part I. Processing and morphology," *Carbohydr. Polym.*, vol. 96, no. 2, pp. 611–620, 2013, doi: 10.1016/j.carbpol.2013.02.068.

[272] N. Bitinis *et al.*, "Poly(lactic acid)/natural rubber/cellulose nanocrystal bionanocomposites. Part II: Properties evaluation," *Carbohydr. Polym.*, vol. 96, no. 2, pp. 621–627, 2013, doi: 10.1016/j.carbpol.2013.03.091.

[273] Z. Shakouri and H. Nazockdast, "Microstructural development and mechanical performance of PLA/TPU blends containing geometrically different cellulose nanocrystals," *Cellulose*, vol. 25, no. 12, pp. 7167–7188, Dec. 2018, doi: 10.1007/s10570-018-2061-3.

[274] Z. Shakouri, H. Nazockdast, and H. Sadeghi Ghari, "Effect of the geometry of cellulose nanocrystals on morphology and mechanical performance of dynamically vulcanized

PLA/PU blend," *Cellulose*, vol. 27, no. 1, pp. 215–231, Jan. 2020, doi: 10.1007/s10570-019-02775-5.

[275] Basf, "Ecoflex - Sense or Nonsense of Bio." [Online]. Available: www.basf.de/plastics.

[276] D. Arslan *et al.*, "Effect of preparation method on the properties of polylactide/cellulose nanocrystal nanocomposites," *Polym. Compos.*, vol. 41, no. 10, pp. 4170–4180, Oct. 2020, doi: 10.1002/pc.25701.

[277] C. Bruel, J. R. Tavares, P. J. Carreau, and M. C. Heuzey, "The structural amphiphilicity of cellulose nanocrystals characterized from their cohesion parameters," *Carbohydr. Polym.*, vol. 205, pp. 184–191, 2019, doi: 10.1016/j.carbpol.2018.10.026.

[278] P. Ma, L. Jiang, M. Yu, W. Dong, and M. Chen, "Green Antibacterial Nanocomposites from Poly(lactide)/Poly(butylene adipate-co-terephthalate)/Nanocrystal Cellulose-Silver Nanohybrids," *ACS Sustain. Chem. Eng.*, vol. 4, no. 12, pp. 6417–6426, Dec. 2016, doi: 10.1021/acssuschemeng.6b01106.